DISSERTATION

WATER OXIDATION CATALYSIS BEGINNING WITH COBALT POLYOXOMETALATES: DETERMINING THE DOMINANT CATALYST UNDER ELECTROCATALYTIC CONDITIONS AND INVESTIGATION OF THE SURFACE PROPERTIES OF Co_3O_4 NANOPARTICLES

Submitted by

Scott Jerald Folkman

Department of Chemistry

In partial fulfillment of the requirements

For the Degree of Doctor of Philosophy

Colorado State University

Fort Collins, Colorado

Summer 2018

Doctoral Committee:

Advisor: Richard G. Finke

James Neilson
Steven Strauss
James Sites

ABSTRACT

WATER OXIDATION CATALYSIS BEGINNING WITH COBALT POLYOXOMETALATES: DETERMINING THE DOMINANT CATALYST UNDER ELECTROCATALYTIC CONDITIONS AND INVESTIGATION OF THE SURFACE PROPERTIES OF Co_3O_4 NANOPARTICLES

Generation of hydrogen as a fuel is one of the most promising technologies for a renewable energy future. Electrocatalytic water splitting can take energy from virtually any power source and split water into oxygen and hydrogen, thereby creating a renewable feedstock of hydrogen. The efficiency of electrocatalytic water splitting is limited by the anodic half reaction, water oxidation. As such, there has been an immense effort to discover and understand water oxidation catalysts (WOCatalysts). The two main classes of WOCatalysts are homogeneous and heterogeneous catalysts. Homogeneous catalysts are typically soluble molecular complexes that have a single type of active site, allowing for rational tuning through synthesis, and mechanistic studies. Heterogeneous catalysts are typically in a different phase from the reaction (i.e. insoluble or electrode-bound) and have a spectrum of active sites that are more difficult to identify.

This Dissertation examines a class of inorganic compounds called polyoxometalates (POMs), and investigates the nature of the kinetically dominant, homogeneous vs heterogeneous catalyst. Chapter I provides an in depth introduction to water oxidation catalysis and in particular with cobalt-based POMS. Chapters II and III focus on the polyoxometalate, $[Co_4(H_2O)_2(VW_9O_{34})_2]^{10-}$ (hereafter **$Co_4V_2W_{18}$**) which has been claimed to be one of the fastest WOCatalysts to date. Those studies demonstrate that **$Co_4V_2W_{18}$** is, in fact, very unstable and

dissociates 87-100% of the Co(II) originally present in **$Co_4V_2W_{18}$** into solution within three hours when dissolved in 0.1 sodium phosphate buffer (NaPi) at pH 5.8 and 8.0 as well as sodium borate buffer (NaB) pH=9.0. The dissociated $Co(II)_{aq}$ then forms heterogeneous cobalt-oxide (CoO_x) on a glassy carbon electrode under electrocatalytic WOCatalysis conditions. The deposited CoO_x accounts for 100±15% of the observed catalysis current. This finding demonstrates that the original **$Co_4V_2W_{18}$** serves only as a precursor to heterogeneous CoO_x which is the dominant WOCatalyst.

Chapter IV details studies using a selection of the most stable and most active Co-POMs to date. These studies demonstrate that none of the Co-POMs examined are 100% stable, and they release between 0.6 and >90% of the cobalt in the original complex within three hours in 0.1 M NaPi pH=5.8 or 8.0 and NaB pH=9.0. Furthermore, in 13 of the 18 cases examined, heterogeneous CoO_x forms on the glassy carbon electrode and accounts for ≥100% of the observed WOCatalysis current. Lastly, under conditions where the Co-POMs are stable (<2% decomposition), the evidence provided implies that some of the Co-POMs are homogeneous WOCatalyst. Other implications regarding the stability trends and nature of the true catalyst are provided.

The last research chapter, Chapter V, consists of the study of Co_3O_4 nanoparticles, which have been shown to be active for WOCatalysis. In this chapter, the synthesis, and surface properties of Co_3O_4 nanoparticles are investigated. It is demonstrated that ethanol/water (EtOH/water) as solvent forms phase-pure Co_3O_4 nanoparticles but following the same procedure in water yields a mixture of products. Therefore, EtOH must affect the product either *thermodynamically* (i.e. through a covalent EtO-Co linkage on the surface) or *kinetically* (i.e., by affecting the nucleation and/or growth of the particles). However, EtOH is not observed in the product; instead, acetate from the cobalt acetate precursor is the only detectable surface ligand. This implies that EtOH does not affect the thermodynamics of the particle formation, instead it must be involved in the kinetics

of nucleation and/or growth of the Co_3O_4 nanoparticles. Through careful examination of the particle size and surface ligand data were able to obtain an average molecular formula of $\{[Co_3O_4(C_2H_3O_2)^-][(NH_4^+)_{0.3}(H^+_{0.7})]^+ \cdot (H_2O)\}_{\sim 216}$ for the nanoparticles that we isolated. This chapter also includes general implications for the synthesis of metal-oxide nanoparticles in alcohol, and methods for identifying surface ligands.

ACKNOWLEDGEMENTS

I would like to thank my research advisor, Rick Finke, for his support and instruction throughout my time as a graduate student. His knowledge and scientific methods have instilled in me a strong approach to not only scientific inquiries, but life itself. I am also grateful to the Colorado State University chemistry department's faculty and scientific staff, especially within the central instrument facility who have provided intellectual support as well as encouragement. Additionally, I'd like to acknowledge the National Science Foundation for funding from CHE-1361515. I would also like to express gratitude to my graduate student colleagues and lab-mates who have listened, encouraged, and especially challenged me. Last I would like to say thank you to my friends and my family, Mom, Dad, and Lauren; I could not have done it without you.

TABLE OF CONTENTS

ABSTRACT ii

ACKNOWLEDGEMENTS v

I. INTRODUCTION 1

II. COBALT POLYOXOMETALATE $CO_4V_2W_{18}O_{68}^{10-}$: A CRITICAL INVESTIGATION OF ITS SYNTHESIS, PURITY, AND OBSERVED ^{51}V QUADRUPOLAR NMR 12
Overview 12
2.1 Introduction 13
2.2 Results and Discussion 21
2.3 Summary and Conclusions 34
2.4 Experimental 37
REFERENCES 46

III. ELECTROCHEMICAL WATER OXIDATION CATALYSIS BEGINNING WITH CO(II) POLYOXOMETALATES: THE CASE OF THE PRECATALYST $CO_4V_2W_{18}O_{68}^{10-}$ 50
Overview 50
3.1 Introduction 51
3.2 Experimental 54
3.3 Results and Discussion 61
3.4 Summary and Conclusions 76
REFERENCES 79

IV. ELECTROCHEMICALLY DRIVEN WATER-OXIDATION CATALYSIS BEGINNING WITH SIX EXEMPLARY COBALT POLYOXOMETALATES: IS IT MOLECULAR, HOMOGENEOUS CATALYSIS OR ELECTRODE-BOUND, HETEROGENEOUS COO_X CATALYSIS? 82
Overview 82
4.1 Introduction 84
4.2 Experimental 93
4.3 Results and Discussion 101
4.4 Summary and Conclusions 122
REFERENCES 126

V. ALCOHOL SOLVENT EFFECTS IN THE SYNTHESIS OF CO_3O_4 METAL-OXIDE NANOPARTICLES: DISPROOF OF A SURFACE-LIGAND THERMODYNAMIC EFFECT EN ROUTE TO ALTERNATIVE KINETIC AND THERMODYNAMIC EXPLANATIONS 129
Overview 129
5.1 Introduction 130
5.2 Experimental 131
5.3 Results and Discussion 136
5.4 Conclusions 152
REFERENCES 154

VI. SUMMARY AND CONCLUSIONS 157

APPENDIX I. SUPPORTING INFORMATION FOR CHAPTER II 162

APPENDIX II. SUPPORTING INFORMATION FOR CHAPTER III 180

APPENDIX III. SUPPORTING INFORMATION FOR CHAPTER IV 198

APPENDIX IV. SUPPORTING INFORMATION FOR CHAPTER V 230

LIST OF ABBREVIATIONS 244

I. INTRODUCTION

This dissertation has been prepared in a "journal's format" meaning that each chapter was prepared as a manuscript for submission and publication in a peer-reviewed chemistry journal. Each chapter, therefore, follows the formatting guidelines for the journal for which the manuscript was submitted. An overview is presented at the beginning of each chapter and the Supporting Information sections are included as separate appendices for each respective chapter at the end of the dissertation. Below is an introduction to the field of solar fuel production through water oxidation and a brief description of each chapter.

Meeting the demand of humanity's enormous (and growing) energy consumption is one of the biggest scientific challenges of the modern age.[1,2] Solar energy is, of course, the ultimate source of renewable energy.[2] However, because solar energy is diffuse and production is intermittent due to the diurnal cycle, storage schemes must be developed.[2] One method to store solar energy is in the form of chemical bonds of H_2 through electrocatalytic water splitting which involves water oxidation at the anode and proton reduction at the cathode (Scheme 1). The efficiency of electrocatalytic water splitting is limited by the water oxidation half reaction due to sluggish kinetics of the $4e^-/4H^+$ transfer, meaning that a large overpotential must be applied to the anode in order to observe the reaction at reasonable rates.[2] In order to expedite this process and increase the overall efficiency of water splitting, a water oxidation catalyst (WOCatalyst) must be employed. As such WOCatalysts have been the subject of many publications.[2,3,4,5,6,7,8,9,10,11,12,13,14,15,16] Ideally, a water oxidation catalyst would be selective for water oxidation (~100% Faradaic efficiency), fast (>10 mA/cm^2 at minimal overpotential), long lived (>10^9 total turn overs), and composed of earth abundant materials.[17]

$$2H_2O_{(l)} \longrightarrow O_{2(g)} + 4H^+_{(aq)} + 4e^-$$
$$4H^+_{(aq)} + 4e^- \longrightarrow 2H_{2(g)}$$
$$2H_2O_{(l)} \longrightarrow O_{2(g)} + 2H_{2(g)}$$

Scheme 1. Balanced equations for water oxidation, proton reduction, and overall water splitting. This reaction yields ΔG=+237 kJ/mol H_2 produced.[18]

There are two overarching types of WOCatalysts, which are homogeneous and heterogeneous, discussed further in several reviews.[19,20,21] Although the precise definition of homogeneous vs heterogeneous catalysis is the subject of some debate, herein we are defining homogeneous as catalysts that consist of a single type of active site that is known.[19] Examples of homogeneous catalysts include the WOCatalyst used by nature, photosystem II,[5] and a handful of other molecular examples such as $[\{Ru_4O_4(OH_2)(H_2O)_4\}(\gamma\text{-}SiW_{10}O_{36})_2]^{10-}$.[4,6,7] Herein we define heterogeneous as catalysts that have many different active sites, and is often (but not necessarily) in a different phase from the reaction (i.e., electrode bound, insoluble).[19,20,21] An example of a heterogeneous WOCatalyst is the cobalt oxide (CoO_x) film that forms from Co^{2+}_{aq} in phosphate buffered solutions under electrochemically oxidizing conditions.[8] Knowing the precise nature of a given WOCatalyst (i.e., homogeneous vs heterogeneous) is necessary before any other mechanistic or computational studies of the catalytic process are possible. Hence, knowing what the active catalyst is under a given set of conditions is a prerequisite to rational development of the next generation of selective, faster, and more stable WOCatalysts.

Polyoxometalates (POMs) are a class of molecular metal-oxide clusters that often consist of tungsten, phosphorous, molybdenum, vanadium, ruthenium, and cobalt.[6,22,23,24] Many research groups have a strong interest in cobalt based POMs (Co-POMs) for WOCatalysis due to their oxidative stability and molecular structure which could allow for mechanistic studies and synthetic tuning if they are, in fact, homogeneous catalysts as is often claimed.[9,10,11,12,13,14,15,16] One

important example is the case of $Co_4(H_2O)_2P_2W_{18}O_{68}^{10-}$ with which one research group conducted chemical WOCatalysis using $Ru(bpy)_3^{3+}$ (bpy=2,2'-bipyridine) as the oxidant with a turnover frequency (TOF) of ~5 s^{-1}, as well as electrochemical WOCatalysis using 60 mM sodium phosphate buffer (NaPi) pH 8.0 (working electrode not specified), and claimed that intact $Co_4(H_2O)_2P_2W_{18}O_{68}^{10-}$ is the sole WOCatalyst.[9] Subsequent research, however, demonstrated that $Co_4(H_2O)_2P_2W_{18}O_{68}^{10-}$ is hydrolytically unstable, a 500 μM solution of $Co_4(H_2O)_2P_2W_{18}O_{68}^{10-}$ decomposes by 4.3 ± 0.6 % after 3 h in 0.1 M NaPi pH=8.0 thereby releasing ~58 μM Co^{2+}_{aq}.[25] The amount of Co^{2+}_{aq} released then forms heterogeneous CoO_x on a glassy carbon electrode during controlled potential electrolysis (1.1 V vs. Ag/AgCl) which quantitatively accounts for all of the observed WOCatalysis current.[25] This finding spurred a series of publications and counter publications as to the dominant catalyst under a given set of conditions for a multitude of different Co-POMs including $Co_4(H_2O)_2P_2W_{18}O_{68}^{10-}$.[26,27,28,29,30,31,32]

One key goal of the present dissertation then is to examine a selection of the most well-known Co-POMs and Co-POMs that are reported to be WOCatalysts under a variety of electrochemically driven WOCatalysis conditions to determine (i) if the Co-POMs examined are stable in solution and under WOCatalyst conditions, (ii) if a CoO_x film is formed on the electrode, (iii) if any of the WOCatalysis current can be attributed to the Co-POMs, and ultimately (iv) what structural/stability factors contribute to the observed WOCatalysis properties of each Co-POM? The Co-POMs chosen for study, along with WOCatalysis background for each Co-POM are summarized in Table 1.[33,34,35]

The studies in this dissertation initially began with the first six entries in Table 1.However, a 2014 *JACS* communication detailing the use of $Na_{10}[Co_4(H_2O)_2(VW_9O_{34})_2]\cdot 35H_2O$ (hereafter **$Co_4V_2W_{18}$**) as a homogeneous WOCatalyst caught and diverted our attention when that

communication came out.[16] The 2014 studies claimed that **$Co_4V_2W_{18}$** was stable in solution and exhibited a TOF > 1 x 10^3 s^{-1} under photochemical WOCatalysis conditions.[16] Our interest in this particular Co-POM stems from the fact that **$Co_4V_2W_{18}$** is the vanadium analog of the controversial **$Co_4P_2W_{18}$** Co-POM discussed above.[9,16,36]Hence, we wondered why **$Co_4V_2W_{18}$** is more stable in solution? Also, why is **$Co_4V_2W_{18}$** ~200 times more active for WOCatalysis than its P-analogue? We ultimately postulated the alternative hypothesis that **$Co_4V_2W_{18}$** is actually, probably not a homogeneous WOCatalyst. Rather, we hypothesized that **$Co_4V_2W_{18}$** serves as a precursor to homogeneous CoO_x as is the case for **$Co_4P_2W_{18}$**.[25] Thus, the first two research chapters of this dissertation (Chapters II and III) involve our studies with **$Co_4V_2W_{18}$**.

Table 1. Co-POMs chosen to study, along with prior studies for WOCatalysis.

Polyoxometalate[a] (Abbreviation)	System[b]	References
$[Co_4(H_2O)_2(PW_9O_{34})_2]^{10-}$ (**$Co_4P_2W_{18}$**)	Chemical Oxidant, Electrochemical, Photochemical. $TOF_{reported}$>5 s^{-1}	**9, 10**
$[Co_9(H_2O)_6(OH)_3(HPO_4)_2(PW_9O_{34})_3]^{16-}$ (**$Co_9P_5W_{27}$**)	Electrochemical.	**13, 32**
$[Co_4(H_2O)_2(P_2W_{15}O_{56})_2]^{16-}$ (**$Co_4P_4W_{30}$**)	Chemical Oxidant. No activity reported.	**9**
$[Co(H_2O)PW_{11}O_{39}]^{5-}$ (**$CoPW_{11}$**)	Chemical Oxidant. No activity reported.	**9**
$[\alpha_1\text{-}CoP_2W_{17}O_{61}]^{8-}$ (**$\alpha_1\text{-}CoP_2W_{17}$**)	No WOC studies to date.	**N/A**
$[\alpha_2\text{-}CoP_2W_{17}O_{61}]^{8-}$ (**$\alpha_2\text{-}CoP_2W_{17}$**)	No WOC studies to date.	**N/A**
$[Co_4(H_2O)_2(VW_9O_{34})_2]^{10-}$ (**$Co_4V_2W_{18}$**)	Photochemical. $TOF_{reported}$=1.6-2.2x 10^3 s^{-1}	**16**

a) Abbreviations are shown in bold. b) Systems are defined as follows: chemical oxidant refers to the use of $Ru(bpy)_3^{3+}$ as oxidant; photochemical refers to WOC using $Ru(bpy)_3^{2+}$ as photosensitizer and $S_2O_8^{2-}$ as sacrificial electron acceptor; and electrochemical refers to a variety of electrochemically driven oxidation conditions, see the cited references for specific conditions.

As Chapter II details,[33] we initially attempted to synthesize **$Co_4V_2W_{18}$** according to literature procedures,[16,36] but immediately experienced issues pertaining to the purity of the material.[33] Hence, Chapter II of this dissertation is based upon our findings pertaining to the synthesis, purity and the ^{51}V nuclear magnetic resonance (NMR) spectrum of the as-synthesized "**$Co_4V_2W_{18}$**" material. Quotations were added for "**$Co_4V_2W_{18}$**" because the material obtained from the synthesis is shown in Chapter II to be both impure and hydrolytically unstable.[33] In fact, we

discovered that the ^{51}V NMR resonance at −510 ppm ($\Delta\nu_{1/2}$=28±7 Hz) previously assigned to **$Co_4V_2W_{18}$** and used as evidence of its hydrolytic stability, actually belongs to *cis*-$V_2W_4O_{19}^{4-}$, present as either an impurity from the synthesis or a decomposition side-product.[33] These findings were formatted for and published in the ACS journal *Inorganic Chemistry* (Folkman, S. J.; Kirner, J. T.; Finke, R. G. *Inorg. Chem.* **2016**, *55*, 5343–5355) of which the author of this dissertation, S. Folkman is the primary experimenter and author J. Kirner was added as an author because of his valuable contributions later in the manuscript writing.

Given that the initial studies claiming **$Co_4V_2W_{18}$** is a homogeneous WOCatalyst[16] were highly questionable after our aforementioned publication,[33] we sought to more fully understand the nature of the high observed WOCatalysis activity beginning with **$Co_4V_2W_{18}$**.[34] The origin of the WOCatalysis activity beginning with **$Co_4V_2W_{18}$** is the subject matter of Chapter III of this dissertation.[34] We conducted highly sensitive and selective Co^{2+} dissociation experiments and found that "**$Co_4V_2W_{18}$**" dissociates 102 ± 12% and 87± 18 % of the Co^{2+} in the complex after just 1 h in 0.1 M NaPi at pH 5.8 and 8.0 respectively, forming $Co(H_2O)_6^{2+}$ (hereafter Co^{2+}_{aq}). This is in stark contrast to the initial **$Co_4V_2W_{18}$** studies by others,[16] but are consistent with our findings that "**$Co_4V_2W_{18}$**" is impure and unstable.[33] We then conducted a series of electrocatalytic WOCatalysis experiments with the "**$Co_4V_2W_{18}$**" material and found that it indeed serves as a precursor to heterogeneous CoO_x formation, which quantitatively accounts for all of the observed WOCatalysis activity.[34] This manuscript was prepared for and published in the journal *ACS Catalysis* (Folkman, S. J.; Finke, R. G. *ACS Catal.* **2017**, *7*, 7–16.) where S. Folkman is again the primary experimenter and author. These two publications concluded our studies with **$Co_4V_2W_{18}$** in which we effectively demonstrated that **$Co_4V_2W_{18}$** is unstable in aqueous solutions, and serves as a precursor to electrode-bound heterogeneous CoO_x which is the true WOCatalyst under

electrochemically driven conditions. The greater observed WOCatalysis activity of **$Co_4V_2W_{18}$** than **$Co_4\underline{P}_2W_{18}$** is due to its greater instability and hence greater amount of Co^{2+}_{aq} present to form CoO_x.[34]

Next, we return to the survey of the other Co-POMs which constitutes Chapter IV of this dissertation.[35] Using Co^{2+}_{aq} detection techniques from previous studies[25,34] the amount of Co^{2+}_{aq} that is dissociated from each Co-POM in a given time frame (typically 3 h) was determined in NaPi at pH 5.8 and 8.0, as well as in sodium borate buffer (NaB) at pH 9.0. Free Co^{2+}_{aq} was detected in every case, with decomposition of the Co-POMs varying from 0.6 ± 0.6% (**α_1-CoP_2W_{17}** in 0.1 M NaPi pH 5.8) to 90 ± 10% (**$CoPW_{11}$** in 0.1 M NaB pH 9.0).[35] The more stable Co-POM complexes highlight the need for selective and sensitive methods focused on detecting decomposition byproducts, rather than trying to "prove" stability because most methods which directly observe the intact Co-POM would not have detected the 0.6% decomposition for **α_1-CoP_2W_{17}** in 0.1 M NaPi pH 5.8 herein. Electrochemical controls were then conducted to determine if CoO_x was formed and accounted for the observed WOCatalysis current. Indeed, CoO_x was formed on the electrode during controlled potential electrolysis and accounts for ≥100% of the observed current in 13 out of the 18 cases examined.[35] Under conditions where the Co-POMs are more stable (<2% decomposition), the evidence provided implies that some of the Co-POMs are homogeneous WOCatalyst. For example, when beginning with **α_1-CoP_2W_{17}** in 0.1 M NaPi at pH=5.8 the amount of $Co(II)_{aq}$ detected only accounts for 30±20 %, of the observed WOCatalysis activity, and no detectable film is formed from 30 min of electrolysis.[35] However, the equivalent amount of $Co(II)_{aq}$ that is leached into solution has a relative rate of at least 10x than that of the Co-POM and is usually 20-300x faster. In summary, this chapter provides a general methodology for distinguishing between homogeneous and heterogeneous WOCatalysis when beginning with

Co-POMs, and provides examples of both homogeneous WOCatalysis from the Co-POM starting material and heterogeneous WOCatalysis from CoO_x that is derived from the Co-POM starting material. These results have been formatted for and submitted to *Journal of American Chemical Society* (Folkman, S. J.; Soriano-Lopez, J.; Galán-Mascarós, J.R.; Finke, R. G. Electrochemically Driven Water-Oxidation Catalysis Beginning with Six Exemplary Cobalt Polyoxometalates: Is It Molecular, Homogeneous Catalysis or Electrode-Bound, Heterogeneous CoO_x Catalysis? Submitted to *JACS*, June 2018).[35]

Next, because all of these Co-POM and several other molecular precatalysts serve as precursors to a more stable, more active heterogeneous CoO_x we began research into WOCatalysis active cobalt-oxide nanoparticles. Spinel-phase Co_3O_4 is a well-known WOCatalyst material that has been used in a variety of water oxidation schemes.[37,38,39,40] The surface properties and catalytic mechanism of the Co_3O_4 nanoparticles are, however, poorly understood. In order to better understand the surface properties of spinel-phase Co_3O_4, we synthesized Co_3O_4 nanoparticles in various alcohols and water using cobalt acetate, O_2 as oxidant, and NH_4OH as base using a procedure adapted from literature methods.[37,41,42] Although our main interest in Co_3O_4 materials was initially for WOCatalysis, novel findings with regard to solvent effects on cobalt-oxide nanoparticle formation and other surface properties prompted us to pursue publication on the nanoparticle synthesis, characterization, and fundamental properties. These studies are the subject of Chapter V of this dissertation.[42] That manuscript demonstrates that the presence of alcohols such as ethanol (EtOH), *tert*-butanol (*t*-BuOH), and benzyl alcohol ($PhCH_2OH$) greatly affected the size, size distribution, and crystallinity of the cobalt-oxide nanoparticles when compared with syntheses in water alone, confirming prior literature observations.[37,41,42] FT-IR of the isolated particles, however, gave evidence of acetate (OAc^-) in the product. Digestion and quantitative ^1H

NMR then demonstrated OAc^- is present as a surface ligand but importantly and previously unknown with no detectable EtOH or *t*-BuOH in the product (~5% detection limit). The fact that the particles synthesized in alcohol have very different size and crystallinity properties than those synthesized in water, yet do not contain EtOH or *t*-BuOH, strongly suggests that the alcohols *kinetically affect the formation of the particles*, and are not thermodynamically contributing to the surface coverage via a covalent linkage to a RO^- moiety. These and other experiments along with the implications for the field of metal-oxide nanoparticle synthesis have are published in *Inorganic Chemistry* (Folkman, S. J.; Zhou, M.; Nicki, M.; Finke, R. G. *Inorg. Chem.* **2018**, *57* (3), 1517–1526.)[42] The initial studies of alcohol solvent effects on the size and crystallinity were conducted by Finke group postdoc M. Zhou along with graduate student M. Nicki. Eventually M. Zhou's postdoc with the Finke group ended and M. Nicki joined a different research group at CSU. S. Folkman finished the studies by synthesizing and characterizing the particles following M. Zhou's procedure, then developing the digestion and quantitative ^{1}H NMR experiments, and being the primary writer of the published manuscript with the main edits made by R. Finke the resultant dissertation chapter is Chapter V.[42]

The final chapter of this dissertation, Chapter VI, provides a summary and outlook from the main findings described in this thesis. The results from each chapter are combined with other literature to generate an overarching outlook for WOCatalysis beginning with molecular catalyst, and in particular Co-POMs.

REFERENCES

1 Turner, J. A. *Science* **1999**, *285*, 687–689.

2 Lewis, N. S.; Nocera, D. G. *PNAS* **2006**, *103*, 15729–15735.

3 Kärkäs, M.; Åkermark, B. *Dalton Trans.* **2016**.

4 Llobet, A. *Molecular Water Oxidation Catalysis*; 1 edition.; Wiley, **2014**.

5 Liu, F.; Concepcion, J. J.; Jurss, J. W.; Cardolaccia, T.; Templeton, J. L.; Meyer, T. J. *Inorg. Chem.* **2008**, *47*, 1727–1752.

6 Geletii, Y. V.; Botar, B.; Kögerler, P.; Hillesheim, D. A.; Musaev, D. G.; Hill, C. L. *Angew. Chem. Intl. Ed.* **2008**, *47*, 3896–3899.

7 Sartorel, A.; Carraro, M.; Scorrano, G.; Zorzi, R. D.; Geremia, S.; McDaniel, N. D.; Bernhard, S.; Bonchio, M *J. Am. Chem. Soc.* **2008**, *130*, 5006–5007.

8 Kanan, M. W.; Nocera, D. G. *Science* **2008**, *321*, 1072–1075.

9 Yin, Q.; Tan, J. M.; Besson, C.; Geletii, Y. V.; Musaev, D. G.; Kuznetsov, A. E.; Luo, Z.; Hardcastle, K. I.; Hill, C. L. *Science* **2010**, *328*, 342–345.

10 Huang, Z.; Luo, Z.; Geletii, Y. V.; Vickers, J. W.; Yin, Q.; Wu, D.; Hou, Y.; Ding, Y.; Song, J.; Musaev, D. G. *J. Am. Chem. Soc.* **2011**, *133*, 2068–2071.

11 Zhu, G.; Geletii, Y. V.; Kögerler, P.; Schilder, H.; Song, J.; Lense, S.; Zhao, C.; Hardcastle, K. I.; Musaev, D. G.; Hill, C. L. *Dalton Transactions* **2012**, *41*, 2084.

12 Zhu, G.; Glass, E. N.; Zhao, C.; Lv, H.; Vickers, J. W.; Geletii, Y. V.; Musaev, D. G.; Song, J.; Hill, C. L. *Dalton Trans.* **2012**, *41*, 13043–13049.

13 Goberna-Ferrón, S.; Vigara, L.; Soriano-López, J.; Galán-Mascarós, J. R *Inorg. Chem.* **2012**, *51*, 11707–11715.

14 Car, P.-E.; Guttentag, M.; Baldridge, K. K.; Alberto, R.; Patzke, G. R. *Green Chemistry* **2012**, *14*, 1680.

15 Evangelisti, F.; Car, P.-E.; Blacque, O.; Patzke, G. R. *Catalysis Science & Technology* **2013**, *3*, 3117.

16 Lv, H.; Song, J.; Geletii, Y. V.; Vickers, J. W.; Sumliner, J. M.; Musaev, D. G.; Kögerler, P.; Zhuk, P. F.; Bacsa, J.; Zhu, G. *J. Am. Chem. Soc.* **2014**, *136*, 9268–9271.

17 McCrory, C. C. L.; Jung, S.; Peters, J. C.; Jaramillo, T. F. *J. Am. Chem. Soc.* **2013**, *135*, 16977–16987.

18 Lide, D. R.; Haynes, W. M. *CRC Handbook of Chemistry and Physics*. 92nd ed. Taylor & Francis. **2012**.

18 Stracke, J. J.; Finke, R. G. *ACS Catal.* **2014**, *4*, 909–933.

20 Fukuzumi, S.; Hong, D. *Inorg. Chem.* **2014**, *2014*, 645–659.

21 Widegren, J. A.; Finke, R. G. *J. Mol. Catal. A: Chemical* **2003**, *198*, 317–341.

22 Pope, M. T. *Heteropoly and Isopoly Oxometalates*; Springer-Verlag, 1983.

23 Yamase, T.; Pope, M. *Polyoxometalate Chemistry for Nano-Composite Design*; Springer Science & Business Media, 2006.

24 Pope, M.; Muller, A. *Polyoxometalates: From Platonic Solids to Anti-Retroviral Activity: From Platonic Solids to Anti-Retroviral Activity*; Springer Science & Business Media, 1994.

25 Stracke, J. J.; Finke, R. G. *J. Am. Chem. Soc.* **2011**, *133*, 14872–14875.

26 Stracke, J. J.; Finke, R. G. *ACS Catal.* **2013**, *3*, 1209–1219.

27 Vickers, J. W.; Lv, H.; Sumliner, J. M.; Zhu, G.; Luo, Z.; Musaev, D. G.; Geletii, Y. V.; Hill, C. L. *J. Am. Chem. Soc.* **2013**, *135*, 14110–14118.

28 Stracke, J. J.; Finke, R. G. *ACS Catal.* **2014**, *4*, 79–89.

29 Vickers, J. W.; Sumliner, J. M.; Lv, H.; Morris, M.; Geletii, Y. V.; Hill, C. L. *Phys. Chem. Chem. Phys.* **2014**, *16*, 11942–11949.

30 Soriano-López, J.; Musaev, D. G.; Hill, C. L.; Galán-Mascarós, J. R.; Carbó, J. J.; Poblet, J. M. *J. Catal.* **2017**, *350*, 56–63.

31 Goberna-Ferrón, S.; Soriano-López, J.; Galán-Mascarós, J. R.; Nyman, M. *Eur. J. Inorg. Chem.* **2015**, *2015*, 2833–2840.

32 Soriano-López, J.; Goberna-Ferrón, S.; Vigara, L.; Carbó, J. J.; Poblet, J. M.; Galán-Mascarós, J. R. *Inorg. Chem.* **2013**, *52*, 4753–4755.

33 Folkman, S. J.; Kirner, J. T.; Finke, R. G. *Inorg. Chem.* **2016**, *55*, 5343–5355.

34 Folkman, S. J.; Finke, R. G. *ACS Catal.* **2017**, *7*, 7–16.

35 Folkman, S. J.; Soriano-Lopez, J.; Galán-Mascarós, J.R.; Finke, R. G. Submitted to *JACS*, June 2018

36 Li, B.; Yan, Y.; Li, F.; Xu, L.; Bi, L.; Wu, L. *Inorg. Chim. Acta* **2009**, *362*, 2796–2801.

37 Grzelczak, M.; Zhang, J.; Pfrommer, J.; Hartmann, J.; Driess, M.; Antonietti, M.; Wang, X. *ACS Catal.* **2013**, *3*, 383–388.

38 Wei, P.; Hu, B.; Zhou, L.; Su, T.; Na, Y. *J Ener Chem* **2016**, *25*, 345–348.

39 Chou, N. H.; Ross, P. N.; Bell, A. T.; Tilley, T. D. *ChemSusChem* **2011**, *4*, 1566–1569.

40 Shi, N.; Cheng, W.; Zhou, H.; Fan, T.; Niederberger, M. *Chem. Commun.* **2014**, *51*, 1338–1340.

41 Dong, Y.; He, K.; Yin, L.; Zhang, A. *Nanotechnology* **2007**, *18*, 435602.

42 Folkman, S. J.; Zhou, M.; Nicki, M.; Finke, R. G. *Inorg. Chem.* **2018**, *57* (3), 1517–1526.

II. COBALT POLYOXOMETALATE $Co_4V_2W_{18}O_{68}^{10-}$: A CRITICAL INVESTIGATION OF ITS SYNTHESIS, PURITY, AND OBSERVED ^{51}V QUADRUPOLAR NMR[i]

Overview

The vanadium-containing cobalt polyoxometalate (Co-POM), $Co_4V_2W_{18}O_{68}^{10-}$ (hereafter **$Co_4V_2W_{18}$)** has been reported to be a stable, homogeneous water-oxidation catalyst, one with a claimed record turnover frequency that is also reportedly 200-fold faster than its phosphorous congener, $Co_4P_2W_{18}O_{68}^{10-}$. The claimed superior water-oxidation catalysis activity of the vanadium congener, **$Co_4V_2W_{18}$**, rests squarely on the reported synthesis of **$Co_4V_2W_{18}$**, its purity, and its stability in both the solid-state and in solution. Attempts to repeat the preparation of **$Co_4V_2W_{18}$** by either of two literature syntheses, along with the other studies reported herein, led to the discovery of multiple, convoluted problems in the prior literature of **$Co_4V_2W_{18}$**. The three most serious of those problems proved to be the prior misunderstanding of the quadrupolar (herein ^{51}V) NMR peak widths in complexes that also contain paramagnetic metals such as Co(II), the incorrect assignment of a −506.8 ppm ^{51}V NMR to **$Co_4V_2W_{18}$**, and then the use of that −506.8 peak to argue for the stability of **$Co_4V_2W_{18}$** in solution. The results are reported in a somewhat

[i] Our initial goal was to study the hydrolytic stability and catalytic properties of the purported homogeneous water oxidation catalyst $Co_4V_2W_{18}O_{68}^{10-}$. However, attempts to synthesize $Co_4V_2W_{18}O_{68}^{10-}$ led to the discovery of several issues regarding the synthesis, purity and ^{51}V NMR of "$Co_4V_2W_{18}O_{68}^{10-}$." Hence, in order to study the stability and catalytic properties of $Co_4V_2W_{18}O_{68}^{10-}$ we were forced to take a step back and more fully understand the fundamental properties of the "$Co_4V_2W_{18}O_{68}^{10-}$" material obtained from literature syntheses .This dissertation chapter contains the entire published manuscript describing our first published work with $Co_4V_2W_{18}O_{68}^{10-}$ and highlights the variable nature of the synthesis, the impurity of the material obtained, the incorrectly assigned ^{51}V NMR peak, and other factors that complicate studies with $Co_4V_2W_{18}O_{68}^{10-}$ (Folkman, S. J.; Kirner, J. T.; Finke, R. G. *Inorg. Chem.* **2016**, *55*, 5343–5355.). Minor formatting edits have been introduced to meet the dissertation requirements. For example, the figure and table numbers have been changed to reflect the dissertation chapter, and the Supporting Information has been moved to Appendix I.

historical, "story" fashion en route to elucidating and fully supporting the 11 insights and take-home messages listed in the Summary and Conclusions section.

2.1 Introduction

The cobalt polyoxometalate (Co-POM), $Co_4V_2W_{18}O_{68}^{10-}$ (hereafter **$Co_4V_2W_{18}$**, Figure 2.1) was reported in a 2014 *J. Am. Chem. Soc.* communication to be an "oxidatively and thermally stable, homogeneous water oxidation catalyst,"[1] one with a turnover frequency (TOF) > 1 x 10^3 s^{-1}, hence ~200-fold faster than its better-known[2,3] phosphorous-based analogue, $Co_4P_2W_{18}O_{68}^{10-}$ (hereafter **$Co_4P_2W_{18}$**).[4,5]

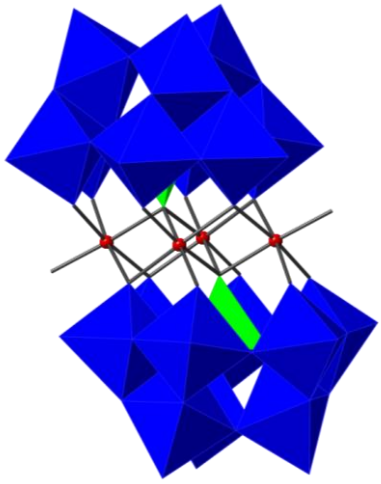

Figure 2.1. Structure of **$Co_4V_2W_{18}$** established by two single-crystal X-ray diffraction structural studies.[1,5] Blue octahedra represent WO_6, green tetrahedra VO_4, and red spheres indicate cobalt.

The reported purity and stability of **$Co_4V_2W_{18}$** deserve special scrutiny in light of the discovery that the **$Co_4P_2W_{18}$** analogue slowly decomposes in solution, resulting in heterogeneous CoO_x as the true water oxidation catalyst (WOCatalyst) under electrochemically driven conditions.[6,7] Specifically, a 2011 report[6] demonstrated that 500 μM **$Co_4P_2W_{18}$** decomposes by 4.3 ± 0.6% after 3 h in pH 8.0 sodium phosphate buffer (0.1 M) releasing 58 ± 2 μM $Co(II)_{aq}$ into

solution. Under electrochemically driven catalysis, that released $Co(II)_{aq}$ forms electrode-bound CoO_x, that then accounts for *all* (100 ± 12%) of the observed, electrochemically driven WOC.

The dissociation of Co(II) from **$Co_4P_2W_{18}$** or analogous POMs comes as no surprise, as the POM is just a ligand, with Co(II) dissociation constants from Co-POMs often in the micromolar range.[6,7] Hence, the type of absolute hydrolytic stability needed for truly sustained, $\geq 10^9$ total turnovers[8] of WOC by molecular Co-POM complexes is, in general, not expected *nor precedented*.[7] The claimed purity and stability of **$Co_4V_2W_{18}$** are, therefore, of special importance and interest in the field of all-inorganic, potentially robust, putatively molecular POM WOC.

The Two Literature Syntheses of $Co_4V_2W_{18}$[1, 5]

The synthesis of **$Co_4V_2W_{18}$** was originally[5] reported in 2009, and slightly modified in 2014 as part of those WOC studies.[1] The syntheses used in both the original[5] and the 2014 studies[1] rely upon self-assembly of **$Co_4V_2W_{18}$** from the corresponding Co^{2+}, VO_4^{3-} and WO_4^{2-} salts in sodium acetate buffer at pH 4.8 (Scheme 2.1). Although self-assembly of POMs from the corresponding sodium or nitrate salts is a common practice,[9] the desired POM is often just one of multiple products produced by self-assembly. A relevant case in point is **$Co_4P_2W_{18}$**,[2,10,11] where the self-assembly synthesis from Co^{2+}, PO_4^{3-} and WO_4^{2-} produce the side product[12] $[Co_9(OH)_3(H_2O)_6(HPO_4)_2(PW_9O_{34})_3]^{16-}$,[11] one that can be avoided by the more convergent synthesis beginning with the lacunary Keggin ion synthon, β-$PW_9O_{34}^{9-}$.[13] Hence if a POM synthesis relies upon self-assembly, then one should expect to obtain a mixture of species that will then need to be separated in either the workup, or more likely by crystallization (and probably recrystallization) step(s).

Synthesis #1: The Original Synthesis of $Na_{10}[Co_4(H_2O)_2(VW_9O_{34})_2]\cdot 30H_2O$

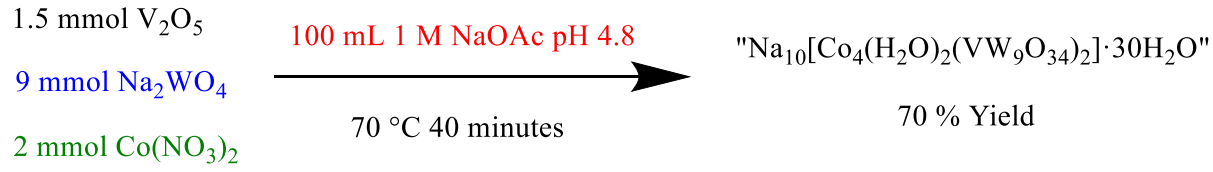

Synthesis #2: The 2014 Synthesis of $Na_{10}[Co_4(H_2O)_2(VW_9O_{34})_2]\cdot 35H_2O$

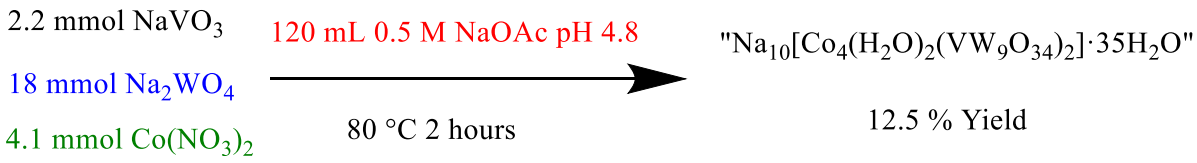

Scheme 2.1. Outline of Synthesis #1, the Original[5] Synthesis of $Na_{10}[Co_4(H_2O)_2V_2W_{18}O_{68}]$ and Synthesis #2, the Synthesis of $Na_{10}[Co_4(H_2O)_2V_2W_{18}O_{68}]$ employed as part of the 2014 WOC studies.[1] The similarities are highlighted in green, blue, and red for the respective $Co(NO_3)_2$ reactant, Na_2WO_4 reactant, and buffer conditions. The "**$Co_4V_2W_{18}$**" products are shown in quotes to indicate that there are issues in the purity and hence absolute identity of the isolated, brown product as detailed in what follows.

Both the original[5] synthesis and the 2014[1] synthesis for **$Co_4V_2W_{18}$** follow very similar procedures, heating the dissolved reactants in approximately stoichiometric ratios for the desired product (except for the original synthesis[5] which uses a 3-fold excess of V), then collecting a brown, microcrystalline product from solution after evaporation over a variable, 1–2 week period. Despite the similar procedures, the original[5] synthesis reports a 70% yield based on tungsten, whereas the 2014[1] synthesis obtained only a 12% yield (without comment or explanation for the nearly 1/6th yield). Because neither synthesis uses a recrystallization purification step or reports removing any other products, the significantly different yields must occur during the crystallization step (neither synthesis reports the exact time, glassware type, temperature, nor other conditions that likely affect the crystallization step and which would make it reproducible in other's hands).

An additional point here is that, especially for a 12% yield where the rest of the mass is unaccounted for, one's working assumption should be that the first crystals observed and collected

are the least soluble species (and / or what nucleates and grows the fastest), and *hence not necessarily representative of the dominant species in the bulk solution*. Furthermore, because the solution composition will be changing as evaporation and precipitation proceed, the composition of the precipitating product(s) may also change over the duration of the crystallization. Hence, the first issue we ran into is the prior assumption[1,5] of purity of "**$Co_4V_2W_{18}$**" in the brown, as-prepared, solid-state product. Accordingly, we necessarily address the issue of the purity of the brown **$Co_4V_2W_{18}$** solid-state product in the next section even though our main interests are the purity, stability, and speciation of **$Co_4V_2W_{18}$** in solution. In all the sections which follow we will strive to be detailed and as rigorous as possible, even if it unavoidably adds some length to the paper, as corrections of the literature demand that level of detail and rigor.

A Look at the Literature Evidence for the Purity of the Brown, $Co_4V_2W_{18}$ Product

Single Crystal X-Ray Diffraction Structure. Both of the two separate literature syntheses contained single crystal, X-ray diffraction structural studies of the $Cation_{10}[Co_4V_2W_{18}O_{68}]\cdot xH_2O$ product (cation = Na^+ or K^+; x = variable hydrates of 30 to 35).[1, 5] The R value for the single crystal refinement of the K^+ salt was noted to have one of the lowest ever reported for a polyoxometalate.[1] A look at these two, independent X-ray diffraction structural studies leaves little doubt as to the existence of **$Co_4V_2W_{18}$** in the *solid state*, and when obtained in *single-crystal form*.[1,5] The evidence for (or against) the purity of the *bulk*, brown **$Co_4V_2W_{18}$** product is, however, another issue, *vide infra*.

Elemental Analysis Data. Just looking at the elemental analyses for the original[5] and modified 2014[1] syntheses of **$Co_4V_2W_{18}$** (summarized in Table 2.1) reveals that *neither of the elemental analyses reported for either of the two literature syntheses yield a publishable, ≤0.4 absolute wt % standard error* vs the expected percentage for each element of **$Co_4V_2W_{18}$**. The

absolute differences in tungsten range from 0.79 to 1.56 wt % high; suggesting that the bulk product is actually not analytically pure **$Co_4V_2W_{18}$**, but rather a composite mixture consisting of **$Co_4V_2W_{18}$** plus unknown impurities. In addition, on the basis of our work to be presented in the sections which follow, we know that at least sodium acetate (NaOAc) is one impurity present in both the literature and our repeats of these syntheses (e.g., a FT-IR peak for NaOAc at ca. 1600 cm^{-1} is observed in *each* of our repeat syntheses of **$Co_4V_2W_{18}$**, Figure S2.1, Table 2.2).[14] Noteworthy in this context is that a carbon analysis that would have detected the NaOAc was not conducted for either of the two syntheses.

Table 2.1. A Comparison of the Elemental Analysis Results for the Two Literature Syntheses of $Co_4V_2W_{18}$.[a]

Synthesis	*Element*	*Calculated wt %*	*Found wt %*	*Difference*
The original synthesis[5]	Co	4.25	4.31	0.06
	W	59.72	60.51	**0.79**
	V	1.84	1.85	0.01
	Na	4.15	4.20	0.05
Synthesis in the 2014 Report [1]	Co	4.21	4.09	−0.12
	W	59.14	60.7	**1.56**
	V	1.82	1.80	−0.02

[a] Differences > ± 0.4 wt % are shown in bold.

FT-IR Data. As further evidence for the presence of impurities in the bulk solid, the FT-IR peaks reported for the original[5] and 2014[1] syntheses are compiled for a comparison in Table 2.2. The data reveal that the FT-IR peak absorbances are not completely reproducible, with peaks shifted somewhat randomly, as much as 3 cm^{-1} higher and 7 cm^{-1} lower peak absorbances for the 2014 synthesis compared to the original (and beyond the estimated instrument error of 1 cm^{-1} in any given band); note that the lack of a systematic shift of the peaks indicates the absence of a systematic error in the positions of the IR peaks. Furthermore, the FT-IR peaks are generally quite

broad, appearing more as bands (Figure S-2 of the original[5] study, Figure S-3 of the 2014[1] study, Figure S2.1 herein) which, therefore, can hide impurity peaks rather easily. In short, inconsistencies in the FT-IR spectra obtained for the two syntheses of **$Co_4V_2W_{18}$**, as well as the broadened, diffuse nature of the observed peaks (bands) and IR evidence for the presence of NaOAc support the elemental analysis results that impurities are present in the brown, solid samples of "**$Co_4V_2W_{18}$**".

Table 2.2. A Comparison of the FT-IR Peaks Reported in the 2014[1] and Original[5] Studies for $Co_4V_2W_{18}$**.**

original[5] synthesis (reported peaks) [a]	2014[1] synthesis (reported peaks)[b]
ca. 3500(br), 1600(s), 958(m), 883(s), 825(s), 757(sh), 698(s), 488(m)	960(m), 882(s), 818(s), 760(sh), 694(s), 513(sh), 485(m)

[a] Peaks shown in red were not reported, yet are readily observable in the Supporting Information of that paper. Peak descriptors were not given in the original paper,[5] so they have been provided where possible as part of the present reinvestigation.
[b] Peak descriptors were given in the Supporting Information of the 2014 paper (m = medium; s = strong; sh = shoulder; br = broad).[1] The spectrum was cut off at 1200 cm^{-1}, so the presence or absence of NaOAc (1600 cm^{1-}) cannot be rigorously demonstrated.

In short, the available data demonstrate that the implied 100% purity, and reported formulas of $Na_{10}[Co_4(H_2O)_2V_2W_{18}O_{68}]\cdot 30H_2O$ for the original[5] and $Na_{10}[Co_4(H_2O)_2V_2W_{18}O_{68}]\cdot 35H_2O$ for the 2014[1] studies, are not completely correct descriptions of the brown, bulk solid products obtained in highly variable yields of 12-70%.

UV-Visible Data in Aqueous Solution. The UV–visible spectrum of "**$Co_4V_2W_{18}$**" in aqueous solution caught our eye early on in this work, especially when compared to its structural analog, **$Co_4P_2W_{18}$**, (Figure S-5 of that study,[1] Figure S2.2 of the current studies), a Co-POM we are quite familiar with because we reported its rational synthesis in 1987.[3] Specifically, the **$Co_4P_2W_{18}$** polyoxoanion is purple in aqueous solution with a cobalt-based d–d absorption[15,16] around 580 nm, whereas the "**$Co_4V_2W_{18}$**" is brown in water while displaying only a poorly

resolved shoulder in the expected d–d range (Figure S2.2). As first suggested by the authors of the 2014 study,[1] it is likely that a ligand-to-metal charge transfer (LMCT) band for V(V) in oxo-ligation extends into the visible, a phenomenon that is well precedented and depends on the ligands and coordination environment of the V atom of interest.[17,18,19] The LMCT of V(V)–O could then obscure the d–d of "**$Co_4V_2W_{18}$**" and other cobalt-containing species. However, the elemental analysis and the FT-IR of the solid material already discussed imply that the UV–vis is likely a convolution of at least several hitherto unidentified species—a prediction with compelling, supporting evidence provided by our reexamination of the ^{51}V NMR of "**$Co_4V_2W_{18}$**" solutions, *vide infra*. Hence, the ≤2% decrease in absorbance in the UV–vis reported for "**$Co_4V_2W_{18}$**" is not sufficient, and certainly not compelling, direct evidence for the stability of **$Co_4V_2W_{18}$** in aqueous solution.

Mass Spectrometry Data of the TBA^+ Salt in Acetonitrile. Mass spectrometry was also used to examine the **$Co_4V_2W_{18}$** product of the 2014 synthesis. Although mass spectrometry can be a powerful method in POM chemistry, a careful examination of the mass spectrometry reported[1] reveals five issues and associated problems. Those issues and problems render the MS results non-definitive—and certainly unable to demonstrate the purity (nor to definitively detect impurities) of the as-prepared **$Co_4V_2W_{18}$**—as discussed in detail in the SI for the interested reader. We also have provided our own MS studies of "**$Co_4V_2W_{18}$**"; those, too, proved non-definitive—and certainly unable to demonstrate the purity (nor to definitively detect impurities) of the as prepared **$Co_4V_2W_{18}$**—as discussed in the Supporting Information for the interested reader (Figures S2.3 and S2.4).

^{51}V NMR Data in Aqueous Solution. The 2014 report states that the "^{51}V NMR spectra of [**$Co_4V_2W_{18}$**] in D_2O or in borate buffer at pH 9.0 exhibit only one peak at −506.8 ppm"[1]. That

single resonance for bulk, redissolved **"$Co_4V_2W_{18}$"** was assigned[1] to the pseudotetrahedral ^{51}V atom within the center of the lacunary Keggin unit[1,5] of **$Co_4V_2W_{18}$** (Figure 2.1). The 2014 report further states that "no changes [in the ^{51}V NMR] were noticed over a period of one month", and that "heating the NMR sample to 80 °C followed by cooling to room temperature gives the same ^{51}V NMR spectrum (same chemical shift and line width), confirming the stability of [**$Co_4V_2W_{18}$**]."[1]

Hereafter we will refer to the −506.8 ppm resonance as −507 ppm ($\Delta\nu_{1/2}$=30.5 Hz), because the error in the chemical shift of the "−506.8 ppm" resonance will prove to be at least an order of magnitude greater than the ±0.05 ppm implied by the inclusion of the right-most, fourth significant figure (−506.**8**) in the literature report.[1] In what follows we will reproducibly observe this main resonance at −510±0.5 ppm, *vide infra*.

The Focus of the Present Studies

Herein, we first attempted to synthesize **$Co_4V_2W_{18}$** three times according to the synthesis outlined in the 2014[1] study; we also repeated the synthesis outlined in the original[5] report of **$Co_4V_2W_{18}$**. As will be detailed in what follows, we immediately ran into concerns about the purity of the sample after collecting ^{51}V NMR with good signal-to-noise, revealing more than one resonance and, therefore, indicating impurities in the brown product obtained. Purification of the material to 99% purity based on the primary resonance at −510 ppm ($\Delta\nu_{1/2}$=28±7 Hz) led to two additional, unexpected, but important observations not previously reported:[1,5] (i) the color of the "purified" product changed from brown *to green*; and (ii) elemental analysis of the "purified" material revealed a very low Co analysis—<1 equiv of Co compared to the 4 expected Co for **$Co_4V_2W_{18}$**! This in turn led us to critically reexamine the two literature syntheses of **$Co_4V_2W_{18}$**, the reported ^{51}V NMR assignments and expected vs observed line widths. Those and other studies

eventually allowed us to deconvolute multiple errors in the prior work that are detailed in what follows.

2.2 Results and Discussion

Repeats of the Previous $Co_4V_2W_{18}$ Syntheses and Attempted Isolation of a "Purified" Material

We repeated the synthesis for **$Co_4V_2W_{18}$** according to the 2014[1] study as closely as possible from the written procedure three times (hereafter syntheses 2A, 2B and 2C). We also repeated the original[5] synthesis (hereafter 1A, see Experimental for details). We collected ^{51}V NMR (Figure S2.5), FT-IR (Figure S2.1), and elemental analysis on the products and compiled a table comparing the yield and spectra of each synthesis, presented in Table 2.3.

From a look at the compiled data in Table 2.3 for the syntheses 1A, 2A, 2B, and 2C, it is clear that the syntheses of "**$Co_4V_2W_{18}$**"are irreproducible for five identifiable reasons, specifically (i) the crystallization time required to observe and obtain the brown microcrystalline product ranges from 11 to 31 days, depending on if a Kimwipe or a watch glass is used to cover the solution (to prevent contamination with dust rather than slow down the evaporation, see the Experimental Section for more details); (ii) the highly variable yield ranges from 8.3 to 46%, no doubt at least in part due to the details of the slow evaporation and associated variable crystallization time; (iii) the "purity" based on ^{51}V NMR ranges from 88 to 97%—a "purity" that will prove to be the purity of *cis*-$V_2W_4O_{19}^{4-}$ as what is actually being detected, not the"**$Co_4V_2W_{18}$**" purity, *vide infra*; (iv) the FT-IR peak maxima are not reproducible; and (v) the elemental analysis of the products varies as much as 4 wt % for tungsten (all tungsten analyses we obtained proving to be systematically low).

Table 2.3. Comparison of the Four Repeat Syntheses and the Preparation of the "Purified" Material

sample number	*evaporation time* [A]	*yield*[b] *(g)*	*yield*[c] *(%)*	*^{51}V NMR*[d] *δ (ppm), $\Delta\nu_{1/2}$ (Hz), (%)*	*FT-IR*[e] *(cm^{-1})*	*elemental*[f] *(%)*
1A	12 days	0.476	8.3	−510, *41* (97) −525, *N.O.* (3)	3400(br), 1620(d), 1405(s), 955, 881, 818, 761, 695, 511, 484	**Co: 3.51** **W: 61.6** V: 1.6 2 **Na: 4.88**
2A	31 days	0.55	9.9	−510, *23* (88) −559, *69* (12)	3400(br), 1620(d), 1400(d), 951, 879, 810, 752, 694, *N.O.*, 469	**Co: 5.05** **W: 54.0** V: 1.88 Na:4.89 **C: 0.55**
2B	13 days	2.55	45.9	−510, *19* (90) −559, *N.O.* (10)	3400(br), 1620(s), 1411(w), 959, 885, 820, 749, 688, *N.O.*, 485,	not conducted
2C	11 days	1.04	18.7	−510, *22* (95) −559, *86* (5)	3400(br), 1620(d), 1405(s), 954, 882, 812, 761, 693, 512, 491	**Co: 4.95** **W: 55.8** V: 1.83 **Na: 5.83**
"purified"	N/A	1.39	–	−510, *28* (99) −517, *N.O.* (0.4) −525, *35* (0.6)	3400(br), 1620(d), 1400(d), 932, 880, 833, *N.O.*, 693, *N.O.*, 485	**Co: 1.00** **W: 52.9** V: 1.80 **Na: 9.56**

[a] A significant amount of brown crystals had visibly accumulated in the beaker used for the slow evaporation at the indicated times. [b] The yield is the mass of the material obtained after drying as described in the Experimental Section.[c] The percent yield is calculated based on tungsten and assuming the empirical formula $Na_{10}[Co_4V_2W_{18}O_{68}]\cdot 26H_2O$ (the number of hydrates determined for 2A from TGA), except for 1A, in which 37 H_2O are used (the number of hydrates determined by TGA for 1A; see the Experimental Section for more details).[d] The ^{51}V NMR resonances observed for the freshly synthesized and freshly dissolved material (5 mg in 1 mL of unbuffered 10% D_2O at room temperature). The peaks are the instrument readings relative to $VOCl_3$ (calculated from the D_2O lock) in ppm; the peak widths are reported in *italics* in Hz (see the Experimental Section for more details); *N.O.* (not observed) is used where the signal-to-noise was too low for accurate determination. The integration is shown in parentheses (the total integration was set to 100).[e] FT-IR peaks of the material obtained, 2 wt % in KBr. Peak descriptors are provided where appropriate, and are not given when the peaks were not well resolved. *N.O* is used for peaks that were observed in the 2014[1] or original[8] syntheses, but not observed herein. br = broad, d = doublet, w= weak, and s = strong. [f] Elemental analysis obtained from Galbraith Laboratories. Differences of greater than 0.4 wt % error are reported in **bold**. The calculated (theoretical) elemental analysis values for each complex are given in the Experimental Section.

At this point, ^{51}V NMR *appeared* to be the most direct and certainly the most convenient spectroscopic handle for following the synthesis. Hence, next we attempted to purify the material, mainly by changing the buffer concentration and filtering off a brown precipitate, while using ^{51}V NMR to monitor the "purity" of the sample judged by the amount of the −510 ppm resonance vs other signals observed. Doing so yielded a *green*, rather than a brown, powder, as further detailed in the Experimental Section—a material that exhibited a *ca.* 99% purity by ^{51}V NMR (Figure S6 and Table 3), pleasingly at the time (but highly misleadingly as we will see) implying that we had isolated "pure **$Co_4V_2W_{18}$**." *However*, elemental analysis on the green product revealed it contained only 1 wt % cobalt, not the expected 4.3 wt % calculated for the full molecular formula of **$Co_4V_2W_{18}$**. Restated, whatever we isolated and is 99% pure according to ^{51}V NMR contained <1 equiv of Co (Table 2.3) and, hence, is not pure **$Co_4V_2W_{18}$** which contains four Co ions. Interestingly, this "purified" material has an IR spectrum that is practically indistinguishable from the as-isolated, brown "**$Co_4V_2W_{18}$**" material (Figure S2.1).

Another strange observation at the time was that, for the freshly prepared brown material from any of the syntheses 2A, 2B, or 2C, the −510 ppm resonance is readily observable immediately upon dissolution (Figure S2.5), but that main resonance was no longer observable for freshly dissolved solid material that had been stored (aged) for at least five months. Rather, the −510 ppm peak reappeared in the ≥5 month aged material only after aging in solution for greater than 30 min, Figure 2.2—observations that remain poorly understood. Clearly, something was amiss with the claimed stability of "**$Co_4V_2W_{18}$**" and perhaps also with its ^{51}V NMR assignment.

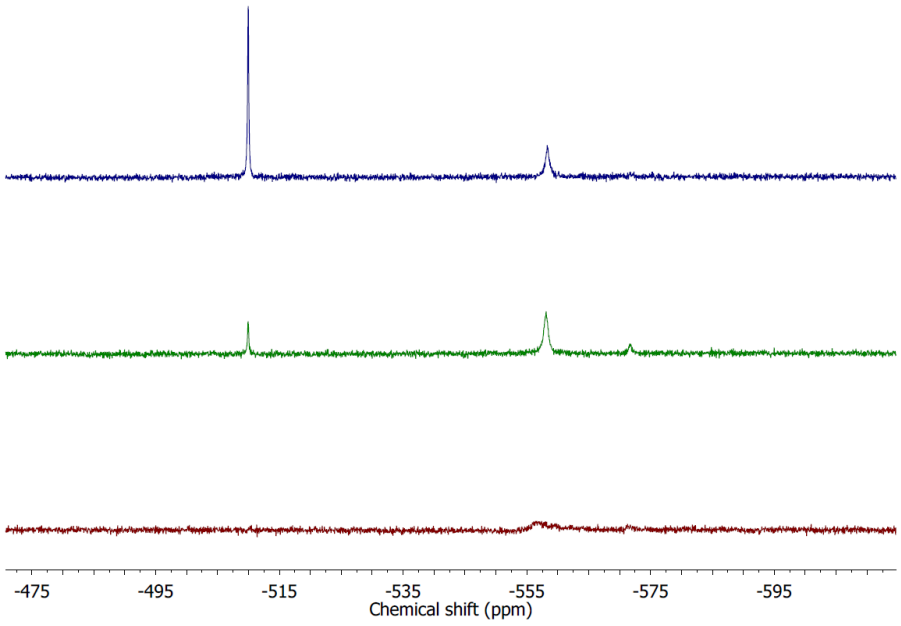

Figure 2.2. Absolute intensities of ^{51}V NMR spectra of the material obtained following the 2014[1] synthesis, 2A, from t = 2, 30, and 60 min following dissolution, from bottom to top. This material had aged approximately five months as a solid prior to dissolution and acquisition of the spectra shown. Spectra were collected on a *ca.* 5 mM aqueous solution (with ~10% D_2O) "**$Co_4V_2W_{18}$**" at room temperature. This experiment demonstrates that the −510 ppm ($\Delta\nu_{1/2}$=28±7 Hz) resonance is absent when aged "**$Co_4V_2W_{18}$**" is freshly dissolved in solution. At the minimum, these experiments by themselves cast considerable doubt on both the assignment of the ^{51}V NMR main peak at −510 ppm ($\Delta\nu_{1/2}$=28±7 Hz) to authentic **$Co_4V_2W_{18}$** as well as doubt on the stability of **$Co_4V_2W_{18}$**, apparently even in the solid-state as its hydrate.

Taking the above observations and phenomena together, we decided to take a step back and reexamine the ^{51}V NMR assignments made in the 2014 study.[1]

A Critical Re-evaluation of the ^{51}V NMR of $Co_4V_2W_{18}$

The Relevant Literature on NMR Peak Widths of Quadrupolar and Paramagnetic Molecules. Upon reviewing the literature, the assignment[1] of the −507 ppm ($\Delta\nu_{1/2}$=30.5 Hz) ^{51}V NMR peak concerned us for four reasons. First, (i) because ^{51}V is a quadrupolar nucleus, ^{51}V NMR line widths are inherently broad.[20,21] The resonance and corresponding line width of quadrupolar nuclei are highly sensitive to electric field gradients and therefore coordination geometry.[20,21] For example, for a pseudo-tetrahedral site within a polyoxovanadate (as are the sites in **$Co_4V_2W_{18}$**) the

narrowest ^{51}V NMR line we could find in the prior literature is *ca.* 60 Hz for $V_4O_{12}^{4-}$.[20] Only octahedral and pseudo-octahedral V sites display narrower line widths, the lowest value we found being 1.4 Hz for [V(CO_6)].[20] Indeed, for vanadium in a pseudo-octahedral symmetry, the vanadotungstate, *cis*-$V_2W_4O_{19}^{4-}$ has a peak width ranging from *23 to 42 Hz*, depending on the precise conditions (i.e. pH, counterion, solvent, and temperature), *within experimental error of that observed in the prior work ($\Delta\nu_{1/2}$=30.5 Hz)*[1] *or with error bars based on the present work ($\Delta\nu_{1/2}$=28±7 Hz)*[22,23] Moreover (ii), **$Co_4V_2W_{18}$** has a molar mass of approximately 5000 AMU and therefore should experience relatively slow tumbling in solution and, hence, at least some NMR line broadening as a result of a shorter T_1 (longitudinal relaxation time).[21] Just these two factors together suggest that the assignment of the reported[1] line with width 30.5 Hz to **$Co_4V_2W_{18}$** cannot be correct—even *before* considering the major line width broadening effects of paramagnetic Co(II), *vide infra*.

Additionally and compellingly, (iii) paramagnetic centers, such as Co(II) with its d^7 electron configuration, are known to cause substantial NMR line broadening due to the fluctuating magnetic field generated by the unpaired electron spins that align with the external magnetic field.[24,25] This fluctuation shortens T_1 and typically increases the peak width in a linear fashion with respect to the correlation time which is dominated by the electron spin relaxation.[24,25] Hence, one would expect *a severely broadened*—most likely broadened beyond detection—^{51}V NMR peak for **$Co_4V_2W_{18}$** due to the four ferromagnetically coupled[1,26] Co(II) centers.

Indeed and in fact, there are only a few examples in the literature of NMR studies on POMs containing paramagnetic nuclei.[3,4,27,28] For the case of non-quadrupolar, spin one-half ^{31}P NMR of POMs containing PO_4^{3-} as a reference point, the ^{31}P NMR line width in α_1-[(H_2O)Co(II)$P_2W_{17}O_{61}$]$^{8-}$ is *ca.* 103 Hz. Hence, the peak is *over 100-fold broadened* compared

to the diamagnetic Zn-substituted analog, which has a line width of <1.0 Hz.[27] For the structurally more relevant case of paramagnetic $Co_4P_2W_{18}O_{68}^{10-}$ and its diamagnetic Zn(II)-containing $Zn_4P_2W_{18}O_{68}^{10-}$ analogue, the ^{31}P NMR line widths are 337 and 2.6 Hz, respectively, as observed herein (see the Supporting Information and the Experimental Section if additional details are required). Hence, in the structurally similar (to $Co_4\mathbf{V}_2W_{18}O_{68}^{10-}$) case of $Co_4P_2W_{18}O_{68}^{10-}$, the *paramagnetic Co(II) broadens the ^{31}P NMR by a factor of ~130* relative to the Zn(II) analogue. A similar broadening of the ^{51}V line, far beyond the observed 30.5 Hz, is expected for the true resonance for **$Co_4V_2W_{18}$**. The caveat here is that the effect of Co(II)-induced NMR line broadening in isotropic, spin 1/2 ^{31}P has the potential to be quite different than anisotropic, quadrupolar, spin 7/2 ^{51}V due to the different relaxation modes for each.[21] Nevertheless, line *narrowing* is not expected quantum mechanically, nor has it ever been observed to our knowledge. The presence of paramagnetic species invariably causes more rapid nuclear spin relaxation, in turn increasing peak width[21,24,25]—in the present case far beyond the reported 30.5 Hz.[1]

Finally (iv) *there is very limited literature precedence for ^{51}V (quadrupolar) NMR of compounds containing paramagnetic ions such as Co(II).* Extensive literature searches that we conducted, for solution-based ^{51}V NMR of compounds containing a paramagnetic ion, yielded only three cases: $Na_{10}[Mn_4(H_2O)_2(VW_9O_{34})_2]$ (hereafter **$Mn_4V_2W_{18}$**),[29] $Na_{17}[(Co(H_2O)Co_2VW_9O_{34})_2(VW_6O_{26})]$ (hereafter **$Co_6V_3W_{24}$**),[30] and the **$Co_4V_2W_{18}$**[1] molecule studied herein, all studies from the same research group, all within the last three years.[1,29,30] The one other independent report[31] we could find for ^{51}V NMR on a sample that also contains paramagnetic Co(II) is the *solid state* ^{51}V NMR of a single crystal of $Co_3V_2O_8$. *The ^{51}V NMR peaks observed therein have a $\Delta\nu_{1/2}\geq$500,000 Hz (*estimated from the figures therein),[31] fully consistent with the above arguments and literature suggesting that ^{51}V NMR lines for Co-

containing vanadium compounds should be quite broad. In short, a careful analysis of the literature of ^{51}V NMR and the NMR of paramagnetic molecules lead to our hypothesis that the prior assignment, of a −507 ppm ($\Delta\nu_{1/2}$=30.5 Hz)[1] ^{51}V NMR peak to **Co$_4$V$_2$W$_{18}$** must be incorrect.

^{51}V NMR of Product from a Control Synthesis Performed without Co(NO$_3$)$_2$. We then designed and performed what proved to be a very telling experiment. Given the discussion on ^{51}V NMR line widths above, one would expect that the chemical species responsible for the observed ^{51}V NMR signal of solutions beginning with "**Co$_4$V$_2$W$_{18}$**" does not actually contain Co(II)—and, hence, might still be observed in a synthesis that repeated the 2014 preparation of "**Co$_4$V$_2$W$_{18}$**", *but in which we deliberately left out the Co(II)*. Therefore, the 2014 synthesis of "**Co$_4$V$_2$W$_{18}$**" was repeated precisely as written, except that the 4 equiv of $Co(NO_3)_2$ were omitted, so that no products containing cobalt (such as **Co$_4$V$_2$W$_{18}$**) could possibly be formed. As the ^{51}V NMR spectra in Figure 2.3 show, *the identical −510±0.5 ppm, relatively narrow ($\Delta\nu_{1/2}$= 28±7 Hz peak width), resonance is seen in this control synthesis as is seen in Syntheses #1 and #2.* The results provide compelling, *prima facie* evidence that the assignment of the −510 ppm peak to the Co(II) containing **Co$_4$V$_2$W$_{18}$** cannot be correct. Instead, the correct assignment of the −510 ppm peak *must be to a species that does not have any Co as part of its chemical composition.*[32]

The Synthesis and ^{51}V NMR of Authentic cis-$V_2W_4O_{19}^{4-}$. A search of the literature revealed that the hexametalate cis-$V_2W_4O_{19}^{4-}$ self assembles under conditions very similar to those employed for the "**Co$_4$V$_2$W$_{18}$**" syntheses (Scheme 2.2).[22,23,33] That literature search also revealed that the ^{51}V NMR resonance reported for authentic cis-$V_2W_4O_{19}^{4-}$ ranges from −506 to −524 ppm, with a peak width ranging from 23 to 42 Hz[22,23] —importantly all within error of the −507, $\Delta\nu_{1/2}$=30.5 Hz peak assigned previously to "**Co$_4$V$_2$W$_{18}$**" and within error of the −510±0.5 ppm, $\Delta\nu_{1/2}$=28±7 Hz peak we see herein for each and every synthesis of "**Co$_4$V$_2$W$_{18}$**" that we performed.

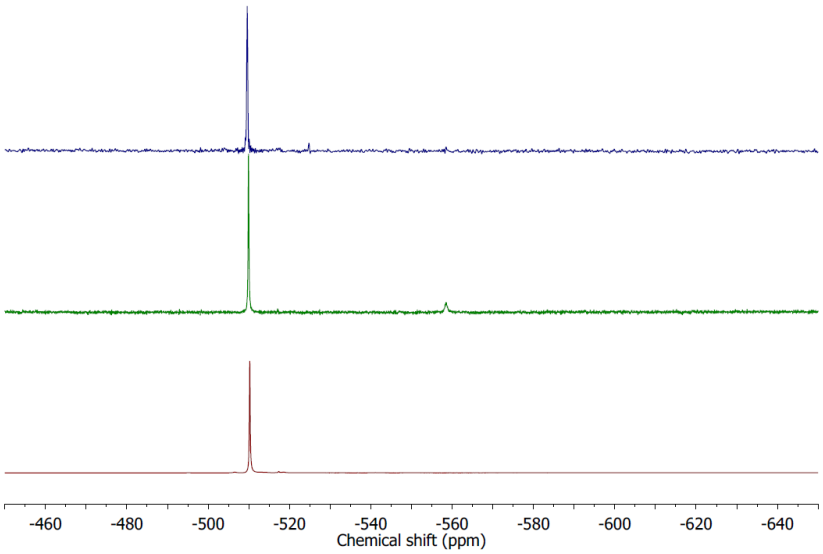

Figure 2.3. ^{51}V NMR spectra of the material obtained following the original[5] synthesis, 1A (top), the 2014[1] synthesis, 2A (middle), and a control synthesis in which Synthesis #2 was repeated *except that Co(II) was deliberately omitted* (bottom). All samples contained *ca.* 27 mg of the material in 1 mL (i.e. approximately 5 mM) unbuffered H_2O with 10% D_2O at 25˚C, which had been aged for 1 h prior to data acquisition. The appearance of the same main resonance in each synthesis provides seemingly incontrovertible evidence that the main resonance at −510 ppm must be for a species that does not contain any Co(II).

Hence, the next set of experiments was obvious: synthesize authentic[22,23] *cis*-$V_2W_4O_{19}^{4-}$ by the literature route (but as the more soluble sodium salt; see the Experimental Section), obtain its ^{51}V NMR, and compare that signal to that for the products obtained from Synthesis #1 and #2 under identical NMR conditions—is the expected −510±0.5 ppm peak observed?

The synthesis was performed (Scheme 2.2), and the ^{51}V NMR was obtained. The results are again both telling and compelling: each synthesis (i.e., that of "**$Co_4V_2W_{18}$**" by the two literature syntheses, and the synthesis of authentic *cis*-$V_2W_4O_{19}^{4-}$) *shows identical, sharp* $\Delta\nu_{1/2}$*=28±7 Hz resonances at −510±0.5 ppm, Figure 2.4.*

The 2014 Synthesis of $Na_{10}[Co_4(H_2O)_2(VW_9O_{34})_2]\cdot 35H_2O$

2.2 mmol $NaVO_3$
18 mmol Na_2WO_4
4.1 mmol $Co(NO_3)_2$

120 mL 0.5 M NaOAc pH 4.8
80 °C 2 hours

"$Na_{10}[Co_4(H_2O)_2(VW_9O_{34})_2]\cdot 35H_2O$"
12.5 % Yield

The Synthesis of $Na_4[cis\text{-}V_2W_4O_{19}]\cdot 11H_2O$

12 mmol $NaVO_3$
24 mmol Na_2WO_4

120 mL 0.6 M HOAc
80 °C 2hours

"$Na_4[V_2W_4O_{19}]\cdot 11H_2O$"
ca. 90 % Yield

Scheme 2.2. A Comparison of the Conditions Used for the 2014 Synthesis[1] of "**$Co_4V_2W_{18}$**"[1] and *cis*-$V_2W_4O_{19}^{4-}$ [22,33]

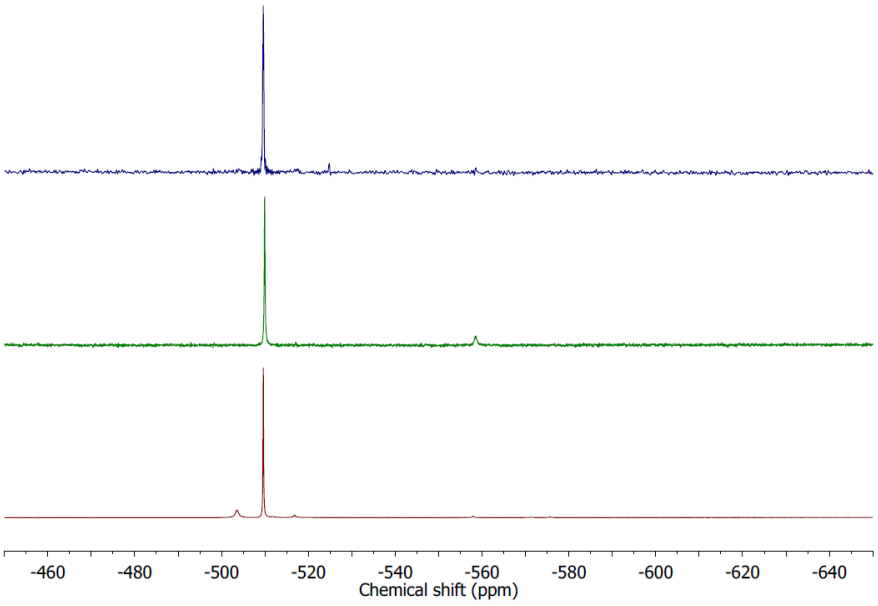

Figure 2.4. ^{51}V NMR of the "**$Co_4V_2W_{18}$**" product obtained from the original[8] "**$Co_4V_2W_{18}$**" synthesis (1A, top), the 2014 synthesis[1] (2A, middle), and for authentic *cis*-$V_2W_4O_{19}^{4-}$ (bottom).[22] Each ^{51}V NMR was obtained under identical conditions (*ca.* 5 mM in POM, post aging 1 h in unbuffered H_2O with 10% D_2O at 25˚C. Note that although several minor resonances are observed in each spectrum, the predominant resonance in each is −510 ppm with the identically narrow, $\Delta\nu_{1/2}$= 28±7 Hz, line width within experimental error.

The identical −510 ppm peaks seen in every synthesis conducted herein, importantly including authentic *cis*-$V_2W_4O_{19}^{4-}$ or repeating synthesis #2 without Co(II), compel one to assign the −510 ppm peak to *cis*-$V_2W_4O_{19}^{4-}$.[34] Our results are also fortified by Pettersson's finding in which he has noted that *cis*-$V_2W_4O_{19}^{4-}$ "dominates the [^{51}V NMR] spectra under most conditions"

when V and W are present in aqueous solutions at near-neutral pH for temperatures from 20 to 89˚C, reflecting the large formation constant for *cis*-$V_2W_4O_{19}^{4-}$ of $K=10^{57}$ at 25 °C in 0.6 M NaCl.[23]

One can now see that the prior misassignment[1] of this ^{51}V NMR resonance to **$Co_4V_2W_{18}$** in turn greatly mislead the authors of the 2014 study[1] about the stability of **$Co_4V_2W_{18}$** ("no changes [in the ^{51}V NMR] were noticed over a period of one month"[1]). *The lack of changes being observed in the ^{51}V NMR is actually indicating the (well-known)[23] stability of cis-$V_2W_4O_{19}^{4-}$, not the stability of "**$Co_4V_2W_{18}$**".*[1]

Resolving the Issue of our −510±0.5 ppm vs the Literature's Reported "−506.8" ppm ^{51}V NMR Resonance. The final issue to be resolved is that we consistently and reproducibly see the major ^{51}V NMR resonance for each and every synthesis herein at −510±0.5 ppm with $\Delta\nu_{1/2}$=28±7 Hz, whereas the literature reports[1] the main peak at *"−506.8"* ppm (no error estimates reported; implied error is ±0.05 ppm) with $\Delta\nu_{1/2}$=30.5 Hz (error bars unstated). The chemical shifts in the literature (as well as our) study are reported as relative to neat $VOCl_3$, referenced as 0 ppm at 25°C, but no control is reported in the prior study of actually measuring the chemical shift of neat $VOCl_3$ on their instrument and in their hands. In our own controls (see the Experimental Section for details and the Supporting Information where those results are presented and discussed, including Figures S2.7, S2.8, and S2.9), we found that the signal for neat $VOCl_3$ comes at +1.4 ppm (i.e., and not 0, Figure S2.8). Hence there is a chemical shift referencing error of ca. ±1.4 ppm, at least in our hands, and on our instrument.

It may be obvious at this point that pretty much the only reasonable explanation, and certainly the simplest ("Ockham's razor") explanation, is that our −510 ppm resonance, and the literature's "−506.8" ppm resonance, correspond to *one and the same species, namely cis-*

$V_2W_4O_{19}^{4-}$. The evidence bearing on this point is at least 5-fold and compelling: (i) the reported ^{51}V NMR resonance for authentic *cis*-$V_2W_4O_{19}^{4-}$ from the literature ranges from −506 to −524 ppm, with a peak width ranging from 23 to 42 Hz,[22,23] all well within error of the −507 ppm, $\Delta\nu_{1/2}$=30.5 Hz peak assigned previously to "**$Co_4V_2W_{18}$**" as well as with the peak at −510±0.5 ppm, $\Delta\nu_{1/2}$=28±7 Hz assigned herein to *cis*-$V_2W_4O_{19}^{4-}$; additionally (ii) we see the −510 ppm peak in *all* our syntheses, be it of *cis*-$V_2W_4O_{19}^{4-}$, synthesis #2 without Co(II), or our repeats of Syntheses #1 and #2 of **$Co_4V_2W_{18}$** which result in the same brown solid as described in the literature;[1,5] moreover (iii) our −510±0.5 ppm peak is the primary peak just as the primary peak in the 2014 study is at "−506.8 ppm"—that is, because the syntheses are the same, and because only a single, main peak is observed in both studies, it follows that these primary peaks correspond to the same product of those (same) syntheses; and fourth (iv) the highly sensitive ^{51}V NMR peak widths *are identical* within experimental error in the two studies, ours is $\Delta\nu_{1/2}$=28±7 and the literature's is $\Delta\nu_{1/2}$=30.5 Hz, by itself compelling evidence the two reported −510±0.5 ppm and "−506.8 ppm" peaks correspond to one and the same species—that is, and given that ^{51}V NMR peak-widths are quite sensitive to a number of factors and generally to the precise identity of the ^{51}V-containing species. That species is *cis*-$V_2W_4O_{19}^{4-}$. Finally, (v) as their TBA^+ salts and in acetonitrile-d_3 both *cis*-$V_2W_4O_{19}^{4-}$ and (impure) **$Co_4V_2W_{18}$** show an identical −507 ppm (but now $\Delta\nu_{1/2}$ = 12 ±1 Hz) resonance, Figure S2.9 of the Supporting Information.

An important corollary here is that the error in the ^{51}V NMR chemical shifts among different laboratories must be more than the ±0.5 ppm *precision* we observe (−510±0.5 ppm) and likely even more than the putative ±1.4 ppm estimated *accuracy* (−510±1.4) revealed by our chemical referencing control. It furthermore follows that the literature report of "−506.8 ppm", and thus its implied ±0.05 ppm (by normal significant figure definitions), overstates even the

precision (much less the accuracy) of that literature chemical shift measurement[1] by at least one, and probably approaching two, orders of magnitude.

Implication of This Work for the Purity and ^{51}V NMR of Other Paramagnetic Metal-Containing POMs in the Literature.

Critical Analysis of the ^{51}V NMR of $Co_6V_3W_{24}$ (i.e., $Na_{17}[(Co(H_2O)Co_2VW_9O_{34})_2(VW_6O_{26})]$). The complex **$Co_6V_3W_{24}$** is of some relevance to the present study because it and **$Co_4V_2W_{18}$** are made under similar conditions (Schemes 2.1 and 2.3)[30] and because the single crystal structure refinement[30] of **$Co_6V_3W_{24}$** has revealed the same structural motif of a pseudotetrahedral, vanadium-centered, lacunary Keggin ion that is in close proximity to several Co(II) paramagnetic centers. Hence, very broad ^{51}V NMR lines for **$Co_6V_3W_{24}$** would be expected, yet the ^{51}V NMR spectrum assigned[30] to "**$Co_6V_3W_{24}$**" has two relatively narrow peaks at −509.6 ($\Delta\nu_{1/2}$= 33.7 Hz) and −524.6 ppm ($\Delta\nu_{1/2}$= 21.6 Hz). Interestingly, the −509.6 ppm resonance was reported to shift to −507.2 ppm ($\Delta\nu_{1/2}$= 35.7 Hz) upon aging in pH 8.0 sodium borate buffer.[30] The authors attributed the new, −507.2 ppm ^{51}V NMR resonance to "**$Co_4V_2W_{18}$**." However, *both of these resonances have the same line width and chemical shift as observed herein for cis-$V_2W_4O_{19}^{4-}$*. Hence, the Ockham's razor hypothesis at this point has to be that the −509.6 ($\Delta\nu_{1/2}$= 33.7 Hz) peak should be reassigned to *cis*-$V_2W_4O_{19}^{4-}$. Note also that the −509.6 ppm peak is equivalent to our −510±0.5 ppm peak (assigned herein to *cis*-$V_2W_4O_{19}^{4-}$) within experimental error.

The species responsible for the −524.6 ppm peak remains unidentified, although we note that a resonance at −524 (line width not determined due to low S/N) is observed as a minor impurity in synthesis 1A—and, importantly, *not* in a 2:1 ratio as previously reported for "**$Co_6V_3W_{24}$**." An educated guess is that the observed[30] signal at −524.6 ppm corresponds to the monovanadium

hexametalate, $VW_5O_{19}^{3-}$, because the literature chemical shift[23] for $VW_5O_{19}^{3-}$ is −526.4 ppm and, hence, likely the same within experimental error as the −524.6 ppm peak. (Note the overstatement of even the precision of the chemical shifts here, again, by approaching 2 orders of magnitude (±0.05 implied; ±1.8 observed).) But, the working hypothesis that the −524.6 ppm signal corresponds to $VW_5O_{19}^{3-}$ remains to be tested by the synthesis of authentic material and its ^{51}V NMR under identical conditions to that employed for "**$Co_6V_3W_{24}$**".

Synthesis #5: The Synthesis of $Na_{10}[Mn_4(H_2O)_2(VW_9O_{34})_2]\cdot 34H_2O$

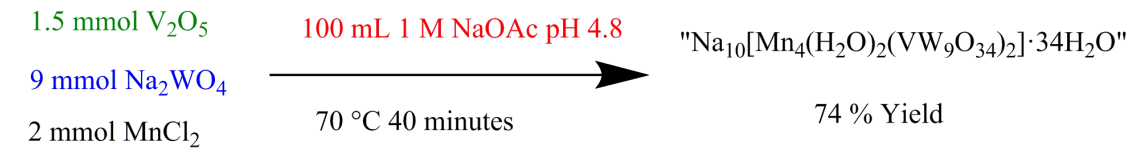

Synthesis #6: The Synthesis of $Na_{17}[(Co(OH_2)Co_2VW_9O_{34})_2(VW_6O_{26})]\cdot 31H_2O$

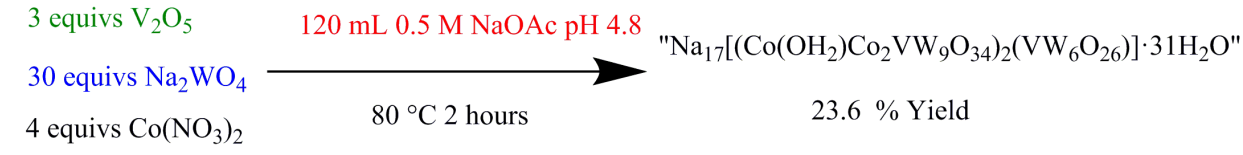

Scheme 2.3. Synthesis Conditions of **$Mn_4V_2W_{18}$**[5] and **$Co_6V_3W_{24}$**.[30]

Critical Analysis of the ^{51}V NMR of $Mn_4V_2W_{18}$ (i.e. $Na_{10}[Mn_4(H_2O)_2(VW_9O_{34})_2]$). The Mn analogue of **$Co_4V_2W_{18}$** is **$Mn_4V_2W_{18}$**, a complex also synthesized under nearly identical conditions to those for **$Co_4V_2W_{18}$**, except using $MnCl_2$ instead of $Co(NO_3)_2$ (Scheme 2.3).[5] Two different X-ray crystal structures were obtained for **$Mn_4V_2W_{18}$**, confirming its structural similarity to **$Co_4V_2W_{18}$**.[5,29] Once again, one expects greatly broadened ^{51}V NMR lines for this Mn congener, **$Mn_4V_2W_{18}$**—which, in turn, means that the relatively narrow, −505.2 ppm ($\Delta\nu_{1/2}$= 73.7 Hz) peak assigned[29] to **$Mn_4V_2W_{18}$** is almost surely incorrect. Indeed, based on the literature, one would expect significantly *more* broadening from the Mn(II) centers than seen for Co(II), due to the longer electronic spin correlation time of Mn(II), which in turn causes more rapid nuclear

relaxation and hence typically extremely broad NMR lines.[21,24,25] Additionally, although the chemical shift of −505.2 ppm is probably within experimental error of the resonance for *cis*-$V_2W_4O_{19}^{4-}$, its peak width is about 3-fold greater than seen so far for authentic *cis*-$V_2W_4O_{19}^{4-}$. Hence, an unequivocal assignment for the −505.2 resonance remains to be accomplished. In summary, the ^{51}V NMR assignments associated with **$Mn_4V_2W_{18}$** are almost surely in error.

2.3 Summary and Conclusions

The main findings and implications of the present studies can be summarized as follows:

• Bulk, solid, brown "**$Co_4V_2W_{18}$**", as synthesized by literature methods,[1,5] is actually an impure, composite mixture consisting of **$Co_4V_2W_{18}$**, NaOAc, plus other impurities, a conclusion fortified by elemental analysis, FT-IR, ^{51}V NMR, and the highly variable, 12–70% yields reported for "**$Co_4V_2W_{18}$**".

• The as-prepared, impure "**$Co_4V_2W_{18}$**" undergoes changes in both the solid and solution: the main ^{51}V NMR resonance due to *cis*-$V_2W_4O_{19}^{4-}$ at −510 ppm, $\Delta\nu_{1/2}$=28±7 Hz is present in solutions of freshly prepared material, yet is initially absent in solid aged for ≥5 months, yet grows in from that aged solid once it is aged further in solution.

• The finding that a cobalt-free synthesis reproduces the same −510 ppm ^{51}V NMR resonance, within experimental error, as the products obtained from Syntheses #1 and #2 for "**$Co_4V_2W_{18}$**" (as well as for "**$Co_6V_3W_{24}$**")[30] means, by itself, that the −510 ppm resonance cannot be due to any species that contains Co(II) (Figure 2.3).

• Alternatively, the −510 ppm resonance can be confidentially assigned to *cis*-$V_2W_4O_{19}^{4-}$, a hexametalate formed under the reaction conditions used for the syntheses of both **"$Co_4V_2W_{18}$**" and "**$Co_6V_3W_{24}$**", (Schemes 2.1, 2.2, and 2.3, Figure 2.4). In addition, authentic *cis*-$V_2W_4O_{19}^{4-}$

has the same chemical shift and peak width within experimental error to that previously assigned to **"$Co_4V_2W_{18}$**" as well as to that previously assigned to "**$Co_6V_3W_{24}$**".

• The unavoidable implication is that use of the −510 ppm (= the literature's −507 ppm[1]) resonance to argue for the stability of **"$Co_4V_2W_{18}$**" (e.g., "no changes [in the ^{51}V NMR] were noticed over a period of one month"[1]) is a flawed, highly misleading argument. Instead, the stability being observed is that of *cis*-$V_2W_4O_{19}^{4-}$, a vanadotungstate known to be relatively stable in the pH range of 3–8, with a formation constant of $K=10^{57}$.[23]

• Also cast in serious doubt, then, is the claim that **$Co_4V_2W_{18}$** is an "oxidatively and thermally stable, homogeneous water oxidation catalyst,"[1] one with a record reported TOF for a Co-POM of $>1x10^3$ s^{-1}.[1] A critical reinvestigation of this claim merits its own separate study, one presently in progress and one which will be reported elsewhere in due course.

• There are additional take-home messages from this work:[35]

(i) The danger in performing POM syntheses, *in the absence of prior full speciation*[36] *studies to guide those synthetic studies*,[23] is again emphasized—a point that likely extends to self-assembly syntheses more generally. However, the present state-of-the-art speciation study in POM chemistry is still a three-component system (e.g., V, W, and H^+ (pH)),[23] while what is needed for **$Co_4V_2W_{18}$** would be an unprecedented four-component speciation study (V, W, Co, and H^+). The interested reader is referred to valuable, state-of-the-art studies that at least bear on the speciation, as well as the stability, of a given POM species, notably the valuable studies by Pettersson,[23] Thouvenot,[28] Hercules,[37] Cronin,[38] Uskokovic´-Markovic´,[39] Nyman,[40,41] and Casey.[42] In addition, a recent Perspective highlights the spectroscopic and computational tools available for those wishing to study speciation and dynamics of aqueous POMs.[43]

(ii) The well-known rule that one needs independent demonstration of purity (i.e., convincing evidence for homogeneity by chromatographic methods, multiple recrystallizations, or other appropriate methods) whenever possible, *before* collecting physical and other characterization data on that material, is once again reinforced by the present example.

(iii) The present study also demonstrates that ^{51}V NMR *fails* as a reliable physical tool for demonstrating the purity of POMs containing paramagnetic atoms. Restated, ^{51}V quadrupolar NMR of paramagnetic-ion-containing POMs is quite a different situation compared to the utility and power of ^{31}P NMR as a direct method for speciation and purity in PO_4^{3-}-containing POMs, including ones containing paramagnetic ions.[27,28]

• The most important take-home message continues to be[6,7] that only by employing a scientific method based on the statement of specific hypotheses, along with the disproof of all reasonable multiple alternative hypotheses—as Chamberlin and Platt long ago urged us all to employ[44]—can one avoid being fooled when trying to extract nature's truths. The (unstated) hypothesis of the prior work[1] was that quadrupolar NMR of paramagnetic-ion-containing POMs could be employed analogously to how spin-1/2 ^{31}P NMR is used in POM chemistry. In hindsight, the first critical alternative hypothesis proved to be that the peaks seen in the ^{51}V NMR of "**$Co_4V_2W_{18}$**" are far too narrow to originate from a species containing paramagnetic Co(II). A more specific, second alternative hypothesis was then generated by a careful scrutiny of the literature: namely that *cis*-$V_2W_4O_{19}^{4-}$ is what is actually responsible for the observed ^{51}V NMR signal. That second alternative hypothesis is a good example of how more specific hypotheses contain more "scientific power"—because they are often testable in a direct, definitive fashion. In the present case resultant telling experiments included (a) leaving Co(II) out of the synthesis and seeing if the -510 ppm,

$\Delta\nu_{1/2}$=28±7 Hz resonance was still observed (as it was), and (b) preparing authentic *cis*-$V_2W_4O_{19}^{4-}$ and seeing if it gave exactly the observed -510 ppm, $\Delta\nu_{1/2}$=28±7 Hz resonance (as it did).

In upcoming papers we will report the results of our studies on the nature of the kinetically dominant WOCatalyst under electrochemically driven conditions derived from the multiple Co-POMs reported in the literature as molecular WOCatalysts, including the case of "**$Co_4V_2W_{18}$**".

2.4 Experimental

General Reagents. $Co(NO_3)_2{\cdot}6H_2O$(ACS Reagent >99%), $Na_2WO_4{\cdot}2H_2O$ (ACS Reagent >99%), and $NaVO_3$ (ACS Reagent >98%) were purchased from Sigma-Aldrich. V_2O_5 (99.2%) was purchased from Alpha Aesar. Sodium acetate (99.6%) and glacial acetic acid (ACS Reagent) were purchased from Mallinckrodt, and KBr (ACS spectral grade) was purchased from Acros. $VOCl_3$ was purchased from Aldrich; it should be handled with care because it is an oxidizer, corrosive, and water-sensitive. Each of the above reagents was used as purchased. All aqueous solutions were made from 18 MΩ water from a Barnstead Nanopure water purification system.

Instrumentation. ^{51}V NMR spectra were collected on a Varian 500 MHz NMR in an aqueous solution containing at least 10% D_2O which was used as an internal lock. Controls show that the percentage of D_2O used had no effects on the chemical shift, line width, or signal to noise in the concentration range investigated (i.e. 2–5 mM POM and 10–99% D_2O). Unless otherwise noted, spectra were collected on *ca.* 2–5 mM solutions of the stated complex (≥1 h after dissolution, unless stated otherwise) in 5 mm O.D. NMR tubes. Spectra were collected from −235 to −691 ppm with 512 scans, 1.0 s relaxation delay, 90° pulse angle, and 0.02 s acquisition time. Line widths were determined by fitting the observed NMR resonance using MestReNova software. The reported error bars are the standard deviation from the NMR spectra obtained on 1A, 2A, 2B, 2C, and the "purified" material. FT-IR was performed on a ThermoScientific Nicolet iS50 FT-IR

spectrometer in transmission mode using KBr pellets containing approximately 2 wt % of the product. External calibration was conducted using a polystyrene standard (peaks were ±1 cm^{-1} of the expected values). Thermogravimetric analysis (TGA) was performed on a TA Instruments TGA 2950 with a 5 ºC/min ramp rate from *ca.* 25 to 500 ºC unless otherwise noted. UV–vis absorption spectra were collected on an Agilent 8453 UV–vis spectrophotometer using a 1 cm path length quartz cuvette and solutions of a *ca.* 5 mM POM in water. ESI-MS was conducted on a Thermo-Finnigan LTQ LC/MS-MS using solutions containing *ca*. 5 mg/mL of TBA^+ salts (*vide infra*) of the chosen POM in acetonitrile. Spectra were collected with a sample flow rate of 10 μL/min, with the capillary voltage ranging from −11.96 to −35.13 V and capillary temperature of 275 °C.

Repeat of Synthesis #1: The Original[5] *Synthesis of* $Na_{10}[Co_4V_2W_{18}O_{68}]\cdot 37H_2O$. The original synthesis of $\mathbf{Co_4V_2W_{18}}$ was followed as closely as possible from the written procedure (and is labeled as 1A herein).[5] Specifically, 0.27 g of V_2O_5 (1.5 mmol) was dissolved into 100 mL of 1 M NaOAc, pH 4.8 solution in a 125 mL Erlenmeyer flask with stirring at *ca.* 600 rpm at room temperature for 5 min, yielding a turbid orange solution (Figure S2.10, left). Then 2.97 g of $Na_2WO_4\cdot 2H_2O$ (9 mmol) was added with stirring followed immediately by addition of 0.58 g of $Co(NO_3)_2\cdot 6H_2O$ (2 mmol). This solution was then placed into an oil bath at room temperature and heated to 70˚C over approximately 10 min, during which time the solution became transparent brown (Figure S2.10, right). The temperature was then maintained at 70˚C for 40 min; no further color changes were observed while maintaining the temperature at 70 °C. The 125 mL Erlenmeyer flask containing the solution was then removed from the oil bath, and the solution was poured into a 250 mL beaker and covered with a Kimwipe to prevent contamination, while still allowing slow evaporation at room temperature. The solvent was allowed to evaporate over the next two weeks

to yield dark-brown microcrystals. The product was collected by filtration using a medium frit glass filter, and 476 mg of the brown block-like microcrystals were collected after drying overnight via aspiration, 8.3% yield based on tungsten. FT-IR (Figure S2.1), ^{51}V NMR (Figure S2.5), and TGA (Figure S2.11) were collected on the product as described in the Instrumentation section. A *ca*. 100 mg sample was sent to Galbraith Laboratories for elemental analysis: calculated for $Na_{10}[Co_4(H_2O)_2(VW_9O_{34})_2]\cdot 37H_2O$: Co 4.16, W 58.4, V 1.80, Na 4.06%; found: Co 3.51, W 61.6, V 1.62, Na 4.88%.

Repeat of Synthesis #2: The 2014[1] Synthesis of $Na_{10}[Co_4V_2W_{18}O_{68}]\cdot 26H_2O$. **$Co_4V_2W_{18}$** was also synthesized following the procedure used for the 2014 WOCatalysis study[1] as closely as possible—although, unfortunately, the 2014[1] synthesis lacks many required details as a word-for-word reproduction of that synthesis in a footnote document.[45] Specifically, three repeat syntheses were conducted (labeled as 2A, 2B, and 2C) to examine the reproducibility of the synthesis as written; the only difference in the conditions was that for synthesis 2A, a watch glass covered the slowly evaporating solution instead of a Kimwipe, which was used for 2B and 2C.

To start, 6.0 g of $Na_2WO_4\cdot 2H_2O$ (18 mmol) and 1.2 g of $Co(NO_3)_2\cdot 6H_2O$ (4.1 mmol) were dissolved into 120 mL of a sodium acetate buffer (0.5 M, pH 4.8) in a 125 mL Erlenmeyer flask with stirring at *ca*. 600 rpm at room temperature. Upon full dissolution of the solids in *ca*. 5 min, 0.27 g of $NaVO_3$ (2.2 mmol) was added all at once to the clear pink solution with stirring (Figure S2.12, left). The solution was then heated to 80 °C over approximately 20 min in an oil bath, after which the temperature was held at 80 °C for 2 h with continued stirring. Upon reaching 80 °C, the solution changed from turbid pink with undissolved $NaVO_3$ to dark brown with no visible precipitate (Figure S2.12, right). The solution was then filtered hot through a medium frit filter to ensure its homogeneity; no precipitate was collected. This solution was then allowed to slowly

evaporate at room temperature in a 250 mL beaker with a Kimwipe covering the top to prevent contamination with dust while allowing slow evaporation over ca. 2-4 weeks (except for 2A, *vida supra*). The resulting characterization data is reported here for synthesis 2A because that is the material that was used for subsequent experiments. After approximately one month, 550 mg of brown, block-like crystals were collected over a medium frit filter, 9.9% yield based on tungsten. ^{51}V NMR (Figure S2.5), FT-IR (Figure S2.1), and TGA (Figure S2.13), were collected on the product as described in the Instrumentation section, and a *ca*. 100 mg sample was sent to Galbraith Laboratories for elemental analysis: calculated for $Na_{10}[Co_4(H_2O)_2(VW_9O_{34})_2]\cdot 26H_2O$: Co 4.30, W 60.31, V 1.86, Na 4.19%; found: Co 5.05, W 54.0, V 1.88, Na 4.89, C 0.55 %. The full characterization data for syntheses 2A, 2B and 2C are available in Table 2.3.

Synthesis of the Green Material "Purified" to the −510 ppm ^{51}V NMR Signal. We optimized the synthesis conditions to obtain a solid material that had the greatest purity of the −510 ppm ^{51}V NMR resonance. To start, 6.0 g of $Na_2WO_4\cdot 2H_2O$ (18 mmol) and 1.2 g of $Co(NO_3)_2\cdot 6H_2O$ (4.1 mmol) were dissolved into 120 mL of a sodium acetate buffer (0.25 M, pH 4.8; half the concentration used in the 2014[1] study). After *ca*. 5 min, 0.27 g of $NaVO_3$ (2.2 mmol) was added all at once to the turbid purple solution with stirring. The solution was then heated to 80 °C over approximately 20 min in an oil bath, after which the temperature was held at 80 °C for 2 h with continued stirring. During this time the solution became turbid and brown. The solution was then removed from the oil bath, and placed into an ice bath for 45 min. During this time, a light-brown precipitate collected at the bottom of the flask leaving a clear green solution. The solution was then filtered through approximately 1 cm of Celite on a coarse frit filter using suction supplied by aspiration. The solution was then rotary evaporated at 40 °C at 300 rpm for approximately 30 min until *ca.* 45 mL of solution remained. This solution was then placed in a

mortar in a vacuum oven at 40 °C overnight. The obtained powder was then ground in the mortar with a pestle, and placed in a medium frit filter. The solution was then suspended in 30 mL of methanol and filtered to dryness four times to remove NaOAc. The product was then dissolved in 30 mL of water and filtered through Celite as described above. The clear green solution was then added to a recrystallization dish and placed in a vacuum desiccator for 1 week. The green powder that resulted was collected and ground in a mortar and pestle to obtain greater particle size homogeneity, 1.39 g collected. ^{51}V NMR (Figure S2.6) and FT-IR (Figure S2.1) were collected as described in the Instrumental section and a *ca*. 100 mg sample was sent to Galbraith Laboratories for elemental analysis: calculated for $Na_{10}[Co_4(H_2O)_2(VW_9O_{34})_2]\cdot 26H_2O$: Co 4.30, W 60.31, V 1.86, Na 4.19%; found: Co 1.00, W 52.9, V 1.80, Na 9.56%.

Synthesis #3: Authentic $Na_4[cis\text{-}V_2W_4O_{19}]\cdot 11H_2O$. The synthesis of $Na_4[cis\text{-}V_2W_4O_{19}]\cdot 8H_2O$ was performed by an adaption of the synthesis of the potassium salt, $K_4[cis\text{-}V_2W_4O_{19}]\cdot 8H_2O$, from a procedure by Pope and Flynn.[33] Specifically, 120 mL of a 0.6 M acetic acid solution was prepared by mixing 4.1 mL glacial acetic acid with 116 mL of water in a 125 mL Erlenmeyer flask. Then 1.46 g of $NaVO_3$ (0.012 mmol) was added to the solution with stirring at *ca*. 600 rpm, after which the solution became red and cloudy. Next, 7.05 g of $Na_2WO_4\cdot 2H_2O$ (0.024 mmol) was added with stirring, and the solution was heated in an oil bath to 80 °C over approximately 30 min; the temperature was then held at 80 °C for 2 h with continued stirring. At the end of the heating, the solution was orange with large red chunks, the orange solution being characteristic of *cis*-$V_2W_4O_{19}^{4-}$. The insoluble red material was removed using a medium frit filter and suction by aspiration. The solution was then placed into a 250 mL beaker and covered with a Kimwipe to prevent contamination with dust and to allow for slow evaporation at room temperature over a two-week period. Large (ca. 1 cm^3) orange crystals were collected by filtration

through a medium frit filter, and the product was rinsed with 50 mL of acetone. After 4 h of aspiration, 2.3 g of an orange powder were collected; 27% yield based on tungsten. ^{51}V NMR (Figure 2.4) and FT-IR (Figure S2.14) were collected as described in the Instrumentation section. TGA was collected by ramping 5 °C/min to 200 °C and holding at 200 °C for 10 min, and then ramping 10 °C/min to 500 °C (Figure S14). The TGA was initially stopped at 200 °C because the literature[33] TGA of *cis*-$V_2W_4O_{19}^{4-}$ reports no mass lost above 200 °C. However, we observed further weight loss above 200 °C, specifically 12.07% and 14.3% weight loss once 200 and 500 °C, respectively, had been reached. The 14.3% weight losses correspond to 11 equiv of water calculated for Na_4[*cis*-$V_2W_4O_{19}$]·$11H_2O$ used herein. For elemental analysis a *ca*. 100 mg sample was sent to Galbraith Laboratories: calculated for Na_4[*cis*-$V_2W_4O_{19}$]·$11H_2O$: W 51.1, V 7.1, Na 6.4%; found: W 47.4, V 7.1, Na 6.8%.

Synthesis #4: Control synthesis Following Synthesis #2 of $Na_{10}[Co_4V_2W_{18}O_{68}]\cdot 35H_2O$, but Omitting the Cobalt(II). This control synthesis was conducted exactly as described in Synthesis #2 except that *no $Co(NO_3)_2\cdot 6H_2O$* was added. The goal of this experiment was to see what tungsto-vanadates or other POMs would form in the absence of cobalt, but under the otherwise identical reaction conditions of Synthesis #2.

In this synthesis 6.0 g of $Na_2WO_4\cdot 2H_2O$ (18 mmol) was dissolved into 120 mL of a sodium acetate buffer (0.5 M, pH 4.8) in a 125 mL Erlenmeyer flask with stirring at *ca*. 600 rpm at room temperature. Upon full dissolution of the solid in *ca*. 5 min, 0.27 g of $NaVO_3$ (2.2 mmol) was added all at once to the solution with stirring. The solution was then heated on an oil bath to 80 °C over approximately 20 min, then the temperature was held at 80 °C for 2 h with continued stirring. Upon reaching 80 °C the solution became clear yellow/orange. ^{51}V NMR was then collected on the resulting solution by mixing 0.75 mL of the solution with 0.25 mL of D_2O and collecting ^{51}V

NMR as described in the Instrumentation section (Figure 2.3). The product was allowed to evaporate slowly from a 250 mL beaker covered with a Kimwipe. After 11 days of slow evaporation, 15.2 g were collected via filtration with a medium frit filter. Note that calculating a percent yield here is not possible because the material obtained is a nonstoichiometric mixture. However, the substantially greater mass of product than originally added (15.2 g obtained vs the *ca.* 6.27 g of $NaWO_3$ + $NaVO_3$) suggested that a substantial amount of NaOAc and/or water are present in the product. The excess NaOAc was removed by resuspending the solid in 60 mL of acetone and filtering twice. After drying via aspiration overnight, 3.41 g of product were collected ^{51}V NMR was collected as described above, no significant changes in the ^{51}V NMR spectra were observed before and after the removal of NaOAc. The NaOAc peak in the FT-IR at ca. 1600 cm^{-1} was still observed, albeit at much lower intensity. Elemental analysis was not conducted on this product because although *cis*-$V_2W_4O_{19}^{4-}$ is the predominant detectable species by ^{51}V NMR, tungsten was added in excess and the bulk product is a mixture.

^{51}V NMR Experiment with "$Co_4V_2W_{18}$", cis-$V_2W_4O_{19}^{4-}$, and Neat $VOCl_3$ at 25 °C to Estimate the Error in Observed Chemical Shifts. To obtain one estimate of the accuracy of the ^{51}V NMR chemical shifts reported herein, we performed the following experiment with "**$Co_4V_2W_{18}$**" (2A), *cis*-$V_2W_4O_{19}^{4-}$, and neat $VOCl_3$ at 25 °C, using the "substitution" method, as $VOCl_3$ cannot be used as an internal standard in aqueous solution due to its spontaneous reaction with water to form polyoxovanadates and HCl. First, a 500 μM solution of *cis*-$V_2W_4O_{19}^{4-}$ (or "**$Co_4V_2W_{18}$**") was prepared in unbuffered 50% D_2O in a 5 mm O.D. NMR tube. The broadband probe was then tuned, and the field was shimmed and locked on the D_2O in the POM solution. A spectrum was collected with a sweep width from +200.5 to −692.4 ppm (117474.3 Hz) with a 0.001 s relaxation delay, 90° pulse angle, 6.4 μs observe pulse, and 1024 scans. Next, that solution was removed, and neat

$VOCl_3$ in a 5 mm O.D. NMR tube was placed into the instrument and allowed to thermally equilibrate for 5 min. A spectrum was then acquired unlocked and without shimming to replicate the ^{51}V NMR conditions used for the acquisition of the POM sample. The observed ^{51}V NMR chemical shift for $VOCl_3$ obtained in this manner was +1.4 ppm (Figure S2.8), that is, positive of the nominally expected 0.0 ppm value for this standard ^{51}V NMR reference compound. No shift in the $VOCl_3$ spectrum was observed when tuning, shimming, and locking on D_2O in the "**$Co_4V_2W_{18}$**" sample instead of the *cis*-$V_2W_4O_{19}^{4-}$ sample, suggesting that the error in chemical shift is a systematic one, of magnitude 1.4 ppm.

Supporting Information. The following Figures and Discussions are available in Appendix I: Supporting Information for Chapter II: Figure S2.1. FT-IR of 1A, 2A, 2B, 2C, and "purified" green material; UV-Vis of $Co_4P_2W_{18}$, $Co_4V_2W_{18}$ and *cis*-$V_2W_4O_{19}^{4-}$: Experiments and Discussion; Figure S2.2. The UV–vis spectra of "$Co_4V_2W_{18}$," $Co_4P_2W_{18}$, and authentic *cis*-$V_2W_4O_{19}^{4-}$; ESI-MS of $Co_4V_2W_{18}$ and *cis*-$V_2W_4O_{19}^{4-}$: Experiments and Discussion; Figure S2.3. ESI-MS of the TBA salt of "**$Co_4V_2W_{18}$**" and *cis*-$V_2W_4O_{19}^{4-}$ in acetonitrile; Figure S2.4. ESI-MS zoom of the −1367 *m/z* peak of the authentic *cis*-$V_2W_4O_{19}^{4-}$ TBA^+ salt, and the simulations for the species fit herein; Figure S2.5. ^{51}V NMR spectra of the product obtained for syntheses 1A, 2A, 2B, and 2C; Figure S2.6. ^{51}V NMR of the "purified" green product; Additional evidence that the ^{51}V NMR chemical shift reported (−507 ppm) for "$Co_4V_2W_{18}$" and that obtained in this work (−510 ppm) are for the same species; Figure S2.7. ^{51}V NMR of "$Co_4V_2W_{18}$" after one hour in 0.1 M NaB buffer pH=9.0; Figure S2.8. ^{51}V NMR of neat $VOCl_3$ reference standard; Figure S2.9. ^{51}V NMR of the TBA^+ salts of 2A and *cis*-$V_2W_4O_{19}^{4-}$; Line widths for $Zn_4P_2W_{18}O_{68}^{10-}$ and $Co_4P_2W_{18}O_{68}^{10-}$; Figure S2.10. Photographs of reaction solution following the Original synthesis procedure; Figure S2.11. TGA of "$Co_4V_2W_{18}$" obtained following the Original synthesis

procedure; Figure S2.12. Photographs of reaction solution following the 2014 synthesis procedure; Figure S2.13. TGA of "$Co_4V_2W_{18}$" obtained following the 2014 synthesis procedure; Figure S2.14. FT-IR and TGA of authentic *cis*-$V_2W_4O_{19}^{4-}$.

REFERENCES

1 Lv, H.; Song, J.; Geletii, Y. V.; Vickers, J. W.; Sumliner, J. M.; Musaev, D. G.; Kögerler, P.; Zhuk, P. F.; Bacsa, J.; Zhu, G.; Hill, C. L. *J. Am. Chem. Soc.* **2014**, *136* (26), 9268.

2 Weakley, T. J. R.; Evans, H. T.; Showell, J. S.; Tourné, G. F.; Tourné, C. M. *J. Chem. Soc., Chem. Commun.* **1973**, No. 4, 139.

3 Finke, R. G.; Droege, M. W.; Domaille, P. J. *Inorg. Chem.* **1987**, *26* (23), 3886.

4 Yin, Q.; Tan, J. M.; Besson, C.; Geletii, Y. V.; Musaev, D. G.; Kuznetsov, A. E.; Luo, Z.; Hardcastle, K. I.; Hill, C. L. *Science* **2010**, *328* (5976), 342.

5 Li, B.; Yan, Y.; Li, F.; Xu, L.; Bi, L.; Wu, L. *Inorg. Chim. Acta* **2009**, *362* (8), 2796.

6 Stracke, J. J.; Finke, R. G. *J. Am. Chem. Soc.* **2011**, *133* (38), 14872.

7 Stracke, J. J.; Finke, R. G. *ACS Catalysis*, **2014**, *4*, 909-933.

8 To be industrially successful, the catalytic lifetime of a truly relevant WOC will reportedly have to be on the order of $10^{8–9}$ total turn overs (TTO's), which means a stable catalyst for approximately126 hours at a reported TOF of ~1000 s^{-1} for "**$Co_4V_2W_{18}$**".

9 (a) Pope, M. T. *Heteropoly and isopoly oxometalates*; Springer-Verlag, 1983. (b) Yamase, T.; Pope, M. *Polyoxometalate Chemistry for Nano-Composite Design*; Springer Science & Business Media, 2006. (c) Pope, M.; Muller, A. *Polyoxometalates: From Platonic Solids to Anti-Retroviral Activity: From Platonic Solids to Anti-Retroviral Activity*; Springer Science & Business Media, 1994.

10Evans, H. T.; Tourné, C. M.; Tourné, G. F.; Weakley, T. J. R. *J. Chem. Soc., Dalton Trans.* **1986**, No. 12, 2699.

11 Weakley, T. J. R. *J. Chem. Soc., Chem. Commun.* **1984**, No. 21, 1406.

12 Goberna-Ferrón, S.; Vigara, L.; Soriano-López, J.; Galán-Mascarós, J. R. *Inorg. Chem.* **2012**, *51* (21), 11707.

13 Finke, R. G.; Droege, M.; Hutchinson, J. R.; Gansow, O. *J. Am. Chem. Soc.* **1981**, *103* (6), 1587.

14 Note that the C=O stretch of NaOAc at ca. 1600 cm^{-1} is present in the FT-IR spectrum given in the SI of the original[5] synthesis, although it was not reported in the main text of that paper.[5] The 2014 paper did not report a peak around 1600 cm^{-1} and the spectrum provided in that SI was cut off at 1200 cm^{-1}. Because no attempts were made to remove NaOAc in the 2014 synthesis,[1] and because we find NaOAc in each of our repeats of these syntheses (as judged by a ca. 1600 cm^{-1}, Figure S1, Table 3), we conclude that NaOAc is in all probability an impurity in the 2014 synthesis as well.

15 Andres, H.; Clemente-Juan, J. M.; Aebersold, M.; Güdel, H. U.; Coronado, E.; Büttner, H.; Kearly, G.; Melero, J.; Burriel, R. *J. Am. Chem. Soc.* **1999**, *121* (43), 10028.

16 The literature on **$Co_4P_2W_{18}$** provides little information as to the exact nature of the observed d–d transition in the visible range. However, since the ground state of pseudo-octahedral Co(II) in a weak field environment is $^4T_1$,[15] the observed transition at 580 nm can be assigned to the $^4T_1(F) \rightarrow {}^4T_1(P)$ transition according to a Tanabe-Sugano diagram. The observed shoulder at ca. 517 nm could be evidence of lowered symmetry due to Jahn–Teller, or spin orbit coupling, as is observed in $Co(OH_2)_2^{2+}$. The lower energy $^4T_1(F) \rightarrow {}^4T_2(F)$ is likely weak, and likely in the near IR, making its detection difficult especially in water.

17 Miranda, C. T.; Carvalho, S.; Yamaki, R. T.; Paniago, E. B.; Borges, R. H. U.; De Bellis, V. M. *Polyhedron* **2010**, *29* (2), 897.

18 Bellenger, J.-P.; Arnaud-Neu, F.; Asfari, Z.; Myneni, S. C. B.; Stiefel, E. I.; Kraepiel, A. M. L. *J. Biol. Inorg. Chem.* **2006**, *12* (3), 367.

19 Morey, M.; Davidson, A.; Eckert, H.; Stucky, G. *Chem. Mater.* **1996**, *8* (2), 486.

20 Rehder, D.; Polenova, T.; Bühl, M. In *Annual Reports on NMR Spectroscopy*; Webb, G. A., Ed.; Academic Press, **2007**; Vol. 62, pp 49–114.

21 Drago, R. S. *Physical methods for chemists*; Saunders College Pub., **1992**.

22 Leparulo-Loftus, M. A.; Pope, M. T. *Inorg. Chem.* **1987**, *26* (13), 2112.

23 Andersson, I.; Hastings, J. J.; Howarth, O. W.; Pettersson, L. *J. Chem. Soc., Dalton Trans.* **1996**, No. 13, 2705.

24 La Mar, G. N.; Horrocks, W. D.; Holm, R. H. *NMR-Paramagnetic Molecules*; Academic Press, **1973**.

25 Bakhmutov, V. *Practical NMR Relaxation for Chemists*; John Wiley & Sons, **2004**.

26 Clemente, J. M.; Andres, H.; Aebersold, M.; Borrás-Almenar, J. J.; Coronado, E.; Güdel, H. U.; Büttner, H.; Kearly, G. *Inorg. Chem.* **1997**, *36* (11), 2244.

27 Jorris, T. L.; Kozik, M.; Casan-Pastor, N.; Domaille, P. J.; Finke, R. G.; Miller, W. K.; Baker, L. C. W. *J. Am. Chem. Soc.* **1987**, 109 (24), 7402.

28 Ruhlmann, L.; Schaming, D.; Ahmed, I.; Courville, A.; Canny, J.; Thouvenot, R. *Inorg. Chem.* **2012**, *51* (15), 8202.

29 Lv, H.; Song, J.; Zhu, H.; Geletii, Y. V.; Bacsa, J.; Zhao, C.; Lian, T.; Musaev, D. G.; Hill, C. L. *Journal of Catal.* **2013**, *307*, 48.

30 Lv, H.; Song, J.; Geletii, Y. V.; Guo, W.; Bacsa, J.; Hill, C. L. Eur. J. *Inorg. Chem.* **2013**, 1720.

31 Ogloblichev, V.; Kumagai, K.; Yakubovsky, A.; Mikhalev, K.; Furukawa, Y.; Verkhovskii, S.; Gerashenko, A.; Barilo, S.; G Bychkov; Shiryaev, S.; Korolev, A. *J. Phys.: Conf. Ser.* **2009**, *150* (4), 042148.

32 We did consider (briefly!) the alternative hypothesis that the cobalt-free species from the control synthesis and **$Co_4V_2W_{18}$** might have coincidentally identical ^{51}V NMR resonances. However, we ruled out this at least conceivable alternative explanation because **$Co_4V_2W_{18}$**

contains four paramagnetic, line-broadening Co(II) ions and under no known circumstances should it give the precise, identically narrow ($\Delta\nu_{1/2}$=28±7 Hz), ^{51}V NMR line width, let alone the same chemical shift. Instead, the observed relatively narrow, $\Delta\nu_{1/2}$=28±7 Hz −510 ppm resonance should be assigned to a V-containing species that does not contain Co(II).

33 Flynn, C. M.; Pope, M. T. *Inorg. Chem.* **1971**, *10* (11), 2524.

34 Note that we considered, but did not try the otherwise obvious experiment of attempting to detect, the ^{51}V NMR resonance actually due to **$Co_4V_2W_{18}$**, for the following reasons: (i) all our evidence is that the as-prepared sample of solid "**$Co_4V_2W_{18}$**" is impure, and apparently also unstable in solution; hence, more than a single resonance is expected; (ii) the correct assignment of any detected resonance to **$Co_4V_2W_{18}$** is at best problematic: the paramagnetic effect of the four Co(II) centers on the V atom is difficult to predict and, depending on the exact contact, polarization, and pseudo-contact shifts, the resonance could be greatly shifted either upfield or downfield,[24,25] so that a mistake in the assignment is possible if not probable; and (iii) the actual detection of the peak promises to be challenging at best due to the rapid relaxation and correspondingly greatly broadened peak width, and probably requires specialized NMR equipment beyond that available to us at least locally, according to our in-house NMR hardware expert, Dr. Chris Rithner.

35 (a) Relevant and worth repeating here is the statement in the classic 1972 Inorganic Chemistry textbook,**Error! Bookmark not defined.**[b] while discussing POMs, that "the fact that a salt with a particular structure crystallizes from solution under certain conditions does not necessarily mean that the same anion is the major species in solution—or, in fact, that it even exists in solution. There are clear cases where the ions in solution and the crystals obtained from them are substantially different."

(b) Cotton, F., A. and Wilkinson, G. *Advanced Inorganic Chemistry A Comprehensive Text*, Third Edition.; Interscience Publishers, **1972**, 950-951.

36 By speciation studies we mean a combination of spectroscopic, potentiometric, and any other applicable technique to identify the precise mixture of complexes present under a given set of conditions used for the synthesis, and ideally where that system of complexes is at equilibrium (i.e., under thermodynamic, not kinetic, control). By the word "speciation" we mean this in the classic sense;[23] we specifically do *not* mean the "stability" of a single compound in solution, as one referee used the concept of "speciation".

37 Truebenbach, C. S.; Houalla, M.; Hercules, D. M. *J. Mass Spectrom.* **2000**, *35* (9), 1121.

38 Surman, A. J.; Robbins, P. J.; Ujma, J.; Zheng, Q.; Barran, P. E.; Cronin, L. *J. Am. Chem. Soc.* **2016**, *138* (11), 3824.

39 Holclajtner-Antunović, I.; Bajuk-Bogdanović, D.; Popa, A.; Uskoković-Marković, S. *Inorg. Chim. Acta* **2012**, *383*, 26.

40 Hou, Y.; Fast, D. B.; Ruther, R. E.; Amador, J. M.; Fullmer, L. B.; Decker, S. R.; Zakharov, L. N.; Dolgos, M. R.; Nyman, M. *J.l of Solid State Chem.* **2015**, *221*, 418.

41 Goberna-Ferrón, S.; Soriano-López, J.; Galán-Mascarós, J. R.; Nyman, M. *Eur. J. Inorg. Chem.* **2015**, *2015* (17), 2833.

42 Ohlin, C. A.; Harley, S. J.; McAlpin, J. G.; Hocking, R. K.; Mercado, B. Q.; Johnson, R. L.; Villa, E. M.; Fidler, M. K.; Olmstead, M. M.; Spiccia, L.; Britt, R. D.; Casey, W. H. *Chem. Eur. J.* **2011**, *17* (16), 4408.

43 Jackson, M. N.; Kamunde-Devonish, M. K.; Hammann, B. A.; Wills, L. A.; Fullmer, L. B.; Hayes, S. E.; Cheong, P. H.-Y.; Casey, W. H.; Nyman, M.; Johnson, D. W. *Dalton Trans.* **2015**, *44* (39), 16982.

44 (a) "Studies for Students. The Method of Multiple Working Hypotheses", Chamberlin, T. C. *J. Geology* **1897**, *5*, 837-848. (b) "Strong Inference", Platt, J. R. *Science* **1964**, *146*, 347.

45 The synthesis in the 2014 paper is the following:[1] "$Co(NO_3)_2 \cdot 6H_2O$ (1.2 g) and $Na_2WO_4 \cdot 2H_2O$ (6.0 g) were dissolved in 0.5 M sodium acetate buffer (120 mL, pH 4.8) and vigorously stirred for about 5 minutes before $NaVO_3$ (0.27 g) was added. The resulting turbid mixture was then heated to 80 °C for 2 hours. The hot, brown mixture was filtered to remove any precipitate and left to crystallize for about one week to give dark block crystals of [$\mathbf{Co_4V_2W_{18}}$]".

III. ELECTROCHEMICAL WATER OXIDATION CATALYSIS BEGINNING WITH CO(II) POLYOXOMETALATES: THE CASE OF THE PRECATALYST $Co_4V_2W_{18}O_{68}^{10-}$[ii]

Overview

The question is addressed of whether the cobalt-polyoxometalate (Co-POM) precatalyst $Co_4V_2W_{18}O_{68}^{10-}$ (hereafter **$Co_4V_2W_{18}$**) is a stable, homogeneous water-oxidation catalyst under electrochemically driven conditions and in 0.1 M pH 5.8 and pH 8.0 NaPi buffer as well as pH 9.0 sodium borate (NaB) buffer. This question is of considerable interest since **$Co_4V_2W_{18}$** has been reported to be highly stable, and 200-fold faster WOC than its P-congener, $Co_4P_2W_{18}O_{68}^{10-}$ (hereafter **$Co_4V_2W_{18}$**), for reasons that were not specified. The nature of the true water-oxidation catalyst when starting with **$Co_4V_2W_{18}$** is of further fundamental interest because a recent report reveals that the ^{51}V NMR peak at ca. −507 ppm assigned by others to **$Co_4V_2W_{18}$** and used to argue for its solution stability is, instead, correctly assigned to the highly stable *cis*-$V_2W_4O_{19}^{4-}$, in turn raising the question of the true stability of **$Co_4V_2W_{18}$** under water oxidation catalysis conditions. A battery of physical methods is used to address the questions of the stability and true water-oxidation catalyst when beginning with **$Co_4V_2W_{18}$** as the precatalyst: ^{31}P line-broadening detection of Co(II) present in solution from leaching or as a counter-ion impurity; a check of those Co(II) concentration results by the second method of cathodic stripping; the O_2 yield (and, hence, Faradaic efficiency) of electrocatalytic water oxidation; electrochemical, SEM, EDX and XPS

[ii] This chapter is a direct follow up to Chapter II and details studies with **$Co_4V_2W_{18}$** wherein, the stability is quantified, and the dominant WOCatalyst is identified from a variety of buffer conditions starting with **$Co_4V_2W_{18}$**. This chapter contains the entire published manuscript and has been reproduced with permission from the journal in which it was originally published (Folkman, S. J.; Finke, R. G. *ACS Catal.* **2017**, *7*, 7–16.). Minor edits have been made in order for the material to be in the same dissertation format.

characterization of CoO_x films produced on the electrode; plus multiple controls and other experiments designed to test alternative hypotheses that might explain the observed results. The collective evidence provides a compelling case that Co(II) derived from **$Co_4V_2W_{18}$** forms a CoO_x film on the electrode which, in turn, carries all the observed, electrochemically driven water-oxidation catalysis current within experimental error. A list of seven bulleted main findings is provided as a summary.

3.1 Introduction

Water oxidation catalysis (WOC) is a topic of intense interest since it is a key reaction for solar fuel production and energy storage.[1] Polyoxometalates (POMs) have attracted attention in the field of WOC because they are all-inorganic, redox active, oxidatively robust, and synthetically tunable ligand systems that can be characterized at the molecular level. Molecular if not atomic-level kinetic and mechanistic studies are possible[2,3,4] with POMs, in turn allowing insights required to rationally fine-tune POM catalyst systems.

Cobalt POMs (hereafter Co-POMs), in particular, have attracted considerable attention as potential water oxidation catalysts (WOCatalysts).[5,6,7,8,9,10,11,12] Indeed, the hypothesis has been advanced that Co-POMs are a (if not *the*) superior class of robust WOCatalysts.[6,12] However, an important alternative hypothesis has also appeared: namely that no Co-POM is sufficiently stable in water to be a long-lived WOCatalyst; instead, Co-POMs often serve as precursors to leached $Co(II)_{aq}$ and, then, heterogeneous cobalt oxide (CoO_x) which acts as the true, kinetically dominant WOCatalyst, especially under electrochemically driven WOC conditions.[13,14] Supporting the latter hypothesis is our 2011 study[13] showing that, when beginning with a 500 μM solution of the PO_4^{3-}-core $Co_4P_2W_{18}O_{68}^{10-}$ (hereafter **$Co_4P_2W_{18}$**)[15] in 0.1 M, pH 8.0 sodium phosphate (NaPi), the **$Co_4P_2W_{18}$** leaches 58 ± 2 μM $Co(II)_{aq}$ after three hours. This amount of $Co(II)_{aq}$ leads to the

formation of electrode-bound, POM-free, Nocera-type CoO_x that carries 100 ± 12 % of the observed, electrochemically driven WOC current.[13]

Hence, a study of considerable interest to the WOC field is the 2014 report[12] that the V-congener $Co_4V_2W_{18}O_{68}^{10-}$ (hereafter **$Co_4V_2W_{18}$**, Figure 3.1)[12,16] exhibits: (i) "high hydrolytic stability;" [12] (ii) two times the oxygen yield using photogenerated $Ru(bpy)_3^{3+}$ as the chemical oxidant with **$Co_4V_2W_{18}$** (and in comparison to **$Co_4P_2W_{18}$**) as the water oxidation (pre)catalyst; and surprisingly that (iii) **$Co_4V_2W_{18}$** has a reported $TOF_{apparent}$ 200x greater than the TOF originally reported[6] for the P-congener, **$Co_4P_2W_{18}$**, albeit an O_2 yield that is only 2-fold higher.[17] This latter report is especially interesting since, if verifiable, then it would appear to hold insight into how to fine-tune even higher activity POM-based catalysts. Why a **V**O_4^{3-} core Co-POM could have a 200-fold higher activity than a **P**O_4^{3-} core one, Figure 1, was left completely unexplained, however, and has no precedent.

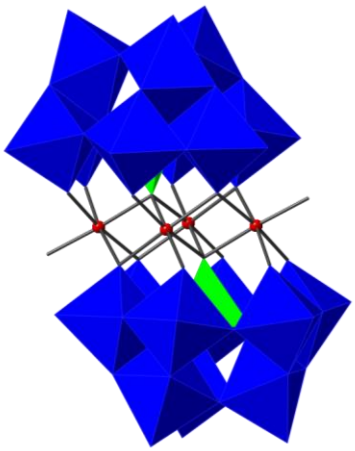

Figure 3.1. Structure of **$Co_4V_2W_{18}$** established by two independent[12,16] single-crystal X-ray diffraction refinements. One of the structures was well refined to a low R = 2.43% value providing confidence in at least the solid-state structure of **$Co_4V_2W_{18}$**.[12] Blue octahedra represent WO_6, green tetrahedra VO_4, and red spheres indicate cobalt. In the P-congener, a PO_4 is present in place of the (green) VO_4.

Highly relevant to the present investigation of **$Co_4V_2W_{18}$** as a WOPrecatalyst is our 2016 report[18] that, despite the well-refined and seemingly unequivocal nature of the composition and structure of **$Co_4V_2W_{18}$** as a *single crystalline solid*, there are multiple issues with the literature syntheses and characterization[12,16] of **$Co_4V_2W_{18}$**. Specifically, the issues uncovered recently[18] that are directly relevant to the current studies are: (i) that brown solid **$Co_4V_2W_{18}$** is impure and contains sodium acetate (NaOAc) and probably some *cis*-$V_2W_4O_{19}^{4-}$; (ii) efforts to purify the as-synthesized **$Co_4V_2W_{18}$** led, instead, to *less pure* **$Co_4V_2W_{18}$** that contained a greater amount of *cis*-$V_2W_4O_{19}^{4-}$; and crucially (iii) that the ^{51}V NMR peak at −506.8 ppm assigned to **$Co_4V_2W_{18}$** is, instead, more accurately reported as −510(±1.4 ppm) as well as correctly reassigned to the very stable[19] *cis*-$V_2W_4O_{19}^{4-}$, which is known to self-assemble under the synthesis conditions for **$Co_4V_2W_{18}$**.[18,19]

Herein we address the following questions: (i) what is the stability of **$Co_4V_2W_{18}$** in aqueous solution using 0.1 M NaPi pH 5.8 and 8.0 as well as sodium borate (NaB) pH 9.0? Does it exhibit "high hydrolytic stability" as previously[12] claimed based on the misassigned ^{51}V NMR, or does **$Co_4V_2W_{18}$** leach $Co(II)_{aq}$ as literature precedent[13,14] suggests one must carefully consider? (ii) What, then, is the true WOCatalytst under the more solar-energy-relevant conditions of electrochemically driven WOC? Is the catalyst **$Co_4V_2W_{18}$** as claimed,[12] or is the catalyst well-precedented[13,14] CoO_x formed from Co(II) dissociated from the Co-POM, or, perhaps, some other catalyst species? (iii) Is the solution stability of **$Co_4V_2W_{18}$** sufficient to even permit a reliable study of its WOC activity? And (iv) more fundamentally, if the stabilities of the V- vs P- congener of **$Co_4X_2W_{18}$** are different (as we will in fact find), then why? What, then, are the implications for POM-based chemistries and catalysis, including Co-POM based WOC? Finally (v) what are the implications of findings for the prior 2014 study[12] and its claim of superior, stable WOC by

$Co_4V_2W_{18}$, in that case with a Ru(III) chemical and photochemical oxidant system? The results that follow paint a rather different picture than the prior report[12] claiming **$Co_4V_2W_{18}$** is a robust, hydrolytically stable, superior activity WOC. The results which follow are also of are of fundamental interest to both POM and WOC chemistries.

3.2 Experimental

General Reagents. $Co(NO_3)_2 \cdot 6H_2O$ (ACS Reagent >99%), $Na_2WO_4 \cdot 2H_2O$ (ACS Reagent >99%), $NaVO_3$ (ACS Reagent >98%), LiBr (ACS Reagent >99%) and $Bi(NO_3)_3$ (ACS Reagent >98%)were purchased from Sigma-Aldrich. Monobasic and tribasic sodium phosphate (ACS Reagent), HCl (12.1 N, ACS Plus), and boric acid (ACS Certified) were purchased from Fisher Scientific. Sodium acetate (99.6%) and glacial acetic acid (ACS Reagent) were purchased from Mallinckrodt. Dimethylglyoxime (DMG, ACS Reagent) was purchased from Fluka. Sodium borate (≥99.5%) was purchased from EM Scientific. Neat (i.e., 200 Proof) EtOH (ACS anhydrous) was purchased from Pharmco-AAPER. The glassy carbon and gold electrodes were polished to a mirror-like sheen using 0.05 μm Al_2O_3 purchased from CH Instruments, rinsed with water, sonicated in water for one minute to remove adsorbed Al_2O_3, rinsed with water, then sonicated in ethanol for one minute and rinsed once more with water prior to use. All reagents were used as purchased without further purification. All aqueous solutions were made from 18 MΩ-cm water from a Barnstead Nanopure water purification system.

Instrumentation. ^{31}P NMR was conducted on a 500 MHz Varian NMR. Spectra were collected at 25 ºC on a 500 MHz Varian NMR spectrometer, the spectral width was −64.9 to +64.9 ppm (26,272.6 Hz) with a 45º pulse angle, 1.000 second relaxation delay and 0.624 second acquisition time. Electrochemistry was performed on a CH Instruments CHI630D using a Ag/AgCl reference electrode purchased from Bioanalytical Systems Inc. (all voltages reported against

Ag/AgCl), a platinum wire counter electrode, and glassy carbon (either 1 cm^2 or 0.071 cm^2) or Au (0.031 cm^2) working electrode, as specified for each experiment. SEM was conducted on a JEOL JSM-6500F, and EDX was collected using a Thermo Electron EDX System. XPS was conducted on a PE-5800 X-Ray Photoelectron spectrometer.

Synthesis of ***$Co_4V_2W_{18}$*** *According to the the 2014*[12] *Study and Its Characterization.* **$Co_4V_2W_{18}$** was synthesized following the 2014 study as close as possible,[12] and characterized extensively.[18] The relevant characterization data are reproduced in Table S3.1 for the convenience of the interested reader. In our recent work, we conducted 3 repeat syntheses of **$Co_4V_2W_{18}$** according to the 2014 studies[12] and labeled them 2A, 2B and 2C in historical order of their synthesis. For all experiments herein, the material from synthesis 2A was used because that material had the closest yield to the 2014 synthesis[12] while following the synthesis in the 2014 report[12] as closely as possible. Sample 2C was also used to test reproducibility. No significant differences were observed, *vide infra*.

Stability of ***$Co_4V_2W_{18}$*** *Determined by* ^{31}*P NMR Line Broadening Analysis of the NaPi Buffer to Quantify* $Co(II)_{aq}$ *Present.* $Co(II)_{aq}$ induced line broadening was used to determine the amount of Co(II) leached from both **$Co_4V_2W_{18}$** and, as a control, **$Co_4P_2W_{18}$** in 0.1 M NaPi pH 5.8 and 8.0. To generate a calibration curve, standard solutions were prepared by diluting stock solutions of $Co(NO_3)_2$, 0.2 M sodium phosphate (NaPi, pH 8.0 or 5.8), and 99.9% D_2O to the concentrations used in the calibration curves to yield 1 mL of 0.1 M NaPi solution with 25% D_2O. The probe was tuned to the ^{31}P signal of the 0.1 M NaPi sample containing no added cobalt. Spectra for the standard curve were collected between data points in the kinetic experiments in order to include any instrument drift in the calibration curve (Figures S3.1 and S3.2 in the Supporting Information). To ensure that precipitation of $Co_3(PO_4)_2$ (K_{sp}= 2.05 x $10^{-35}M^5$)[20] was not

contributing significantly to the analysis (i.e., and under our relatively dilute Co(II) conditions), several standards were monitored over 24 hours. No significant decrease in line broadening over those 24 hrs was observed in samples containing less than 100 μM $Co(II)_{aq}$. The full width at half maximum (FWHM) of the peaks were determined using the VnmrJ instrument software and plotted against the $[Co(II)_{aq}]$ to obtain the calibration curves and corresponding linear regressions (Figures S3.1 and S3.2).

For the stability determination of $\mathbf{Co_4V_2W_{18}}$, 5.5 mg (1.0 μmol) of $\mathbf{Co_4V_2W_{18}}$ was weighed in a 1 dram vial, and dissolved into 4 mL of water with 45 seconds of sonication and mixing using a 1 mL autopipette to ensure complete dissolution of the $\mathbf{Co_4V_2W_{18}}$ powder (yielding a 250 μM $\mathbf{Co_4V_2W_{18}}$ solution). A 20 μL aliquot of this solution was then mixed with 230 μL water, 250 μL D_2O and 500 μL of the appropriate 0.2 M phosphate buffer to yield a final 1.0 mL solution containing 5 μM $\mathbf{Co_4V_2W_{18}}$ and 0.1 M NaPi with 25% D_2O. Time t=0 was set with the addition of water to the $\mathbf{Co_4V_2W_{18}}$ powder; typically 3−4 minutes elapsed between sample mixing and the first ^{31}P NMR spectrum acquisition. Spectra were then obtained approximately every 30 min for 3 h; the exact time of acquisition was variable due to delays in the auto sampler; therefore, the reported time in the NMR file log was used to determine the exact elapsed time.

Controls were performed in which ^{31}P NMR spectra were obtained as described above except with the presence of 25 μM EDTA to chelate $Co(II)_{aq}$. Those crucial controls gave a ^{31}P NMR line width for P_i approximately 2 Hz, *hence within experimental error of the observed line width for Pi in the absence of* $Co(II)_{aq}$*, thereby indicating that intact* $\mathbf{Co_4V_2W_{18}}$ *makes no observable contribution to the observed* ^{31}P *NMR line broadening of the NaPi buffer within experimental error*. The $[Co(II)_{aq}]$ vs Time profiles for $\mathbf{Co_4V_2W_{18}}$ in 0.1 M NaPi pH 8.0 and 5.8 are shown in Figure 3.2.

As a further control, the stability of **$Co_4P_2W_{18}$** was also determined by dissolving 5.4 mg (1.0 μmol) of the sample into 0.5 mL of water, 0.5 mL D_2O, and 1 mL of 0.2 M NaPi pH 8.0 or 5.8 to yield a 2 mL solution containing 500 μM **$Co_4P_2W_{18}$**, 0.1 M NaPi, and 25 % D_2O. Spectra were obtained on 1.0 mL of the Co-POM solution using the same methodology described for **$Co_4V_2W_{18}$**, except data points for pH 5.8 were collected every 90 min (Figure S3.3). An additional control was conducted in which 50 μM EDTA was present in the final dilution of the pH 8.0 solution as a further test if any of the observed line broadening was caused by the intact Co-POM, *vide supra*. A more in depth discussion of this additional control is presented in the Supporting Information for the interested reader.

*Stability of **$Co_4V_2W_{18}$** Determined by a Secondary Method: Cathodic Stripping.* A modified procedure of Krolicka *et al*[21] was used to determine [$Co(II)_{aq}$] via an adsorptive cathodic stripping procedure. This procedure involves the chelation of $Co(II)_{aq}$ by dimethylglyoxime (DMG), followed by $Co(DMG)_2$ adsorption to a glassy carbon electrode, and finally differential pulse voltammetry (DPV) to determine the [$Co(II)_{aq}$]. This is the same general experimental protocol for cathodic stripping that we used in our 2011 paper.[13]

To generate a calibration curve for the cathodic stripping, $Co(NO_3)_2$ was used as an authentic $Co(II)_{aq}$ source with [$Co(II)_{aq}$] ranging from 0 to 20 μM. Each cathodic stripping experiment was conducted in three stages: (i) first a bismuth film was prepared by inserting the working (0.071 cm^2 glassy carbon), counter, and reference electrodes into a 3 dram vial containing a solution with $Bi(NO_3)_3$ (0.02 M), LiBr (0.5 M) and HCl (1.0 M), followed by vigorous stirring for 10 seconds using a 1.5 x 1.0 cm oval magnetic stir bar. After the stirring was stopped, chronoamperometry was conducted at −0.26 V, and the experiment was set to stop after 10 mC of charge had accumulated (typically about 45 seconds). (ii) The electrodes were then removed from

the solution, gently rinsed with water, and then the electrodes were placed into the analyte solution (*vide infra*), followed by vigorous stirring for 10 seconds with a 1.0 x 0.5 cm oval magnetic stir bar. Chronoamperometry was then again conducted at −1.3 V for 15 seconds to allow adsorption of the $Co(DMG)_2$ complex. (iii) Next, the solution was stirred 3 seconds, and DPV was conducted on unstirred solutions from −0.7 to −1.3 V with a 0.004 V increment, 0.05 V amplitude, 0.1 second pulse width, 0.0167 second sampling width, 0.2 second pulse period, and 2 second quiet time. The calibration curve was generated using the peak height of the current response of the DPV plotted against the $[Co(II)_{aq}]$ (Figures S4 and S5 of the Supporting Information). The peak heights of the DPV waves were determined by background subtraction using the CHInstruments software. Background currents were usually 1-2 μA.

To determine the amount of $Co(II)_{aq}$ leached from the complex after 3 hours, a 5 μM solution of $\mathbf{Co_4V_2W_{18}}$ was prepared by dissolving 5.5 mg (1.0 μmol) of 2A into 2.0 mL of water (yielding a 500 μM solution), then diluting 150 μL of the 500 μM solution into 7.35 mL of water and 7.5 mL of the appropriate 0.2 M buffer. This solution was then allowed to age for 3 h prior to addition of DMG. To prepare the analyte solution, 1.0 mL of the resultant aged 5 μM $\mathbf{Co_4V_2W_{18}}$ solution was mixed with 500 μL of a 400 μM DMG solution and 500 μL of the appropriate buffer to yield a 2.0 mL solution containing 2.5 μM $\mathbf{Co_4V_2W_{18}}$, 100 μM DMG, and 0.1 M buffer. This solution was then used as the analyte solution in the cathodic stripping procedure described above. The $[Co(II)_{aq}]$ present in the $\mathbf{Co_4V_2W_{18}}$ solutions was determined using the calibration curves developed for pH 8.0 NaPi and pH 9.0 NaB; the observed value was doubled to account for the 1:1 dilution required for analysis to determine the $[Co(II)_{aq}]$ in the aged solution. The error bars for pH 8.0 0.1 M NaPi and for pH 9.0 0.1 M NaB were determined via three repeated trials in each case. The results of this experiment are given in Table 3.1.

Electrocatalytic WOC of Solutions Beginning with ***$Co_4V_2W_{18}$****: O_2 Quantification.* For O_2 quantification experiments, a custom built two-compartment cell was used (see Figure S3.6 of the Supporting Information). The working compartment was sealed with a Teflon septum and contained 6 mL of the argon-flushed buffer solution with 5 μM Co-POM or 23 μM $Co(NO_3)_2$ (the amount of $Co(II)_{total}$ expected in solution),[22] the working (1 cm^2 glassy carbon), and the reference electrode as well as the O_2 sensor (Ocean Optics FOSPOR-R probe) plus a magnetic stir bar. The counter compartment, separated by a medium glass-frit filter contained the appropriate argon-flushed buffer as well as the platinum counter electrode. The O_2 sensor was calibrated using a two-point calibration of air saturated DI water (typically *ca.* 220 μM, at 22±2°C and approximately 0.84 atm, a typical barometric pressure in mile-high Fort Collins, CO) and O_2-free solutions (generated by adding excess sodium sulfite to the aqueous solution yielding sodium sulfate as a byproduct). Electrolysis was conducted at 1.1 V for five minutes stirring at a rate of 600 rpm. The [O_2] was monitored throughout the reaction using the O_2 sensor. The Faradaic efficiency was determined by comparing the final measured [O_2] with the theoretical [O_2] calculated by integrating the current and converting the total charge to equivalents of O_2, assuming 4e⁻ per O_2 produced. The results are shown in Figure S3.7 of the Supporting Information and Table 3.2.

Electrocatalytic WOC of Fresh and Aged Solutions of ***$Co_4V_2W_{18}$****: Constant Potential Electrolysis.* The long term electrochemical current response of freshly dissolved **$Co_4V_2W_{18}$** was compared with **$Co_4V_2W_{18}$** that had been aged 3 and 24 h, respectively. Hence, electrolysis was conducted at 1.1 V for 1 h on 2.0 mL solutions containing either 23 μM $Co(NO_3)_2$, or 5 μM **$Co_4V_2W_{18}$** (aged less than 5 minutes, aged 3 hours and aged 24 hours, respectively) in each of the three buffer conditions with stirring at 600 rpm in a 1 dram vial. A gold working electrode was used for the prolonged electrolysis because the films showed poor stability on glassy carbon

electrodes (Figure S3.8). The results are given in Figure 3.3 and Figure S3.9 of the Supporting Information.

Electrochemical Characterization of Electrodeposited Films. For the film deposition experiments, a 0.071 cm^2 glassy carbon working electrode was used (polished and rinsed as described in the Materials section), and constant potential electrolysis was carried out at 1.1 V for 30 min with stirring at 600 rpm from a solution containing 5 μM $\mathbf{Co_4V_2W_{18}}$ and 0.1 M of the appropriate buffer (Figures 3.4A, and S3.10). Cyclic voltammetry (CV) was then conducted from 0.5 to 1.2 V at scan rate of 20 mV/s with a positive initial scan polarity and two sweep segments. The electrodes were then removed from the original solution, rinsed gently with water, and placed in a solution containing the buffer-only solution. CV was then conducted on the film in the solution containing only the buffer. Constant potential electrolysis was then conducted in the buffer solution as described above. The resulting voltammograms are shown in Figure 3.4B and Figure S3.11 of the Supporting Information.

Morphological and Compositional Analysis of Electrochemically Deposited Films. The catalytically active film was deposited on a 1 cm^2 glassy carbon electrode (polished as described in the Materials section) by constant potential electrolysis at 1.1 V for 30 min with stirring at 600 rpm in a solution containing 5 μM $\mathbf{Co_4V_2W_{18}}$ and 0.1 M of the appropriate buffer. These films were then gently rinsed with water and allowed to dry in a vacuum desiccator overnight prior to SEM, EDX, and XPS analysis as described in the Instrumentation Section. As an additional control, $\mathbf{Co_4V_2W_{18}}$ was drop cast onto a 1 cm^2 glassy carbon electrode for SEM (Figure 3.5), EDX (Figure S3.12 of the Supporting Information) and XPS (Figure S3.13 of the Supporting Information).

3.3 Results and Discussion

^{31}P NMR Line Broadening Quantification of Co(II)$_{aq}$: Determination of the Stability of ***Co$_4$V$_2$W$_{18}$.*** The [Co(II)$_{aq}$] in solutions of **Co$_4$V$_2$W$_{18}$** was determined employing a method first observed by Klanberg and Dodgen[23] and then developed as an analytical technique by Nocera and co-workers.[24,25] This powerful, sensitive, and relatively direct method is based on the fact that aqueous solutions of paramagnetic cations such as Co(II) or Mn(II) will cause line broadening of the ^{31}P NMR resonance of $H_xPO_4^{-x-3}$ in the NaPi buffer employed.[23] An in depth-discussion of the Co(II)$_{aq}$-induced line broadening is presented in the Supporting Information for the interested reader. The most important parts of that discussion are that the ^{31}P line broadening has a *ca.* 2 μM Co(II) detection limit, *is selective to Co(II)$_{aq}$* (with no detectable contribution from the intact Co-POM as demonstrated herein, *vide infra*, and as discussed further in the Supporting Information), is non-destructive to the Co-POM, is quantitative, and can be conducted *in situ*.

Calibration Curves. Calibration curves were generated in 0.1 M NaPi both pH 5.8 and 8.0 using $Co(NO_3)_2$ as a source of authentic Co(II)$_{aq}$, with [Co(II)$_{aq}$] ranging from 0 to 100 μM (example spectra are provided in Figure S1). The full width at half max (FWHM) was plotted against the [Co(II)$_{aq}$] to generate the calibration curves and corresponding linear regressions (Figure S2 of the Supporting Information). The linear regressions obtained at pH = 5.8 (FWHM = 0.784 [Co(II)] + 2.50; R^2 = 0.998; Figure S2) and pH = 8.0 (FWHM = 1.18 [Co(II)] + 1.97; R^2 = 0.993; Figure S2) were then used for *in-situ* determination of the [Co(II)$_{aq}$] present in solutions containing the Co-POMs.

[Co(II)] Determinations. The ^{31}P NMR-detected [Co(II)$_{aq}$] vs time when beginning with a 5 μM solution of **Co$_4$V$_2$W$_{18}$** is shown in Figure 3.2. The first point to note is that in either pH = 5.8, or pH 8.0 buffer, *the amount of Co(II) detected after just ca. 3 minutes (the earliest point*

possible in the ^{31}P NMR experiment) is between 44-50% of the total Co(II) present in the system (Figures 3.2A and 3.2B, initial point on the blue lines therein)! This experiment by itself answers question (iii) raised in the Introduction, namely if the stability of **$Co_4V_2W_{18}$** in solution is sufficient to even allow a reliable study of its WOC activity? The answer is clearly "no", especially when one considers that the dissociated Co(II) is known to[13,14] form a very active, electrode-bound, CoO_x WOCatalyst—and does herein as well, *vide infra*. That is, doomed to failure is any study that would try to determine the WOC activity of (rapidly decomposing) **$Co_4V_2W_{18}$** in the presence of the (increasing) formation of a very active, electrode-bound CoO_x WOCatalyst. One might even wonder why one would want to know the putative WOC activity of any species as unstable in solution as **$Co_4V_2W_{18}$**.

The second main observation from Figures 3.2A and 3.2B is that **$Co_4V_2W_{18}$** *decomposes 100% within experimental error within one hour at either pH 5.8 or 8.0!* Clearly, according to the direct measurement of Co(II) in solution **$Co_4V_2W_{18}$** is <u>not</u> *"highly stable"*[12] in solution as previously incorrectly claimed based on monitoring a ^{51}V NMR peak that is actually due to[12] *cis*-$V_2W_4O_{19}^{4-}$, a very stable impurity that is present.[18]

Note that the above conclusions do require that an important alternative hypothesis here be disproven, namely the alternative hypothesis that some (to all) of the line broadening conceivably could be caused by the intact Co-POM (i.e., in which intact, POM-bound paramagnetic Co(II) could in principle coordinate to $H_xPO_4^{-x-3}$, thereby inducing line broadening). This alternative hypothesis was disproved via several, what proved to be definitive, control experiments. In the first control, a 500 μM solution of **$Co_4P_2W_{18}$** in 0.1 M NaPi pH 8.0 was used and the ^{31}P NMR line width of the NaPi buffer was measured every 30 min for 3 h to test the accuracy of the ^{31}P NMR method compared to our previously published results[13] for **$Co_4P_2W_{18}$** (that, for a 500 μM

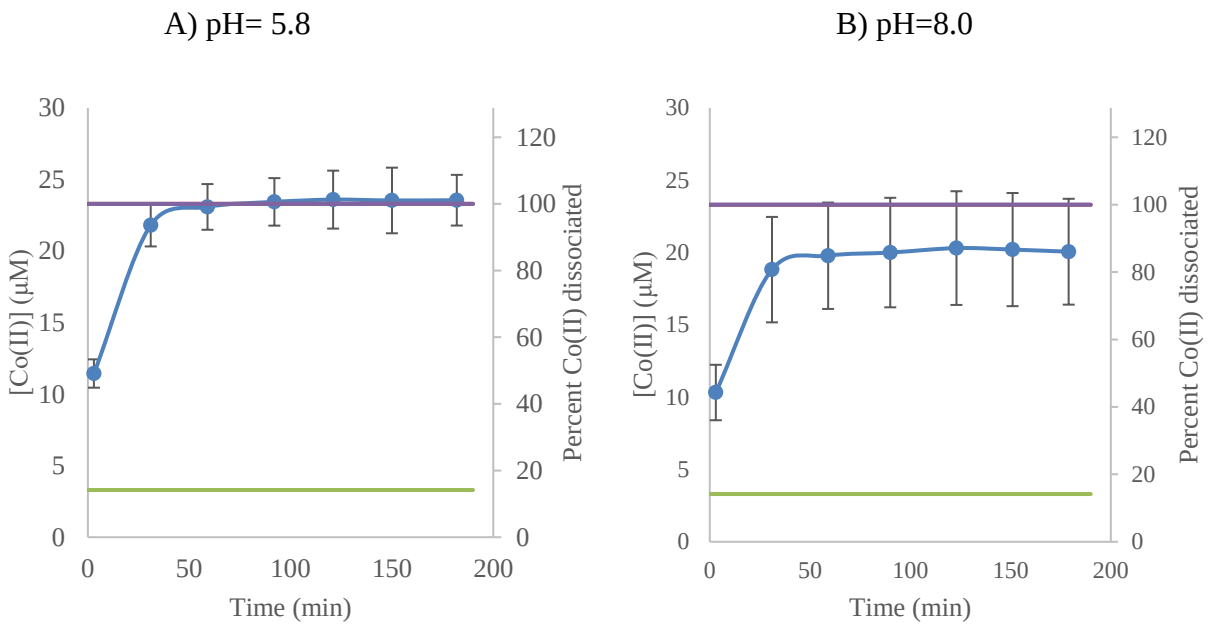

Figure 3.2. [Co(II)aq] (left y-axis) and the percent of total Co(II) dissociated (right y-axis) vs. time as determined by ^{31}P NMR line broadening for a 5 μM solution of **$Co_4V_2W_{18}$** at 25 ºC in 0.1 M NaPi pH 5.8 (A; left) and pH 8.0 (B; right). Purple lines represent the total maximum cobalt concentration in solution calculated if all 4 Co(II) present initially in **$Co_4V_2W_{18}$** are dissociated into solution (20 μM) plus if the the excess Co(II) present present as an impurity by elemental analysis (e.g., Co(II) as a counter cation; 3.3±0.3 μM) is added to the total possible Co(II), for a total 23.3 ± 0.3 μM Co(II), defined as 100% Co(II). The green lines represent the 3.3±0.3 μM Co(II) impurity found by elemental analysis.[22] The blue lines are just lines to guide the eye (i.e., and are not curve-fits). The end percentage in Figures 2A and 2B are nominally 102(±12)% and 87(±18)%, that is, 100% within experimental error. *Note that even the earliest point experimentally possible at ~3 minutes shows the formation of ~44-50% Co(II).*

solution of **$Co_4P_2W_{18}$**, in 0.1 M NaPi pH 8.0, at room temperature and after three hours of aging, the [$Co(II)_{aq}$] measured previously was 56 ±2 μM (by cathodic stripping) and 58 ± 2 μM (by linear sweep voltammetry[13]). The [$Co(II)_{aq}$] value determined herein by the (more direct) ^{31}P NMR line-broadening method after three hours is [$Co(II)_{aq}$] = 55 ± 3 μM, *within experimental error of the two previously determined values of 56 ±2 μM and 58 ± 2 μM*,[13] Figure S3.3 of the Supporting Information. Next, to determine if there is any measurable line broadening caused by the intact Co-POM, 50 μM EDTA was added to the solution to complex the free $Co(II)_{aq}$ and remove aqueous Co(II) from any observed, residual line broadening (the 50 μM EDTA is a 10-fold lower

concentration than the starting [Co-POM], but is a 5-fold excess of the beginning [$Co(II)_{aq}$] that is detected). The resultant ^{31}P NMR line width for **$Co_4P_2W_{18}$** in the presence of 50 μM EDTA *is just the background level of 2 Hz,* that is, identical to the natural line width of Pi in the absence of Co(II) within experimental error. (Additional discussion of this crucial control experiment is presented in the Supporting Information for the interested reader.) Just to be sure, we then conducted a second control with **$Co_4V_2W_{18}$**, but now with half the amount (25 μM) EDTA (i.e., in slight excess of the total [Co(II)] detected of 23 μM). Again, no additional line broadening beyond the natural, 2 Hz line width for Pi under our NMR conditions was observed. *These controls demonstrate that all of the observed ^{31}P NMR line broadening is caused by $Co(II)_{aq}$ and not intact* ***$Co_4V_2W_{18}$****, or any other conceivable Co-POM fragment,* within experimental error of the measurement and under the stated conditions.

Stability of ***$Co_4V_2W_{18}$*** *Determined By a Second Method: Adsorptive Cathodic Stripping.* To verify the [$Co(II)_{aq}$] determined by ^{31}P NMR line broadening by a second independent physical method, adsorptive cathodic stripping was used. As already noted, this technique was successfully used previously to quantify the amount of Co(II) leached from the phosphorus analog, **$Co_4P_2W_{18}$.**[13] Importantly, cathodic stripping also allows [$Co(II)_{aq}$] quantification in buffers other than phosphate, notably in pH = 9.0 sodium borate. The cathodic stripping technique consists of complexation of $Co(II)_{aq}$ by dimethylglyoxime (DMG) followed by adsorptive stripping of this complex on an electrochemically deposited bismuth film premade on a glassy carbon electrode.[21]

To start, an adsorptive cathodic stripping calibration curve was created using $Co(NO_3)_2$ as an authentic source of $Co(II)_{aq}$ for both pH 8.0 NaPi and pH 9.0 NaB, Figures S3.4 and S3.5 of the Supporting Information. (Attempts at generation of a calibration curve in *pH 5.8* NaPi showed little current response in the desired cobalt concentration range and hence proved unsuccessful;

this likely indicates poor formation or adsorption of $CoDMG_2$ to the Bi film electrode at this more acidic pH.) Next, the $[Co(II)_{aq}]$ by cathodic stripping of aqueous solutions of 5 μM **$Co_4V_2W_{18}$** was obtained in pH 8.0 NaPi and pH 9.0 NaB. The resulting $[Co(II)_{aq}]$ values are 25.5 ± 2.3 and 24.2 ±0.9 μM, corresponding to 109(±15)% and 104(±11)% decomposition (again after three hours of aging in 0.1 M pH 8.0 NaPi and pH 9.0 NaB, respectively). A few potential caveats associated with the $[Co(II)_{aq}]$ values determined by cathodic stripping are discussed in a footnote for the interested reader.[26] A comparison of all the Co(II) values is presented in Table 3.1. The results demonstrate that the Co(II) values determined by cathodic stripping are the same within experimental error of the Co(II) values as seen by ^{31}P NMR, adding confidence to both the values and to each method.

In short, the data from the two independent, ^{31}P NMR and cathodic stripping techniques demonstrate conclusively that **$Co_4V_2W_{18}$** is *not* hydrolytically stable in 0.1 M NaPi at pH 5.8, 8.0 or NaB pH 9.0. Instead, 100(±≤15)% of the cobalt initially present in "**$Co_4V_2W_{18}$**" is leached into solution within three hours. The bottom line here is both unequivocal and quite clear: the results compellingly demonstrate that, regardless of the buffer or pH, *all of the cobalt presently initially in the* ***$Co_4V_2W_{18}$*** *precatalyst winds up as aqueous Co(II) in solution in three hours within the stated experimental error.*

Table 3.1. Comparison of [$Co(II)_{aq}$] at three hours as determined by ^{31}P NMR vs that determined by cathodic stripping. The upper limit is again 23.3 ± 2.3 μM Co(II) present in the starting **$Co_4V_2W_{18}$** in each case (as detailed in the caption for Figure 2). Shown in bold below the Co(II) concentration is the percent of total Co(II) present initially in **$Co_4V_2W_{18}$** that is accounted for by the detected amount of $Co(II)_{aq}$.

Buffer	*[$Co(II)_{aq}$] by 31P NMR (μM)* *(% Co(II))*	*[$Co(II)_{aq}$] by cathodic stripping (μM)* *(% Co(II))*
0.1 M NaPi pH 8	20 ± 4 **87 ±18**	25.5 ± 2.3 **109 ± 15**
0.1 M NaPi pH 5.8	24 ± 2 **102 ± 12**	NA
0.1 M NaB pH 9	NA	24.2 ± 0.9 **104 ± 11**

These results are, unfortunately, completely opposite to those reported in the 2014 publication[12] which claimed that **$Co_4V_2W_{18}$** "exhibits high hydrolytic stability."[12] That prior claim is fully disproven by the results herein. Additionally, we now know[18] that the prior claim of stability was based on a misassignment of the ^{51}V NMR peak at -510(±1.4) ppm to **$Co_4V_2W_{18}$** when that resonance is actually due to the known, very stable,[19] *cis*-$V_2W_2O_{19}^{4-}$ that is an impurity in the synthesis as well as one of the hydrolysis products formed from **$Co_4V_2W_{18}$**.[18] Restated, the stability being measured previously by ^{51}V NMR was that of *cis*-$V_2W_2O_{19}^{4-}$, not **$Co_4V_2W_{18}$** as believed.[12]

Electrocatalytic WOC Beginning with ***$Co_4V_2W_{18}$*** *and* O_2 *quantification.* The next tasks were (a) to determine the WOC activity and associated O_2 yield, and (b) to determine what percentage of that observed yield/activity is accounted for by the leached $Co(II)_{aq}$.

Choice of Aging Time and Other Standard Conditions. For these experiments, we had to choose a set of "Standard Conditions", and specifically the aging time. Post some reflection, we chose a 3 hour aging time as before[13] as it is actually *a very minimalistic time frame* if one considers that any WOC catalyst of true practical interest might have to perform $10^{3\text{-}4}$ *or more hrs* of WOC to achieve lifetimes (TTOs, total turnovers) that may approach 10^9 or more. For example, suppose that a Co-POM has a TOF ~10^3 s^{-1} as originally claimed for **$Co_4V_2W_{18}$**.[12] Hence, for 10^9 TTOs, **$Co_4V_2W_{18}$** would have had to have been table for $\geq 10^6$ sec (which is ≥277 hrs), nearly 100 times the chosen 3 hr stability test employed as part of the present studies as a *minimalistic test*.[27]

WOC Activity and Associated O_2 *Faradic Efficiencies.* Following our published protocol,[13] **$Co_4V_2W_{18}$** was aged three hours in the respective buffers (pH 5.8, 8.0, 0.1 M NaPi or pH 9.0 NaB) and the WOC activity was then determined at 1.1 V corresponding to 410, 540 and 600 mV overpotential for water oxidation at pH 5.8, 8.0 and 9.0, respectively. Electrolysis was conducted on a 1 cm^2 glassy carbon electrode for five minutes in a custom built U-cell (Figure S3.6). Because studies[25] by Nocera *et al.* demonstrate that glassy carbon electrodes can oxidize to CO_2 at potentials greater than 1.2 V vs Ag/AgCl, all of our WOC studies were conducted at 1.1 V vs. Ag/AgCl. Figure S8 of the Supporting Information shows a representative O_2 evolution profile beginning, in that example, with 5 μM **$Co_4V_2W_{18}$** precatalyst in 0.1 M NaPi pH 8.

The deposition of an iridescent blue/black film upon electrolysis performed as above is observable to the naked eye. The theoretical O_2 produced was obtained by integrating the current; in Figure S3.7 the theoretical [O_2] vs time is compared to the [O_2] measured by the Ocean Optics

probe. The observed experimental O_2 yield was always greater than 80%, and usually closer to 100 ± 5%. Any lower yields are likely due to O_2 escape from the cell, and not from a side reaction such as glassy carbon decomposition.[25]

Because the O_2 yield was close to 100%, we used the total charge passed (i.e., the integrated current) to calculate the μmol amount of O_2 as our metric for catalyst comparison, with 23 μM $Co(NO_3)_2$ as the "standard" (i.e., recall from the caption to Figure 3.2 that 23 μM $Co(II)_{aq}$ is the amount of Co(II) expected from 100% dissociation of the four Co(II) in **$Co_4V_2W_{18}$** plus the amount of Co(II) present as a counter-cation impurity according to elemental analysis).

Table 3.2. A comparison of the O_2 yield (μmol) for each of the buffer conditions from: 23 μM $Co(NO_3)_2$ as the standard for comparison; 3 h aged solutions of 5 μM **$Co_4V_2W_{18}$**; 5 μM *cis*-$V_2W_4O_{19}^{4-}$; and 5 μM *cis*-$V_2W_4O_{19}^{4-}$ plus 23 μM $Co(NO_3)_2$.

	0.1 M NaPi pH 5.8	*0.1 M NaPi pH 8.0*	*0.1 M NaB pH 9.0*
$Co(NO_3)_2$	**0.027 ± 0.003**	**0.35 ± 0.02**	**0.5 ± 0.1**
$Co_4V_2W_{18}$	0.030 ± 0.001	0.36 ± 0.05	0.7 ± 0.2
cis-$V_2W_4O_{19}^{4-}$	0.01 ± 0.002	0.007± 0.003	0.1 ± 0.1
cis-$V_2W_4O_{19}^{4-}$ with $Co(NO_3)_2$	0.037 ± 0.001	0.28 ± 0.04	0.7 ± 0.2

The data in Table 3.2, second entry left to right, make apparent that the amount of free cobalt detected after 3 hrs aging accounts for 90 ± 32, 97 ± 15, and 71 ± 25 % of the observed WOC activity when beginning with **$Co_4V_2W_{18}$**, at pH 5.8, 8.0 and 9.0, respectively, and within the stated error limits (which are a bit larger than desired, but not unexpected, because variables such as the film deposition rate, resulting film thickness, morphology, and microstructure that can influence the observed WOC activity). Also given in Table 3.2 are the controls of using *cis*-$V_2W_4O_{19}^{4-}$ without, and with, added $Co(NO_3)_2$, controls done since *cis*-$V_2W_4O_{19}^{4-}$ is a detected

decomposition product of **$Co_4V_2W_{18}$.** The results show that *cis*-$V_2W_4O_{19}^{4-}$ is, as expected, a poor WOCatalyst: adding *cis*-$V_2W_4O_{19}^{4-}$ does not improve the observed WOC beyond experimental error vs $Co(NO_3)_2$ alone. The data at pH 5.8 is arguably an exception to this statement, but not at 3σ error bars.

Overall, the bottom line of the O_2 quantification is that *when conducting electrocatalytic WOCatalysis beginning with **$Co_4V_2W_{18}$**, the equivalent amount of $Co(NO_3)_2$ to the Co(II) detected in solution can account for 100 (*±15-32*)% of the observed, electrochemically driven water-oxidation catalysis*. *(IV) Comparison of Electrocatalytic WOC Activity from Fresh and Aged Solutions of **$Co_4V_2W_{18}$** and $Co(NO_3)_2$ via Prolonged Electrolysis on a Gold Electrode for Each Buffer Condition.* Because aging the solution could, in principle, lead to the formation of a different catalyst, we wanted to compare the WOC activity of **$Co_4V_2W_{18}$** after aging less than 5 minutes, and after aging 3 hours and 24 hours. Conducting extended electrolysis experiments allows for the observation of the more thermodynamically stable catalyst that forms under the reaction conditions. These particular electrolysis experiments were carried out using a gold electrode because a current decay is observed when using glassy carbon electrodes (Figure S3.8).

The current density (J) vs time curves are presented in Figure 3.3, and Figure S3.9 of the Supporting Information. Note that because we have demonstrated that the O_2 Faradaic is ~100% within experimental error, the current (J) can be taken as a reliable measure of the WOC.

The J vs t profiles for solutions beginning with **$Co_4V_2W_{18}$** shown in Figures 3.3 and S3.9 do not show steady current density with time, as is expected for a molecular catalyst (basically a curve similar to the blank in Figure 3.3, but at a higher J value). Instead, the current grows over time to ca. ≥8 times the starting current density, which is consistent with the formation of a new, more active, (CoO_x, vide infra) catalyst. Furthermore, for every buffer condition, a slight increase

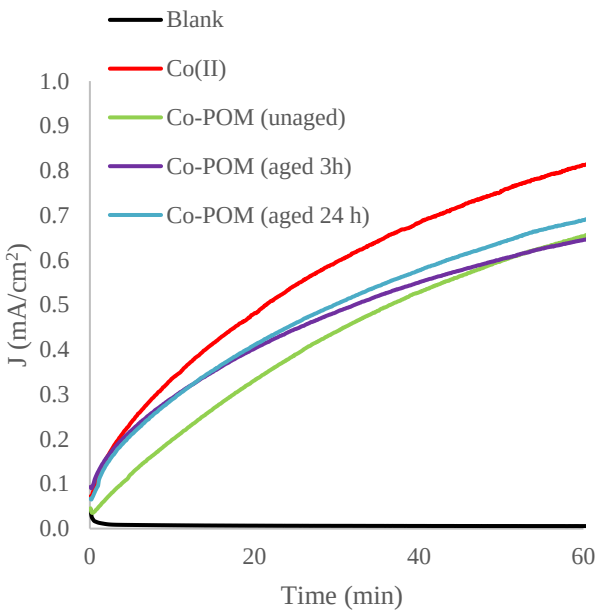

Figure 3.3. Current Density (mA/cm^2) vs time (min) of **$Co_4V_2W_{18}$**: unaged (less than 5 min); aged 3 h; and aged 24 h, and 23 μM $Co(NO_3)_2$ (each in 0.1 M pH 5.8 NaPi). This same experiment conducted in both 0.1 M pH 9.0 NaB and 0.1 M pH 8.0 NaPi is presented in the Supporting Information, Figure S9. The data demonstrate the expected result[13,14] that the Co(II) released in solution can account for all (actually more than) the activity seen when beginning with the **$Co_4V_2W_{18}$** precatalyst.

in the initial activity is observed after aging the Co-POM solutions. This observation is consistent with the release of $Co(II)_{aq}$ (as indicated by ^{31}P NMR line broadening analysis) as a precursor to form a well-precedented[13] heterogeneous CoO_x WOCatalyst. However, the freshly dissolved solutions and the aged solutions display characteristically similar J vs. t profiles. Moreover, because they approach the same steady state current density, we can conclude that *aging the solutions does not have a significant effect on the formation of a more thermodynamically favored catalyst* (than CoO_x, *vide infra*).

While there are small (≤30%), interesting differences in the activity of the films compared to the films formed from only $Co(II)_{aq}$ and NaPi (a point discussed more in the Supporting Information along with Figure S3.9), the bottom line of the J vs time experiments is that they are

fully consistent with and supportive of Co(II) as a precatalyst to the kinetically dominant WOCatalyst, CoO_x.

Electrochemical Characterization of the Deposited Films: Demonstration that the Catalytic Activity is Predominantly Carried by the Deposited Film. Following our 2011 protocol,[13] constant potential electrolysis was carried out in a 5 μM **$Co_4V_2W_{18}$** solution with a 0.1 M solution of the appropriate buffer at 1.1 V at a 0.071 cm^2 glassy carbon electrode for 30 minutes (Figure 3.4A, S3.10) to obtain an electrocatalytically active film. The growth of the catalytic current with time is shown in Figure 3.4A, blue trace, consistent with the formation of a more active catalyst. Cyclic voltammetry (CV) was then conducted on the electrodeposited film in the original 5 μM **$Co_4V_2W_{18}$** solution (Figure 3.4B, blue trace).

Next, the resultant electrodes with the deposited film were removed, rinsed gently with water and placed into a solution containing only the buffer as a supporting electrolyte (i.e., without any Co-POM in solution). In this buffer-only solution, the CV of the film was repeated (Figure 3.4B, red trace). Finally, constant potential electrolysis was again conducted using the film in the buffer-only solution (Figure 3.4A, red trace). The fact that the current density for this film in the buffer-only solution begins at approximately the same value as in the Co-POM solution indicates that essentially all of the catalytic activity is retained by the film itself. The current subsequently decays over time in the buffer-only solution because of poor film adhesion to glassy carbon (Figure 3.4A, red trace) as seen previously.[13] The preservation of the catalytic activity of the film is also demonstrated by the nearly identical CV traces of the film in the original 5 μM **$Co_4V_2W_{18}$** solution (Figure 3.4B, blue trace) in comparison with the CV of the film in the buffer-only solution (Figure 3.4B, red trace). These two controls taken together effectively demonstrate that *the heterogeneous, electrode-bound film accounts for all of the catalytic current.*

A) Prolonged Electrolysis

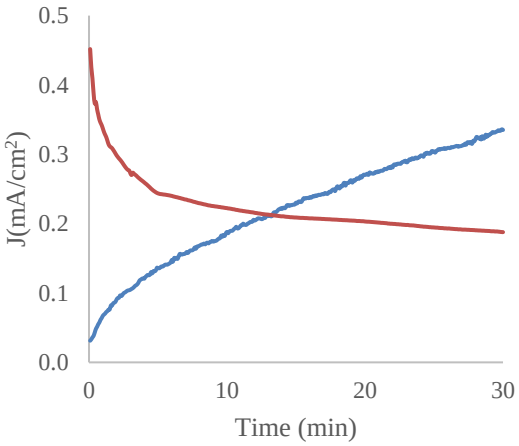

B) Cyclic Voltammetry

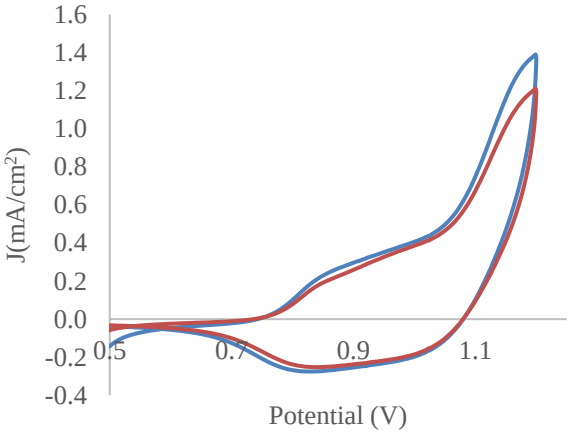

Figure 3.4. A) Constant potential electrolysis of 5 μM **$Co_4V_2W_{18}$** in pH 5.8, 0.1 M NaPi at 1.1 V for 30 minutes (blue trace) and constant potential electrolysis of the deposited film in pH 5.8, 0.1 M NaPi at 1.1 V for 30 minutes in the absence of **$Co_4V_2W_{18}$** dissolved in solution (red trace). The observation of catalytic current in buffer-only solution demonstrates that the electrode bound film formed is the dominant electrochemical catalyst derived from solutions of **$Co_4V_2W_{18}$**. B) CV of the deposited film in the original 5 μM **$Co_4V_2W_{18}$** in pH 5.8, 0.1 M NaPi solution (blue trace) and CV of the deposited film in buffer-only, pH 5.8, 0.1 M NaPi. The two CV's are nearly identical, thereby demonstrating that the electrode-bound film is the dominant WOC when beginning with **$Co_4V_2W_{18}$**. This experiment was repeated for both 0.1 M pH 9.0 NaB and 0.1 M pH 8.0 NaPi, results presented as Figures S3.10 and S3.11 in the Supporting Information.

Morphological and Compositional Characterization of the Electrodeposited Film. Electrodes for SEM, EDX, and XPS were prepared using the 30 minute bulk electrolysis and film-deposition time in 5 μM **$Co_4V_2W_{18}$** solution with a 0.1 M solution of the appropriate buffer, all at 1.1 V using a 1.0 cm^2 glassy carbon electrode. The electrodes were then immediately removed from solution, rinsed with water, and allowed to dry slowly in air before being placed in a vacuum desiccator.

SEM images of the samples displayed a morphology similar to the well-known CoO_x catalyst formed from aqueous Co(II), including the presence of nodules (Figure 3.5).[24,28] Significantly, EDX collected on the same samples (Figure S3.12) displayed *no detectable tungsten or vanadium (i.e., "no" being below the* instrumental detection limit of at least 1 wt%, and probably closer to 0.1 wt%), indicating the absence of any detectable **$Co_4V_2W_{18}$** or other, W or V-containing fragment. This is the same result we obtained before when starting with the P-congener, **$Co_4P_2W_{18}$**.[13]

XPS was also conducted on the electrodeposited film for a more surface-sensitive analysis and as an additional control (Figure S3.13). Once again, no detectable (i.e., <1 wt%) tungsten or vanadium is observed in the XPS spectra. The observed Co:P ratios are 1.2:1 and 2.1:1 for electrolysis carried out at pH 8.0 and 5.8, respectively, comparable to the CoO_x film prepared by Nocera *et al.* which exhibited a Co:P ratio of 2.1:1.[28] Hence, the heterogeneous films deposited from solutions of **$Co_4V_2W_{18}$** show similar compositions and morphological properties to authentic CoO_x films derived from $Co(NO_3)_2$. The results point squarely to CoO_x as the predominant WOC under electrocatalytic conditions when beginning with **$Co_4V_2W_{18}$** as a precatalyst and under electrochemically driven WOC in 0.1 M NaPi pH = 5.8, 8.0 and NaB pH =9.0 with an applied potential of 1.1 V vs. Ag/AgCl. Overall, the film characterization results *corroborate the*

hypothesis that the in situ formed CoO_x film is the active, electrochemically derived and driven WOCatalyst derived from ***$Co_4V_2W_{18}$.***

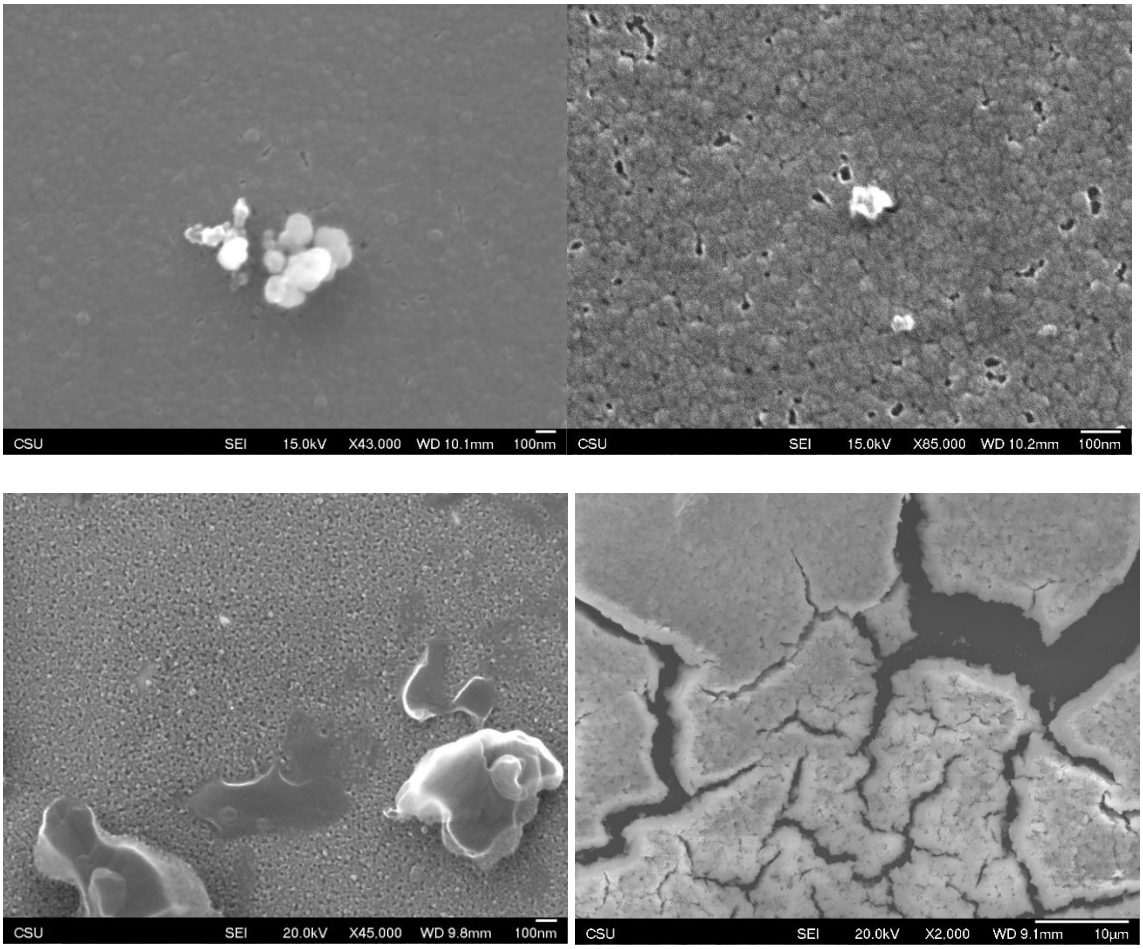

Figure 3.5. SEM of CoO_x film deposited from bulk electrolysis of 5 µM **$Co_4V_2W_{18}$** conducted at 1.1 V vs. Ag/AgCl for 30 minutes in 0.1 M NaPi, pH 8 or 5.8 (top left and right respectively), 0.1 M NaB, pH 9 (bottom left), and a 5 µM unbuffered aqueous solution of **$Co_4V_2W_{18}$** drop cast onto a glassy carbon electrode (bottom right).

Discussion of the Different Stabilities Observed for $Co_4V_2W_{18}O_{68}^{10-}$ vs $Co_4P_2W_{18}O_{68}^{10-}$.

An interesting finding when the present work is combined with our prior study[18] is that **$Co_4\underline{V}_2W_{18}$** shows significantly *decreased* solution hydrolytic stability compared to its P-analog, **$Co_4\underline{P}_2W_{18}$**. Because the V vs P (i.e., VO_4^{3-} vs PO_4^{3-}) central core is the only difference in these two isostructural compounds,[12,15,16] the difference in their solution stabilities must derive from the V vs. P substitution. Hence, it is of fundamental interest to POM chemistry to try to understand this

difference. Moreover, understanding what decreases the stability of the V-congener could, at least in principal, provide the insights needed to go the other direction and synthesize hydrolytically *more stable* Co-POMs for WOC.

A look at the bond distances from the crystal structures[12,15,16,29] of the two Co-POMs reveals that the Co-O bonds are largely unaffected, both average 2.09 Å. However, *the average V–O bond distance of 1.70 Å compared to the phosphorous analog which has an average P–O bond distance of 1.57 Å (a change of 0.13 Å) is a non-negligible change*, and leads to the hypothesis that this V–O vs P–O bond distance is related to the relative instability of the V-congener. A second possible factor is the huge formation constant for the formation of stable *cis*-$V_2W_4O_{19}^{4-}$, *ca.* 10^{59} in 0.6 M NaCl solution at 25 ˚C,[19] which could serve as a driving force for decomposition of $\mathbf{Co_4V_2W_{18}}$ by scavenging V(IV) and W(VI) released by hydrolysis of $\mathbf{Co_4V_2W_{18}}$.

However, overall, the greater instability of the isostructural V- vs P- $\mathbf{Co_4X_2W_{18}O_{68}^{10-}}$ merits additional study, including answering the following questions: (i) is that stability difference primarily thermodynamic or kinetic in origin? (ii) What are the full hydrolysis product stoichiometry and accompanying kinetics and mechanism of the V- and P- $\mathbf{Co_4X_2W_{18}O_{68}^{10-}}$ decomposition reaction? (iii) Is Co(II) leaching primarily dissociative or associative (and what is the latter as a function of the [Pi], for example)? The needed, additional V- and P- $\mathbf{Co_4X_2W_{18}O_{68}^{10-}}$ degradation and Co(II) leaching mechanism studies promise to be of fundamental interest to POM and related chemistries, but are beyond the scope of the present study.

Implications of This Work for Previous Studies with $\boldsymbol{Co_4V_2W_{18}}$. The stability findings presented in this paper, of 40-50% $\boldsymbol{Co_4V_2W_{18}}$ decomposition in 3 minutes and ~100% decomposition within experimental error within 3 hrs in pH 5.8 to 8.0 buffers raises serious questions about the prior claim that $\boldsymbol{Co_4V_2W_{18}}$ serves as an intact WOCatalyst—it is conceivable

that it does, but unlikely given the hydrolytic instability of ***$Co_4V_2W_{18}$***. The similarities and differences between the systems employed in the present study vs the literature 2014 study are summarized and discussed in the Supporting Information for the interested reader (Table S3.2). A discussion of the previous study's[12] attempt to disprove CoO_x as a catalyst in that chemical oxidant system is also presented in the Supporting Information for the interested reader.

3.4 Summary and Conclusions

Herein, we demonstrate the following key findings:

• The decomposition of **$Co_4V_2W_{18}$** in both NaPi and NaB buffer occurs in a smooth fashion over time, with the Co(II) quickly growing in over time as seen in Figure 3.2, reaching 40-50% even after ~3 minutes.

• Over 3 hrs, 5 μM **$Co_4V_2W_{18}$** in 0.1 M NaPi and NaB buffer, pH 5.8-9.0, decomposes by 87(±18)-102(±12)% (Table 3.1, Figure 3.2), a result confirmed by the two independent physical techniques, ^{31}P NMR line broadening and cathodic stripping.

• The rapid decomposition of **$Co_4V_2W_{18}$** to $Co(II)_{aq}$ then forms the expected[13,14] electrode bound CoO_x. That CoO_x film WOCatalyst accounts for 100 (±15-32)% of the observed electrocatalytic WOC during even the first five minutes of electrolysis (Table 3.2) and under conditions where the Faradaic efficiency is 100% within experimental error.

• Prolonged electrolysis plus cyclic voltammetry demonstrate that the resultant film carries all of the catalytic current within experimental error (Figures 3.4, S3.10, and S3.11). The heterogeneous phase formed *in situ* was analyzed via SEM (Figure 3.5), EDX (Figure S3.12) and XPS (Figure S3.13). Its composition and morphology are consistent with the well-known CoO_x phase, one shown to *contain no detectable amounts of tungsten or vanadium*, consistent with that new, catalytically active phase being precedented CoO_x.

• The data taken together demonstrate that, under electrocatalytic conditions in pH 5.8 or 8.0 0.1 M NaPi and pH 9.0 0.1 M NaB, the dominant electrochemically driven WOCatalyst beginning with 5 μM **$Co_4V_2W_{18}$** *is the Nocera type heterogeneous CoO_x derived from Co(II) leached from the hydrolytically very unstable polyoxometalate,* **$Co_4V_2W_{18}$** plus any Co(II) impurity present inintially as a counter-cation.

• Efforts to understand the dramatic difference in the stability of the X = V- vs P- congener of **$Co_4X_2W_{18}$** suggest hypotheses related to the (longer) V–O vs P–O bonds, and / or the high formation constant and resultant stability of *cis*-$V_2W_4O_{19}^{4-}$ that, as a decomposition product for just the V-congener, could contribute to its lower kinetic stability. Further experimental and computational investigations of the stability difference between the V and P congeners of **$Co_4X_2W_{18}O_{68}^{10-}$** would be welcome, however.

• The prior 2014 study,[12] in which a misassigned ^{51}V NMR −507 peak actually due to stable *cis*-$V_2W_4O_{19}^{4-}$ was used to argue for the stability of **$Co_4V_2W_{18}$**, is therefore and hereby cast into serious doubt. A careful and critical reinvestigation of that work will be required to determine if any of the **$Co_4V_2W_{18}$** remaining in solution at a given time can be a homogeneous WOC with $Ru(bpy)_3^{3+}$ as the chemical oxidant, as has been claimed.[12] Regardless of the outcome of that needed study, the claim that **$Co_4V_2W_{18}$** has "high hydrolytic stability"[12] is disproven by the present study.

Supporting Information. **Table S3.1.** Characterization data for the **$Co_4V_2W_{18}$** used herein. **Figure S3.1.** Example ^{31}P NMR spectra **Figure S3.2.** Calibration curve 0.1 M NaPi pH 8.0 and 5.8. **Figure S3.3.** $[Co(II)]_{aq}$ vs. time for **$Co_4P_2W_{18}$** *Phenomenological Discussion of $Co(II)_{aq}$ Induced Line Broadening and Implications for Ion Pairing, Exchange Rates of Co(II)/HPO_4^{2-} or PO_4^{3-}, and Rationalization of Why the Intact POMs Do Not Contribute to the Observed Line*

Broadening. **Figure S3.4.** Example differential voltammograms of $Co(NO_3)_2$ in 0.1 M NaPi pH = 8.0. **Figure S3.5.** Calibration curve 0.1 M NaPi pH 8.0 and NaB pH 9.0. **Figure S3.6.** Photograph of the custom built U-cell employed for O_2 quantification experiments. **Figure S3.7.** Representative O_2 evolution profile **Figure S3.8.** Prolonged WOC beginning with 5 μM **$Co_4V_2W_{18}$** in pH 8.0 0.1 M NaPi on the 0.071 cm^2 glassy carbon electrode. **Figure S3.9.** Prolonged Electrolysis of 23 μM $Co(NO_3)_2$ and 5 μM **$Co_4V_2W_{18}$** on a gold electrode in pH 8.0 NaPi and pH 9.0 NaB; both buffers were 0.1 M. *Discussion of the Prolonged Electrolysis Experiments.* **Figure S3.10.** Prolonged electrolysis of 5 μM **$Co_4V_2W_{18}$** in 0.1 M NaPi pH 8.0 and 0.1 M NaB pH 9.0 on a glassy carbon electrode. **Figure S3.11.** Cyclic voltammograms of the films **Figure S3.12.** EDX spectra of the CoO_x films obtained from the electrolysis of **$Co_4V_2W_{18}$**. **Figure S3.13.** XPS of the CoO_x films obtained from the electrolysis of **$Co_4V_2W_{18}$.** *Discussion of the similarities and differences between the present and the 2014 study.* **Table S3.2.** A comparison of the similarities and differences of the present vs the 2014 study. *Discussion of previous literature attempts to disprove CoO_x when studying $Co_4V_2W_{18}$ for WOC.*

REFERENCES

1 Lewis, N. S.; Nocera, D. G. *PNAS* **2006**, *103*, 15729-15735.

2 Pope, M. T. *Heteropoly and isopoly oxometalates*; Springer-Verlag, 1983.

3 Pope, M.; Müller, A. *Polyoxometalates: From Platonic Solids to Anti-Retroviral Activity*: Springer Science & Business Media, 1994.

4 Yamase, T.; Pope, M. *Polyoxometalate Chemistry for Nano-Composite Design*; Springer Science & Business Media, 2006.

5 Sartorel, A.; Carraro, M.; Scorrano, G.; Zorzi, R. D.; Geremia, S.; McDaniel, N. D.; Bernhard, S.; Bonchio, M. *J. Am. Chem. Soc.* **2008**, *130*, 5006-5007.

6 Yin, Q.; Tan, J. M.; Besson, C.; Geletii, Y. V.; Musaev, D. G.; Kuznetsov, A. E.; Luo, Z.; Hardcastle, K. I.; Hill, C. L. *Science* **2010**, *328*, 342-345.

7 Besson, C.; Huang, Z.; Geletii, Y. V.; Lense, S.; Hardcastle, K. I.; Musaev, D. G.; Lian, T.; Proust, A.; Hill, C. L. *Chem. Commun.* **2010**, *46*, 2784-2786.

8 Zhu, G.; Geletii, Y. V.; Kögerler, P.; Schilder, H.; Song, J.; Lense, S.; Zhao, C.; Hardcastle, K. I.; Musaev, D. G.; Hill, C. L. *Dalton Trans.* **2012**, *41*, 2084-2090.

9 Zhu, G.; Glass, E. N.; Zhao, C.; Lv, H.; Vickers, J. W.; Geletii, Y. V.; Musaev, D. G.; Song, J.; Hill, C. L. *Dalton Trans.* **2012**, *41*, 13043-13049.

10 Goberna-Ferrón, S.; Vigara, L.; Soriano-López, J.; Galán-Mascarós, J. R. *Inorg. Chem.* **2012**, *51*, 11707-11715.

11 Evangelisti, F.; Car, P.-E.; Blacque, O.; Patzke, G. R. *Catal. Sci. Technol.* **2013**, *3*, 3117-3129.

12 Lv, H.; Song, J.; Geletii, Y. V.; Vickers, J. W.; Sumliner, J. M.; Musaev, D. G.; Kögerler, P.; Zhuk, P. F.; Bacsa, J.; Zhu, G.; Hill, C. L. *J. Am. Chem. Soc.* **2014**, *136*, 9268-9271.

13 Stracke, J. J.; Finke, R. G. *J. Am. Chem. Soc.* **2011**, *133*, 14872-14875.

14 Stracke, J. J.; Finke, R. G. *ACS Catal.* **2014**, *4*, 909-933.

15 (a) Weakley, T. J. R.; Evans, H. T.; Showell, J. S.; Tourné, G. F.; Tourné, C. M. *J. Chem. Soc., Chem. Commun.* **1973**, 139-140. (b) Finke, R. G.; Droege, M. W.; Domaille, P. J. *Inorg. Chem.* **1987**, *26*, 3886-3896.

16 Li, B.; Yan, Y.; Li, F.; Xu, L.; Bi, L.; Wu, L. *Inorg. Chim. Acta* **2009**, *362*, 2796-2801.

17 (a) One reason the TOFs claimed for $\mathbf{Co_4V_2W_{18}}$ vs that for $\mathbf{Co_4P_2W_{18}}$ exhibit a 200-fold difference, yet show only a 2-fold difference in oxygen yield, is due to the reported TOFs being based on the rate of $[Ru(III)(bpy)_3]^{3+}$ disappearance. That rate measures primarily (the dominant[17b]) side reaction of oxidation of the bpy ligands, and not just the desired O_2 production.[17b]

That said, the factor of 200 difference in rate claimed for **$Co_4V_2W_{18}$** vs **$Co_4P_2W_{18}$** remains unexplained by the prior work.[12]

(b) Stracke, J. J.; Finke, R. G. *ACS Catalysis,* **2014**, *4*, 79-89.

18 Folkman, S. J.; Kirner, J. T.; Finke, R. G. *Inorg. Chem.* **2016**, *55*, 5343-5355.

19 Andersson, I.; Hastings, J. J.; Howarth, O. W.; Pettersson, L. *J. Chem. Soc., Dalton Trans.* **1996**, 2705-2711.

20 Haynes, W. M.; Lide, D. R. *Handbook of Chemistry and Physics*, 92nd ed.; Taylor and Francis Group, **2011**.

21 Krolicka, A.; Bobrowski, A.; Kalcher, K.; Mocak, J.; Svancara, I.; Vytras, K. *Electroanalysis* **2003**, *15*, 1859-1863.

22 The amount of $Co(II)_{total}$ was determined from the elemental analysis for Co of 5.5 mg of solid 2A material. That Co analysis revealed 5.05 % Co by weight; hence of the 5.5 mg of 2A weighed out for the analysis, 0.27 mg is Co(II). This in turn 23 μM $Co(II)_{total}$ in solution, slightly higher than the 20 μM $Co(II)_{total}$ expected from a 5 μM solution of pure **$Co_4V_2W_{18}$**. The assumption is that the excess Co(II) is mostly likely present as a counter-cation impurity.

23 Klanberg, F.; Hunt, J. P.; Dodgen, H. W. *Naturwissenschaften* **1963**, *50*, 90-91.

24 Surendranath, Y.; Lutterman, D. A.; Liu, Y.; Nocera, D. G. *J. Am. Chem. Soc.* **2012**, *134*, 6326-6336.

25 Ullman, A. M.; Liu, Y.; Huynh, M.; Bediako, D. K.; Wang, H.; Anderson, B. L.; Powers, D. C.; Breen, J. J.; Abruña, H. D.; Nocera, D. G. *J. Am. Chem. Soc.* **2014**, *136*, 17681-17688.

26 (a) Caveats in the cathodic stripping experiment include: that DMG has a binding constant of logK=11.5± 0.3 at pH 8.0[26b] so that it can, at least thermodynamically speaking, shift the Co(II) dissociative equilibrium out of Co-POMs such as **$Co_4V_2W_{18}$**. The kinetics—that is how fast—additional Co(II) would be formed is another issue. To minimize the time during with the Co(II) dissociative equilibrium might be shifted, the aging of **$Co_4V_2W_{18}$** in the presence of DMG was kept to a minimum of six minutes (the minimum time required for the experiment). Relevant to this discussion is that our previous studies[13] with the P-analog, **$Co_4P_2W_{18}$**, found only ~4.3 % of the total Co(II) is present as $Co(II)_{aq}$ in aged aqueous solutions in pH 8.0 NaPi—a value far smaller than the *ca.* 100% decomposition observed herein for **$Co_4V_2W_{18}$**. Hence, the DMG in the cathodic stripping experiments does not seem to be drastically altering the stripping-determined Co(II) values. Nevertheless, *$[Co(II)_{aq}]$ values determined by adsorptive stripping with DMG are considered to be an upper limit to the true $[Co(II)_{aq}]$ present.* (b) Saito, M. A.; Moffett, J. W. *Marine Chemistry* **2001**, *75*, 49-68.

27 Oxidizing the Co(II) to Co(III) in **$Co_4V_2W_{18}$** or other Co-POMs could in principle increase the stability of the Co-POM. However, arguing against this hypothesis at least presently is that reversible Co(II)/(III) waves have not been observed in Co-POM's to our knowledge—suggesting that Co(II)/(III) oxidation in Co-POMs has a high Marcus-type intrinsic barrier, as one might expect from the different intrinsic sizes of Co(II) vs Co(III). Moreover, any Co(III/II) WOC cycle

then necessarily produces substitutionally labile Co(II), which in turn is more likely at least kinetically to dissociate that Co(II) from the Co-POM.

28 Kanan, M. W.; Nocera, D. G. *Science* **2008**, *321*, 1072-1075.

29 Evans, H. T.; Tourné, C. M.; Tourné, G. F.; Weakley, T. J. R. *J. Chem. Soc., Dalton Trans.* **1986**, 2699-2705.

IV. ELECTROCHEMICALLY DRIVEN WATER-OXIDATION CATALYSIS BEGINNING WITH SIX EXEMPLARY COBALT POLYOXOMETALATES: IS IT MOLECULAR, HOMOGENEOUS CATALYSIS OR ELECTRODE-BOUND, HETEROGENEOUS COO_X CATALYSIS?[iii]

Overview

A carefully selected series of six exemplary cobalt-polyoxometalate (Co-POM) precatalysts have been chosen for examination of whether they are molecular water-oxidation catalysts (WOCatalysts) or if, instead, they actually form heterogeneous, electrode-bound CoO_x as the true WOCatalyst under electrochemically driven water-oxidation catalysis (WOCatalysis) conditions. Specifically, the WOCatalysis derived from the following six Co-POMs was examined at pH 5.8, 8.0, and 9.0: $[Co_4(H_2O)_2(PW_9O_{34})_2]^{10-}$ (**$Co_4P_2W_{18}$**), $[Co_9(H_2O)_6(OH)_3(HPO_4)_2(PW_9O_{34})_3]^{16-}$ (**$Co_9P_5W_{27}$**), [*ββ*-$Co_4(H_2O)_2(P_2W_{15}O_{56})_2]^{16-}$ (**$Co_4P_4W_{30}$**) , $[Co(H_2O)PW_{11}O_{39}]^{5-}$ (**$CoPW_{11}$**), [α_1-$Co(H_2O)P_2W_{17}O_{61}]^{8-}$ (**α_1-CoP_2W_{17}**), and [α_2-$Co(H_2O)P_2W_{17}O_{61}]^{8-}$ (**α_2-CoP_2W_{17}**). To probe the true WOCatalyst from each of these Co-POMs and under the three pH conditions and associated buffers, the alternative hypothesis was tested that leached (or counter-cation) $Co(II)_{aq}$ is present and forms electrode-bound CoO_x as the true WOCatalyst under electrocatalytic conditions. The amount of $Co(II)_{aq}$ in 500 μM solutions of

[iii] This chapter is the most comprehensive survey of Co-POMs for WOCatalysis to date. Herein, the stability of six exemplary Co-POMs is quantified under three different buffering conditions. Furthermore, the contribution to catalysis from the amount of $Co(II)_{aq}$ that is present is quantified and compared to the WOCatalysis activity from the Co-POMs. This chapter has been submitted to the *Journal of the American Chemical Society*, and includes co-authors Joaquin Soriano-Lopez, and José Ramón Galán-Mascarós, who supplied the $[Co_9(H_2O)_6(OH)_3(HPO_4)_2(PW_9O_{34})_3]^{16-}$ material used in the study in addition to edits during the final phases of writing and publication. The entirety of the other experiments were performed by the author of this dissertation, S. Folkman. Minor changes were made to meet dissertation formatting guidelines.

each Co-POM was measured after 3 hrs of aging as well as from t = 0. For pH=5.8 and 8.0 0.1 M sodium phosphate buffer (NaPi), $Co(II)_{aq}$-induced line broadening of the ^{31}P NMR resonance was used in comparison to calibration curves for authentic $Co(II)_{aq}$ to quantitate the $Co(II)_{aq}$ present. For 0.1 M sodium borate (NaB) pH=9.0 solution (i.e., a system without the ^{31}P handle), cathodic stripping was used to determine the amount of $Co(II)_{aq}$ in 500 μM Co-POM solutions, again after 3 h aging. The amount of detectable $Co(II)_{aq}$ after 3 hours for the six Co-POMs ranges from ~0.6 to ~90% of the total cobalt initially present in the Co-POM. The amount of WOCatalysis accounted for by the $Co(II)_{aq}$ from each Co-POM was then determined for each of the six Co-POMs and under the three pH=5.8, 8.0, and 9.0 buffer conditions. For each of the six Co-POMs at the more basic pH 8.0 and 9.0 (i.e., for 12 out of 18 total cases), the amount of freely diffusing $Co(II)_{aq}$ detected after 3 hrs forms detectable, heterogeneous CoO_x which, in turn, is able to account for ≥100% of the observed WOCatalysis activity—that is, at pH 8.0 and 9.0, the evidence strongly suggests that none of the six Co-POMs function as a molecular, homogeneous WOCatalyst within experimental error. *However*, under 0.1 M NaPi, pH 5.8 conditions and for **$CoPW_{11}$** and **α_1-CoP_2W_{17}** where <2% detectable $Co(II)_{aq}$ is seen, the detected $Co(II)_{aq}$ *cannot* account for the observed WOCatalysis, implying that these Co-POMs are primarly molecular, Co-POM-based, WOCatalysts under electrochemically driven, pH 5.8, phosphate buffer conditions, albeit with the CoO_x formed under those conditions being an estimated ~20-300x faster at pH =5.8, and an estimated ~740x faster a pH=8, than that of the single most stable Co-POM, **α_1-CoP_2W_{17}**. The results obtained (i) are the most definitive look to date at the true catalyst derived from the range of 6 prototype Co-POM precatalysts; (ii) go far in suggesting that even more hydrolytically stable Co-POM and other Metal-POM WOCatalysts merit development; and most importantly and notably (iii) illustrate a successful, arguably preferred methodology for distinguishing molecular

homogeneous from metal-oxide heterogeneous WOCatalysts and when metal-leaching or counter-cation contamination is present at just trace, μM levels.

4.1 Introduction

Meeting the growing global energy demand requires the development of new technologies and energy-storage schemes.[1,2] Electrocatalytic water splitting is one widely discussed scheme for generating hydrogen as a renewable fuel.[2] The bottleneck of the needed electrocatalytic water splitting is the anodic half reaction, catalytic water oxidation. As such, there has been a tremendous interest in, and resultant publication on, the development and screening of water oxidation catalysts (WOCatalysts) (a SciFinder search of "water oxidation" yields 6550 hits while "water oxidation catalysis" yields 281 references since 2000, and as of March 2018).[3,4,5,6,7,8,9,10,11,12,13,14,15,16] The identification of the kinetically dominant WOCatalyst—the primary focus of the present study—is directly relevant the rational development of selective, active, and long-lived WOCatalysts.

Polyoxometalates (POMs), and in particular cobalt based polyoxometaltes (Co-POMs), have attracted huge interest in the WOCatalysis area.[6,7,9,10,11,12,13,14,15,16,17] POMs are discrete metal-oxide compounds that can be readily synthesized on the gram to kilogram or larger scale via self-assembly. POMs are typically composed of high valent (and therefore oxidatively stable) elements such as W(VI), P(V), Mo(VI), and V(V). Interest in POMs for WOCatalysis comes from the fact that POMs are known to incorporate redox active metal centers such as cobalt and ruthenium, both of which are active towards WOCatalysis.[18,19,20]

However, no known Co-POM is *100%* hydrolytically stable over a wide range of pH values. The few Co-POMs that have had their Co(II) binding constants measured show that those Co(II) binding constants are in the μM range.[21,22] The μM amount of $Co(II)_{aq}$ that is leached when the Co-POMs are aged in buffered solutions can then deposit onto anodes during controlled

potential WOCatalysis, in turn creating a well-known heterogeneous CoO_x film[8] as the active, electrochemically driven WOCatalyst. Such CoO_x films have been shown to account quantitatively for all of the observed electrocatalytically driven WOCatalysis current in the case of $[Co_4(H_2O)_2(PW_9O_{34})_2]^{10-}$ (**$Co_4P_2W_{18}$**) in 0.1 M sodium phosphate pH=8.0 buffer and also for $[Co_4(H_2O)_2(VW_9O_{34})_2]^{10-}$ (**$Co_4V_2W_{18}$**) in 0.1 M sodium phosphate pH=8.0 and 5.8 buffers, as well as 0.1 M sodium borate pH=9.0 buffer.[21,23,24,25,26,27]

Our 2014 review entitled "Distinguishing Homogeneous from Heterogeneous Water Oxidation Catalysis When Beginning with Polyoxometalates" highlights the issues in, as well as preferred techniques for, distinguishing between homogeneous and heterogeneous WOCatalysis when beginning with POMs.[25] The main findings of that review include that: (i) multiple complimentary methods are necessary en route to determining the Co-POM speciation, stability, and ultimately the identity of the true WOCatalyst;[17,25,26] (ii) the amount of redox active metal such as $Co(II)_{aq}$ that is leached into solution (or present as a counter-cation impurity, as discovered herein) needs to be determined quantitatively; (iii) one needs to perform control experiments examining authentic heterogeneous CoO_x self-assembled from $Co(II)_{aq}$ under the catalytic reaction conditions; (iv) the contribution to catalysis of heterogeneous CoO_x or other metal-oxides must then be quantified; and, overall, (v) the stability of each POM is dependent upon the unique POM structure, the structural metals (e.g., W, Mo), the heteroatoms (e.g., P, Si, others), the redox-active metal (e.g., Co, Ru), and the reaction conditions, notably the pH, buffer type, and buffer concentration. Additionally, the true WOCatalyst is often dependent on the method of oxidation (e.g., chemical, photochemical, or electrochemical).

Unfortunately, of the many studies using Co-POMs or other M-POMs (M= catalytically active metal) employed as water oxidation *precatalysts*, very few publications conduct the

necessary experiments to provide *compelling* evidence for or against homogeneous molecular vs heterogeneous metal-oxide WOCatalysis. There are important exceptions,[13,17,23,26,28] that are discussed where relevant in the sections that follow. Other studies that use POMs for WOCatalysis, but which are not specifically treated in the main text of the present contribution, are summarized for the interested reader in Table S4.1 of the Supporting Information.

The $[Co_4(H_2O)_2(PW_9O_{34})_2]^{10-}$ Prototype Co-POM WOPrecatalyst

The early prototype of a Co-POM WOCatalysis precatalyst system is $[Co_4(H_2O)_2(PW_9O_{34})_2]^{10-}$ (**$Co_4P_2W_{18}$**) in 0.1 M sodium phosphate pH=8.0.[9,23,24] Previous work has shown that, after 3 hours of aging in 0.1 M NaPi solution, 500 μM $[Co_4(H_2O)_2(PW_9O_{34})_2]^{10-}$ dissociates a mere 58 μM Co(II) corresponding to just 4.3% decomposition (assuming the loss of a single Co(II) from the parent Co-POM).[23] That 58 μM $Co(II)_{aq}$ forms a highly catalytically active heterogeneous CoO_x films on tin-doped indium oxide (ITO) or glassy carbon electrodes under constant potential electrolysis.[23] The resultant CoO_x film accounts for 100±12% of the WOCatalysis current under the 0.1 M NaPi buffer and electrochemically driven WOCatalysis conditions.[23]

However and in experiments designed to deliberately favor molecular WOCatalysis by **$Co_4P_2W_{18}$**, when 2.5 μM $[Co_4(H_2O)_2(PW_9O_{34})_2]^{10-}$ is dissolved in NaPi pH 8.0 or 5.8 with ≥ 600 mV overpotential, the detected amount of Co(II) *cannot* account for the observed WOCatalysis current under the stated conditions—evidence that CoO_x is *not* the dominant catalyst under those only modestly different conditions.[24] The now classic **$Co_4P_2W_{18}$** system is a good example of how seemingly small changes in conditions can alter the kinetically dominant form of the Co-POM-derived WOCatalyst.

A second important example of a system where the formation of CoO_x from a Co-POM has been carefully examined is a 2012 *Inorg. Chem*. publication[13] in which the Co-POM

$[Co_9(H_2O)_6(OH)_3(HPO_4)_2(PW_9O_{34})_3]^{16-}$ (**$Co_9P_5W_{27}$**) was shown to form CoO_x under controlled potential electrolysis.[13] Addition of bipyridine to starting solutions of **$Co_9P_5W_{27}$** chelates leached $Co(II)_{aq}$ and prevents the formation of CoO_x under electrocatalytic conditions.[13] WOCatalysis current was still observed in the presence of bipyridine, consistent with molecular **$Co_9P_5W_{27}$** being a true, electrochemically driven, homogeneous WOCatalyst, albeit one with only ~2% of the WOCatalysis current of CoO_x formed in the absence of bipyridine.[13] This is another, important conclusion from prior studies: when molecular WOCatalysis from Co-POMs is seen, that activity (at least to date) is often only 1/2-1/11th that of the activity of CoO_x examined under identical conditions.[23,24,25,26]

Identifying the kinetically dominant WOCatalyst from a molecular precatalyst is often difficult,[9,13,23,24,25,26] especially in cases where as much as >95-99% of the initial POM remains intact under the reaction conditions. Only the scientific method of multiple alternative hypotheses is able to provide convincing, compelling evidence for the kinetically dominant, "true" WOCatalyst.[25,29] Scheme 4.1 presents 6 alternative hypotheses for the true catalyst when beginning with molecular, M-POM precatalysts (M = metal such as Co, Ru). The first hypothesis is that the precatalyst remains intact and is a homogeneous WOCatalyst, as the evidence strongly supports for the Ru_4-POM, $Cs_{10}[Ru_4(\mu\text{-}O)_4(\mu\text{-}OH)_2(H_2O)_4(\gamma\text{-}SiW_{10}O_{36})_2]$.[7] A second hypothesis is that there is insidious Co(II) (e.g., present as a counter-cation from the synthesis) which then forms heterogeneous CoO_x as the dominant catalyst; Co_4O_4 cubanes are a case in point.[28] A third hypothesis is that the precatalyst (Co-POM) is hydrolytically unstable, and leaches $Co(II)_{aq}$ into solution which then forms heterogeneous CoO_x as the WOCatalyst. Such leaching of $Co(II)_{aq}$ and then the formation of CoO_x is observed for both **$Co_4P_2W_{18}$** and **$Co_4V_2W_{18}$**, as already noted.[23,26] A fourth alternative hypothesis is that electrode-bound Co-POM serves as a direct precursor to

CoO_x on the electrode without yielding solution-deteactable $Co(II)_{aq}$. A fifth, quite reasonable hypothesis is that a fragment of the original Co-POM, POM-stabilized CoO_x nanoparticles, or perhaps some other at present unidentified species is actually the true catalyst. Lastly, it is always possible that more than one of the five hypotheses listed might be occurring simultaneously, as was the case with the formation of CoO_x from **$Co_9P_5W_{27}$** where WOCatalysis activity is still observed when $Co(II)_{aq}$ is removed by chelation with bipyridine (*vide supra*).[13]

1. The Co-POM is the true molecular catalyst.

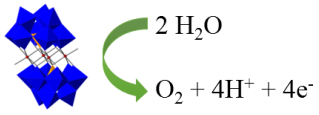

2. There is insidious Co(II) counter ion impurity which forms the catalyst.

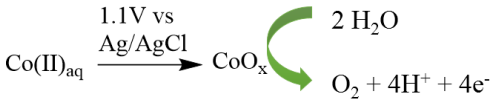

3. The Co-POM releases Co(II) to form CoO_x as the catalyst.

4. The Co-POM acts as a direct precursor to CoO_x on the electrode

5. An unidentified species is the catalyst.

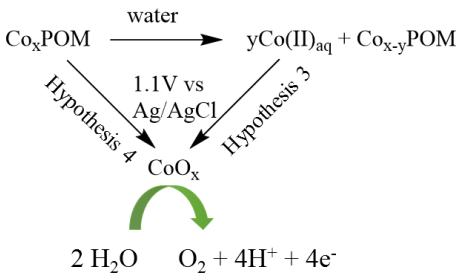

6. A combination of any of the above.

Scheme 4.1. List of six alternative hypotheses for the kinetically dominant WOCatalyst under a specific set of conditions.

Focus of the Present Studies

The focus of the current study is to establish the stability, speciation, and kinetically dominant WOCatalysts from the six exemplary Co-POMs shown in Figure 4.1 and under three carefully selected buffer and pH 5.8, 8.0, and 9.0 conditions. These exemplary Co-POMs allow examination of the observed WOCatalysis as a function of varied Co(II) coordination environments (e.g., single vs multiple redox centers), and as a function of different Co(II) binding sites. The six Co-POMs chosen for study are: the prototype $[Co_4(H_2O)_2(PW_9O_{34})_2]^{10-}$ (**$Co_4P_2W_{18}$**)

(because it is relatively well-studied,[9,17,23,24] and, therefore, is a benchmark system for controls and comparisons of methods); $[Co_9(H_2O)_6(OH)_3(HPO_4)_2(PW_9O_{34})_3]^{16-}$ (**$Co_9P_5W_{27}$**), which has been reported to exhibit homogeneous WOCatalysis under electrocatalytically driven conditions (*vida supra*), and has also shown very interesting, high WOCatalysis activity (η=189 mV at 1mA/cm^2) as an insoluble Ba^{2+} salt embedded within amorphous carbon paste;[13,30,31,32,33] then [*ββ*-$Co_4(H_2O)_2(P_2W_{15}O_{56})_2]^{16-}$ (**$Co_4P_4W_{30}$**) is the third Co-POM selected because its Co centers are isostructural with **$Co_4P_2W_{18}$**, yet this Co-POM was previously reported, surprisingly, as not exhibiting WOCatalysis using $Ru(bpy)_3^{3+}$ as the oxidant[9,34,35] and even though its close congener **$Co_4P_2W_{18}$** does.[9] The final three of the six Co-POMs are: single Co-containing $[Co(H_2O)PW_{11}O_{39}]^{5-}$ (**$CoPW_{11}$**), which has been shown to form CoO_x under electrocatalytic conditions in pH 7 phosphate buffer solutions,[9,36,37,38,39,40] yet is reported to not exhibit WOCatalysis activity using $Ru(bpy)_3^{3+}$ as the chemical oxidant;[9] and finally [α$_1$-$Co(H_2O)P_2W_{17}O_{61}]^{8-}$ (**α_1-CoP_2W_{17}**) and [α$_2$-$Co(H_2O)P_2W_{17}O_{61}]^{8-}$ (**α_2-CoP_2W_{17}**), two isomeric, single-cobalt Co-POMs[21,22,41,42,] chosen because they have literature precedent[43] as WOPrecatalysts and because they therefore allow insights into the role of different Co(II)-to-POM binding sites and structures on the resultant WOCatalysis and kinetically dominant WOCatalyst.

Meriting mention here is that the dicobalt(IV)-μ-oxo dimer of **α_2-CoP_2W_{17}**, [(α$_2$-$Co^{IV}P_2W_{17}O_{61})_2O]^{14-}$ (formed from **α_2-CoP_2W_{17}** using ozone as the oxidant and as an inner-sphere oxo transfer reagent) has been shown to generate O_2 from water in ~95% yield, according to Equation 1.[44] However, it is not currently known if [(α$_2$- $Co^{IV}P_2W_{17}O_{61})_2O]^{14-}$ can form from [α$_2$-$Co^{II}(H_2O)P_2W_{17}O_{61}]^{8-}$ under electrochemical oxidation. If formation of the μ-oxo dimer did occur, then one might expect to observe homogeneous WOCatalysis from **α_2-CoP_2W_{17}**.

$$[(\alpha_2\text{-}Co^{IV}P_2W_{17}O_{61})_2O]^{14-} + 3H_2O \longrightarrow 2[\alpha_2\text{-}Co^{II}(OH_2)P_2W_{17}O_{61}]^{8-} + O_2 + 2H^+ \quad (1)$$

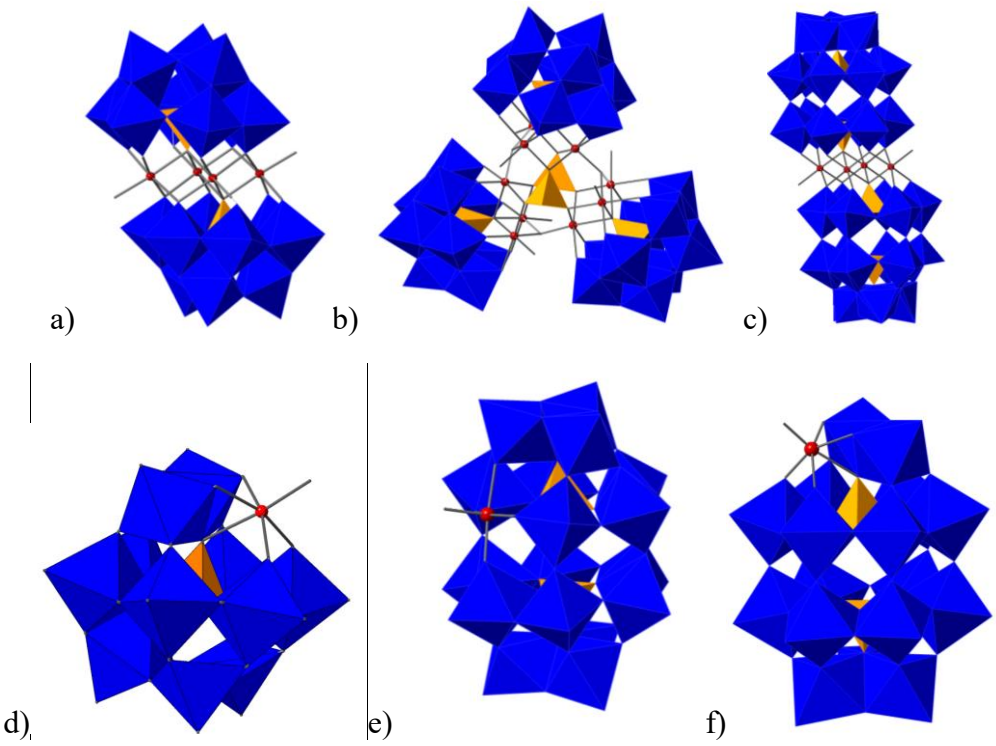

Figure 4.1. Polyhedral representations of the structure of the Co-POMs: a) $\mathbf{Co_4P_2W_{18}}$;b) $\mathbf{Co_9P_5W_{27}}$; c) $\mathbf{Co_4P_4W_{30}}$; d) $\mathbf{CoPW_{11}}$; e) $\mathbf{\alpha_1\text{-}CoP_2W_{17}}$; and f) $\mathbf{\alpha_2\text{-}CoP_2W_{17}}$. Blue octahedra represent WO_6, orange tetrahedra represent PO_4, and red spheres are Co(II). The coordination site on the Co atoms typically bind H_2O and is where WOCatalysis is generally postulated to occur if the Co-POMs are indeed homogeneous, molecular WOCatalysts.

Choice of reaction conditions and key experimental methodologies.

The conditions chosen to examine the Co-POMs in Figure 4.1 include: sodium phosphate buffer (NaPi) at both pH 5.8 (favoring the stability of the Co-POMs) and 8.0 (favoring the thermodynamics of water oxidation). We also used sodium borate buffer (NaB) at pH 9.0 to compare the effect of buffer, since Co-POMs tend to be more stable in NaB buffer,[17] and because NaPi can, at least in principle, drive the decomposition of Co-POMs due to the formation of insoluble $Co_3(PO_4)_2$ ($K_{sp}\approx10^{-35}$).[45] Similar to our previous publications, we aged the Co-POMs in each respective buffer for three hours as a relatively minimal solution lifetime.[23,26]

Note that 3 h aging is at most a *minimum test* of the stability of the Co-POMs, because any truly useful WOCatalyst will need to be active for $>10^8$ total turnovers, so that even if the Turnover

Frequency was among the highest reported for a Co-POM (i.e., 200 s^{-1})[16], then any molecular Co-POM WOCatalyst would still need to be active for >140 h—meaning that our 3 h test is only 2% of that required catalytic lifetime. However and importantly, we also examine the amount of $Co(II)_{aq}$ formation at $t \approx 0$ and as a function of time by ^{31}P NMR in what follows.

In order to quantify the amount of Co(II) that dissociates from the complexes, $Co(II)_{aq}$-induced ^{31}P NMR line broadening of the P atom in the phosphate buffer was used.[26,28,46,47,48] Adsorptive cathodic stripping was used as a secondary method to quantify the $Co(II)_{aq}$ in NaPi and the primary method to quantify the $Co(II)_{aq}$ leached from the Co-POMs in NaB.[23,26,49] Once the stability of each Co-POM was established under a given set of conditions, controlled potential electrolysis was conducted in the Co-POM solutions, followed by cyclic voltammetry in the original Co-POM solution and then cyclic voltammetry of the working electrode in a fresh, buffer-only solution, thereby obtaining the CV of any deposited film. The deposited films were also characterized by scanning electron microscopy (SEM) and x-ray photoemission spectroscopy (XPS) in what follows. The sum of these experiments were then used collectively to provide evidence for the kinetically dominant WOCatalyst under a stated set of conditions.

Finally, a historical note is perhaps of some interest: we never started out to pursue the "Who's the true catalyst?" question in the WOCatalysis area and despite our background in this question in the area of hydrogenation catalysis with low valent metal nanoparticles.[50] *Instead, this key question quickly found us in the area of Co-POMs as WOPrecatalysts*. Our original goal, and hence first experiments, were using $\mathbf{Co_4P_2W_{18}}$ as a WOPrecatalyst in our OPV-driven WOC half-cell,[51] the Co-POM $\mathbf{Co_4P_2W_{18}}$ being "close to our intellectual hearts" since we discovered the rational synthesis of and $\mathbf{Co_4P_2W_{18}}$, $\mathbf{Co_4P_4W_{30}}$, and the other members of this class of M_4-containing POMs in 1981.[52] *The very first experiments with* $\boldsymbol{Co_4P_2W_{18}}$ *provided evidence that an*

electrode-bound catalyst, the same color as Nocera's CoO_x/Pi catalyst[8] *that we had been examining, had formed on the ITO anode from the* ***$Co_4P_2W_{18}$*** *precatalyst*.[23] The findings quickly followed that the **$Co_4P_2W_{18}$** POM leached Co(II) into solution from just 4.3% decomposition over 3 hrs, and that the resultant 58 μm Co(II) formed electrode-bound CoO_x that accounted for 100 ± 12% of the observed, electrochemically driven, WOCatalysis current.[23] A similar situation occurred for the V-based congener, **$Co_4V_2W_{18}$**: we were intrigued by the claim of 100% hydrolytic stability, and 200-fold higher catalytic activity compared to the P-congener.[16] Yet when we prepared **$Co_4V_2W_{18}$** by the literature route and tried to purify it to the ^{51}V NMR resonance assigned in the literature to **$Co_4V_2W_{18}$**, the resultant, different color POM contained only ~1 Co per $V_2W_{18}O_{68}^{18-}$ unit—yet had the same ^{51}V NMR resonance ascribed to "**$Co_4V_2W_{18}$**".[53] The 100% hydrolytic *instability* of **$Co_4V_2W_{18}$**, its decomposition to Co(II) that forms electrode-bound CoO_x/Pi that, once again, carried 100% of the observed WOC within experimental error, as well as assignment of the observed ^{51}V NMR resonance to the impurity $V_2W_4O_{19}^{6-}$ followed after considerable effort.[26,53] In short, the "Who's the true catalyst?" question has raised its omnipresent head each and every time we tried to build off the literature of Co-POMs as WO(Pre)Catalysts. That observation is, actually, not surprising at least in hindsight: the identity of the true catalyst in any and all catalytic reactions is an important, often overlooked, typically challenging, critical question in catalysis. Reflection makes the latter claim obvious once one realizes that *all catalytic properties* of interest derive from the precise composition and nature of the actual catalyst, including the: catalytic activity, selectivity, lifetime, poisoning, re-isolation, and catalyst regeneration, for example. The "Who's the catalyst?" question, and the associated "Is it homogeneous or heterogeneous catalysis?" question, had not been fully raised nor critically addressed for cobalt or other POM-based WOCatalysts before our 2011 study that has (as of May

2018) over 244 citations.[23] The present work brings to completion our studies of the kinetically dominant, "true" catalyst(s) derived from exemplary Co-POMs in buffer solutions under electrochemically driven and the other stated, specific WOCatalysis conditions—conditions that matter greatly, *vide infra*. It is hoped that the WOCatalysis community can use methods and approach herein to provide evidence for the kinetically dominant WOCatalyst as a critical part of their own WOCatalysis studies.

4.2 Experimental

General Considerations. All reagents used were the highest purity available and were used without further purification. 18 MΩ water was obtained from an in house Barnstead Nanopure filtration system. FT-IR were collected using a ThermoScientific Nicolet iS50 FT-IR spectrometer in transmission mode using KBr pellets containing approximately 2 wt% of the analyte. Thermogravimetric analysis (TGA) was performed using a TA Instruments TGA 2950 with a 5°C/min ramp rate to 500° C on a platinum sample pan. TGA was used to determine the waters of hydration because water is the only volatile component of the Co-POMs at ≤500 °C. ^{31}P NMR was collected using either an Agilent (Varian) 400 MHz NMR or an Agilent Inova 500 MHz NMR—the spectral ranges and pulse sequences were optimized for the resonance of the ^{31}P atom of interest. Elemental analyses were obtained from Galbraith Laboratories in Knoxville, TN.

Electrochemically driven WOCatalysis experiments were conducted in 0.1 M sodium phosphate buffer (NaPi) either at pH 5.8 or 8.0 or in 0.1 M sodium borate (NaB) pH 9.0.[54] All stability, electrochemistry and WOCatalysis experiments were conducted with a 500 μM Co-POM concentration, chosen because the stability of the complexes can be difficult to quantify, and hence employing this higher, 500 μM concentration allows detection of decomposition byproducts by ^{31}P NMR, for example (*vide infra*).

All of the electrochemistry was performed using a CH Instruments CHI630D with a three electrode set up. All potentials are referenced to Ag/AgCl, with a platinum wire as the counter electrode, and glassy carbon either 1.0 or 0.071 cm^2 as the working electrode. SEM was conducted on a JEOL JSM-6500F microscope with magnification from 1000 to 20,000. XPS was conducted on a PE-5800 X-ray photoelectron spectrometer; full scans were collected on deposited films as well as high resolution scans for individual elements.

Syntheses of the Co-POMs were conducted according to literature methods and characterized via FT-IR, ^{31}P NMR, TGA and elemental analysis. The procedures followed and resulting characterization data are presented in the Supporting Information for the interested reader (Figures S4.1-S4.8).[9,13,21,23,30,31,34-43,52] Characterization of the Co-POMs was consistent with prior literature, and are isomerically pure samples, with the exception of $K_8[\alpha_1\text{-}Co(H_2O)P_2W_{17}O_{61}]$ which contains a presently inseparable 5% impurity of the isomeric $K_8[\underline{\alpha_2}\text{-}Co(H_2O)P_2W_{17}O_{61}]$.

Stability of the Co-POMs in Buffered Solutions

Stability of the CoPOMs determined by Co(II) induced ^{31}P NMR line broadening. The well-established method of $Co(II)_{aq}$ induced ^{31}P NMR line broadening of the sodium phosphate buffer, first observed by Klanberg and Dodgen[46] and used later by Nocera and others to quantify aqueous Co(II) leached out of CoO_x film or molecular Co-complexes,[26,47,28,48] was used to detect the amount of $Co(II)_{aq}$ present in NaPi buffered solutions for each Co-POM. This ^{31}P NMR technique is powerful because it is selective towards $Co(II)_{aq}$ (i.e., and insensitive to Co(II) within a Co-POM) while also having a detection limit of ~2 μM $Co(II)_{aq}$.[26] Further precedent for this ^{31}P NMR methodology is its recent use to quantify the amount of Co(II) leached from $[Co_4V_2W_{18}O_{68}]^{10-}$ as well as $[Co_4P_2W_{18}O_{68}]^{10-}$, results which demonstrate that the ^{31}P method agrees with cathodic

stripping determinations of Co(II) to within ±5% for both $[Co_4V_2W_{18}O_{68}]^{10-}$ and $[Co_4P_2W_{18}O_{68}]^{10-}$ in 0.1 M NaPi pH=8.0.[26]

We followed the same general procedure outlined in our 2016 *Inorg. Chem.* paper[26] for the ^{31}P NMR determinations of $Co(II)_{aq}$, except the Co-POM concentrations employed herein are 500 μM. (The lower concentration of 5 μM Co-POM used in our 2016 paper was chosen because $[Co_4V_2W_{18}O_{68}]^{10-}$ decomposes 100% resulting in $Co(II)_{aq}$ concentrations too high to measure reliably at more than 5 μM of that particular Co-POM). First, a calibration curve was developed using $Co(NO_3)_2$ as an authentic source of Co^{2+}_{aq} for the line broadening experiments in both pH 5.8 and 8.0 NaPi (as 100 mM solutions in 25% D_2O, Figure S4.9 in the Supporting Information). Next, the appropriate amount of Co-POM was weighed in a 1 dram vial. To prepare 2 mL of a 500 μM solution, 1 μmol of each POM is required; therefore the following masses of each indicated Co-POM were used: **$Co_9P_5W_{27}$**, 8.97 mg; **$Co_4P_4W_{30}$**, 8.77 mg; **$CoPW_{11}$**, 3.20 mg; **α_1-CoP_2W_{17}**, 4.86 mg; **α_2-CoP_2W_{17}**, 4.82 mg. Next, 1 mL of 200 mM NaPi (pH 5.8 or 8.0), 500 μL D_2O, and 500 μL water were added to the Co-POM powder in the 1 dram vial, yielding 2 mL of a solution with 500 μM Co-POM, 100 mM NaPi, and 25% D_2O. The timer was started immediately upon addition of the buffer solution to the solid Co-POM. A 1 mL aliquot was then transferred into a 5 mm OD NMR tube which was then inserted into the NMR. ^{31}P NMR was then collected on the sample without shimming and under identical conditions to those used for the calibration curve. A 500 MHz Varian NMR spectrometer was used at 25° C with scans from +64.9 to −64.9 ppm, a 45° pulse angle, a 1.000 s relaxation delay, and a 0.624 s acquisition time. The peak width of the ^{31}P NMR peaks were determined using the instrument's VNMRJ software after phase correction.

To confirm the line broadening is caused almost completely by $Co(II)_{aq}$, and not by the Co(II) present within the intact Co-POM, we conducted the same experiments as above except in

the presence of 92 μM EDTA to complex any free Co(II) (i.e., an amount of EDTA in excess of the $Co(II)_{aq}$ detected by the initial ^{31}P NMR experiment). Any residual line broadening over that original ^{31}P NMR was then assigned to the intact Co-POM, an amount that ranged from just 2 to 8 Hz, so only between 1.3 and 6 μM $Co(II)_{aq}$ for **$Co_4P_2W_{18}$** and **$Co_4P_4W_{30}$** in 0.1 M NaPi pH=8.0. This in turn means that the contribution from the intact Co-POMs to the observed ^{31}P NMR line broadening is at most only 8% of the $Co(II)_{aq}$ detected for **$Co_4P_4W_{30}$** in 0.1 M NaPi pH=8.0. The residual line broadening from the added EDTA experiment was subtracted from the raw FWHM values for the particular Co-POM being examined before the FWHM values were fit to the calibration curve to calculate the final $Co(II)_{aq}$ concentration.

Stability of the Co-POMs as determined by cathodic adsorptive stripping as a confirmatory technique. The reliability of the ^{31}P NMR technique for the quantitation of $Co(II)_{aq}$ has been demonstrated for both **$Co_4P_2W_{18}$** and **$Co_4V_2W_{18}$**.[23,26] However, we wanted to determine the amount of $Co(II)_{aq}$ present in the 500 μM Co-POM solutions *in pH 9.0 NaB* after three hours of aging (i.e., and under conditions where no P_i is available for the use of the ^{31}P NMR method). Therefore, and as before[23,26] an adsorptive cathodic stripping method was employed that quantifies $Co(II)_{aq}$ by adsorption of the neutral cobalt dimethylglyoxime (DMG) complex on a bismuth electrode and subsequent reductive stripping.[23,26,49]

Electrode preparation. The Bi-film electrode was prepared using a method adapted from previous studies.[23,26,49] First, a clean glassy carbon electrode (3 mm diameter), a Ag/AgCl reference electrode, and a Pt wire counter electrode were placed into an aqueous solution containing 0.02 M $Bi(NO_3)_3$, 0.5 M LiBr, and 1 M HCl. Then constant potential electrolysis was conducted at -0.25 V until 10 mC of charge had accumulated (~45 s). The electrodes were then

removed and rinsed gently with water prior to being placed into the analyte solution containing either $Co(NO_3)_2$ for the calibration curve, or the aged Co-POM solutions.

Calibration Curve. A calibration curve was developed using $Co(NO_3)_2$ as an authentic source of $Co(II)_{aq}$, with concentrations ranging from 1.0 to 50 μM $Co(II)_{aq}$ in NaPi pH 8.0 and NaB pH 9.0 (Figure S4.10 in the Supporting Information). Using freshly plated Bi films, the electrodes were placed into a 1 dram vial containing a buffered solution (either 0.1 M NaPi pH 8.0 or 0.1 M NaB pH 9.0) that contained the desired $Co(NO_3)_2$ concentration and 100 μM DMG. Then, the solution was stirred for 3 s, allowed to reach stillness, and then the $CoDMG_2$ was adsorbed by applying -1.3 V to the Bi film electrode for 15 s. The solution was again stirred for 3 seconds and allowed to settle before differential pulse voltammetry (DPV) from -0.7 to -1.3 V using a 0.1 sec pulse width, 50 mV amplitude, and a 0.0167 s sampling width. The height of the DPV waves were measured from the background using the CH Instruments software, and plotted against the known $Co(II)_{aq}$ concentration for the calibration curves (Figure S4.10 in the Supporting Information). Worth noting is that the use of pH=8.0 to 9.0 buffer is essential, because at pH=5.8 the adsorptive cathodic stripping is not responsive to the $Co(II)_{aq}$ concentration—likely because the DMG must be deprotonated by pH > 5.8 to form $Co(DMG)_2$ that is an intermediate in the Co-stripping on the Bi film.

Aging of the Co-POMs and cathodic stripping. First, 500 μM solutions of the Co-POMs were prepared by weighing the appropriate amount of the solid Co-POM material into a 1 dram vial, then adding 2 mL of either 0.1 M NaPi pH 8.0 or NaB pH 9.0. The solutions were then aged 3 h before an aliquot, typically 200 μL, was used in the same analyte solution as the calibration curve. (While as noted the aliquot was typically 200 μL, the actual μL volume of the aliquot adjusted such that the detected $Co(II)_{aq}$ concentration was within the calibration curve's linear

range of 1-10 μM, as explained in greater detail below.) Because DMG binding of Co(II) could, in principle, shift the Co-POM dissociative equilibrium yielding a larger $Co(II)_{aq}$ concentration than without DMG, the time between aliquot addition and cathodic stripping was kept to a minimum (<1 min). The $Co(DMG)_2$ deposition and the DPV were conducted in the same manner as for the calibration curve above. The peak height of the DPV was fit to the calibration curves (Figure S4.10 of the Supporting Information), and the results were used to calculate the $Co(II)_{aq}$ concentration in the analyte solutions. The $Co(II)_{aq}$ concentration in the original solution was determined by taking into account the 1:10 dilution from the original solution to the analyte solution. For cases where the measured $Co(II)_{aq}$ was not within the linear range of the calibration curve, the dilution factor from the original to the analyte solution was adjusted so that the detected $Co(II)_{aq}$ concentration was within the range of the linear calibration curve. For example, the $Co(II)_{aq}$ detected from a 1:10 dilution of **$CoPW_{11}$** is >>10 μM and therefore outside the linear range of the calibration curve. Instead, a 20 μL aliquot of the aged **$CoPW_{11}$** was used (a 1:100 dilution) and the $Co(II)_{aq}$ concentration in the diluted solution was determined to be 4.4 ±0.5 μM, meaning that the actual $Co(II)_{aq}$ concentration in the original, undiluted **$CoPW_{11}$** solution was 100-fold larger, specifically 440 ± 50 μM.

Electrocatalytically driven water oxidation catalysis beginning with the Co-POMs.

Electrolysis using the Co-POMs in buffered solutions in comparison with $Co(II)_{aq}$. From the ^{31}P NMR and cathodic stripping studies, the amount of $Co(II)_{aq}$ that dissociates into buffered solution after 3 hours is known. Comparing the observed activity of the aged Co-POM solutions with solutions containing authentic $Co(II)_{aq}$ tests if the WOCatalysis activity can be accounted for by the dissociated $Co(II)_{aq}$ or, alternatively, if WOCatalysis by the Co-POM itself is indicated. Hence, we conducted bulk electrolysis using a 1 cm^2 working electrode in buffered solutions that

either contained a 500 μM Co-POM solution that had aged 3 h, or an amount of authentic $Co(II)_{aq}$ that matched the measured $Co(II)_{aq}$ after 3 h, as determined by ^{31}P NMR or cathodic stripping.

Electrolysis was conducted in the same manner as previous studies using **$Co_4V_2W_{18}$** as a WOPrecatalyst.[26] Briefly, the experiments were conducted in a custom built U-cell with a medium fritted glass filter separating the working and counter electrodes. The working compartment was sealed using a Teflon lid pierced to accommodate the working electrode, the reference electrode, and the O_2 detection sensor (NeoFox; FOSPOR-R probe), all in a 6 mL, argon-purged solution. The O_2 sensor was calibrated using a 2-point calibration curve consisting of air-saturated DI water (~220 μM at 22 °C, for a typical barometric pressure of 0.84 atm for Fort Collins, CO), and O_2-free solutions were generated by addition of excess sodium sulfite to the solution. Electrolysis was conducted at 1.1 V for 5 min with stirring at ~600 rpm. The final faradaic efficiency was determined by comparing the final O_2 concentration to the O_2 concentration expected from the total charge passed during the experiment (i.e., 4 e^- passed per 1O_2 produced).

Electrochemical and morphological characterization of the films electrodeposited from the Co-POM solutions.

Deposition and cyclic voltammograms of CoO_x films. Previous work has documented the effectiveness of controlled potential electrolysis and subsequent analysis of deposited films from Co-POMs.[23,26] As such, controls were conducted in a similar manner in which constant potential electrolysis was conducted at 1.1 V on a glassy carbon electrode for 5 to 30 min to allow accumulation of an electrodeposited film visible to the naked eye. After electrolysis, cyclic voltammetry was conducted on the film in the same Co-POM solution. The electrodes were subsequently removed from the original Co-POM solution, rinsed with water and placed into a buffer-only solution. Cyclic voltammetry was then conducted on the electrodeposited film in the

buffer-only solution—this allows comparison of the observed WOCatalysis activity from the deposited film to the starting Co-POM solution. Electrolysis was then conducted on the deposited film in the buffer-only solution under otherwise identical conditions to the Co-POM solution.

To test the hypothesis that CoO_x forms from $Co(II)_{aq}$, and not directly from Co-POM bound to the electrode surface, EDTA was added at a concentration 10 times the measured $Co(II)_{aq}$. Constant potential electrolysis at 1.1 V was then conducted. Controls with $Co(NO_3)_2$ and EDTA present demonstrate that no film is deposited from the Co•EDTA complex. This, in turn, means that if a film is observed from any Co-POM solution containing 10 equiv. EDTA/$Co(II)_{aq}$, then that film would have to be formed from some route not involving freely diffusing $Co(II)_{aq}$, for example from directly from Co-POM adsorbed on the electrode.

Morphological and compositional analysis of the deposited films. The electrodeposited films were examined by XPS and SEM to quantify elements in the surface of the film, and to capture morphological features, respectively. The films were deposited on glassy carbon (1 cm^2) at 1.1 V for 30 min from Co-POM solutions in 0.1 M NaPi pH 5.8 and 8.0 as well as 0.1 M NaB pH 9.0. The electrodes were then removed from solution and allowed to air dry on the bench before being placed into a desiccator overnight. XPS was conducted on a PE-5800 X-ray photoelectron spectrometer; survey scans were collected from 10 to 1100 eV with 1.6 eV/step and 187.85 eV pass energy. High resolution scans were collected for each element detected from the survey (such that sufficient background was included with 0.1 eV/step and 23.5 eV pass energy). SEM was conducted on a JEOL JSM 6500F scanning electron microscope. Images were collected from 1,000 to 20,000x magnification to demonstrate the homogeneity of the film as well as to visualize morphological details.

4.3 Results and Discussion

Stability of the Co-POMs assayed by $Co(II)_{aq}$-induced ^{31}P NMR line broadening. Quantitative knowledge of the stability of any precatalyst under a given set of conditions is crucial to understanding the kinetically dominant, most active form of the catalyst.[23,25,26] Using the $Co(II)_{aq}$-induced, ^{31}P NMR line broadening experiments first developed by Klanberg and Dodgen[46] and then Nocera and co-workers,[28,47] the amount of $Co(II)_{aq}$ present as a function of time for each Co-POM was measured in NaPi pH 5.8 and 8.0. The $Co(II)_{aq}$ vs time traces for selected Co-POMs are shown in Figure 4.2 and Figure S4.11 of the Supporting Information. The percent of total Co(II) in the Co-POM solution that is present as aqueous $Co(II)_{aq}$ after 3 hours of aging is presented in Figure 4.3 and Table 4.1. *All of the Co-POMs examined showed some detectable $Co(II)_{aq}$ over 3 hrs in NaPi buffer* ranging from ~0.6 to 50% of the total Co(II) present in the given Co-POM solution, the exact % depending on the Co-POM and the precise pH and buffering conditions, *vide infra.*

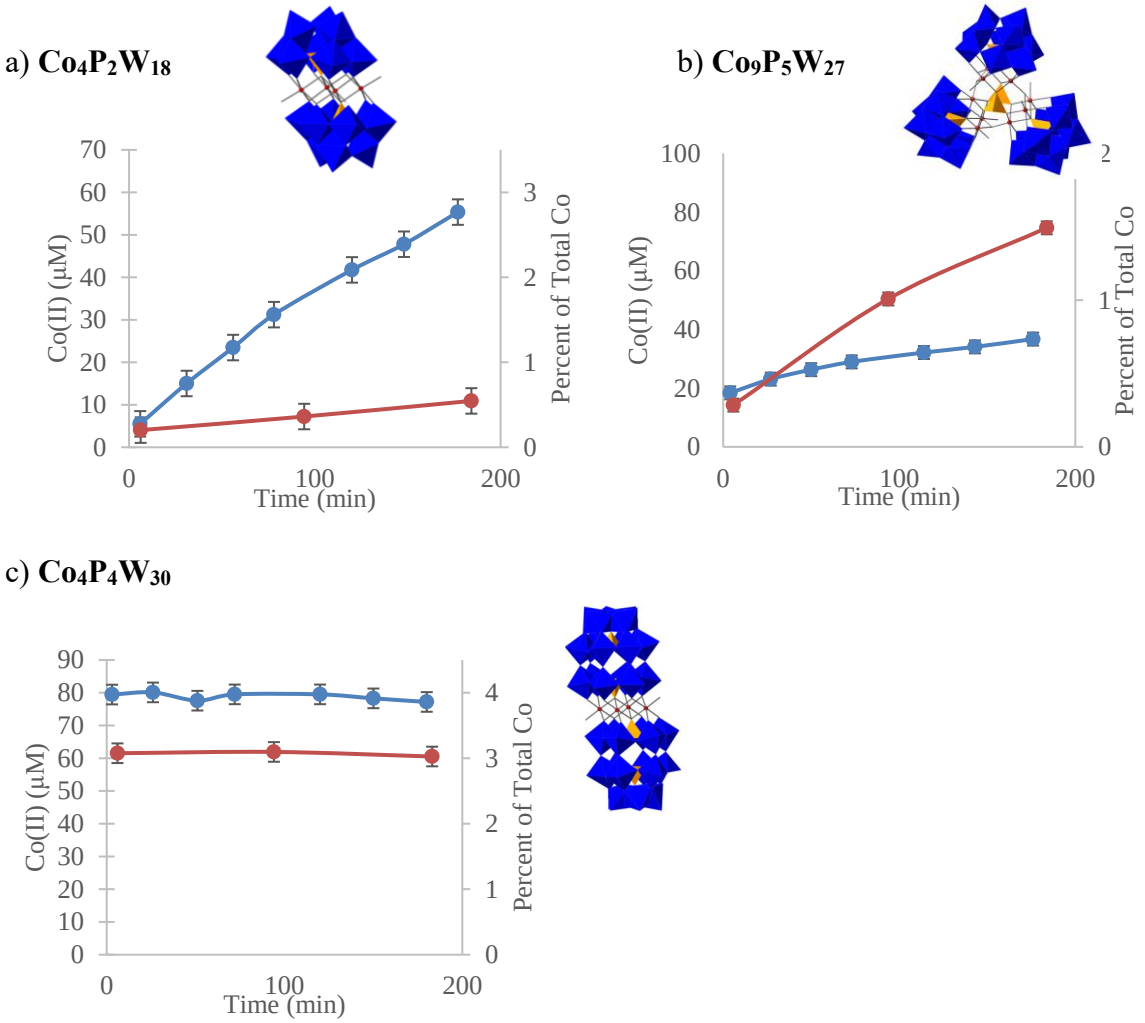

Figure 4.2. The $Co(II)_{aq}$ concentration vs time determined by $Co(II)_{aq}$ induced line broadening in 0.1 M NaPi (pH 5.8, red and pH 8.0, blue) for 500 μM solutions of a) **$Co_4P_2W_{18}$** (adapted with permission from Reference 26, Copyright 2017 American Chemical Society); b) **$Co_9P_5W_{27}$**; and c) **$Co_4P_4W_{30}$**. The value for the $Co(II)_{aq}$ concentration was determined by fitting the observed ^{31}P NMR linewidths of the NaPi to the calibration curve generated with authentic $Co(NO_3)_2$. The percent of total cobalt refers to the percent of cobalt that is detected in solution compared to the total Co(II) present initially in the specific Co-POM. Error bars are the standard deviation from three repeat experiments. The lines between points have been added to guide the eye and, hence, are not fits to any specific equation. The $Co(II)_{aq}$ vs time plots for the other Co-POMs are shown in Figure S4.11 of the Supporting Information.

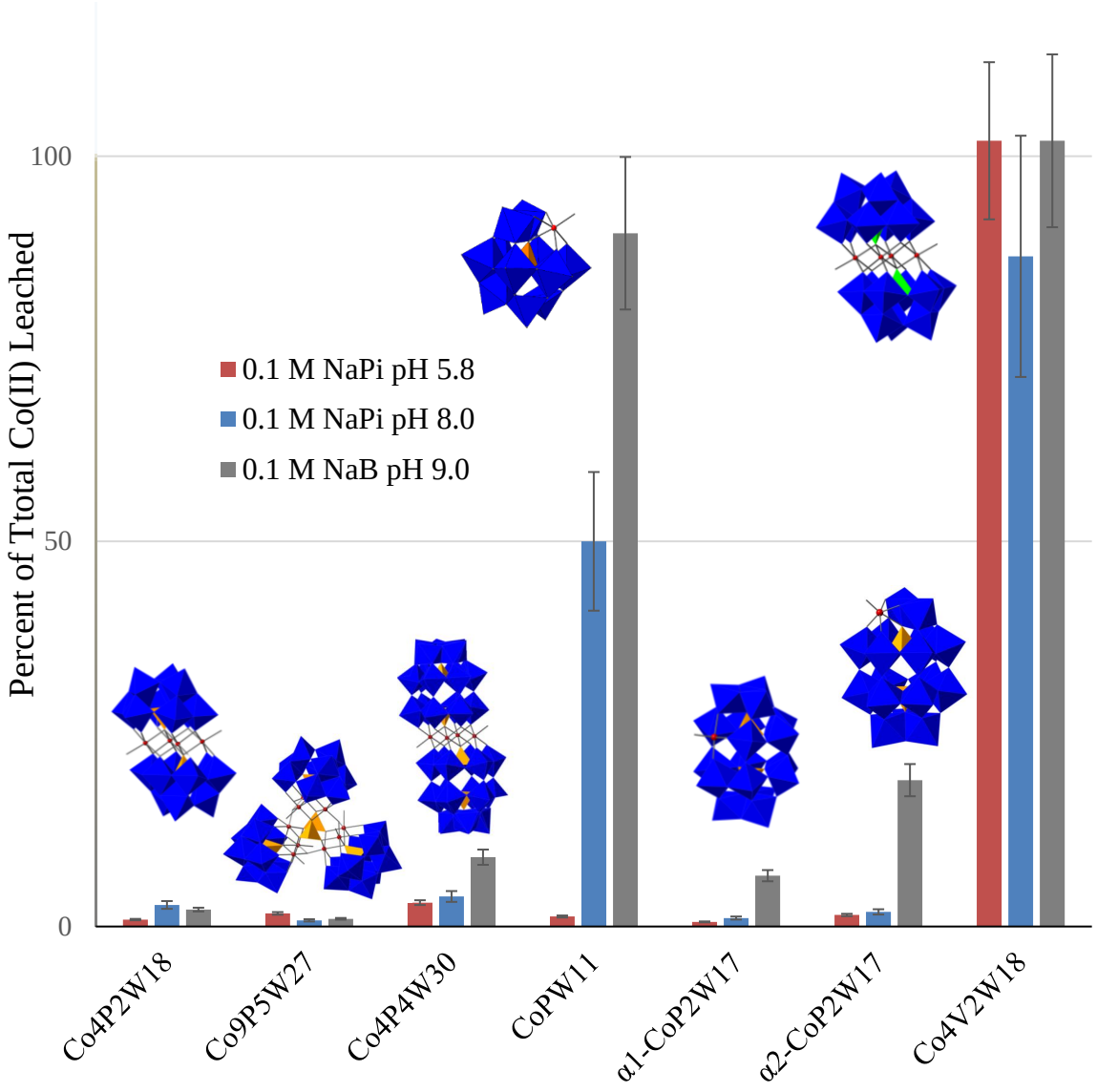

Figure 4.3. Percent of total cobalt that is present as $Co(II)_{aq}$ after three hours of aging in solution for 500 μM solutions of each Co-POM in 0.1 M NaPi pH=5.8 (red), and pH=8.0 (blue) as well as in 0.1 M NaB pH=9.0 (grey). Decomposition data for $\mathbf{Co_4V_2W_{18}}$ has been adapted from reference 26 with permission for comparison with the other Co-POMs, albeit with a 5 μM Co-POM concentration under otherwise identical conditions. The lower concentration of $\mathbf{Co_4V_2W_{18}}$ had to be used because $\mathbf{Co_4V_2W_{18}}$ is so unstable that, at 500 μM, the $Co(II)_{aq}$ detected is outside the linear range of the calibration curve. Copyright 2017 American Chemical Society.

Table 4.1. Comparison of the leached $Co(II)_{aq}$ (μM) after 3 hours of solution aging from 500 μM Co-POM solutions under the three buffer conditions (values shown in **bold** in parentheses are the percent of cobalt that has dissociated from the Co-POM compared to the total cobalt present initially in the Co-POM). The $Co(II)_{aq}$ values in 0.1 M NaPi at pH 5.8 and 8.0 were determined using $Co(II)_{aq}$ induced line broadening ^{31}P NMR. The $Co(II)_{aq}$ values in 0.1 M NaB pH 9.0 were determined using cathodic stripping.

	[$Co(II)_{aq}$] by ^{31}P NMR , μM **(Co(II) %**; after 3 hours) [Data Range]		[$Co(II)_{aq}$] by Cathodic Stripping, μM **(Co(II)%** after 3 hours) [Data Range]
Polyoxometalate	**0.1 M NaPi pH 5.8** [Data Range]	**0.1 M NaPi pH 8.0** [Data Range]	**0.1 M NaB pH 9.0** [Data Range]
$Co_4P_2W_{18}$	11 ± 3 **(0.5 ± 0.2%)** [8-15]	55 ± 3 **(2.8 ± 0.3%)** [52-58]	44 ± 5 **(2.2 ± 0.3%)** [38-49]
$Co_9P_5W_{27}$	75 ± 2 **(1.7 ± 0.1%)** [73-77]	37 ± 2 **(0.8 ± 0.1%)** [35-39]	44 ± 5 **(1.0 ± 0.1%)** [39-50]
$Co_4P_4W_{30}$	62 ± 3 **(3.1 ± 0.4%)** [59-66]	79 ± 3 **(3.9 ± 0.1%)** [77-82]	170 ± 20 **(9 ± 1%)** [150-192]
$CoPW_{11}$	6 ± 3 **(1.3 ± 0.6%)** [3-9]	247 ± 3 **(50 ± 5%)** [245-250]	440 ± 50 **(90 ± 10%)** [390-490]
α_1-CoP_2W_{17}	2.9 ± 3 **(0.6 ± 0.6%)** [0.2-6.0]	6 ± 3 **(1.2 ± 0.6%)** [3-9]	33 ± 5 **(6.6 ± 0.6%)** [29-38]
α_2-CoP_2W_{17}	7.7 ± 3 **(1.5± 0.6%)** [4-11]	10 ± 3 **(1.9 ± 0.6%)** [7-12]	97 ± 9 **(19 ± 2%)** [88-106]

Three of the Co-POMs examined, specifically **$Co_4P_2W_{18}$**, **$Co_9P_5W_{27}$**, and **$CoPW_{11}$**, show increasing concentration of Co(II) leached into solution over 3 h at pH=8.0 and 5.8, Figure 4.2 and S11 of the Supporting Information. For these cases, the detected, *increasing* $Co(II)_{aq}$ is most simply attributed to (continued) dissociation of Co(II) from the Co-POM precatalyst. One interesting point

to note is that while **$Co_4P_2W_{18}$** is more stable at pH=5.8, **$Co_9P_5W_{27}$** is more stable at pH=8.0. This is consistent with the fact that a mixture of **$Co_4P_2W_{18}$** and **$Co_9P_5W_{27}$** is obtained from reactions of HPO_4^{2-}, Co(II), and WO_4^{2-},[30] with **$Co_9P_5W_{27}$** being more prevalent at the more basic pH>7.[31] Restated, this evidence suggests unsurprisingly that individual Co-POMs tend to be more stable in the pH range where they are synthesized. Leaching of $Co(II)_{aq}$ from the complex is consistent with hypothesis #3 from Scheme 4.1.

The other three Co-POMs, **$Co_4P_4W_{30}$**, **α_1-CoP_2W_{17}**, and **α_2-CoP_2W_{17}**, show detectable, 0.6(±0.6)% [range 0.04 to 1.2%] to 3.9(±0.1)%, but relatively flat, $Co(II)_{aq}$ over 3 h at pH 5.8 and 8.0 (with the exception of **α_2-CoP_2W_{17}** at pH 8.0, *vide infra*). Note here that the ~0.6% *is experimentally non-zero in each measurement*, but at the lower limits (and hence ±0.6%) error bars of even our sensitive, uM measurement of $Co(II)_{aq}$.

A flat $Co(II)_{aq}$ vs time dependence implies either: (i) that rapid $Co(II)_{aq}$ dissociation from the Co-POM to reach equilibrium quickly has occurred, or (ii) that the $Co(II)_{aq}$ is present as a counter cation to the Co-POM from the synthesis (or, conceivably (iii) a combination of (i) and (ii)). If the $Co(II)_{aq}$ is, in fact, present as a counter cation, then one might expect to observe a high Co(II) weight percent (wt.%) in the elemental analysis.

However, as an example, the wt.% of Co by elemental analysis for $Na_{16}[\beta\beta\text{-}Co_4(H_2O)_2(P_2W_{15}O_{56})]\cdot 39H_2O$ (**$Co_4P_4W_{30}$**) is 2.62% vs the expected 2.69%—so is not high. Furthermore, the molar amount of Co(II) present in the **$Co_4P_4W_{30}$** solutions (14 to 16 % mol Co(II)/mol Co-POM) is not distinguishable if one assumes an error of ±0.4 absolute wt.%. Indeed, the expected wt. % cobalt would change from <u>2.69%</u> for the elemental formula of the pure $Na_{16}\beta\beta\text{-}[Co_4(H_2O)_2(P_2W_{15}O_{56})]\cdot 39H_2O$ to <u>2.81%</u> for the case where 16 mol% of Co(II)/ **$Co_4P_4W_{30}$** as a counter cation was present for a hypothetical elemental formula of $Na_{15.68}$**<u>$Co_{0.16}$</u>**$[\beta\beta\text{-}$

$Co_4(H_2O)_2(P_2W_{15}O_{56})]\cdot 39H_2O$, a difference of only 0.11 wt. %. In short, a publishable (±0.4% absolute wt.%) *elemental analysis is not sufficient evidence to disprove Co(II) impurities* as counter cations present in **$Co_4P_4W_{30}$** nor, by analogy, more generally in other Co-POMs.

To provide evidence for or against $Co(II)_{aq}$ being present as a counter cation vs the rapid dissociation of Co(II) from **$Co_4P_4W_{30}$** to an equilibrium value, we conducted ^{31}P NMR control experiments by adding 1 equiv. EDTA/$Co(II)_{aq}$ to the **$Co_4P_4W_{30}$** solutions and then conducting the ^{31}P NMR line-broadening experiment, Figure 4.4. The results of that experiment show that addition of 1 equiv. of EDTA/$Co(II)_{aq}$ lowers—*but does not remove all*—of the $Co(II)_{aq}$ (black dashed line, Figure 4.4). Furthermore, an important observation is that the $Co(II)_{aq}$ concentration does not immediately return to the higher, 60-80 μM value, thereby ostensibly ruling out a fast, initial release of $Co(II)_{aq}$ to reach an equilibrium level at either pH of 8.0 or 5.8. Addition of a higher, 100 μM amount of EDTA does, however, remove all of the observed $Co(II)_{aq}$, which then *remains at zero* and hence constant within experimental error over the 3 hour experiment (black solid line, Figure 4.4). In short, the data suggest that the $Co(II)_{aq}$ being detected is present initially at a counter-cation attached tightly to the highly negatively charged, [*ββ*-$Co_4(H_2O)_2(P_2W_{15}O_{56})_2]^{16-}$ polyoxopolyanion and, therefore, not available to contribute to the phosphate line broadening to any great extent. Such tight-ion pairing between a dicationic $Co(II)^{2+}$ and the 16 minus POM, [*ββ*-$Co_4(H_2O)_2(P_2W_{15}O_{56})_2]^{16-}$, even in water is not unreasonable nor unexpected, at least in hindsight.

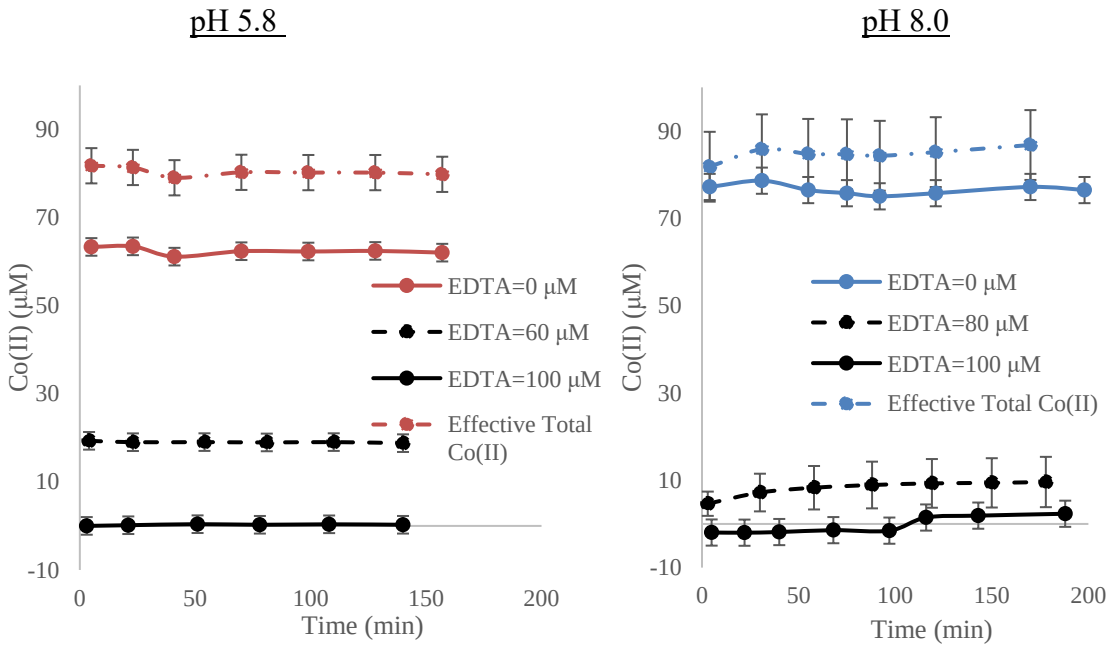

Figure 4.4. Plots of $Co(II)_{aq}$ concentration vs time for a 500 μM solution of **$Co_4P_4W_{30}$** in 0.1 M NaPi (pH 5.8, left and pH 8.0, right). The red and blue lines are for **$Co_4P_4W_{30}$** in the absence of any added EDTA (i.e., the same as Figure 4.2), the dashed black lines are for experiments where 1 equiv. of EDTA/$Co(II)_{aq}$ has been added (60 and 80 μM for pH 5.8 and 8.0 respectively), and solid black lines represent the addition of excess EDTA (100 μM). The dashed red and blue lines represent the true $Co(II)_{aq}$ concentration (i.e., the sum of the solid colored line with the dashed black line for each pH condition.

The evidence provided above demonstrates that that is an EDTA-removable amount of additional ^{31}P NMR line broadening in the **$Co_4P_4W_{30}$** system, consistent with an additional amount of tight ion paired Co(II) attached to the $[\beta\beta\text{-}Co_4(H_2O)_2(P_2W_{15}O_{56})_2]^{16-}$. It is therefore reasonable to sum the observed $Co(II)_{aq}$ in the absence of EDTA with the observed $Co(II)_{aq}$ seen upon the addition of 1 equiv. of EDTA to give the total apparent Co(II)aq as shown in Figure 4.4. Specifically, one can calculate that in pH=5.8 buffer, the total $Co(II)_{aq}$ value = 62(±1) + 19(±2) = 81(±2) μM (i.e., the solid red line plus the dashed black line yields the dashed red line in Figure 4.4), while in pH=8.0 the total $Co(II)_{aq}$= 78(±2) + 10(±3) = 88(±4) (i.e., the solid blue line plus the dashed black line yields the dashed blue line in Figure 4.4). Averaging the pH 5.8 and 8.0 data yields a $Co(II)_{aq}$ value of 85(±4) μM as an estimate of the amount of $Co(II)_{aq}$ present as a counter

cation from the synthesis in **$Co_4P_4W_{30}$**. The systematic difference of the measured $Co(II)_{aq}$ in pH 5.8 vs 8.0 of 62(±1) vs 78(±2) μM, respectively, is discussed in the Supporting Information for the interested reader.

The prevalence of Co(II) as a counter cation is an important finding for at least two reasons, the first of which is because it is evidence for hypothesis #2 from Scheme 4.1, where Co(II) is present as a normally undetected impurity in the post-synthesis **$Co_4P_4W_{30}$**.[28] Second, the results in Figure 4.4 are significant as they imply that the presence of dication impurities in the syntheses of highly charged POMs is very likely a little recognized, but more general, phenomenon in polyoxometalate and other polyanionic self-assembly syntheses. Because of the intrinsically high molecular weight of large POM anions, low levels of counter-cation impurities are difficult to detect via standard elemental analysis methods such as ICP-OES (*vide supra*). This highlights the power of the $Co(II)_{aq}$-induced ^{31}P NMR line broadening technique because it has high selectivity towards $Co(II)_{aq}$ with a detection limit of ~2 μM $Co(II)_{aq}$, which in turn corresponds to ~0.4 mol% regardless of the molar mass of the Co-POM. Future research using Co-POMs for WOCatalysis should use ^{31}P NMR line broadening to quantify $Co(II)_{aq}$ because it is likely always present in as-synthesized Co-POMs that are not run down ion-exchange columns or not exposed to multiple recrystallizations from, say, Na^+, K^+, or other desired cation-containing recrystallization solutions.

^{31}P NMR Line Broadening Data for the Relatively Stable Co-POMs, α_1-CoP_2W_{17} and α_2-CoP_2W_{17}

For the case of **α_1-CoP_2W_{17}** and **α_2-CoP_2W_{17}** at pH=5.8 and 8.0 and because these Co-POMs appear relatively "stable" in initial $Co(II)_{aq}$ detection experiments, we conducted ^{31}P NMR experiments over a longer time-scale, 7-10 h, Figure S4.12 of the Supporting Information. These longer timescale experiments show that at pH = 5.8, little change beyond experimental error is

observed. Addition of excess EDTA (92 μM) to **α_1-CoP_2W_{17}** and **α_2-CoP_2W_{17}** at pH=5.8 returns the ^{31}P NMR linewidth of NaPi to its natural width of ~2 Hz. Looking closely at Figure S4.12, however, the $Co(II)_{aq}$ concentration increases by ~0.5 μM over the first 3 h, but then appears to reach a steady state of 2.9 ± 3 μM and 7.7 ± 3 μM, ostensibly the equilibrium value of $Co(II)_{aq}$ that dissociates from **α_1-CoP_2W_{17}** and **α_2-CoP_2W_{17}**, respectively, at pH=5.8.

Assuming that the observed $Co(II)_{aq}$ concentration values are in fact the equilibrium $Co(II)_{aq}$ concentrations, estimates of the K_{diss} of the complexes at 25 °C in 0.1 M NaPi at pH=5.8 are 2(±3) x 10^{-8} and 2(±3) x 10^{-10} M for **α_1-CoP_2W_{17}** and **α_2-CoP_2W_{17}**, respectively. While imprecise and order-of-magnitude estimates only, the K_{diss} value for **α_1-CoP_2W_{17}** of 2(±3) x 10^{-8} M is close to the literature K_{diss} value of 1 x $10^{-7.7}$ M for **α_1-CoP_2W_{17}** (in 1 M $Li(NO_3)_2$ and at 25 °C). The K_{diss} value for **α_2-CoP_2W_{17}** estimated herein is 2(±3) x 10^{-10} M, which is 10^4 smaller than the literature value of 1 x $10^{-5.6}$ M for **α_2-CoP_2W_{17}** in 1 M $Li(NO_3)_2$ at 25 °C.[22] Overall, the results teach that **α_1-CoP_2W_{17}** and **α_2-CoP_2W_{17}**, contain from ~0.6 to ~1.5% of their Co(II) in solution and apparently reach equilibrium within three hours in 0.1 M NaPi pH=5.8.

As for the pH=8.0 experiments, observing the $Co(II)_{aq}$ concentration from **α_1-CoP_2W_{17}** over longer time-scales (10 h) at pH=8.0 demonstrates that the $Co(II)_{aq}$ concentration increases at a slow rate without plateauing—even after 10 h. This indicates that **α_1-CoP_2W_{17}** is unstable at pH=8.0 and dissociates $Co(II)_{aq}$, Figure S4.12. Intriguingly, the $Co(II)_{aq}$ concentration from **α_2-CoP_2W_{17}** actually *decreases* over time in the pH 8.0 solution (Figure S4.11 and S4.12 of the Supporting Information). Possible explanations for this interesting observation, notably the possible consumption of Co(II) by the conceivable formation of **$Co_4P_4W_{30}$**, are discussed in the Supporting Information for the interested reader.[55,56]

To summarize the $Co(II)_{aq}$-induced ^{31}P NMR line broadening experiments, *all of the Co-POMs examined show non-zero detectable amounts of $Co(II)_{aq}$ under the buffer conditions specified.* The amount of $Co(II)_{aq}$ released into solution ranges from ~0.6% to 50% of the total cobalt. Furthermore, due to the large molecular mass of the Co-POMs, cobalt elemental analysis is insufficient to quantify Co(II) present as a counter cation and at the low levels that can matter for WOCatalysis by electrode bound and formed CoO_x. However, $Co(II)_{aq}$-induced line broadening of the ^{31}P NMR peak of NaPi is a much more useful, powerful, and relatively direct technique to quantify the amount of $Co(II)_{aq}$ either leached into solution, or present initially as a Co(II) counter ion inpurity from syntheses employing Co(II).

Stability of the Co-POMs—cathodic stripping. Because ^{11}B is a quadrupolar nucleus with relative receptivity of 0.165 compared to ^{1}H, and perhaps also because borate buffer has a complex speciation, especially near its pK_a, with at least 5 boron species being present,[54] $Co(II)_{aq}$-induced ^{11}B NMR line broadening is unknown at present. Hence, to measure the amount of $Co(II)_{aq}$ that leaches from the Co-POMs after 3 hours of aging in *0.1 M NaB pH 9.0 buffer*, cathodic stripping was employed as the most convenient, sensitive, and selective method presently available.

The results of the cathodic stripping studies are summarized in Figure 4.3 and Table 4.1. The amount of $Co(II)_{aq}$ detected for the 6 prototype Co-POMs by ^{31}P NMR at pH 5.8 and 8.0 are also summarized in Table 4.1 for comparison. The amount of $Co(II)_{aq}$ detected by cathodic stripping for the 0.1 M NaPi pH=8.0 conditions proved to be the same within experimental error to the $Co(II)_{aq}$ detected by ^{31}P NMR (the error bars are much larger for cathodic stripping, that method often complicated by W reduction waves in the differential pulse voltammetry).

The results in Table 4.1 further demonstrate that all of the Co-POMs show some detectable $Co(II)_{aq}$ under any of the conditions examined, ranging from ~0.6% to now ~90%of the total cobalt

present initially in the Co-POMs in the more basic, pH = 9.0 solution. Additionally, clear solution pH-dependent trends are apparent for each Co-POM, Table 4.1. For example, after 3 hrs the relatively stable **$CoPW_{11}$** dissociates just 1.3(±0.6) % of its Co(II) in pH 5.8, but dissociates 50(±5) and 90(±10)% of its Co(II) in pH 8.0 and 9.0 solution, respectively. The pH stability of **$CoPW_{11}$** makes sense considering that the synthesis of **$CoPW_{11}$** relies on the partial degradation of the parent $PW_{12}O_{40}^{3-}$ Keggin ion occurrs at pH ~5[38] (the parent $PW_{12}O_{40}^{3-}$ itself being prepared using concentrated HCl[36]). Hence, **$CoPW_{11}$** is more stable at the mildly acidic pH 5.8 NaPi buffer employed, and then is as expected less stable at the higher, pH 8-9 values.

Overall, our results reiterate an undeniable fact about Co-POMs, namely that Co-POM precatalysts cannot be generally described as 100% "stable"[25] over time under a variety of common buffer and WOCatalysis pH conditions, at least as judged by whether or not $Co(II)_{aq}$ is detectable at the ~0.6% or higher, μM level. Instead, each of **$Co_4P_2W_{18}$**, **$Co_9P_5W_{27}$**, **$Co_4P_4W_{30}$**, **$CoPW_{11}$**, **α_1-CoP_2W_{17}**, and **α_2-CoP_2W_{17}** show somewhere between the limits seen of ~0.6% to ~90% detectable $Co(II)_{aq}$ in 0.1 M, NaPi pH=5.8 or 8.0 and NaB pH=9.0 buffer solutions. The percentage of the WOCatalysis observed that can, therefore, be attributed to CoO_x formed from even those trace levels of $Co(II)_{aq}$ has to be carefully examined to answer the question of if the observed WOCatalysis is by the intact, molecular Co-POM or the often low-level amount of, however, high activity CoO_x formed by even trace levels of $Co(II)_{aq}$.

WOCatalysis activity: confirming the anodic current is due to water oxidation. To ensure that the anodic current being observed is from water oxidation, and not some other process such as oxidation of the glassy carbon electrode (which has been observed in potentials greater than +1.4 V vs. Ag/AgCl),[28] we quantified the O_2 produced under standard conditions of 500 μM Co-POM aged 3 h or $Co(NO_3)_2$ (6-500 μM), 0.1 M NaPi pH=5.8 or 8.0, and NaB pH=9.0 and at 1.1

V vs Ag/AgCl for 5 min. The theoretical O_2 yield for each electrolysis experiment was calculated by dividing the total charge passed in coulombs (determined by integrating the current over time) by the charge of an electron (1.602×10^{-19} C/e$^-$) and using the stoichiometry of 4 e$^-$ passed per each 1O_2 produced. The O_2 concentration was monitored using an Ocean Optics NEOFOX O_2-detection probe. By dividing the measured O_2 yield at the end of the reaction by the theoretical O_2 yield, the faradaic efficiency of the reaction was also determined.

The observed faradaic efficiency *ranged from 80-100%* and is likely closer to ~100% in all cases. Evidence in support of this statement is that a steady decline in the detected O_2 concentration is after electrolysis stops observed, specifically a ca. 8% decline over a ~1 min period, likely due to O_2 equilibration with the reaction vessel headspace or even escape from the electrochemical cell. Nevertheless, the O_2 determinations do allow two important conclusions: first, the Faradaic efficiency of O_2 production is ≥80-100%, and second, because the faradaic efficiency is 100% within 20% error, the anodic current can be used as a semi-quantitative metric to compare WOCatalysis activity of the Co-POMs and authentic CoO_x (i.e., and to within a tolerable, ±<20% error).

WOCatalysis activity: O_2 evolution from Co-POMs in comparison with the $Co(II)_{aq}$ released. Constant potential electrolysis was conducted on 3 h aged 500 μM solutions of the Co-POMs and $Co(NO_3)_2$ in each of the buffer conditions. The $Co(NO_3)_2$ concentrations chosen to compare with each Co-POM were based upon the amount of $Co(II)_{aq}$ that was detected in each buffer condition, Table 4.1, *vide supra*. The O_2 produced by each Co-POM is summarized in Table S4.2 of the Supporting Information. The amount of WOCatalysis activity that can be attributed to $Co(II)_{aq}$ is shown in Table 4.2, in which the O_2 yield from $Co(II)_{aq}$ is divided by the O_2 yield from the Co-POM. *A value of 100% (or more) means that all of the catalysis is quantitatively accounted*

for by Co(II)$_{aq}$. For example, the percentage of WOCatalysis activity that can be attributed to Co(II)$_{aq}$ for **$Co_4P_2W_{18}$** in NaPi pH=8.0 is 150±50%. Such values near or >100% mean that the Co(II)$_{aq}$ present is able to account for all of the WOCatalysis under those specific conditions.

Table 4.2. Percent of WOCatalysis activity that can be accounted for by Co(II)$_{aq}$ for the Co-POMs in each buffer condition. The Co-POMs (500μM) were aged 3 h in each buffer condition. Electrolysis was then conducted at 1.1 V vs Ag/AgCl. The O_2 yield (μmol) was determined as described in the text and is listed in Table S4.2 of the Supporting Information. To compare with the amount of Co(II)$_{aq}$ that is leached, $Co(NO_3)_2$ was used in the concentrations determined and summarized in Table 4.1. The amount of O_2 produced from the Co(II)$_{aq}$ was divided by the amount of O_2 produced from the Co-POMs to determine the percent of WOCatalysis activity that can be accounted for by the Co(II)$_{aq}$ present.

	Buffer System		
Polyoxometalate	**0.1 M NaPi pH 5.8**	**0.1 M NaPi pH 8.0**	**0.1 M NaB pH 9.0**
$Co_4P_2W_{18}$	60 ± 30%	150 ± 50%	400 ± 200%
$Co_9P_5W_{27}$	70 ± 60%	96 ± 24%	300 ± 200%
$Co_4P_4W_{30}$	60 ± 40%	140 ± 70%	140 ± 70%
$CoPW_{11}$	20 ± 20%	180 ± 40%	100 ± 40%
α_1-CoP_2W_{17}	30 ± 20%	90 ± 30%	350 ± 40%
α_2-CoP_2W_{17}	60 ± 60%	90 ± 50%	800 ± 300%

Values significantly above 100% (e.g., for **α_2-CoP_2W_{17}** at pH 9.0, 800 ± 300%, Table 4.2) indicate that the Co(II)$_{aq}$ and subsequent CoO_x films have *greater* WOCatalysis activity than the films generated from the measured amount of Co(II)$_{aq}$ and in the presence of the Co(II)-leaching Co-POMs. The >>100% values are interesting, and suggest several possible situations, including: (i) that the Co-POM somehow poisons the CoO_x film; (ii) that the NO_3^- somehow enhances the catalysis in CoO_x made from $Co(NO_3)_2$; (iii) that the Co(II)$_{aq}$ values determined by ^{31}P NMR or cathodic stripping are somewhat higher than the true Co(II)$_{aq}$ values; or (iv) that the film formation (and for example possible surface area and number of active sites) is affected by the pH[54] or the presence of POMs, which in turn affects the observed WOCatalysis.

Values <100% are also of considerable interest because they imply molecular, homogenous Co-POM WOCatalysis. Specifically, the percentage of WOCatalysis activity that can be attributed to $Co(II)_{aq}$ for **$CoPW_{11}$** and **α_1-CoP_2W_{17}** in NaPi pH=5.8 are 20(±20)% and 30(±20)%, respectively, meaning that *intact **$CoPW_{11}$** and **α_1-CoP_2W_{17}** are the dominant electrochemically driven WOCatalyst at pH=5.8 for 80(±20)% and 70(±20)%* of the observed *current, an important, previously unavailable insight.* The data are compelling in that the most stable Co-POMs examined, **$CoPW_{11}$** and **α_1-CoP_2W_{17}**, can serve as electrochemically driven, molecular WOCatalysts.

Looking more broadly at Table 4.2, there are several overarching trends in the data and even at the inherently large error bars (as discussed more in the Supporting Information) that derive from having to detect mere μM levels of $Co(II)_{aq}$: at lower pH the Co-POMs account for a greater amount of the WOCatalysis. At higher pH the WOCatalysis current from $Co(II)_{aq}$ becomes increasingly prevalent, with Co(II) accounting for 100% (to 800%) of the observed WOCatalysis activity. This pH trend in $Co(II)_{aq}$ contribution to WOCatalysis activity makes sense considering that the Co-POMs examined are often (although not always) more stable at the lower pH, for example, **$CoPW_{11}$** decomposes by only 1.3(±0.6)% at pH 5.8 but decomposes by 50(±5)% and 90(±10)% at pH 8.0 and 9.0, respectively. Hence, unsurprisingly, the Co-POMs examined are more likely to be intact WOCatalyst under conditions where they are demonstrably more stable, pH values closer to the pHs at which they form and are synthesized. Also worth noting here is that the CoO_x catalyst is also affected by pH as previously reported,[57] with CoO_x being more active at higher pH, albeit not being stable below pH = 3.5.[57]

The Greater WOCatalysis Activity of CoO_x vs the That of the Most Stable Co-POMs.

Lastly, although our evidence demonstrates that at pH=5.8 **$CoPW_{11}$** and **α_1-CoP_2W_{17}** are homogeneous WOCatalysts, *a critical point is that the CoO_x that is formed from the equivalent amount of $Co(II)_{aq}$ is an estimated ~20-300-fold faster WOCatalyst at pH=5.8 than is the corresponding homogeneous Co-POM*. Even using the ranges and error bars on the data in Tables 4.1 and 4.2 to bias the estimate as positive as possible in favor of the Co-POM (and then also for the single most stable Co-POM examined, **α_1-CoP_2W_{17}**) still yields the released $Co(II)_{aq}$ in the form of CoO_x as *at least* 10-fold more active than **α_1-CoP_2W_{17}**, as detailed further in the Supporting Information.

If one does this same calculation for, again, the most stable **α_1-CoP_2W_{17}** but now at pH = 8, the CoO_x is ~740-fold more active (and at least 80-fold more active if one biases the calculation as much as the data allow in favor of Co-POM-based catalysis; see the Supporting Information for details of these estimates).

To summarize, comparing the WOCatalysis activity of the 3 h aged Co-POMs with the amount of detected $Co(II)_{aq}$ reveals that at pH=8.0 in 0.1 M NaPi and pH=9.0 in 0.1 M NaB, all of the six exemplary Co-POMs examined give rise to heterogeneous CoO_x as the dominant WOCatalyst. However, at pH=5.8 in 0.1 M NaPi and under electrochemically driven WOCatalysis conditions, the evidence suggests that **$CoPW_{11}$** and **α_1-CoP_2W_{17}**, and perhaps also **$Co_4P_2W_{18}$** and **α_2-CoP_2W_{17}**, can serve as homogeneous, molecular WOCatalysts, albeit with CoO_x being ~20-300x faster at pH=5.8, and ~740x faster at pH=8.

Electrochemical characterization of the deposited films. Previous studies have shown that electrode-bound heterogeneous CoO_x formed from aged Co-POM solutions is active towards WOCatalysis.[23,26] Additionally, such CoO_x films remain active when the working electrode is

removed from the original Co-POM solution and placed in a fresh, buffer-only solution,[23,26] thereby providing a way to characterize what amount of the WOCatalysis current detected is attributable to the film.

Controls similar to those performed before[23,26] were therefore conducted as part of the present studies in which controlled potential electrolysis (5 to 30 min) was conducted in 500 μM solutions of Co-POM that had been aged 3 hours. Cyclic voltammetry (CV) was then conducted first in the original Co-POM solution. The electrodes were subsequently removed, rinsed gently with water, replaced into a fresh, buffer-only solution, and a second CV was obtained. The resultant before and after CVs for selected Co-POMs are shown in Figure 4.5; the rest of the CVs for the Co-POMs and additional CV experiments are provided in Figure S4.13 Supporting Information. Figure 4.5a is a control demonstrating that the previously reported, known[23,24] catalytically active film from **$Co_4P_2W_{18}$** can be reproducibly formed as part of the present studies from a 500 μM solution of **$Co_4P_2W_{18}$** in 0.1 M NaPi at pH 8.0 after 3 h aging. Figure 4.5b is a second control that tests the possibility raised previously[24] (but heretofore not tested) that CoO_x might directly form from Co-POMs as well as from $Co(II)_{aq}$ at sufficiently oxidizing potentials. Hence, the experiment reported in Figure 4.5b also contains 500μM **$Co_4P_2W_{18}$** in 0.1 M NaPi at pH 8.0 that has aged 3h, but now has been spiked after aging with 120 μM EDTA to chelate the free ~60 μM $Co(II)_{aq}$ known to be formed. Almost all of the WOCatalysis activity is diminished and no significant film is formed, implying that **$Co_4P_2W_{18}$** does not serve as a direct precursor to CoO_x at pH 8.0, thereby disproving hypothesis #4 from Scheme 4.1.

The CVs shown in Figures 4.5c and 4.5d present the CVs after electrolysis in the original buffer solution, and then in a buffer-only solution for **α_1-CoP_2W_{17}** in 0.1 M NaPi at pH 5.8 and **α_2-CoP_2W_{17}** in 0.1 M NaPi at pH 8.0, respectively (both after 3 hours of solution aging). The

significantly higher current and unique CV features of the original Co-POM solution, vs those for the rinsed electrode replaced into buffer-only solution CV, provide additional evidence for a solution-based species having a role in the observed WOCatalysis for **α_1-CoP_2W_{17}**, **α_2-CoP_2W_{17}**, and **$CoPW_{11}$**. The Ockham's razor-based hypothesis is that, under conditions where a Co-POM such as **α_1-CoP_2W_{17}** in 0.1 M NaPi at pH 5.8 is relatively stable (less than 2% detectable $Co(II)_{aq}$), the **α_1-CoP_2W_{17}** is serving as a molecular, homogeneous WOCatalysts—albeit one with 5-10x lower WOCatalysis current than the CoO_x films formed from the less stable Co-POMs (Table S4.2).

a) $\mathbf{Co_4P_2W_{18}}$ in 0.1 M NaPi pH 8.0

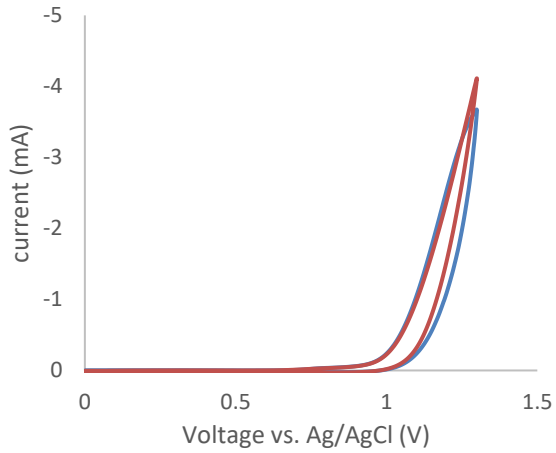

b) $\mathbf{Co_4P_2W_{18}}$ in 0.1 M NaPi pH 8.0 w/EDTA

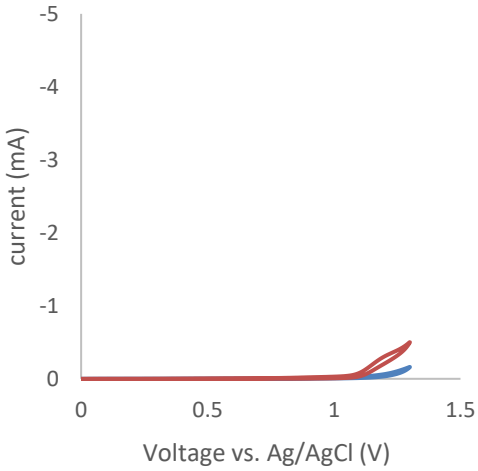

c) $\mathbf{\alpha_1\text{-}CoP_2W_{17}}$ in 0.1 M NaPi pH 5.8

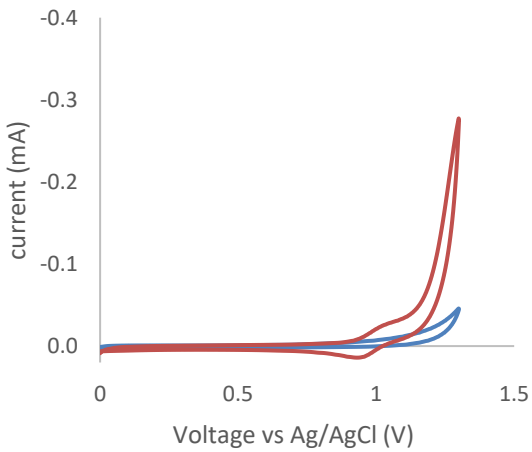

d) $\mathbf{\alpha_2\text{-}CoP_2W_{17}}$ in 0.1 M NaPi pH 8.0

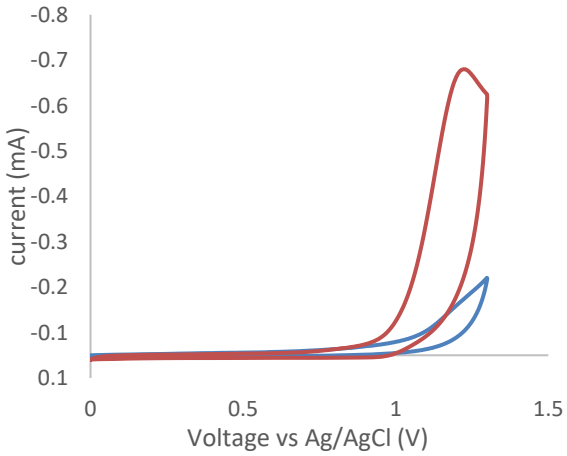

Figure 4.5. Selected CVs of electrodes after 5 min controlled potential electrolysis in the original Co-POM solution (red) and once the electrodes were removed, rinsed, and replaced into a fresh, buffer-only solution (blue). a) $\mathbf{Co_4P_2W_{18}}$ in 0.1 M NaPi pH 8.0 b) $\mathbf{Co_4P_2W_{18}}$ in 0.1 M NaPi pH 8.0 with 120 μM EDTA (2 equiv./ $Co(II)_{aq}$) c) $\mathbf{\alpha_1\text{-}CoP_2W_{17}}$ in 0.1 M NaPi pH 5.8 and d) $\mathbf{\alpha_2\text{-}CoP_2W_{17}}$ in 0.1 M NaPi pH 8.0. The remainder of the CVs are shown in the Supporting Information.

In summary, electrolysis and CV of the electrodes in the electrolyzed solutions (red traces in Figures 4.5 and S4.13 of the Supporting Information) followed by electrolysis in buffer-only

solutions (blue traces in Figures 4.5 and S4.13 of the Supporting Information) helps illuminate whether the active catalyst is a solution-based species or an electrode bound species. The results are in good agreement with the percent WOCatalysis activity from the previous section. For example, at pH 5.8 the percent WOCatalysis evidence suggests that **$Co_4P_2W_{18}$**, **$CoPW_{11}$**, **α_1-CoP_2W_{17}**, and **α_2-CoP_2W_{17}** can serve as molecular, homogeneous, and the CVs for those Co-POMs in pH 5.8 also provide evidence for a solution-based WOCatalyst (Figures 4.5 and S4.13 of the Supporting Information). Other Co-POMs that show evidence of a solution-based WOCatalyst in NaPi at pH=8.0 are **$Co_9P_5W_{27}$**, **α_1-CoP_2W_{17}**, and **α_2-CoP_2W_{17}**, whereas in NaB pH=9.0 only **α_1-CoP_2W_{17}** has evidence of a solution-based WOCatalyst (Figures 4.5 and S4.13 of the Supporting Information). Note that although the CVs of **$Co_9P_5W_{27}$**, **α_1-CoP_2W_{17}**, and **α_2-CoP_2W_{17}** at pH=8.0 and **α_1-CoP_2W_{17}** at pH=9.0 provide evidence of a solution-based WOCatalyst, the results in Table 4.2 provide evidence that under those conditions, CoO_x is still the dominant WOCatalyst.

Morphological and compositional characterization of deposited films. Most of the Co-POMs showed an increase in WOCatalysis activity for longer electrolysis times, which is characteristic of CoO_x film deposition (Figure S4.14 of the Supporting Information).[8,23,26] Hence, we conducted electrolysis for 30 minutes to allow film accumulation and then dried the films for SEM and XPS characterization.

Figure 4.6 shows a typical electrode-bound film of globular particles that are formed from 3 h aged solutions of 500 μM **α_2-CoP_2W_{17}** in 0.1 M NaPi pH 8.0. The XPS of the film from **α_2-CoP_2W_{17}** contains carbon (from the glassy carbon substrate), oxygen, cobalt, sodium, phosphorous, *and tungsten*, Figure 4.6 (right). The presence of tungsten is surprising given that CoO_x films that form from **$Co_4P_2W_{18}$** and **$Co_4V_2W_{18}$** do not contain tungsten.[23,26] The Co:W atom

ratio from the high resolution XPS scans was determined to be 2.1:1.3 whereas the Co:W ratio in the structure is 1:17, meaning that although W incorporation of some type does occur, the original Co-POM is not a major component. This experiment was reproduced twice and similar XPS spectra were obtained, demonstrating reproducible W incorporation—albeit in an unknown form—into CoO_x films produced from 500 μM **α_2-CoP_2W_{17}** in 0.1 M NaPi pH 8.0.

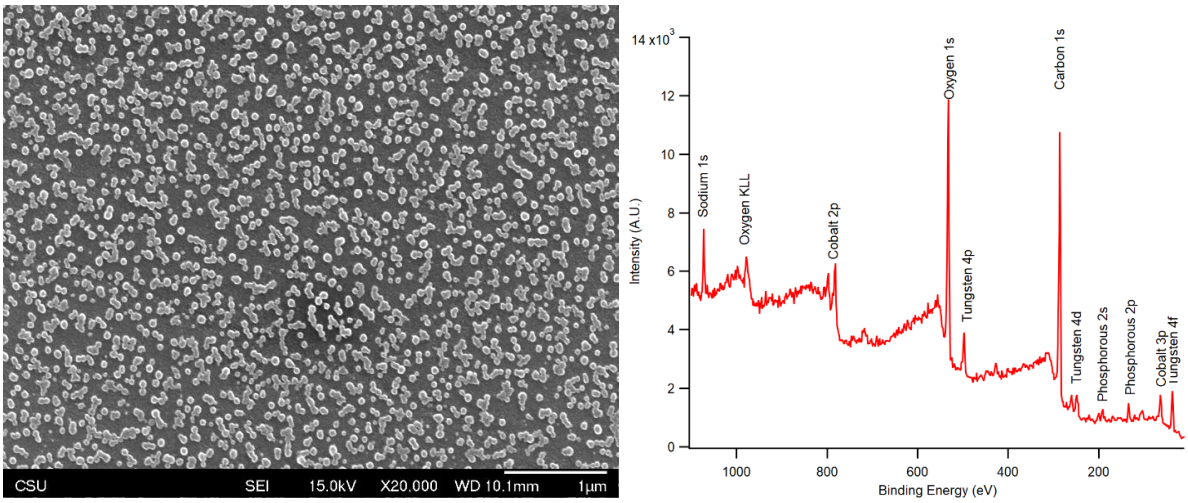

Figure 4.6. SEM micrograph (left) and XPS (right) of electrodes after 30 min bulk electrolysis from a 3 h aged solution of 500 μM **α_2-CoP_2W_{17}** in 0.1 M NaPi pH 8.0. The globular nature of the film is similar to previously observed films from Co(II) or Co-POMs.[8,23,26] The i vs t curve for the film deposition is presented in Figure S4.14 of the Supporting Information.

Next, 30 min. electrolysis was conducted on 3 h aged solutions of 500 μM **$Co_4P_2W_{18}$** in 0.1 M NaPi pH 8.0 with 10 equiv. EDTA/$Co(II)_{aq}$ added after 3 h aging, but prior to electrolysis. The SEM and XPS of that particular electrode is presented in Figure 4.7, and confirms that heterogeneous CoO_x does not form in the presence of excess EDTA from 3 h aged solutions of 500 μM **$Co_4P_2W_{18}$** in 0.1 M NaPi pH 8.0. This finding provides further evidence that the Co-POM cannot form CoO_x directly from, for example, putative electrode-bound Co-POM. Instead, the CoO_x film observed when starting with the **$Co_4P_2W_{18}$** precatalyst is formed by **$Co_4P_2W_{18}$** releasing $Co(II)_{aq}$, consistent with hypothesis #3 (i.e., and not #4) from Scheme 4.1, *vide supra*.

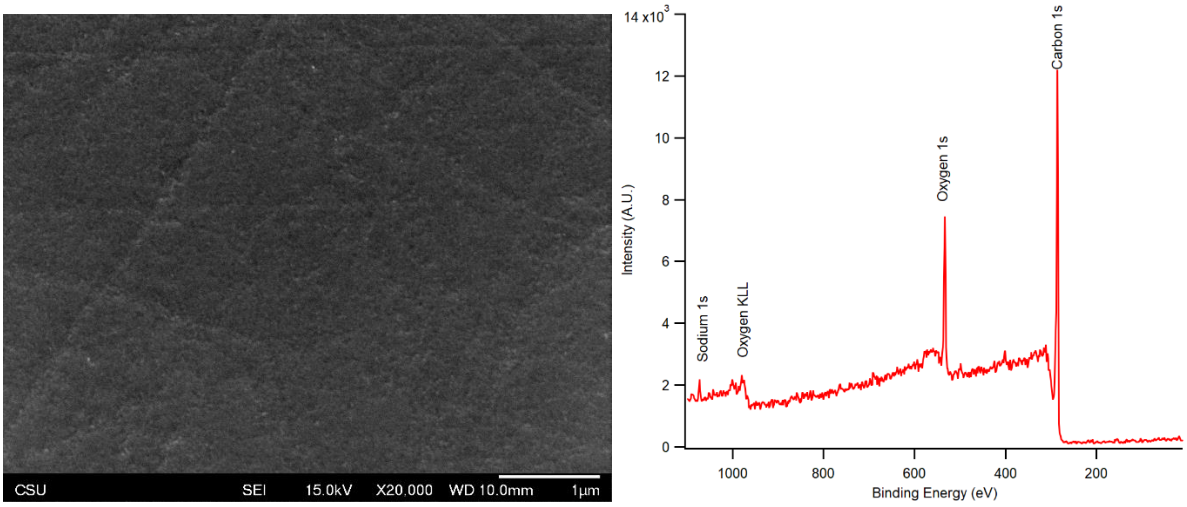

Figure 4.7. SEM micrograph (left) and XPS (right) of electrodes after 30 min bulk electrolysis from a 3 h aged solution of 500 µM **$Co_4P_2W_{18}$** in 0.1 M NaPi pH 8.0 with 600 µM EDTA (10 equiv./ $Co(II)_{aq}$). The i vs t curve for the film deposition is presented in Figure S4.14 of the Supporting Information.

Additional CV experiments using 3 h aged 500 µM **α_1-CoP_2W_{17}** in 0.1 M NaPi pH 5.8 are discussed in the Supporting Information (Figures S4.15 and S4.16). The main results from those experiments using this more stable Co-POM is that no detectable film is formed from the bulk electrolysis of the Co-POM solution.

To summarize the experiments on the electrochemical and morphological characterization of the deposited films, under conditions where the Co-POMs show >2% detectable $Co(II)_{aq}$, CoO_x is formed and that film accounts quantitatively for the observed WOCatalysis (Table 4.2, Figures 4.3, S4.13, and S4.16 of the Supporting Information). However, under conditions where the Co-POMs are more stable (<2% detectable $Co(II)_{aq}$) such as with **α_1-CoP_2W_{17}**, not detectable electrode-bound CoO_x is seen. Rather, a solution-based species is responsible for the observed WOCatalysis current (Table 4.2, Figures 4.5, S4.13 and S4.15 of the Supporting Information), ostensibly the starting Co-POM at the Ockham's razor level of interpretation. Lastly, addition of a 10-fold excess of EDTA (vs the amount of free $Co(II)_{aq}$ detected) prevents the formation of CoO_x, at least with 3 h aged solution of 500 µM **$Co_4P_2W_{18}$** in 0.1 M NaPi pH 8.0 (Figure 4.7).

This, too, is evidence that CoO_x is formed from $Co(II)_{aq}$ and not from intact, electrode-bound Co-POM.

4.4 Summary and Conclusions

The present study details the broadest and most detailed examination to date of the stability and electrochemically driven WOCatalysis from Co-POM precatalysts. Six exemplary Co-POMs $[Co_4(H_2O)_2(PW_9O_{34})_2]^{10-}$ (**$Co_4P_2W_{18}$**), [*β,β*-$Co_4(H_2O)_2(P_2W_{15}O_{56})_2]^{16-}$(**$Co_4P_4W_{30}$**), $[Co_9(H_2O)_6(OH)_3(HPO_4)_2(PW_9O_{34})_3]^{16-}$ (**$Co_9P_5W_{27}$**), $[Co(H_2O)PW_{11}O_{39}]^{5-}$ (**$CoPW_{11}$**), [α_1-$Co(H_2O)P_2W_{17}O_{61}]^{8-}$ (**α_1-CoP_2W_{17}**);], and [α_2-$Co(H_2O)P_2W_{17}O_{61}]^{8-}$ (**α_2-CoP_2W_{17}**) were synthesized, their structural integrity established, and then their stability and electrochemically driven WOCatalysis examined under carefully chosen pH 5.8, 8.0, and 9.0 buffer conditions. Importantly, the amount of $Co(II)_{aq}$ leached from the Co-POMs into solution was quantified directly using $Co(II)_{aq}$-induced line broadening of the ^{31}P NMR resonance of phosphate buffer at pH 5.8 and 8.0, and by cathodic stripping in the case of pH 9.0 borate buffer. The WOCatalysis activity derived from the Co-POM precatalysts was then compared with the WOCatalysis activity of the equivalent amount of $Co(II)_{aq}$ present in solution from each of the Co-POMs.

The main conclusions from this study are the following:

• Significantly, $Co(II)_{aq}$ at the μM or higher level was detected for every Co-POM under each set of pH and buffer conditions. The amount of detectable $Co(II)_{aq}$ as a percentage of the total cobalt present in each Co-POM varies from ~0.6% to 90% after 3 hours in solution, the precise amount being unique to the POM structure / Co(II) binding site and notably the pH, higher pH values in general leading to higher levels of $Co(II)_{aq}$ (Figure 4.2 and Table 4.1, *vide supra*).

• In the case of highly anionically charged Co-POMs such as [*β,β*-$Co_4(H_2O)_2(P_2W_{15}O_{56})_2]^{16-}$(**$Co_4P_4W_{30}$**), Co(II) can be present as a counter-cation impurity which

is likely a more general phenomenon for M^{n+} ions used in the synthesis of M-POMs (and unless ion-exchange resin, recrystallization from counter-ion-controlled solutions, or other counter-cation control efforts have been taken).

• In 12 out of the 18 Co-POM cases at pH 8.0 and 9.0, the amount of heterogeneous CoO_x generated from the detected $Co(II)_{aq}$ accounts for ≥100% of the observed activity—meaning that under those higher pH conditions the kinetically dominant, electrochemically driven WOCatalyst is heterogeneous CoO_x (Table 4.2). In those cases, just using Co(II) salts to prepare the resultant, high-activity CoO_x would be a better, easier, greener use of chemicals, time, and synthetic effort.

• In terms of catalytic rate, at pH 8.0 and for the single most stable Co-POM, **α_1-CoP_2W_{17}**, the CoO_x catalyst formed from $Co(II)_{aq}$ is an estimated ~740-fold more active than any (undetectable) Co-POM based WOC. As an illustrative example, this means that even ~0.14% of decomposition of **α_1-CoP_2W_{17}** to $Co(II)_{aq}$ can in turn, at pH = 8.0, carry ≥99% of the catalytic WOCatalysis current.

• However, under pH 5.8 conditions where the Co-POMs are generally more stable, the amount of $Co(II)_{aq}$ detected *cannot* account for the observed WOCatalysis. Specifically, for **$CoPW_{11}$** and **α_1-CoP_2W_{17}** at pH 5.8 where <2% detectable $Co(II)_{aq}$ is seen, ≥70-80% (±≤30%) of the observed WOCatalysis activity can be ascribed to *molecular, Co-POM-based catalysis*, Table 2, *vide supra*. That said, the Co-POM-based WOCatalysis rate is still an estimated ~20-300-fold lower than that for an equivalent amount of CoO_x for even the most stable Co-POM examined, **α_1-CoP_2W_{17}**.

• In general, our findings confirm and fully support those of prior workers who have concluded that the reaction conditions are hugely important in determining the identity of the kinetically dominant WOCatalyst derived from Co-POMs.[17,24,25,26]

• A summary of additional POMs used in WOCatalysis, but which are not discussed in the main text yet merit further study in several cases as to the identity of the true catalyst, are presented in Table S4.1 of the Supporting Information for the interested reader.

Finally and overall, the results obtained and presented herein in combination with prior notable work in the field of electrocatalytic WOCatalysis,[13,17,23,24,25,26] go far in suggesting that even more hydrolytically stable Co-POM and other Metal-POM WOCatalysts merit development, and most importantly illustrate a successful, arguably preferred methodology for distinguishing molecular homogeneous from metal-oxide heterogeneous WOCatalysts and when metal-leaching or counter-cation contamination is present at just μM levels. It is hoped that these efforts will allow even more stable and active Co-POM based WOCatalysts to be developed in studies that use the methodology herein and report compelling evidence for or against molecular, Co-POM-based vs heterogeneous, CoO_x-based WOCatalysis.

Supporting Information. The Supporting Information can be found in Appendix III and contains: **Table S4.1. Compilation of POMs used in WOCatalysis that are not mentioned in the main text.** **Synthesis of $Na_{16}[\beta,\beta\text{-}Co_4(H_2O)_2(P_2W_{15}O_{56})_2]\cdot 39H_2O$.** **Figure S4.1.** FT-IR of $Na_{16}[\beta,\beta\text{-}Co_4(H_2O)_2(P_2W_{15}O_{56})_2]\cdot 39H_2O$. **Figure S4.2.** ^{31}P NMR of $Na_{16}[\beta,\beta\text{-}Co_4(H_2O)_2(P_2W_{15}O_{56})_2]\cdot 39H_2O$. **Synthesis of $K_5[Co(H_2O)PW_{11}O_{39}]\cdot 14H_2O$.** **Figure S4.3.** FT-IR of $K_5[Co(H_2O)PW_{11}O_{39}]\cdot 14H_2O$. **Figure S4.4.** ^{31}P NMR of $K_5[Co(H_2O)PW_{11}O_{39}]\cdot 14H_2O$. **Synthesis of $K_8[\alpha_1\text{-}Co(H_2O)P_2W_{17}O_{61}]\cdot 17H_2O$.** **Figure S4.5.** FT-IR of $K_8[\alpha_1\text{-}Co(H_2O)P_2W_{17}O_{61}]\cdot 17H_2O$. **Figure S4.6.** ^{31}P NMR of $K_8[\alpha_1\text{-}Co(H_2O)P_2W_{17}O_{61}]\cdot 17H_2O$. **Synthesis of $K_8[\alpha_2\text{-}Co(H_2O)P_2W_{17}O_{61}]\cdot 15H_2O$.** **Figure S4.7.** FT-IR of $K_8[\alpha_2\text{-}Co(H_2O)P_2W_{17}O_{61}]\cdot 15H_2O$. **Figure S4.8.** ^{31}P NMR of $K_8[\alpha_2\text{-}Co(H_2O)P_2W_{17}O_{61}]\cdot 15H_2O$. **Figure S4.9.** Calibration curves for the $Co(II)_{aq}$-induced line broadening of the NaPi ^{31}P NMR peak.

Figure S4.10. Calibration curve for the adsorptive cathodic stripping experiments in 0.1 M NaPi pH=8.0 and 0.1 M NaB pH=9.0. **Figure S4.11.** Plots of $Co(II)_{aq}$ concentration vs time for a 500 μM solution of **$CoPW_{11}$** **α_1-CoP_2W_{17}** and **α_2-CoP_2W_{17}** in 0.1 M NaPi pH 5.8 and 8.0. *The pH 5.8 vs 8.0 ^{31}P Line-Broadening Data for $Co_4P_4W_{30}$: A Discussion of An Apparent Systematic Difference of ~20%, ~16(±~3) μM Apparent $Co(II)_{aq}$.* **Figure S4.12.** Longer time-scale ^{31}P NMR line broadening of a) **α_1-CoP_2W_{17}** pH=5.8 NaPi; b) and **α_2-CoP_2W_{17}** pH=5.8; c) **α_1-CoP_2W_{17}** pH=8.0; d) **α_2-CoP_2W_{17}** NaPi pH= 8.0. *Discussion of the Decrease in $Co(II)_{aq}$ concentration from α_2-CoP_2W_{17} in 0.1 M NaPi pH= 8.0.* **Table S4.2.** Theoretical O_2 (μmol) from 5 min electrolysis of 3 h aged Co-POMs. *Discussion of the WOCatalysis activity of CoO_x derived from $Co(II)_{aq}$ compared with the WOCatalysis activity from the Co-POMs.* **Cyclic voltammograms of 3 h aged Co-POMs after 5 min electrolysis in the original Co-POM solution (red) and the same electrode in a buffer-only solution (blue). Figure S4.13.** Additional cyclic voltammograms experiments with select Co-POMs. *Discussion of the prolonged electrolysis of 3 h aged 500 μM α_1-CoP_2W_{17} in 0.1 M NaPi pH 5.8.* **Figure S4.14.** Current vs. time for the electrodes used for SEM and XPS in the main text. **Figure S4.15.** CVs and constant potential electrolysis curves of 3 h aged 500 μM α_1-CoP_2W_{17} in 0.1 M NaPi pH 5.8. **Figure S4.16.** XPS of the glassy carbon electrode from the constant potential electrolysis of 3 h aged 500 μM **α_1-CoP_2W_{17}** in 0.1 M NaPi pH 5.8. **A** *Brief Discussion of the Error Bars in Table 4.2.*

REFERENCES

1 Turner, J. A. A Realizable Renewable Energy Future. *Science* **1999**, *285*, 687–689.

2 Lewis, N. S.; Nocera, D. G. *PNAS* **2006**, *103*, 15729–15735.

3 Kärkäs, M.; Åkermark, B. *Dalton Trans.* **2016**.

4 Llobet, A. *Molecular Water Oxidation Catalysis*; 1 edition.; Wiley, 2014.

5 Liu, F.; Concepcion, J. J.; Jurss, J. W.; Cardolaccia, T.; Templeton, J. L.; Meyer, T. J. *Inorg. Chem.* **2008**, *47*, 1727–1752.

6 Geletii, Y. V.; Botar, B.; Kögerler, P.; Hillesheim, D. A.; Musaev, D. G.; Hill, C. L. *Angew. Chem. Intl. Ed.* **2008**, *47*, 3896–3899.

7 Sartorel, A.; Carraro, M.; Scorrano, G.; Zorzi, R. D.; Geremia, S.; McDaniel, N. D.; Bernhard, S.; Bonchio, M. *J. Am. Chem. Soc.* **2008**, *130*, 5006–5007.

8 Kanan, M. W.; Nocera, D. G. *Science* **2008**, *321*, 1072–1075.

9 Yin, Q.; Tan, J. M.; Besson, C.; Geletii, Y. V.; Musaev, D. G.; Kuznetsov, A. E.; Luo, Z.; Hardcastle, K. I.; Hill, C. L. *Science* **2010**, *328*, 342–345.

10 Huang, Z.; Luo, Z.; Geletii, Y. V.; Vickers, J. W.; Yin, Q.; Wu, D.; Hou, Y.; Ding, Y.; Song, J.; Musaev, D. G. *J. Am. Chem. Soc.* **2011**, *133*, 2068–2071.

11 Zhu, G.; Geletii, Y. V.; Kögerler, P.; Schilder, H.; Song, J.; Lense, S.; Zhao, C.; Hardcastle, K. I.; Musaev, D. G.; Hill, C. L. *Dalton Trans.* **2012**, *41*, 2084.

12 Zhu, G.; Glass, E. N.; Zhao, C.; Lv, H.; Vickers, J. W.; Geletii, Y. V.; Musaev, D. G.; Song, J.; Hill, C. L. *Dalton Trans.* **2012**, *41*, 13043–13049.

13 Goberna-Ferrón, S.; Vigara, L.; Soriano-López, J.; Galán-Mascarós, J. R. *Inorg. Chem.* **2012**, *51*, 11707–11715.

14 Car, P.-E.; Guttentag, M.; Baldridge, K. K.; Alberto, R.; Patzke, G. R. *Green Chem.* **2012**, *14*, 1680.

15 Evangelisti, F.; Car, P.-E.; Blacque, O.; Patzke, G. R. *Catal. Sci. Technol.* **2013**, *3*, 3117.

16 Lv, H.; Song, J.; Geletii, Y. V.; Vickers, J. W.; Sumliner, J. M.; Musaev, D. G.; Kögerler, P.; Zhuk, P. F.; Bacsa, J.; Zhu, G. *J. Am. Chem. Soc.* **2014**, *136*, 9268–9271.

17 Vickers, J. W.; Lv, H.; Sumliner, J. M.; Zhu, G.; Luo, Z.; Musaev, D. G.; Geletii, Y. V.; Hill, C. L. *J. Am. Chem. Soc.* **2013**, *135* (38), 14110–14118.

18 Pope, M. T. *Heteropoly and Isopoly Oxometalates*; Springer-Verlag, 1983.

19 Yamase, T.; Pope, M. *Polyoxometalate Chemistry for Nano-Composite Design*; Springer Science & Business Media, 2006.

20 Pope, M.; Muller, A. *Polyoxometalates: From Platonic Solids to Anti-Retroviral Activity: From Platonic Solids to Anti-Retroviral Activity*; Springer Science & Business Media, 1994.

21 Contant, R.; Ciabrini, J.-P. *J. Chem. Res.* **1982**, 50–51.

22 Contant, R. *J. Chem. Res.* **1984**, 120–121.

23 Stracke, J. J.; Finke, R. G. *J. Am. Chem. Soc.* **2011**, *133*, 14872–14875.

24 Stracke, J. J.; Finke, R. G. *ACS Catal.* **2013**, *3*, 1209–1219.

25 Stracke, J. J.; Finke, R. G. *ACS Catal.* **2014**, *4*, 909–933.

26 Stracke, J. J.; Finke, R. G. *ACS Catal.* **2014**, *4* (1), 79–89.

27 Folkman, S. J.; Finke, R. G. *ACS Catal.* **2017**, *7*, 7–16.

28 Ullman, A. M.; Liu, Y.; Huynh, M.; Bediako, D. K.; Wang, H.; Anderson, B. L.; Powers, D. C.; Breen, J. J.; Abruña, H. D.; Nocera, D. G. *J. Am. Chem. Soc.* **2014**, *136* (50), 17681–17688.

29Platt, J. R. Strong Inference. *Science* **1964**, *146* (3642), 347–353.

30Weakley, T. J. R. *J. Chem. Soc., Chem. Commun.* **1984**, No. 21, 1406–1407.

31 Galán-Mascarós, J. R.; Gómez-Garcia, C. J.; Borrás-Almenar, J. J.; Coronado, E. *Adv. Mater.* **1994**, *6* (3), 221–223.

32 Soriano-López, J.; Goberna-Ferrón, S.; Vigara, L.; Carbó, J. J.; Poblet, J. M.; Galán-Mascarós, J. R. *Inorg. Chem.* **2013**, *52* (9), 4753–4755.

33 Blasco-Ahicart, M.; Soriano-López, J.; Carbó, J. J.; Poblet, J. M.; Galan-Mascaros, J. R. *Nat. Chem.* **2018**, *10* (1), 24–30.

34 Darensbourg, M. *Inorg. Synth.*; John Wiley & Sons, 1998; Vol. 32, pages 175-182.

35 Ruhlmann, L.; Costa-Coquelard, C.; Canny, J.; Thouvenot, R. *Eur. J. Inorg. Chem.* **2007**, *2007*, 1493–1500.

36 Bailar, J. C.; Booth, H. S.; Grennert, M. *Inorg. Synth.*; Booth, H. S., Ed.; John Wiley & Sons, Inc., 1939; pp. 132–133.

37 Weakley, T. J. R.; Malik, S. A. *J. Inorg. Nucl. Chem.* **1967**, *29*, 2935–2944.

38 Tourné, C. M.; Tourné, G. F.; Malik, S. A.; Weakley, T. J. R. *J. Inorg. Nucl. Chem.* **1970**, *32*, 3875–3890.

39 Jorris, T. L.; Kozik, M.; Casan-Pastor, N.; Domaille, P. J.; Finke, R. G.; Miller, W. K.; Baker, L. C. W. *J. Am. Chem. Soc.* **1987**, *109*, 7402–7408.

40 Li, J.; Wang, J.; Zhang, L.; Sang, X.; You, W. *J. Coord. Chem.* **2017**, *70*, 2950–2957.

41 Contant, R.; Klemperer, W. G.; Yaghi, O. *Inorg. Synth.*; Ginsberg, A. P., Ed.; John Wiley & Sons, Inc., 1990; pp. 104–111.

42 Samonte, J. L.; Pope, M. T. *Can. J. Chem.* **2001**, *79*, 802–808.

43 Lyon, D. K.; Miller, W. K.; Novet, T.; Domaille, P. J.; Evitt, E.; Johnson, D. C.; Finke, R. G. *J. Am. Chem. Soc.* **1991**, *113*, 7209–7221.

44 Barats-Damatov, D.; Shimon, L. J. W.; Weiner, L.; Schreiber, R. E.; Jiménez-Lozano, P.; Poblet, J. M.; de Graaf, C.; Neumann, R *Inorg. Chem.* **2014**, *53* (3), 1779–1787.

45 Haynes, W. M.; Lide, D. R. *Handbook of Chemistry and Physics*, 92nd ed.; Taylor and Francis Group, 2011.

46 Klanberg, F.; Hunt, J. P.; Dodgen, H. W. *Naturwissenschaften* **1963**, *50* (3), 90–91.

47 Surendranath, Y.; Lutterman, D. A.; Liu, Y.; Nocera, D. G. *J. Am. Chem. Soc.* **2012**, *134* (14), 6326–6336.

48 Bazzan, I.; Volpe, A.; Dolbecq, A.; Natali, M.; Sartorel, A.; Mialane, P.; Bonchio, M. *Catal. Today*. **2017**, 39-50.

49 Krolicka, A.; Bobrowski, A.; Kalcher, K.; Mocak, J.; Svancara, I.; Vytras, K. *Electroanalysis* **2003**, *15* (23–24), 1859–1863.

50 Widegren, J. A.; Finke, R. G. *J. Mol. Cat. A: Chemical* **2003**, *198* (1), 317–341.

51 Kirner, J. T.; Stracke, J. J.; Gregg, B. A.; Finke, R. G. *ACS Appl. Mater. Interfaces* **2014**.

52 Finke, R. G.; Droege, M.; Hutchinson, J. R.; Gansow, O. *J. Am. Chem. Soc.* **1981**, *103* (6), 1587–1589.

53 Folkman, S. J.; Kirner, J. T.; Finke, R. G. *Inorg. Chem.* **2016**, *55* (11), 5343–5355.

54 Baes, C.; Mesmer, R. *The Hydrolysis of Cations*; John Wiley & Sons, 1976.

55 Finke, R. G.; Droege, M. W.; Domaille, P. J. *Inorg. Chem.* **1987**, *26* (23), 3886–3896.

56 Ruhlmann, L.; Nadjo, L.; Canny, J.; Contant, R.; Thouvenot, R. *Inorg. Chem.* **2002**, *2002*, 975–986.

57 Gerken, J. B.; McAlpin, J. G.; Chen, J. Y. C.; Rigsby, M. L.; Casey, W. H.; Britt, R. D.; Stahl, S. S. *J. Am. Chem. Soc.* **2011**, *133* (36), 14431–14442.

V. ALCOHOL SOLVENT EFFECTS IN THE SYNTHESIS OF Co_3O_4 METAL-OXIDE NANOPARTICLES: DISPROOF OF A SURFACE-LIGAND THERMODYNAMIC EFFECT EN ROUTE TO ALTERNATIVE KINETIC AND THERMODYNAMIC EXPLANATIONS[iv]

Overview

The synthesis of Co_3O_4 core nanoparticles from cobalt acetate is explored in alcohol solvents plus limited water using O_2 as oxidant and NH_4OH as the base, all in comparison to controls in water alone employing the otherwise identical synthetic procedure. Syntheses in EtOH or *t*-BuOH co-solvents with limited water yield phase-pure and size-controlled (3 ± 1 nm) Co_3O_4-core nanoparticles. In marked contrast, the synthesis in water alone yields mixed phases of Co_3O_4 and β-$Co(OH)_2$ with a very large particle-size range (14 to 400 nm). Importantly, acidic reductive digestion of the Co_3O_4 particles followed by ^{1}H NMR on the resultant solution yields *no detectable EtOH* in nanoparticles prepared in EtOH, nor any detectable *t*-BuOH in nanoparticles prepared in *t*-BuOH (~5% detection limits for each alcohol), despite the dramatic effect of each alcohol co-solvent on the resultant cobalt-oxide product. Instead, in both cases *HOAc* is detected and quantified, indicative of OAc^- as a surface ligand—and not EtO^- or *t*-BuO^- as the surface ligand. The resultant ROH co-solvent-derived particles were characterized by PXRD, FT-IR, HRTEM, plus elemental analysis to arrive at an approximate, average molecular formula in the case of the

[iv] This chapter details our studies of the synthesis and characterization of Co_3O_4 nanoparticles. The main findings are that the solvent used in the synthesis greatly affects the crystallinity and size of the isolated nanoparticles but the solvent is not detected in the product. Instead, acetate from the cobalt acetate precursor is detected and quantitated as the only detectable surface ligand from several alcohol solvents. The general implications of these findings and other aspects of the synthesis are explored in what follows. This chapter is a reproduction of the full published manuscript from *Inorganic Chemistry* with permission (Folkman, S. J.; Zhou, M.; Nicki, M.; Finke, R. G. *Inorg. Chem.* **2018**, *57* (3), 1517–1526.)

particles prepared in EtOH, $\{[Co_3O_4(C_2H_3O_2)]^-[(NH_4^+)_{0.3}(H^+_{0.7})]^+\bullet(H_2O)\}_{\sim 216}$. The key finding is that, because EtOH and *t*-BuOH have a substantial effect on the phase- and size-dispersion of the cobalt-oxide nanoparticle product, yet the intact alcohol does not show up in the final Co_3O_4 nanoparticle product, the effect of these alcohols cannot be a surface-ligand thermodynamic effect on the net nanoparticle formation reaction. A careful search of the literature provided scattered, but consistent, literature in which anions or other additives have large effects on metal-oxide nanoparticle formation reactions, yet also do not show up in the nanoparticle products—that is, where the observed effects are again not due to binding by that anion or other additive in a surface-ligand thermodynamic effect on the overall reaction. Alternative hypotheses are provided as to the origin of ROH solvent effects on metal-oxide nanoparticles.

5.1 Introduction

Cobalt-oxide nanoparticles are an archetypal class of metal-oxide nanoparticles that have applications in a variety of areas including catalysis,[1,2,3,4,5] batteries,[6,7,8,9,10] sensors,[11,12,13,14,15,] supercapacitors,[16,17,18] and electrochemical water splitting.[3,4,19,20,21] These applications depend on the size, crystallinity, surface ligands, and resultant properties of the cobalt-oxide nanoparticles. An important 2007 study by Zhang and co-workers examined the size and crystallinity differences of Co_3O_4 nanoparticles synthesized from $Co(OAc)_2\bullet 4H_2O$ (OAc = acetate^{1-}), with NH_4OH as the base, O_2 as the oxidant, and EtOH/water as the solvent.[2] In addition, the effect of alcohols on metal-oxide nanoparticle formation have been known since 2002 when Stucky and co-workers discovered the marked effects of benzyl alcohol (hereafter $PhCH_2OH$) on TiO_2 nanoparticle formation.[22,23] However, the precise origins of the effect(s) of alcohols on metal-oxide nanoparticle formation remain unknown. More specifically, no prior study that we can find has tested if the observed, often dramatic effect of alcohol solvents on metal-oxide nanoparticle syntheses is a

surface ligand effect and, hence, primarily thermodynamic in origin, or if those dramatic effects on metal-oxide nanoparticle syntheses might be primarily kinetic in origin, as one other possibility.

Herein, Co_3O_4 nanoparticles are synthesized and characterized by a procedure[2,3] in which $Co(OAc)_2•4H_2O$ in EtOH, and aqueous NH_4OH are combined with bubbling of atmospheric air to yield spinel-phase, 3±1 nm Co_3O_4 nanoparticles. A set of control syntheses were also performed using water, *t*-BuOH, or $PhCH_2OH$ as the alcohol (ROH) solvent.[21,22,23,24] The resultant cobalt-oxide nanoparticles are characterized by PXRD, FT-IR, HRTEM, and, importantly, also by acidic reductive dissolution followed by quantitative ^1H NMR. This dissolution plus ^1H NMR procedure addresses for the first time the key questions of whether the alcohol is present as a RO^- surface ligand or if other surface-ligand species can be detected.

5.2 Experimental

General Reagents. $Co(OAc)_2•4H_2O$ (Reagent Grade), Benzyl alcohol ($PhCH_2OH$, Reagent Plus ≥99%), and NH_4OH (ACS Grade, 28-30%) were purchased from Sigma-Aldrich. Neat (i.e., 200 Proof, ACS anhydrous) ethanol (EtOH) was purchased from Pharmco-AAPER. *tert*-Butyl alcohol (*t*-BuOH, ACS Reagent) was purchased from J.T. Baker. D_2O (99.9%) was purchased from Cambridge Isotope Laboratories. Concentrated sulfuric acid (95-98%) was purchased from EMD chemicals. All aqueous solutions were prepared with 18 MΩ-cm water from an in-house Barnstead Nanopure water purification system.

Synthesis of Co_3O_4 Nanoparticles. Co_3O_4 nanoparticles were synthesized using a procedure adapted from literature methods.[2,3] To start, 0.5 g $Co(OAc)_2•4H_2O$ was weighed and placed into a 3-neck 50 mL round-bottomed flask affixed with a thermometer, reflux column open to ambient air, and a rubber septum pierced with a steel syringe for bubbling air. Next, 2 mL of water was added at room temperature with magnetic stirring resulting in a pink solution. Then, 23

mL of solvent (anhydrous EtOH, water, anhydrous *t*-BuOH, or anhydrous $PhCH_2OH$ for each of the respective syntheses) were added while stirring and then heated (sand bath/heating mantle) to a solution temperature of 45 ± 5 °C and holding this temperature for 10 min. (Anhydrous alcohols were employed when alcohols are the primary solvent to control the precise amount of water present.) During this time, the solution changed from pink to blue (except in the case of the water-only synthesis, which remained pink, *vide infra*); the pH of the EtOH / water / $Co(OAc)_2$ solution was pH ~6.3). With the solution still at 45 °C, 2.5 mL of NH_4OH (28%, aqueous) was added dropwise over two minutes, during which the solution became darker blue, then black. The pH after the addition of the NH_4OH was pH ~9.8. Once NH_4OH addition was complete, the solution was subjected to constant flow of ambient atmosphere via a Whisper 40 Aquarium air pump. The flow rate of bubbling was controlled using a clamp on the air line, adjusted to ~600 mL/min. Bubbling with air proved necessary for a reproducible synthesis—likely because O_2 functions as the oxidant and is present in excess when bubbling. The solution was then heated to 75 °C and held at that temperature for three hours under continuous air-bubbling and stirring. The solution was then removed from the sand bath, bubbling and stirring were stopped, and the flask was placed into a room-temperature water bath for ≥20 min until the solution cooled to 25 °C.

The resulting brown solution (~25 mL) was then partitioned equally into four separate 50 mL plastic centrifuge tubes, ~6 mL each. Then, 10 mL of MeOH was used to collect any solid that remained in the flask, which was added approximately evenly to each centrifuge tube. Acetone was added to each of the centrifuge tubes until the total solution volume in each tube was 30 mL, causing the precipitation of the cobalt-oxide nanoparticles. The centrifuge tubes were then vortex stirred for 30 s before centrifugation at 1500 rpm for 20 min resulting in a brown pellet at the bottom of each of the centrifuge tubes. The pink supernatant (presumably containing unreacted

$Co(OAc)_2$, EtOH, water, *t*-BuOH, $PhCH_2OH$, MeOH, and NH_4OH / NH_4OAc) was discarded. The brown particle precipitates were suspended in 3 mL of MeOH via pipette and then vortex stirred for 30 s. Acetone was again added until the solution volume was 30 mL, and the particles were vortex-stirred and centrifuged as before. After the second wash, the supernatant was light brown to colorless and was discarded. The resulting four samples of particles were suspended in 3 mL of MeOH and combined in a pre-weighed 20 mL scintillation vial. Volatiles were removed under reduced pressure via rotary evaporation at 35 °C, followed by drying overnight on a Schlenk line with vacuum supplied by a mechanical pump. The scintillation vial was then weighed again; particle yields ranged between 115 and 200 mg corresponding to a 12 to 22% yield based on $Co(OAc)_2 \cdot 4H_2O$. The samples were found to be hygroscopic and were thus stored in a vacuum desiccator over desiccant. Elemental analysis results are provided and discussed in the SI.

Powder X-Ray Diffraction (PXRD). Samples for PXRD were ground in a mortar and pestle prior to data acquisition. The dark brown/black powder was loaded onto a zero diffraction Si wafer that was spun at 0.5 Hz using the instrument sample holder. PXRD was collected on a Bruker AXS using a Cu x-ray source with an accelerating voltage of 40 KeV. Data were collected from 5 to 70° with 0.05° step size and 1 s step time. The acquired data were smoothed and the Kα2 was stripped using DIFFRAC.EVA software. A library search confirmed that Co_3O_4 (PDF: 00-001-1152) and β-$Co(OH)_2$ (PDF: 00-030-0443) are the best matches for the cobalt oxide phases, depending on the precise synthesis. The crystallite size was determined using the Scherrer analysis in the DIFFRAC.EVA software by defining the peak regions manually.

High resolution transmission electron microscopy (HRTEM) and selected area electron diffraction (SAED). Samples for HRTEM were prepared by suspending 1 mg of nanoparticles in approximately 4 mL of methanol and dropping the solution onto a silicon nitride

TEM grid purchased from SimPore Inc. Samples were examined both before and after 30 min of sonication; no significant difference in particle size, morphology, or crystallinity were observed between the two. HRTEM, and SAED were collected on a JEOL JEM-2100F transmission electron microscope with 200 KeV accelerating voltage. The particle size histograms were acquired by manually measuring ≥30 individual particles in the imageJ program.

Dynamic light scattering (DLS) and zeta potential. Samples for DLS were prepared by dissolving 4 mg of the particles in 1 mL of water and diluting 1:10 to obtain a solution that was 0.4 mg/mL. DLS was collected using a Malvern Zeta Sizer nano-ZS. Approximately 0.3 mL of the 0.4 mg/mL solution was filtered through a 200 nm nylon filter and examined using a pre-rinsed Zen 0040 disposable cuvette. Data were collected at 173° backscatter with 8 runs per measurement, 3 mm working position and without any attenuation.

Fourier transform infra-red spectroscopy (FT-IR). Samples for FT-IR were prepared by grinding in a mortar at approximately 2 wt. % with anhydrous KBr. The resulting powder mixture was then pressed into pellets. FT-IR spectra were collected from 400−4000 cm^{-1} with 1 cm^{-1} resolution. Spectra were collected for cobalt-oxide particles synthesized herein, and as controls for comparison purposes on bulk (commercial) Co_3O_4 powder (~400 mesh, purchased from Alfa Aesar), $Co(OAc)_2•4H_2O$ starting material, and NH_4OAc.

Digestion of the Co_3O_4 Nanoparticles. The samples were digested using an adapted protocol from Suri et al,[25] in which concentrated sulfuric acid and sodium sulfite are used to digest the oxide and reduce the Co^{III} to Co^{II} to yield the pink, substitutionally labile hexahydrate, $Co^{II}(H_2O)_6^{2+}$, thereby freeing any surface ligands into solution. To start, 15 mg of the particles was weighed in a 1 dram vial and 6 mg anhydrous Na_2SO_3 was added. Next, 780 μL water was added, yielding a black/brown solution, and 220 μL of concentrated H_2SO_4 was added with stirring at

room temperature, yielding a 1 mL solution with 15 mg/mL particles, 50 mM Na_2SO_3, and 4 M H_2SO_4. After the addition of the H_2SO_4 the solution bubbled and became pink with some dark particles that dissolved within 5 min, except in the case of the larger CoO_x nanoparticles synthesized in water, which took >2 hours to dissolve fully. This solution was then used as the analyte solution in the following quantitative ^{1}H NMR section.

Quantitative ^{1}H NMR. A quantitative NMR protocol was developed in which the absolute integration of the peak was used to determine the amount of liberated HOAc. First the T_1 of acetate in the digested solutions was determined using inversion recovery, so that reliable quantification of the species present was possible using a relaxation delay of >5 times the T_1 to allow for >95% recovery of the magnetization. The T_1 of HOAc in the digested solution was determined to be 2.75 sec, hence the relaxation delay was set to 18 seconds. ^{1}H QNMR were collected using solvent suppression of the water peak so that the receiver gain could be increased to maximize the signal-to-noise of the HOAc peak. Spectra were collected from −2.0 to 14 ppm, with 30 dB gain, 2.047 s acquisition time, 5.75 μs (90°) pulse, 18 s relaxation delay, 8 scans, and using solvent suppression of the largest (water) peak at ~4.8 ppm. The amount of HOAc was determined using the method of standard additions to account for any matrix effects. The total solution volume was 0.5 mL with 250 μL D_2O, 50 μL of the analyte solution (*vide supra*), and the remainder of the solution (200 μL) was either water or an aqueous HOAc stock solution used for the standard additions. The final NMR solutions consisted of 0.5 mL of 50% D_2O with 1.5 mg/mL digested CoO_x nanoparticles and added HOAc ranging from 0 to 30 μM. Each data point was repeated at least twice and the integration was determined using MestReNova NMR software. The peak integrations were plotted against the added HOAc concentration and fit using a linear regression (R^2 of 0.9999 and 0.9989 for the EtOH and t-BuOH, respectively). The linear regression was extrapolated to the x-intercept

to determine the HOAc concentration in the NMR solution; the concentration of HOAc in the original digested solution was calculated by multiplying by 10 for the 1:10 dilution used in preparing the NMR solution. The detection limit of EtOH was determined by spiking the solution with known amounts of EtOH so that the resulting signal was approximately 3x the noise.

5.3 Results and Discussion

Synthesis and Characterization of Co_3O_4-core Nanoparticles in Ethanol/Water. Various routes have been used to synthesize CoO_x nanoparticles, including sol-gel,[1,2,3] and electrochemical-based syntheses.[26] Herein, a sol-gel method was adapted from the literature[2,3] but modified to avoid the need for an autoclave, thereby making it less cumbersome and more convenient. Specifically, a simple procedure was developed using a 3-neck round-bottomed flask equipped with an inexpensive aquarium pump to bubble atmosphere (O_2) through the reaction solution (Scheme 1). A constant bubbling of O_2 from the atmosphere proved necessary for reproducibility, consistent with prior studies showing that O_2 affects the formation of cobalt-oxide nanoparticles.[2] Control syntheses without the bubbler (i.e., deficient in O_2) gave low (to no) particle yields. The bubbling also cools the solution by supplying room-temperature air to the reaction, so care must be taken to maintain the solution temperature at ~75 °C while bubbling. A second control synthesis was performed (as described in the Supporting Information) in which an eight-fold longer, 24 hr reflux was performed to see if it increased the yield above the best, 200 mg (22% yield based on $Co(OAc)_2•4H_2O$) of Co_3O_4 observed for the 3 hr reflux conditions in Scheme 5.1. That synthesis did not, instead yielding 176 mg of product contaminated with a β-CoOOH phase.

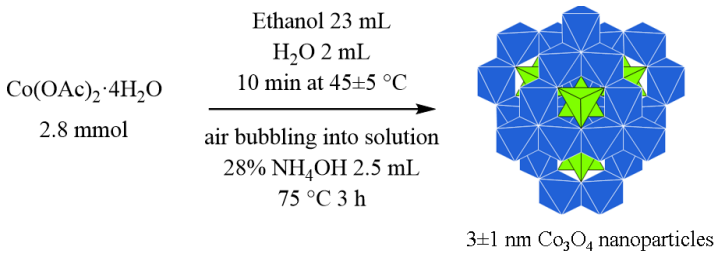

Scheme 5.1. Synthesis of Co_3O_4 nanoparticles. Blue octahedra are $Co(III)O_6$ and green tetrahedra are $Co(II)O_4$ of the A_2BO_4 spinel structure.

The PXRD pattern of the resultant nanoparticles synthesized in EtOH/water as detailed in the Experimental section showed broad, but distinguishable, Bragg reflections consistent with spinel Co_3O_4, Figure 5.1a.[2,3] The peak widths were fit using the Scherrer equation in the DIFFRAC.EVA software and the crystallite size of 3 ± 1 nm was averaged from the different reflections. HRTEM of the Co_3O_4 nanoparticles show 3.0 ± 0.6 nm particles, Figure 5.1b and Figure S5.1 of the Supporting Information, of manually counted (~70) particles, Figure 5.1b, in good agreement with the diffraction results. SAED confirms the crystallinity of these particles (Figure S5.2). The results demonstrate that *the particles synthesized in EtOH have a narrow size distribution and only one crystalline phase, spinel Co_3O_4.*

DLS data for the resultant particles dissolved in water (0.4 mg/mL) show 5.0 ± 1.3 nm number average *hydrodynamic* radius, Figure S5.3. As expected, this radius value is larger than the 3 nm diameter XRD- and HRTEM-determined size because any double layer present will also contribute to the observed (larger) hydrodynamic radius.

The FT-IR spectrum of the solid particles is consistent with prior literature:[4] the observed peak at 3400 cm^{-1} (broad) assigned to water, peaks at 1552 and 1409 cm^{-1} (143 cm^{-1} splitting, *vide infra*) previously assigned to Co-OH surface hydroxyls[4], and peaks at 571 and 655 cm^{-1} assigned to Co-O stretching modes (Figure S5.4) all being observed as before.[4] Interestingly, peaks at 1552 and 1409 cm^{-1} are not observed for commercial Co_3O_4 powder, but are observed for the

a.

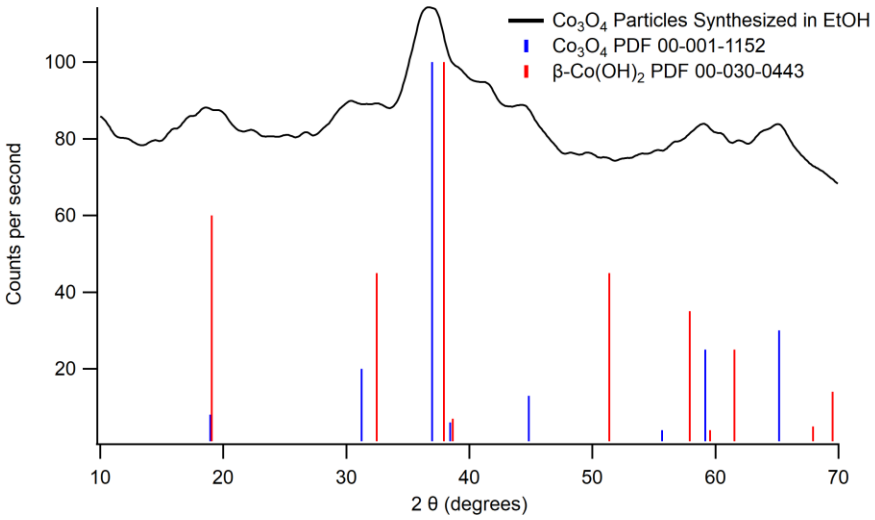

b.

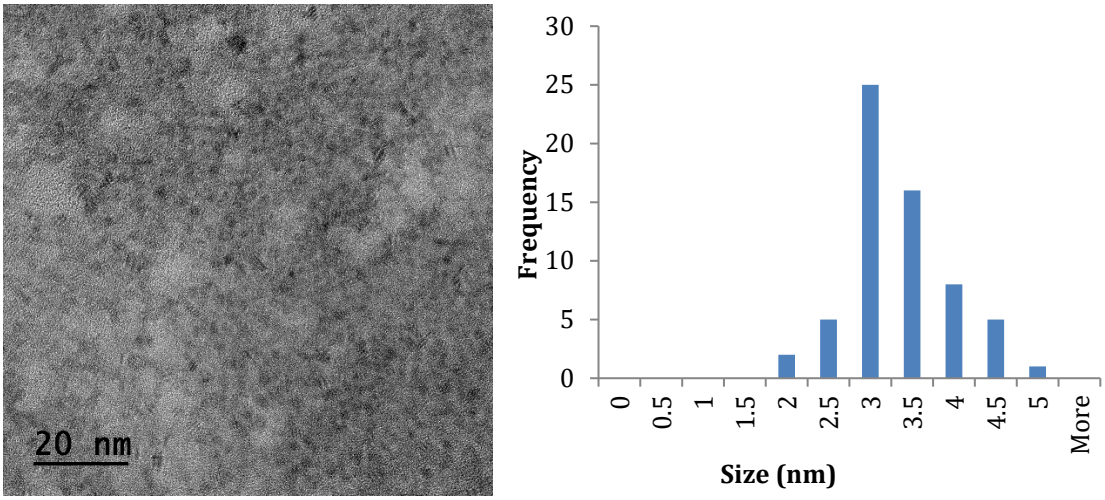

Figure 5.1. a) PXRD pattern of the Co_3O_4 nanoparticles synthesized in EtOH/water. The blue and red lines in the PXRD are expected diffraction peaks for Co_3O_4 and β-$Co(OH)_2$ respectively. Although some of the expected peaks overlap, the absence of detectable β-$Co(OH)_2$ is indicated by the absence of a peak at 51° 2θ meaning that the observed spinel phase Co_3O_4 is the dominant crystal phase as desired. b) HRTEM and size histogram (frequency vs diameter) of the Co_3O_4 nanoparticles synthesized in EtOH/water.

$Co(OAc)_2•4H_2O$ precursor and NH_4OAc (Figure S5.4). The absence of these peaks in the commercial powder suggests the IR peaks at 1552 and 1409 cm^{-1} should be reassigned to OAc^- in the product rather than to surface hydroxyls.[4]

To provide further evidence for or against the presence of OAc^-, the particles were also characterized by elemental analysis, which showed 56.0% cobalt, 34.4% oxygen, 7.5% carbon, 2.0% hydrogen, and 1.2% nitrogen, totaling to 101.1%. Assuming a standard 0.4 absolute weight percent error for each element, the resultant empirical formula is $Co_{3.00\pm0.01}O_{6.80\pm0.01}C_{1.97\pm0.05}H_{6.3\pm0.2}N_{0.3\pm0.3}$, demonstrating the presence of an organic component as well as some nitrogen within experimental error. These results confirm the nanoparticle product *is not pure* Co_3O_4, as has been previously suggested,[2,3] not unexpectedly since nanoparticles generally contain some type of surface ligand, with $EtO^-(H^+)$, $OAc^-(H^+)$, and then also $NH_3(H^+)$ being the most plausible species based on the evidence presented so far.

Synthesis and Characterization of Mixed-Phase Cobalt-Oxide Nanoparticles in Water. This key control experiment was conducted to compare the cobalt-oxide nanoparticles obtained *from water alone* to the cobalt-oxide nanoparticles obtained from the otherwise identical synthesis in EtOH/water (i.e., in the absence of any alcohol co-solvent; see the Experimental section). The water-prepared particles obtained were characterized via PXRD, HRTEM, and FT-IR.

The PXRD pattern of the resultant cobalt-oxide material synthesized in water shows that the particles are mostly β-$Co(OH)_2$ phase[27] with a small amount of Co_3O_4 and unidentified peaks at 11° and 23° 2θ which likely belong to a disordered layered phase[28] that could contain intercalated OAc^-, Figure 5.2a.[29] The greater observed intensity for the (001) reflection at ~19° compared to the (101) reflection at ~38° differs from the expected relationship of the (101) peak

having greater intensity than the (100). This difference in intensity is likely caused by preferred orientation of the crystalline material, which is common in layered materials. Fitting the peak widths to the Scherrer equation[30] yields a crystallite size of ~400 nm (i.e., between 360 and 440 nm) for the β-$Co(OH)_2$ phase. *Peaks for the Co_3O_4 phase are too weak or too broad to be readily detected in the observed PXRD pattern*.

TEM images of the particles, Figure 5.2b, show the two phases obtained and a broad particle size range of 14-60 nm (for the better defined spherical and cubic particles) and ~400 nm for the β-$Co(OH)_2$ phase. The TEM size histogram for the Co_3O_4 particles is shown in Figure S5.5 of the Supporting Information. The large disparity between the TEM-determined size, vs that from the Scherrer equation, likely stems from the mixed-phase nature of the sample and the breakdown of assumptions in the Scherrer equation, where the peak broadening becomes limited by the instrument broadening and not the particle size.

FT-IR spectra (KBr pellet) of the particles show peaks at 3625 (sharp), 3400 (broad) cm^{-1} for the surface hydroxyl of β-$Co(OH)_2$ and adsorbed or intercalated water. Peaks at 1563 and 1360 cm^{-1} are consistent with intercalated OAc^- plus a broad peak at 500 cm^{-1} consistent with the β-$Co(OH)_2$ phase (Figure S5.6).[31,32]

In short, the synthesis of cobalt-oxide nanoparticles in water without any ROH co-solvent yields mixed phases of Co_3O_4, and β-$Co(OH)_2$ (and possibly amorphous phases as well) with little size control (as demonstrated by the broad particle-size range of 14 to 400 nm)—*a dramatic difference in comparison to the cobalt-oxide nanoparticles synthesized in EtOH/water which produce phase-pure spinel, near-monodisperse 3.0±1.0 nm Co_3O_4 nanoparticles.*[2,3] The dramatically different CoO_x particles obtained from the two otherwise identical syntheses demonstrates the importance of EtOH, for example either thermodynamically (i.e., as a capping

a.

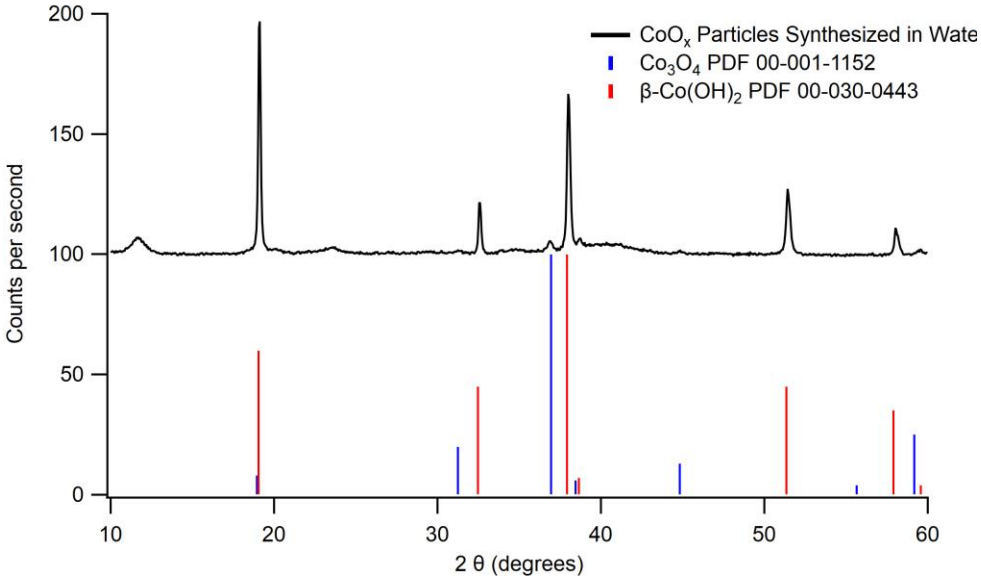

b.

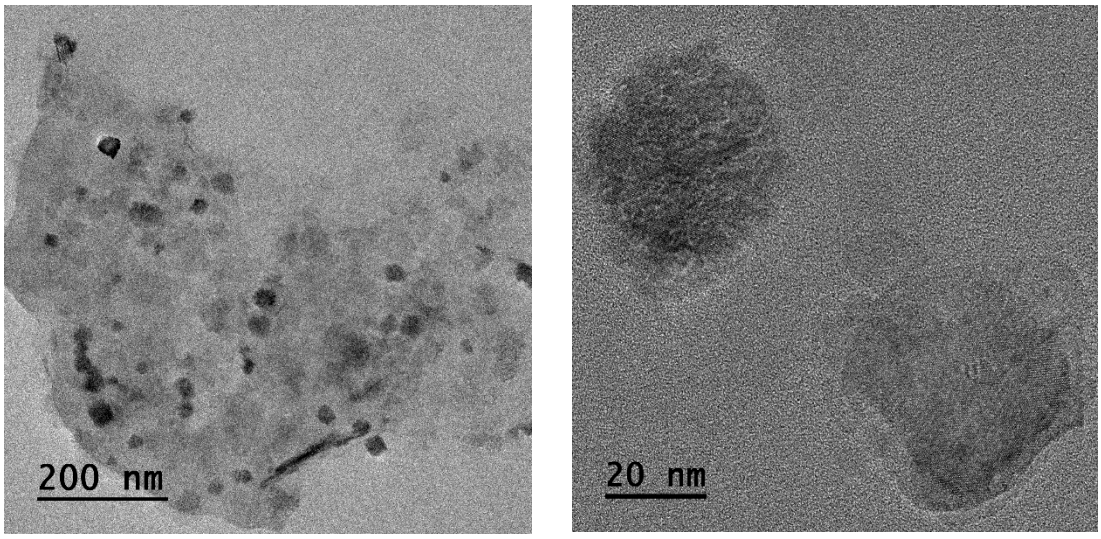

Figure 5.2. a) PXRD, the blue and red lines in the PXRD are expected diffraction peaks for Co_3O_4 and β-$Co(OH)_2$ respectively. b) Selected TEM images of cobalt-oxide nanoparticles synthesized in water.

ligand), or as some type of more general thermodynamic solvent effect on the reaction, or kinetically (i.e., affecting the nucleation and growth of the particles by changing the speciation of

the Co(II) precursor), or conceivably some combination of the above (or other, presently unknown) explanations.

Determining Surface Ligands on the Ethanol /Water Prepared Co_3O_4 Nanoparticles. Given the pronounced effect of EtOH on the synthesis of cobalt-oxide nanoparticles, as well as the evidence by FT-IR and elemental analysis requiring the presence of an organic component in the nanoparticles, the identity of that organic, surface-ligand component was examined next using quantitative ^{1}H NMR. First, we collected ^{1}H NMR on a freshly dissolved sample of the Co_3O_4•(organic component) nanoparticles in water (25% D_2O / 75% H_2O, 1.5 mg/mL total volume, Figure S5.7, left). Importantly, the only ^{1}H NMR peak observable is water (Figure S5.7, left). *However*, if the particles are first digested using a precedented literature procedure in 4 M sulfuric acid under reducing (50 mM Na_2SO_3) conditions, a single new ^{1}H NMR peak is observed at ca. 1.7 ppm (Figure S5.7, right). Spiking the digested solutions with HOAc increases the absolute intensity of the 1.7 ppm peak; hence, we assign the 1.7 ppm resonance to the methyl protons of CH_3CO_2H. No EtOH (≤5% detection limit) is observed indicating that EtO^- or EtOH are not present as a primary surface ligand (≤5%).

Next, using the method of standard additions, a quantitative NMR experiment was performed in which we obtained and plotted the absolute integration of the 1.7 ppm peak vs the concentration of added, authentic HOAc, $[HOAc]_{added}$. By extrapolating the linear regression to the x-intercept, the amount of HOAc in 1.5 mg/mL digested solutions of the Co_3O_4 nanoparticles (i.e. without any added HOAc) is 4.3 ± 0.6 mM, Figure 5.3. The fact that there are no observable ^{1}H NMR peaks for the freshly dissolved (i.e., intact) nanoparticles suggests that the OAc^- is a surface-ligand on the nanoparticles and that the ^{1}H NMR signal for the methyl protons are significantly shifted and/or broadened beyond detection in the surface-attached OAc^- ligand, a

topic discussed further in the Supporting Information.[33] Furthermore, because we have detected spinel phase Co_3O_4 by PXRD (which does not have vacancies to allow for intercalation), and because we have FTIR evidence for a bridging mode of OAc^- being present (*vide infra*; see also the Supporting Information), the simplest explanation consistent with all the data is that OAc^- is serving as a *surface ligand* to the Co_3O_4 particles.

Noteworthy is that the above results are in stark contrast to the cited literature of metal-oxide nanoparticle syntheses in EtOH,[2,3] benzyl alcohol, [21,22,23,24] and other alcohols[34,35,36,37,38,39] that strongly implies that the alcohol winds up as a surface ligand—that is, in turn implying that the effects of alcohols are primarily thermodynamic in origin. In the case of *non-hydrolytic* syntheses, there *is* evidence that ROH solvents can supply O in the final metal-oxide, M_xO_y product.[35,36,37] Note here that the conceivable possibility that some EtOH-derived O winds up in the Co_3O_4 product in our ROH / H_2O / OH^- system is highly unlikely because: (i) the OH^- present in our (basic) system is a ready source of O^{2-} from, formally, "2 $OH^- \rightarrow O^{2-} + H_2O$", (ii) any putative Co-OR formed can readily be hydrolyzed, Co-OR + $H_2O \rightarrow$ Co-OH + ROH, and because (iii) facile 2 Co-OH $\rightarrow$ Co-O-Co + H_2O will drive this hydrolysis and is expected to be much faster than the more difficult, known to be slower, 2 Co-OR $\rightarrow$ Co-O-Co + ROR.

Hence, our results demand a different explanation: *rather than as a surface-ligand in what would be a thermodynamic effect on the net nanoparticle formation reaction, because no intact EtOH is contained in the products, yet the EtOH has a profound effect on the observed phase and size distribution of the cobalt-oxide product, the role of EtOH must occur by either some other thermodynamic effect (i.e., some type of little precedented, general solvent effect on the overall reaction), or a primarily kinetic effect (or some combination of such effects is of course also conceivable).*

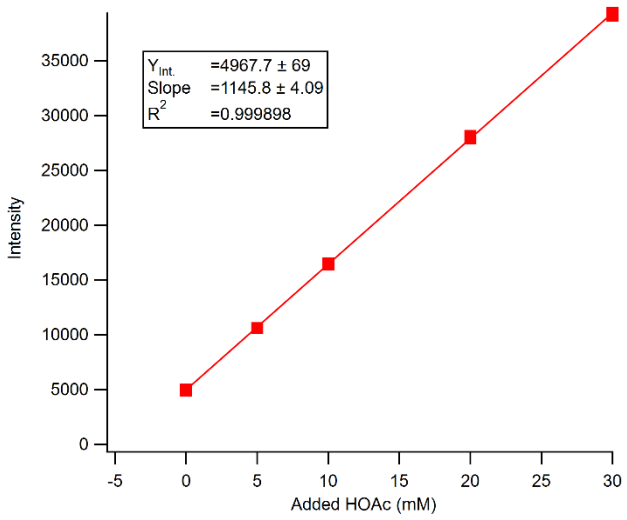

Figure 5.3. Intensity of the quantitative NMR peak of HOAc vs. added [HOAc] for the digested EtOH synthesized Co_3O_4 nanoparticles. By extrapolating to the X intercept, the [HOAc] in the 1.5 mg/mL digested solution of Co_3O_4 is determined to be 4.34 ± 0.6 mM.

Additional experiments and analyses are presented in the Supporting Information, the results of which show: (i) that the elemental analysis agrees quantitatively with the amount of acetate determined by the digestion and quantitative ^{1}H NMR; (ii) that an approximate, average molecular formula of the Co_3O_4 nanoparticles can be formulated as $\{[Co_3O_4(C_2H_3O_2)]^-[(NH_4^+)_{0.3}(H^+_{0.7})]^+\bullet(H_2O)\}_{\sim 216}$; (iii) that each surface bound acetate has, on average, 13 Å^2 of surface area / OAc^- to which the acetate can bind—meaning that the Co_3O_4 nanoparticle's surface is only partially covered by acetate; and (iv) that based on the splitting of the C=O stretching mode, one can infer the acetate binds in a bridging or chelating fashion. In short, the additional results summarized briefly above, and detailed further in the Supporting Information, support the assignment of OAc^- as the primary surface ligand of the Co_3O_4 nanoparticles synthesized in EtOH/water. Additionally, (v) zeta potential experiments on the $\{[Co_3O_4(C_2H_3O_2)]^-[(NH_4^+)_{0.3}(H^+_{0.7})]^+\bullet(H_2O)\}_{\sim 216}$ particles dissolved in deionized water yield a surface zeta potential

of 58 ± 6 mV implying, interestingly, that the particles become positively charged when dissolved in unbuffered water, indicate of the apparent basicity and resultant apparent protonation of the $\{[Co_3O_4(C_2H_3O_2)]^-\}_{\sim 216}$ core of the particles. The positive zeta potential under near neutral conditions is consistent with the point of zero charge (PZC) for Co_3O_4 of PZC=7.5—which is expected to be variable depending upon surface properties.[40]

Overall, then, a net, slightly idealized reaction stoichiometry to the resultant, acetate-stabilized Co_3O_4 nanoparticles is given in eq. 1 in which the only counter cation shown is NH_4^+, thereby simplifying the observed mixed $[(NH_4^+)_{0.3}(H^+_{0.7})]$ (which, if that had been written instead, would then just require 0.7 equiv of NH_3 to also be among the products):

$$\begin{array}{l} 3Co(OAc)_2\cdot 4H_2O \\ +\ \ 6NH_4OH \\ +\ \ 1/2O_2 \end{array} \xrightarrow[\begin{array}{c}75\ ^\circ C \\ 3\ \ h\end{array}]{EtOH/water} \begin{array}{l} 1/\sim 216[Co_3O_4(OAc^-)(NH_4^+)\cdot(H_2O)]_{\sim 216} \\ +\ \ 5(NH_4)(OAc) \\ +\ 14H_2O \end{array} \qquad (1)$$

Note that establishment of even the approximate, average molecular formula cite above also bears on the possibility of some type of "general solvent, thermodynamic effect *on the overall reaction*" as being responsible for controlling the formation of the Co_3O_4 core (when ROH is present) vs the formation a mixture of Co_3O_4, and β-$Co(OH)_2$ that is formed in just H_2O (*vide supra*). Given that in $\{[Co_3O_4(C_2H_3O_2)]^-[(NH_4^+)_{0.3}(H^+_{0.7})]^+\bullet(H_2O)\}_{\sim 216}$ there are thousands of Co-O-Co and other bonds, it makes little chemical sense that some type of "general solvent effect" *on just the surface* of that ~3 nm nanoparticle can lead to its formation vs β-$Co(OH)_2$. What makes much more sense, at least to us, is that ROH co-solvent maybe controlling *the formation of much smaller, sub-nanometer clusters* (such as prenucleation clusters, *vide infra*).

Testing the Generality of the Alcohol Solvent Influence and of OAc^- as a Surface Ligand: Studies Employing *t*-Butanol and Benzyl Alcohol. Our findings that EtOH is not operating by a surface-ligand thermodynamic effect, and that OAc^-, not EtO^-, is the sole detectable

surface ligand, begs the question of how general are these results, at least in the synthesis of Co_3O_4? Do they also extend to other solvents such as *t*-BuOH that others[39] have reported in an autoclave-based synthesis of Co_3O_4 nanoparticles? Do our findings also extend to the widely cited "benzyl alcohol route"[21,22,23,24] employed in the synthesis of a range of metal-oxide nanoparticles? Relevant here is that synthesis of various metal-oxide nanoparticles in benzyl alcohol at elevated temperatures (>250 °C) and putatively "water-free" conditions (i.e., the trace amounts of H_2O possibly present were not quantified) leads to the formation of benzoate, which subsequently is reported to act as the capping ligand of the metal oxide nanoparticles.[41,42,43]

The use of especially *t*-BuOH also tests the arguably remote possibility that some of the oxygen in the Co_3O_4 product could conceivably come from the ROH, since the sterically encumbered *t*-BuOH does not have back-side attack, "S_N2-like" mechanisms to cleave its C-O bond. Hence, if analogous results are obtained with *t*-BuOH as with EtOH (as we will see is the case, *vide infra*), then this is additional evidence against ROH-derived O in the final product in at least the case of *t*-BuOH/H_2O, and by inference more generally in ROH/**H_2O** mixed solvent systems.

To probe the above questions, we conducted analogous cobalt-oxide nanoparticle syntheses by changing only the alcohol co-solvent to *t*-BuOH and, in separate experiments, $PhCH_2OH$. The cobalt-oxide nanoparticles so synthesized were again characterized using PXRD, DLS, TEM, and digestion and quantitative ^1H NMR experiments to determine if OAc^-, *t*-BuO^-, or $PhCH_2O^-$ were detectable in the cobalt-oxide nanoparticle products.

Our synthesis in *t*-BuOH/water yielded similar 3-5 nm Co_3O_4 particles to those synthesized in EtOH/water (Figures S5.8-S5.10), particles a bit smaller than the ~7 nm Co_3O_4 particles prepared previously from $Co(OAc)_2$ / HNO_3 / Pluronic P123 in a 120 ºC autoclave for 17

hrs.[39] Crucially, the acidic reductive digestion and quantitative ^{1}H NMR of our Co_3O_4 nanoparticles prepared in *t*-BuOH reveal that *t*-BuOH *is absent* from among the detectable products (~5% detection limit). Instead and again, HOAc is the only detectable organic species, again implying OAc^- as the primary surface ligand (Figure S5.10) for Co_3O_4 nanoparticles synthesized in *t*-BuOH / H_2O.

Contrasting the syntheses involving *t*-BuOH and EtOH, which yielded phase-and size-controlled Co_3O_4 product, the particles synthesized in $PhCH_2OH$/water exhibit multiple phases, including spinel Co_3O_4, layered β-$Co(OH)_2$, and rock salt CoO (Figures S5.11-S5.13). Revealingly, the digestion and quantitative NMR experiments of the $PhCH_2OH$-prepared nanoparticles showed that (i) neither OAc^- nor $PhCH_2OH$ are present in the ^{1}H NMR spectrum prior to digestion, but now that (ii) *primarily* OAc^-, but also some $PhCH_2OH$, are present at 4.1 ± 0.3 mM and 0.78 ± 0.02 mM in a 1.5 mg/mL solution, respectively (Figure S5.13), resulting in a ~5/1 ratio of OAc^- / $PhCH_2OH$. Hence, *OAc^- is once again the dominant ligand present.* Moreover, the sample is biphasic and the minor amount of $PhCH_2OH$ present may be simply physically trapped/intercalated within the layered β-$Co(OH)_2$ phase rather than a ligand for the Co_3O_4 phase present.

Overall, what is clear is that when a tight size distribution to a single phase Co_3O_4 product is seen as with EtOH and *t*-BuOH, then in those preferred syntheses to a single product *no detectable ROH is in the resulting product*. The Ockham's razor hypothesis at this point for $PhCH_2OH$ is that it, too, may often also be operating by some pathway that does not lead to $PhCH_2O^-$ as a surface-ligand on the metal-oxide, at least when employed in $PhCH_2OH$ / H_2O co-solvent systems.

In hindsight, the finding that acetate is the dominant surface ligand for Co_3O_4 nanoparticles, when beginning with $Co(OAc)_2$ and in alcohol/water mixtures, makes chemical sense—one reason we expect our "acetate as a ligand" finding to likely be more general for other metal-oxide nanoparticle syntheses in alcohol / water co-solvent systems. The reason why is that the pK_a for acetate is 4.8, whereas the pK_a of ethanol is 16, meaning that HOAc will be fully deprotonated and exist as OAc^- at the initial pH = 9.8 of our synthesis. On the other hand, relatively little EtO^- should be present, and hence little Co-OEt formed, given EtOH's pKa of 16 (and even if one postulates a conceivable ~2-4 unit lowering of the $pK_{a(apparent)}$ to, say, 12-14 that would be expected if Co-OEt formed). Furthermore, acetate can bind in a bidentate fashion—and does, *vide supra*—whereas EtO^- binding is expected to occur in a primarily monodentate fashion. In short, our finding of acetate and not the alcohol conjugate base as a surface ligand in the present metal-oxide nanoparticle synthesis makes chemical sense. Hence, we *hypothesize* that OAc^- and other RCO_2^- as surface ligands is likely a more general phenomenon for other metal-oxide nanoparticles synthesized in alcohol co-solvents with water from OAc^- or RCO_2^- precursors at pH values where the alcohol is not significantly deprotonated.

Literature Hinting at the Potential Broader Generality of the "Not A Surface-Ligand Thermodynamic Effect on the Overall Reaction" Uncovered in the Present Work. Our findings led us to peruse the literature of other ligands that have large effects on metal-oxide nanoparticle shapes and sizes. That scrutiny of the metal-oxide nanoparticle formation literature is revealing and at least hints at the potentially broader relevance of the key finding uncovered in the present work, namely that "it's not a surface ligand thermodynamic effect on the overall reaction".

As one important example, in his classic, elegant studies of the syntheses of nearly monodisperse metal-oxide particles of many different metal oxides, Matijevic´ finds that

ellipsoidal rather than cubic particles of hematite, α-Fe_2O_3, are formed when a small amount of phosphate is added, phosphate which Matijevic´ notes is "*not incorporated into the solid*" (italics have been added).[38] Note that the effect of phosphate in this example is almost surely purely kinetic on at least the overall reaction, as it's not a surface-ligand thermodynamic effect, and some other thermodynamic effect on the overall reaction by small amounts of phosphate (and analogous to some type of putative general solvent effect, *vide supra*) both makes little chemical sense and has no precedent that at least we have been able to find.

Another example is the formation of WO_3 nanorods.[44] There, the use of different alcohols (MeOH, EtOH, *i*-PrOH, $PhCH_2OH$) results in *different aspect ratios* for the resultant WO_3 nanorods, yet ROH is not at least written in the final product. (A caveat regarding that work is that clear evidence demonstrating a lack of ROH in the final product was not reported.) However and still, a leading hypothesize going forward has to be that there likely are other, presently hidden examples in the literature of dramatic effects of alcohol solvent, anions, and other "potential ligand" additives on metal-oxide particle shapes, sizes, and distributions that, however and significantly, do not yield metal-oxide products containing those additives as surface ligands. Worthy of closer scrutiny in this regard is an interesting 2012 paper claiming $PhCH_2OH$ as a surface ligand for In/SnO_x and ZrO_2 metal-oxide nanoparticles, but where, strangely, the *loss* of some of that $PhCH_2OH$ is claimed to be important for *increased* nanoparticle stability.[45] Finally, also meriting mention here is the use of ROH solvents in the important 1968 Stöber process[46] (7,750 citations as of December 2017) for making very narrow size distributions of widely used silica particles, a classic system where ROH solvents again have dramatic effects, but the origin(s) of those effects remain obscure.

A caveat here is that *truly non-hydrolytic, "no water" systems* are ostensibly different, as consulting the reviews by Vioux[35,36] or Niederberger[37] suggests, systems where the ROH solvent is postulated to provide much of the O in the metal-oxide products (although trace water from hydrated starting materials, as a reaction by-product, in the ROH co-solvent, or on glassware surfaces is rarely ruled out as Niederberger notes on p. 7285 of his review,[37] a reason he prefers the term "non-aqueous sol-gel" rather than "non-hydrolytic sol-gel" chemistry). In that "low water" chemistry, evidence exists for ROH-based surface-ligands in at least some cases (e.g., the 3-4 nm zirconia nanoparticles prepared in neat $PhCH_2OH$[36]). However, Vioux's 1997 concluding statement,[35] that "Further insights into kinetics are needed to determine the factors governing the mechanisms of non-hydrolytic sol-gel processes…" rings true even now, 20 years later, and is a statement fortified by the results of the present study—that strongly hint at important kinetic effects as well, *vide infra*.

Conceivable, Reasonable Hypotheses for the Observed Effects of Alcohol Solvents on Metal-Oxide Nanoparticle Syntheses

What, then, is the origin(s) of the observed, dramatic effects of alcohol co-solvents in metal-oxide nanoparticle syntheses documented in the present work, and also observed in the literature cited herein? We know it is not a surface-ligand, thermodynamic based effect on the overall reaction based on the present studies, at least for the Co_3O_4 nanoparticle system explored in the present work. Conceivable, reasonable alternative hypotheses include: (i) some presently ill-defined, general "solvent (thermodynamic) effect" on the overall nanoparticle formation reaction—of a type and magnitude that, however, has little precedent that at least we have been able to find; or (ii) a kinetic and mechanistic effect on the metal-oxide nanoparticle formation reaction (i.e., on its nucleation, growth and / or agglomeration steps); or (iii) some other, presently

unknown, as of yet unconceived explanation (or, conceivably, (iv) some combination of the above possibilities).

The fact that nanoparticle syntheses are, in general, *kinetically controlled* in comparison to the formation of the thermodynamically most stable, extended bulk material, by itself argues that the ROH solvents in the present example, and the anion effects from the literature cited above, in all probability likely have a strong component of kinetic control *of the overall reaction*. Intriguing *possibilities* here include: (a) ROH effects on any prenucleation clusters[47] formed in ROH/water mixtures and, hence effects primarily on the nucleation step (i.e., on the *speciation* of the sol-gel). Note here that if correct, such an underlying effect of ROH co-solvents might be primarily *thermodynamic in origin* by controlling *smaller cluster, prenucleation speciation equilibria* (i.e., shifting the K_{eq} between such species, and if the interconversion of those species is fast relative to the rate of product formation), even if the net effect on *the overall reaction* looks to be primarily kinetic because no RO(H) fragment shows up in the Co_3O_4 product and because some type of "general ROH solvent effect" is unlikely to be able to produce the dramatic effects observed. Also possible are (b) ROH and other additive kinetic as well as thermodynamic effects on the growth or agglomeration steps of the metal-oxide nanoparticle formation reaction.

Needed future work is obviously multifold and includes: (i) verifying or refuting the findings herein for other metal-oxide nanoparticles / ROH plus water combinations; (ii) checking in detail the widely employed synthesis of metal-oxide nanoparticles in $PhCH_2OH$, including determining if $PhCH_2O^-$ is a surface ligand in the resultant products[36]; (iii) verifying by *O (* = 17 or 18) labeling studies the source of the O in metal oxides made by both ROH / H_2O co-solvent as well as ostensibly "non-hydrolytic" routes; (iv) seeing if a broader range of other additives, such as added anions that are known to influence metal-oxide nanoparticle compositions, shapes, sizes,

and size distributions,[38] do or don't show up in the reaction products; and especially (v) obtaining the kinetics by for example combined XAFS / SAXS en route to providing detailed, direct kinetic evidence for the underlying mechanistic steps and any role(s) of ROH co-solvents, including on any observable, but also shown to be kinetically competent, prenucleation clusters. Further exploration of (vi) the established kinetic roles of ROH in "non-hydrolytic" routes[35,36,37] also merit consideration and additional scrutiny in especially mixed ROH / H_2O systems involving low water.

5.4 Conclusions

Herein, a simple and reproducible synthesis of crystalline, spinel-phase-pure 3±1 nm Co_3O_4 nanoparticles is reported that uses readily available glassware and equipment. The resultant nanoparticles have been characterized using PXRD, HRTEM, SAED, DLS, zeta potential measurements, elemental analysis, FT-IR, and particle digestion followed by quantitative ^1H NMR. The particles have been shown to have an approximate, average molecular formula of $\{[Co_3O_4(C_2H_3O_2)]^-[(NH_4^+)_{0.3}(H^+_{0.7})]^+\bullet(H_2O)\}_{\sim 216}$, a rare but fundamentally invaluable demonstration of the actual (average) molecular formula of a metal-oxide nanoparticle—one that allows for the first time a known number of mmoles the isolated "Co_3O_4" product to be precisely weighed out and employed in other studies! The results also yield the important discovery that, in the case of EtOH or *t*-BuOH co-solvents that lead to the preferred narrow distribution of phase-pure Co_3O_4 nanoparticles, those alcohols are *not present in any form in the Co_3O_4 product* (~5% alcohol detection limit). Instead, OAc^- is the main, detectable species present that can serve as a surface-ligand for Co_3O_4 nanoparticles synthesized from $Co(OAc)_2$ in alcohol co-solvents. Even for $PhCH_2OH$, a relatively small, ca. 1:5 ratio of that alcohol compared to OAc^- is observed in the isolated product, an amount of $PhCH_2OH$ that may well be trapped in a second, non-Co_3O_4 product. The take-home message is unequivocal for at least EtOH and *t*-BuOH: these alcohols

have a dramatic effect on the phase-purity and size-distribution of the Co_3O_4 nanoparticle products, yet no intact EtOH or *t*-BuOH within experimental error winds up in the isolated Co_3O_4 product. The precise chemical reason(s) for the dominant effect of those alcohols on Co_3O_4 nanoparticle and other M_xO_y nanoparticle syntheses remains to be examined, as do the list of alternative hypotheses generated above en route to understanding the underlying mechanism by which ROH solvents have their dramatic kinetic and / or thermodynamic effects.

Supporting Information.

The Supporting Information can be found in Appendix IV of the dissertation and contains: the TEM histogram and FT-IR of the water synthesized CoO_x nanoparticles; TEM histogram, SAED, DLS, FT-IR, and quantitative ^1H NMR of the Co_3O_4 nanoparticles synthesized in EtOH/water; PXRD, HRTEM, SAED, FT-IR, and quantitative ^1H NMR of the particles synthesized in *t*-BuOH/water or in $PhCH_2OH$/water; Control synthesis employing an eight-fold longer reaction time of 24 hrs in search of a higher yield of the Co_3O_4 product; PXRD pattern of Co_3O_4 nanoparticles synthesized in ethanol for three hours and, separately, for 24 hours.

REFERENCES

1 Zhou, L.; Xu, J.; Miao, H.; Wang, F.; Li, X. *Applied Catalysis A: General* **2005**, *292*, 223–228.

2 Dong, Y.; He, K.; Yin, L.; Zhang, A. *Nanotechnology* **2007**, *18*, 435602.

3 Grzelczak, M.; Zhang, J.; Pfrommer, J.; Hartmann, J.; Driess, M.; Antonietti, M.; Wang, X. *ACS Catal.* **2013**, *3*, 383–388.

4 Wei, P.; Hu, B.; Zhou, L.; Su, T.; Na, Y. *Journal of Energy Chemistry* **2016**, *25*, 345–348.

5 Banerjee, D.; Jagadeesh, R. V.; Junge, K.; Pohl, M.-M.; Radnik, J.; Brückner, A.; Beller, M. *Angew. Chem. Int. Ed.* **2014**, *53*, 4359–4363.

6 Poizot, P.; Laruelle, S.; Grugeon, S.; Dupont, L.; Tarascon, J.-M. *Nature* **2000**, *407*, 496–499.

7 Kim, J.-C.; Hwang, I.-S.; Seo, S.-D.; Kim, D.-W. *Materials Letters* **2013**, *104*, 13–16.

8 Shen, L.; Wang, C. Hierarchical *Electrochimica Acta* **2014**, *133*, 16–22.

9 Park, J.; Moon, W. G.; Kim, G.-P.; Nam, I.; Park, S.; Kim, Y.; Yi, J. *J.Electrochim. Acta* **2013**, *105*, 110–114.

10 Garakani, M. A.; Abouali, S.; Zhang, B.; Takagi, C. A.; Xu, Z.-L.; Huang, J.; Huang, J.; Kim, J.-K. *ACS Appl. Mater. Interfaces* **2014**, *6*, 18971–18980.

11 Li, S.-J.; Du, J.-M.; Zhang, J.-P.; Zhang, M.-J.; Chen, J. *Microchim Acta* **2014**, *181*, 631–638.

12 Kundu, S.; Nelson, A. J.; McCall, S. K.; Buuren, T. van; Liang, H. *J. Nanopart. Res.* **2013**, *15*, 1587.

13 Zheng, Y.; Li, P.; Li, H.; Chen, S. *Int. J. Electrochem. Sci.* **2014**, *9*, 7369–7381.

14 Raj, V.; Silambarasan, J.; Rajakumar, P. *RSC Adv.* **2014**, *4*, 33874–33882.

15 Li, S.-J.; Du, J.-M.; Chen, J.; Mao, N.-N.; Zhang, M.-J.; Pang, H. *J Solid State Electrochem* **2014**, *18*, 1049–1056.

16 Vijayakumar, S.; Ponnalagi, A. K.; Nagamuthu, S.; Muralidharan, G. *Electrochimica Acta* **2013**, *106*, 500–505.

17 Zhi, J.; Deng, S.; Zhang, Y.; Wang, Y.; Hu, *J. Mater. Chem. A* **2013**, *1*, 3171–3176.

18 Zheng, C.; Cao, C.; Ali, Z.; Hou, J. *J. Mater. Chem. A* **2014**, *2*, 16467–16473.

19 Chou, N. H.; Ross, P. N.; Bell, A. T.; Tilley, T. D. *ChemSusChem* **2011**, *4*, 1566–1569.

20 Kanan, M. W.; Nocera, D. G. *Science* **2008**, *321*, 1072–1075.

21 Shi, N.; Cheng, W.; Zhou, H.; Fan, T.; Niederberger, M. *Chem. Commun.* **2014**, *51*, 1338–1340.

22 Niederberger, M.; Bartl, M. H.; Stucky, G. D. *Chem. Mater.* **2002**, *14*, 4364–4370.

23 Niederberger, M.; Bartl, M. H.; Stucky, G. D. *J. Am. Chem. Soc.* **2002**, *124*, 13642–13643.

24 Bilecka, I.; Djerdj, I.; Niederberger, M. *Chem. Commun.* **2008**, 886–888.

25 Hubli, R. C.; Mittra, J.; Suri, A. K. *Hydrometallurgy* **1997**, *44* (1), 125.

26 Kanan, M. W.; Surendranath, Y.; Nocera, D. G. *Chem. Soc. Rev.* **2008**, *38*, 109–114.

27 Liu, Z.; Ma, R.; Osada, M.; Takada, K.; Sasaki, T. *J. Am. Chem. Soc.* **2005**, *127*, 13869–13874.

28 Neilson, J. R.; Schwenzer, B.; Seshadri, R.; Morse, D. E. *Inorg. Chem.* **2009**, *48*, 11017–11023.

29 Poul, L.; Jouini, N.; Fiévet, F. *Chem. Mater.* **2000**, *12*, 3123–3132.

30 Patterson, A. L. *Phys. Rev.* **1939**, *56*, 978–982.

31 Xu, Z. P.; Zeng, H. C. *Chem. Mater.* **1999**, *11*, 67–74.

32 Jayashree, R. S.; Kamath, P. V. *J. Mat. Chem.* **1999**, *9*, 961–963.

33 Folkman, S. J.; Finke, R. G. *ACS Catal.* **2017**, *7*, 7–16.

34 Zhao, Q.; Yan, Z.; Chen, C.; Chen, J. *Chem. Rev.* **2017**, ASAP.

35 Vioux, A. *Chem. Mater.* **1997**, *9*, 2292-2299.

36 Mutin, P. H.; Vioux, A. *J. Mater. Chem. A.* **2013**, *1*, 11504-11512.

37 Neiderberger, M.; Garnweitner, *Chem. Eur*. **2006**, *12,* 7282-7302.

38 Matijevic´, E. *Chem. Mater.* **1993**, *5*, 412-426; see the statement on p. 415.

39 Feckl, J. M.; Dunn, H,. K.; Zehetmaier, P. M.; Pendlebury, S. R.; Zeller, P.; Fominykh, K.; Kondofersky, I.; Döblinger, M.; Durrant, J. R.; Scheu, C.; Peter, L.; Dattakhova-Rohlfing, D.; Bein, T. Mater. *Interfaces* **2015**, *2*, 1500358.

40 Pirovano, C.; Trasatti, S. *Journal of Electroanalytical Chemistry and Interfacial Electrochemistry* **1984**, *180*, 171–184.

41 Pinna, N. *J. Mater. Chem.* **2007**, *17*, 2769–2774.

42 Bai, X.; Pucci, A.; Freitas, V. T.; Ferreira, R. A. S.; Pinna, N. *Adv. Funct. Mater.* **2012**, *22*, 4275–4283.

43 Caputo, G.; Pinna, N. *J. Mater. Chem. A* **2013**, *1*, 2370–2378.

44 Liu, J.; Margeat, O.; Dachraoui, W.; Liu, X.; Fahlman, M.; Ackermann, J. *Adv. Funct. Mater.* **2014**, *24*, 6029–6037.

45 Grote, C.; Cheema, T. A.; Garnweitner, G. *Langmuir* **2012**, *28*, 14395–14404.

46 Stöber, W.; Fink, A.; Bohn, E. *Journal of Colloid and Interface Science* **1968**, *26*, 62–69.

47 Gebauer, D.; Kellermeier, M.; Gale, J. D.; Bergström, L.; Cölfen, H *Chem. Soc. Rev.* **2014**, *43*, 2348-2371.

VI. SUMMARY AND CONCLUSIONS

This dissertation explores the identity of the true water oxidation catalyst (WOCatalyst) under electrocatalytic conditions when beginning with cobalt based polyoxometalates (Co-POMs), as well as the fundamental properties of Co_3O_4 nanoparticles that could be used as WOCatalysts. Each of the research chapters, Chapters II-V, are reproductions of peer-reviewed published manuscripts that were primarily written by the author of this dissertation, S. Folkman.[1,2, 3,4] The main findings of each chapter and the overarching conclusions of the dissertation in totality is discussed in what follows as the final chapter of this dissertation.

Chapter II details our studies[1] of the synthesis, purity and ^{51}V NMR of $[Co_4(H_2O)_2(VW_9O_{34})_2]^{10-}$ (hereafter **$Co_4V_2W_{18}$**), which was claimed to be 200x faster than its P-analog $[Co_4(H_2O)_2(PW_9O_{34})_2]^{10-}$ and purportedly the fastest Co-POM WOCatalyst to date.[5] The main findings of that chapter are as follows: (i) the literature syntheses[5,6] of **$Co_4V_2W_{18}$** yield material that is an impure composite mixture, containing sodium acetate (NaOAc), among other impurities, as demonstrated by elemental analysis, FT-IR, ^{51}V NMR, and the highly variable 12-70% yields for "**$Co_4V_2W_{18}$**"; (ii) the primary observed ^{51}V NMR resonance for the as-synthesized "**$Co_4V_2W_{18}$**" at −510 ppm ($\Delta\nu_{1/2}$=28±7 Hz) that was originally assigned to intact **$Co_4V_2W_{18}$** actually belongs to *cis*-$V_2W_4O_{19}^{4-}$, which is present either as an impurity or decomposition side-product; (iii) the as-synthesized "**$Co_4V_2W_{18}$**" undergoes chemical changes in both the solid state and when dissolved in aqueous solution; and (iv) the previous studies[5] using "**$Co_4V_2W_{18}$**" as a WOCatalyst are called into question because the main claims of that paper hinged on the stability of "**$Co_4V_2W_{18}$**", which was determined using the incorrectly assigned ^{51}V NMR peak at −510 ppm ($\Delta\nu_{1/2}$=28±7 Hz).

Given the findings summarized above, we sought to re-examine the stability and WOCatalysis characteristics "**$Co_4V_2W_{18}$**" under electrocatalytic conditions, which is the subject of Chapter III.[2] The main findings of Chapter III are: (i) **$Co_4V_2W_{18}$** is hydrolytically unstable and dissociates 87-100% of the Co(II) originally present in **$Co_4V_2W_{18}$** into solution within three hours when dissolved in 0.1 sodium phosphate buffer (NaPi) at pH 5.8 and 8.0 as well as sodium borate buffer (NaB) pH=9.0 (determined by $Co(II)_{aq}$-induced line broadening of the phosphate buffer and adsorptive cathodic stripping);[2] (ii) the $Co(II)_{aq}$ that dissociates from the "**$Co_4V_2W_{18}$**" deposits onto a glassy carbon electrode and forms electrode-bound CoO_x; and (iii) the CoO_x film formed from "**$Co_4V_2W_{18}$**" accounts for 100±15% of the observed catalysis. This study provided yet another case where a Co-POM is a precursor to heterogeneous CoO_x under electrocatalytic conditions. From the studies described herein with **$Co_4V_2W_{18}$**, and our previous studies[7,8] with **$Co_4P_2W_{18}$** a reliable methodology for distinguishing between homogeneous and heterogeneous WOCatalysis had been established.

To further establish the generality of our methods for distinguishing between homogeneous and heterogeneous WOCatalysis, and to gain structure-property relationships, we conducted a survey of the most stable and well-studied Co-POMs which constitutes the material in Chapter IV.[3] The conclusions drawn in Chapter IV are: (i) none of the Co-POMs examined are 100% stable, and they release between 0.6 and >90% of the cobalt in the original complex within three hours in 0.1 M NaPi pH=5.8 or 8.0 and NaB pH=9.0; (ii) the stability is highly dependent upon conditions, for example the stability of $[Co(H_2O)PW_{11}O_{39}]^{5-}$ is highly pH dependent and dissociates 1.3±0.6, 50±5, and 90±10% of the cobalt in pH 5.8, 8.0, and 9.0, respectively; (iii) in 13 of the 18 cases examined, heterogeneous CoO_x forms and accounts for ≥100% of the observed WOCatalysis current; (iv) under conditions where the Co-POMs are stable, the evidence provided implies that

some of the Co-POMs are homogeneous WOCatalyst. For example, when beginning with **α_1-CoP_2W_{17}** in 0.1 M NaPi at pH=5.8 the amount of $Co(II)_{aq}$ detected only accounts for 20±14 %, of the observed WOCatalysis activity, and no detectable film is formed from 30 min of electrolysis—implying that **α_1-CoP_2W_{17}** is a homogeneous WOCatalyst under those conditions; and finally (v) the methodologies presented in this study demonstrate cases where a Co-POM forms heterogeneous CoO_x as the dominant WOCatalyst and distinguishes cases where the same Co-POM is a homogeneous WOCatalyst, providing additional, now validated methods of distinguishing homogeneous and heterogeneous WOCatalysis.[2,3,7,8]

Our previous studies using Co-POMs as WOPrecatalysts demonstrated the formation of a more thermodynamically stable CoO_x phase that is also a more active WOCatalyst than the Co-POM starting material.[2,3] As such, we hoped to find a more stable cobalt phase that could be stabilized or modified for use in WOCatalysis. One of the most interesting prospects is spinel phase Co_3O_4 nanoparticles.[4,9,10,11,12] As such, we synthesized and characterized Co_3O_4 nanoparticles from a procedure adapted from the literature.[9,10] Chapter V details the studies conducted on the isolated Co_3O_4 nanoparticles and has implications for the synthesis and surface properties of metal-oxide nanomaterials in general.[4] Specifically, the main findings for the work in Chapter V are: (i) phase pure Co_3O_4 nanoparticles are synthesized in ethanol/water, but a mixture of phases is observed when only water is used as solvent—meaning that the ethanol (EtOH) must be involved in the formation of the particles, either *thermodynamically* as a surface ligand (i.e., EtO^- covalently linked to surface Co) or *kinetically* (i.e., by somehow affecting the nucleation and/or growth of the particles); (ii) digestion of the particles through an acidic reduction followed by quantitative ^1H NMR demonstrates that the only detectable organic species is acetate (OAc^-), which is present from the cobalt acetate starting material; and (iii) through elemental analysis and quantitative ^1H

NMR we were able to obtain an average molecular formula of $\{[Co_3O_4(C_2H_3O_2)^-][(NH_4^+)_{0.3}(H^+_{0.7})]^+ \cdot (H_2O)\}_{\sim 216}$ for the nanoparticles that we obtained—a rare demonstration of the average molecular formula for a cobalt-oxide nanoparticle. In addition, (iv) we conducted the same synthesis in *tert*-butanol, and benzyl alcohol and demonstrated that in both of those cases, OAc^- is the dominant surface ligand—implying the generality of acetate (or other anions) from the starting material as surface ligands for metal-oxide nanoparticles. Although this manuscript did not directly address the use of Co_3O_4 nanoparticles for WOCatalysis, it does provide methodology to probe the surface and composition of metal-oxide nanoparticles that will be relevant to future studies using metal-oxide nanoparticles in WOCatalysis.

In summary, this dissertation has developed and demonstrated the utility of methods for distinguishing between homogeneous and heterogeneous WOCatalysis when beginning with Co-POMs. Although this work has focused on Co-POMs and WOCatalysis, many of the same methods and principles apply to catalysis in general. Namely, (i) identity of the true catalyst is a difficult and often cumbersome task and involves vigilant experimentation and disproof of multiple alternative hypotheses; (ii) stability and speciation are fundamental details that must be known before catalytic and mechanistic studies; (iii) multiple, independent and complementary methods are often necessary to determine a starting material's stability *in situ* and to elucidate the true catalyst; and finally (iv) the identity of the true catalyst is highly dependent upon reaction conditions and must be verified through the methodologies outline here[1,2,3] and elsewhere[8,13] for legitimate claims of homogeneous WOCatalysis.

REFERENCES

1 Folkman, S. J.; Kirner, J. T.; Finke, R. G.. *Inorg. Chem.* **2016**, *55* (11), 5343–5355.

2 Folkman, S. J.; Finke, R. G. *ACS Catal.* **2017**, *7* (1), 7–16.

3 Folkman, S. J.; Soriano-Lopez, J.; Galán-Mascarós, J.R.; Finke, R. G. Submitted to *JACS*, June **2018**.

4 Folkman, S. J.; Zhou, M.; Nicki, M.; Finke, R. G. *Inorg. Chem.* **2018**, *57* (3), 1517–1526.

5 Lv, H.; Song, J.; Geletii, Y. V.; Vickers, J. W.; Sumliner, J. M.; Musaev, D. G.; Kögerler, P.; Zhuk, P. F.; Bacsa, J.; Zhu, G. *J. Am. Chem. Soc.* **2014**, *136* (26), 9268–9271.

6 Li, B.; Yan, Y.; Li, F.; Xu, L.; Bi, L.; Wu, L. *Inorg. Chim. Acta* **2009**, *362* (8), 2796–2801.

7 Stracke, J. J.; Finke, R. G. *J. Am. Chem. Soc.* **2011**, *133* (38), 14872–14875.

8 Stracke, J. J.; Finke, R. G. *ACS Catal.* **2014**, *4* (3), 909–933.

9 Grzelczak, M.; Zhang, J.; Pfrommer, J.; Hartmann, J.; Driess, M.; Antonietti, M.; Wang, X. *ACS Catal.* **2013**, 3, 383−388.

10 Wei, P.; Hu, B.; Zhou, L.; Su, T.; Na, Y. *J. Energy Chem.* **2016**, 25, 345−348.

11 Chou, N. H.; Ross, P. N.; Bell, A. T.; Tilley, T. D. *Chem. Sus. Chem* **2011**, 4, 1566−1569.

12 Shi, N.; Cheng, W.; Zhou, H.; Fan, T.; Niederberger, M. *Chem. Commun.* **2015**, 51, 1338−1340.

13 Widegren, J. A.; Finke, R. G. *J. Mol Catal. A: Chem.* **2003**, 198, 317−341.

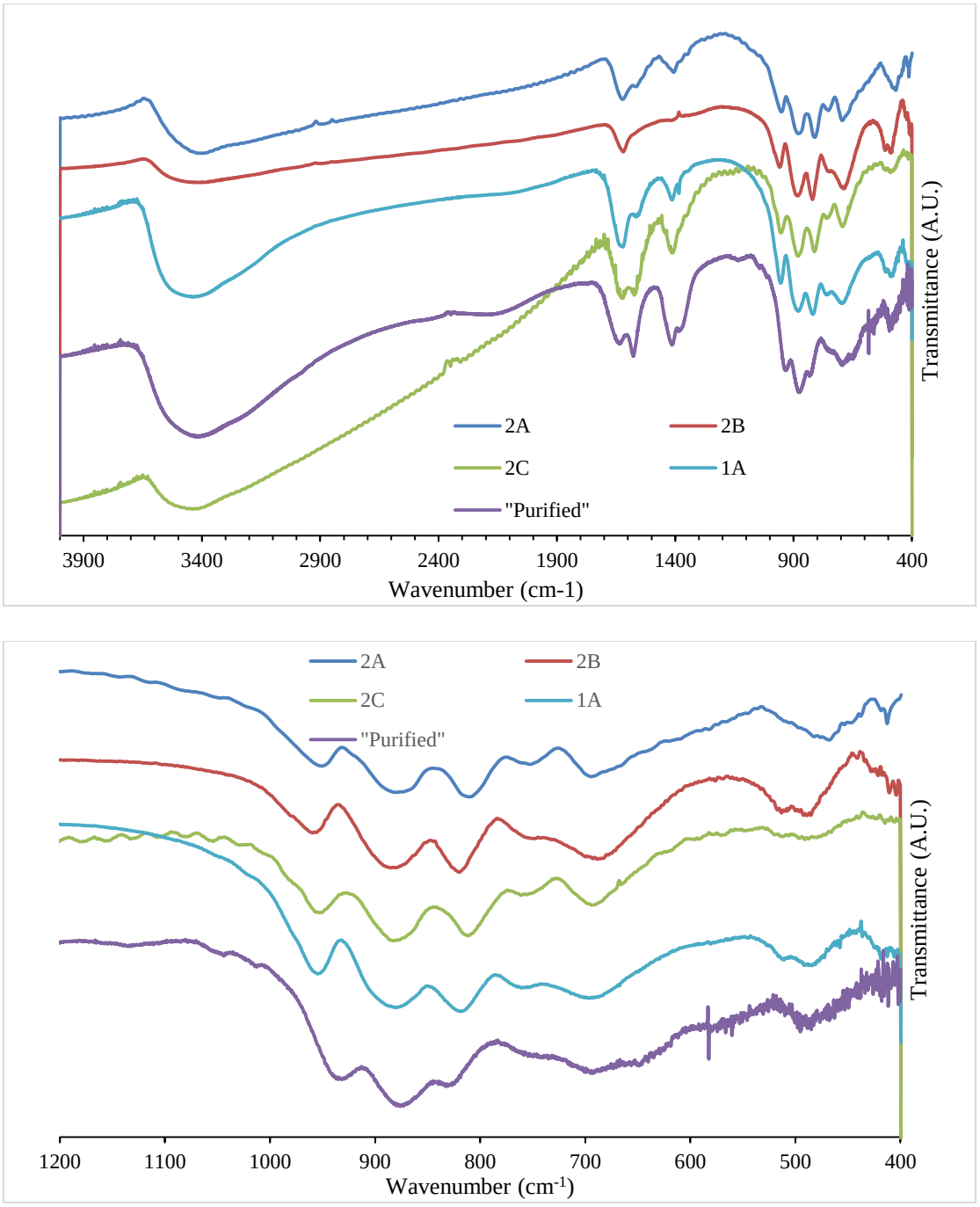

Figure S2.1. FT-IR of the products obtained following the Original[1] synthesis (1A, cyan), three 2014[2] syntheses (2A, 2B, and 2C: blue, red and green lines, respectively), and the "Purified" green material (purple line). All spectra were collected on the products at *ca.* 2 wt % in KBr.

These IR spectra demonstrate that even when following the exact same procedures[1,2] multiple times, variation in the FT-IR spectra is observed. In addition, even the "Purified" green material has a spectrum similar to that of "**$Co_4V_2W_{18}$**." The top spectrum shows the full 400–4000 cm^{-1} range, and the bottom spectrum shows the fingerprint region from 400–1200 cm^{-1}. Note that the C=O doublet stretch at *ca.* 1600 cm^{-1} assignable to acetate is visible in each spectrum.

Discussion on the UV–vis of "$Co_4V_2W_{18}$," $Co_4P_2W_{18}$, and *cis*-$V_2W_4O_{19}^{4-}$

As discussed in the Introduction in the main text, the UV–vis of "**$Co_4V_2W_{18}$**" is likely a convolution of several species existing simultaneously in solution, and in unknown amounts. Indeed, the UV–visible spectrum obtained for authentic *cis*-$V_2W_4O_{19}^{4-}$ at the same total concentration of vanadium as "**$Co_4V_2W_{18}$**", Figure S2, shows a LMCT centered at *ca*. 380 nm. As such, the fairly broad, ill-defined UV–visible spectrum for "**$Co_4V_2W_{18}$**" must, on the basis of the ^{51}V NMR results, be a convolution of absorptions from at least *cis*-$V_2W_4O_{19}^{4-}$ and **$Co_4V_2W_{18}$** as well as other unidentified species, some of which likely contain cobalt.

Overall, our UV–vis results were quite similar to the 2014 study,[2] including that we have observed a small, 2% decrease in the absorbance at several points along the absorption spectrum over two hours.

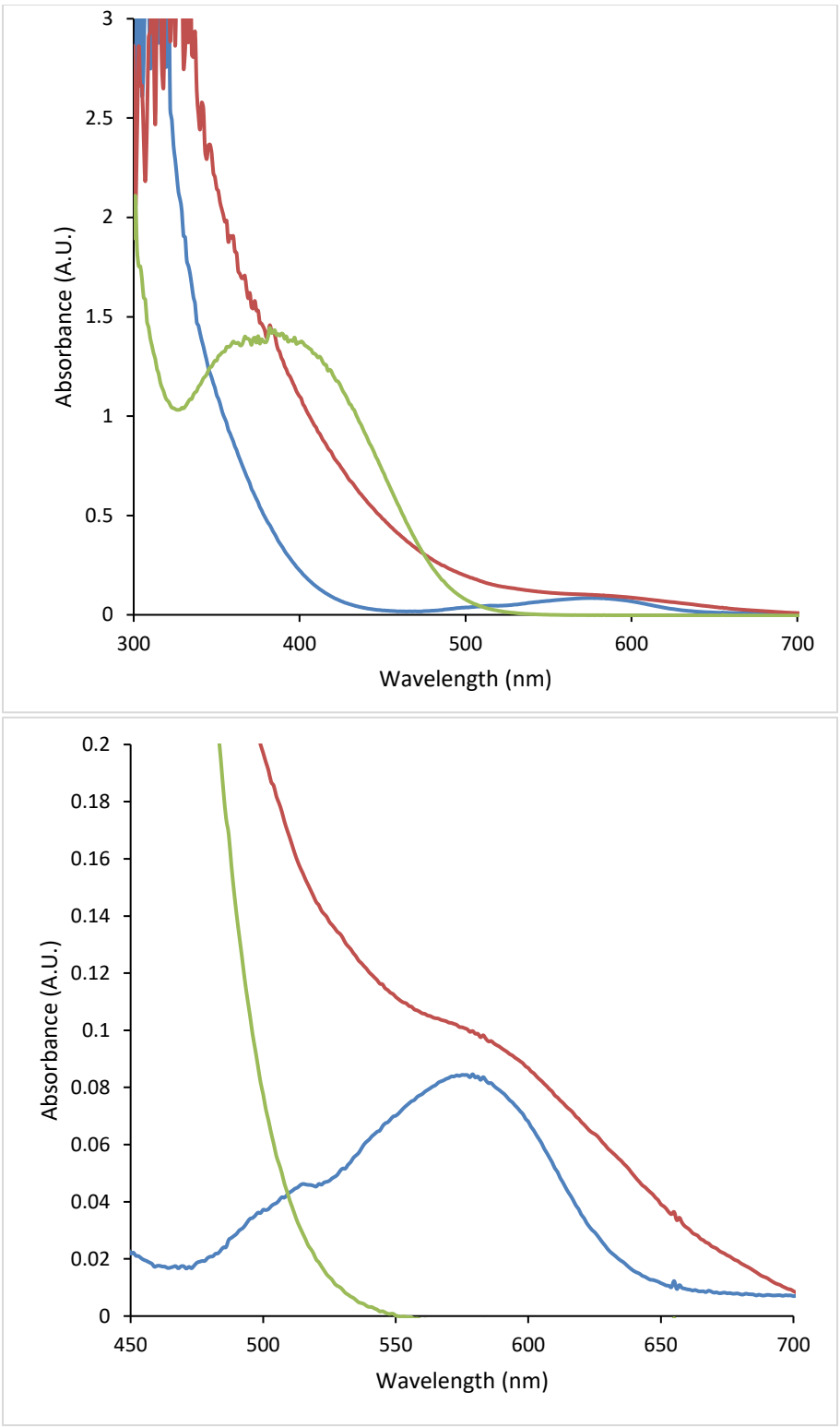

Figure S2.2. The UV–visible spectra of "**$Co_4V_2W_{18}$**" (red), **$Co_4P_2W_{18}$** (blue) and authentic *cis*-$V_2W_4O_{19}^{4-}$ (green) each sample is 500 µM in DI water. The top spectrum shows the full 300–700 nm UV–vis, and the bottom spectrum shows a zoom of the visible d–d transition.

ESI-MS of $Co_4V_2W_{18}$ and *cis*-$V_2W_4O_{19}^{4-}$: Experiments and Discussion

(i) ESI-MS in the 2014 Study. A species with a most abundant mass of −1366 m/z was observed in the 2014[2] study, which the authors attributed to a −4 charged species—if true, then consistent with $(TBA)_2(CH_3CN)_5H_4[Co_4(H_2O)_2(VW_9O_{34})_2]^{4-}$. *However*, (i) the peak spacing is neither reported nor distinguishable in the reported figure (Figure S10 in the SI of that paper[2]), so that one cannot verify the claimed −4 charge via the expected 0.25 m/z isotopic peak spacing. Additionally, (ii) simulations to match the predicted isotopic abundances to those observed for the peaks centered at −1366 were not performed in that study. Furthermore, (iii) even if isotopic simulations were conducted and the simulations matched the observed peak intensities, the assignments are not unique, nor therefore absolutely definitive, due to the large number of possible species that could fit the peak.[3] (The inability to reliably distinguish high molecular weight species by mass spectrometry is well-known and discussed elsewhere for larger MW materials such as polystyrene, glucagon, and phosphazine.[3]) Additionally, (iv) the samples used for mass spectrometry were prepared by converting the **$Co_4V_2W_{18}$** product to the TBA^+ salt and extracting into acetonitrile solution,[2] but no experimental details were provided as to exactly how this extraction was conducted, so that we could repeat it only approximately, but not exactly. Note also that because the speciation and stability of POMs are often drastically different in organic solvents,[4,5] the implication being that *CH_3CN may change the speciation and stability of the cobalt and other POMs present in "**$Co_4V_2W_{18}$**" in aqueous solution*. What's more, possible impurity species may be easily mistaken for fragmentation species of the desired compound. In short, the above points cast serious doubt on the prior assignment[2] of the −1366 m/z species to $(TBA)_2(CH_3CN)_5H_4[Co_4(H_2O)_2(VW_9O_{34})_2]^{4-}$.

(ii) Preparation of tetrabutylammonium salts of "$Co_4V_2W_{18}$" from Synthesis #2 and cis-$V_2W_4O_{19}^{4-}$ from Synthesis #3 for ESI-MS as Part of the Present Studies. The purpose of the experiments which follow is to conduct mass spectrometry on the TBA^+ salt of "**$Co_4V_2W_{18}$**" (prepared from the sodium salt collected from Synthesis #2) and compare this with the mass spectrum obtained from the TBA^+ salt of authentic *cis*-$V_2W_4O_{19}^{4-}$. To prepare the TBA^+ salts, we used a method adapted from the metathesis of $K_7[\alpha_2\text{-}P_2W_{17}O_{61}(Mn(III)\cdot OH_2)]$ to $(TBA)_{8-x}H_x[\alpha_2\text{-}P_2W_{17}O_{61}(Mn(III)\cdot Br)]$.[6] Specifically, a 12.5 mL solution of *ca.* 5 mM of the POM (either **$Co_4V_2W_{18}$** or *cis*-$V_2W_4O_{19}^{4-}$) was prepared in unbuffered water. Next, 14 equivalents of $Bu_4N^+Br^-$ was added with stirring. The resulting Bu_4N^+/H^+ salts were then extracted with 12.5 mL of a 1:1 mixture of CH_3CN and CH_2Cl_2 by mixing vigorously and separating the aqueous and organic phase with a separatory funnel. The product, in the upper organic phase, was then isolated via rotary evaporation at 60 ºC with rotation at 200 rpm. A brown powder was obtained when the TBA^+ salt metathesis was conducted on "**$Co_4V_2W_{18}$**" and an orange powder was obtained with *cis*-$V_2W_4O_{19}^{4-}$. These TBA^+ salts were then used directly in the ESI-MS as described in the Instrumentation section in Chapter II of the main text.

(iii) ESI-MS Repeated as Part of the Present Study. ESI-MS was obtained on the TBA^+ salt of "**$Co_4V_2W_{18}$**," prepared as in (ii) above by the 2014[2] Synthesis #2, and of authentic *cis*-$V_2W_4O_{19}^{4-}$, via metathesis of the sodium salt precursors with TBA^+Br^- (see the Experimental details provided in (ii) above; unfortunately the precise conditions of the TBA^+ salt metathesis and subsequent extraction are not given in the 2014 study[2] and, hence, could not be repeated exactly). ^{51}V NMR (Figure S2.9) of the products in acetonitrile is consistent with the expected metathesis reaction. Our ESI-MS of "**$Co_4V_2W_{18}$**," differ from the ESI-MS in the 2014 report[2] in that we observe many more peaks, Figure S3, than seen in the 2014 studies. In addition, the observed ESI-

MS are quite different for the "**Co$_4$V$_2$W$_{18}$**" and *cis*-$V_2W_4O_{19}^{4-}$, with "**Co$_4$V$_2$W$_{18}$**" sample displaying main peaks at m/z = −723, −1369 and −1690, for example, while the base peak for *cis*-$V_2W_4O_{19}^{4-}$ is −1368, *close to* but *not exactly the same as* the −1369 peak seen in the "**Co$_4$V$_2$W$_{18}$**" sample due to the differences in isotopic peak spacing, Figure S3.

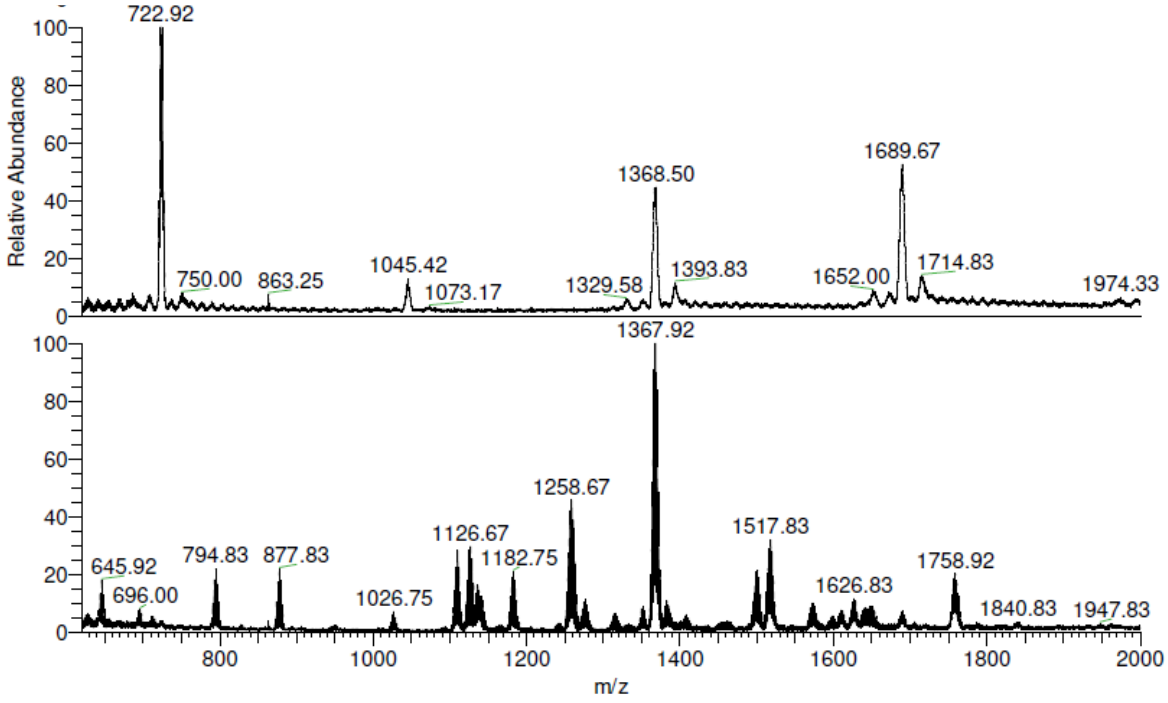

Figure S2.3. ESI-MS of the TBA salts of "**Co$_4$V$_2$W$_{18}$**" (top) and *cis*-$V_2W_4O_{19}^{4-}$ (bottom) in acetonitrile.

Focusing in on the ESI-MS of *cis*-$V_2W_4O_{19}^{4-}$, the isotopic spacing for the −1368 peak is 1 amu so that the charge on the complex giving rise to that peak must be −1. However, when attempting to fit the observed peak at −1368 m/z with −1 charged species of the general nominal formula "$TBA_aNa_bH_{4-a-b}$[*cis*-$V_2W_4O_{19}$]•$(CH_3CN)_c$•$(H_2O)_d$" we were able to match the observed isotopic ratios for a −1 species within experimental error *with at least five different specific compositions*: "$H_3[V_2W_4O_{19}](CH_3CN)_5(H_2O)^{1-}$", "$H_3[V_2W_3O_{16}](CH_3CN)_1(H_2O)_{23}^{1-}$", "$(TBA)_2H_1[V_2W_3O_{16}](CH_3CN)_3(H_2O)_5^{1-}$", "$Na_2H[V_2W_3O_{16}](CH_3CN)_3(H_2O)_{16}^{1-}$", and

"$Na_2H[V_2W_3O_{16}](CH_3CN)_{10}^{1-}$" where $V_2W_3O_{16}$ represents a fragment of $V_2W_4O_{19}^{4-}$ in which a WO_3 has been removed (as has been observed using fast atom bombardment MS of polyoxometalates).[7,8] The simulations are shown in Figure S2.4. This illustrates that the isotopic distribution of high molecular weight species such as POMs can match many proposed compound formulas, and is therefore not definitive evidence for the existence of a single species. This is a well-known problem in the MS of high molecular weight compounds.[3] In short, the ESI-MS results, while interesting, are not definitive evidence for **$Co_4V_2W_{18}$** in either the literature, nor in our, studies.

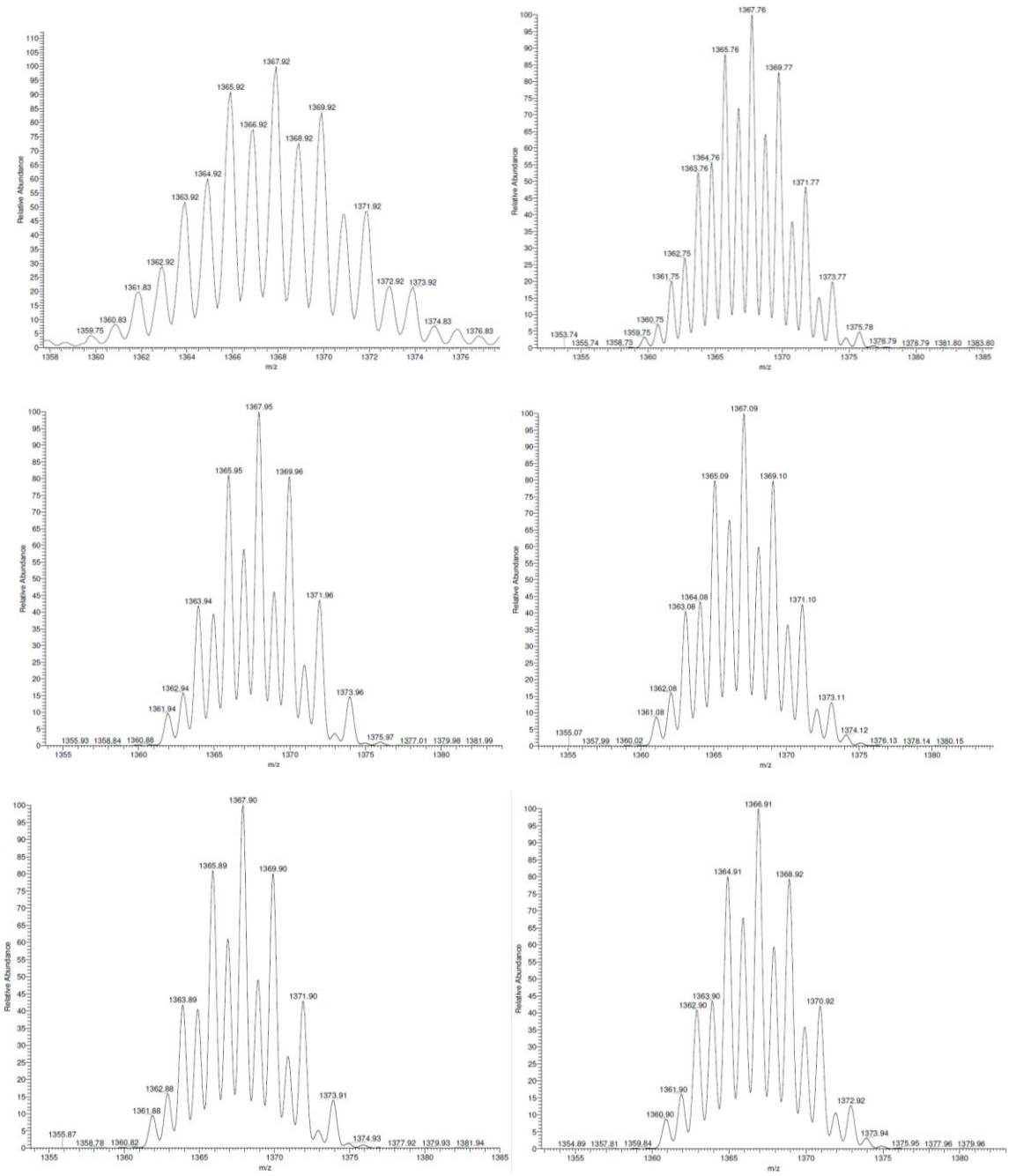

Figure S2.4. ESI-MS zoom of the −1367 of the authentic *cis*-$V_2W_4O_{19}^{4-}$ TBA^+ salt (top left), and the simulations for $H_3[V_2W_4O_{19}](CH_3CN)_5(H_2O)^{1-}$ (top right), $H_3[V_2W_3O_{16}](CH_3CN)_1(H_2O)_{23}^{1-}$ (middle left), $(TBA)_2H_1[V_2W_3O_{16}](CH_3CN)_3(H_2O)_5^{1-}$ (middle right), $Na_2H[V_2W_3O_{16}](CH_3CN)_3(H_2O)_{16}^{1-}$ (bottom left), and $Na_2H[V_2W_3O_{16}](CH_3CN)_{10}$ (bottom right) demonstrating that all of these species fit the spectrum relatively well. The simulations represent Gaussian profiles for 0.5 Dalton resolution.

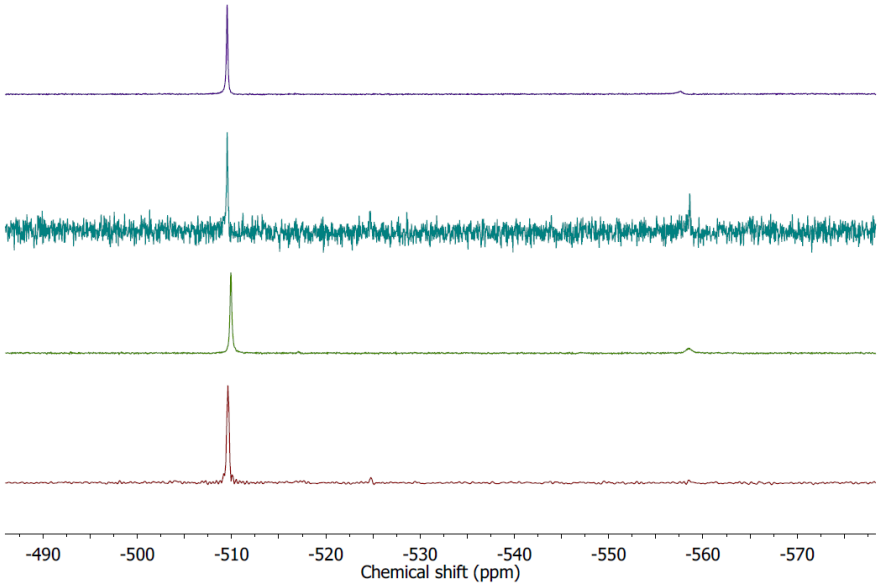

Figure S2.5. ^{51}V NMR spectra of the product obtained for syntheses 2A, 2B, 2C (the three repeats of the 2014 study[2]) and 1A (from the original study[1]) from top to bottom. All of these spectra were collected on *ca.* 5 mM solutions of "**$Co_4V_2W_{18}$**" in 10% D_2O. This demonstrates that some impurities are always observed in the ^{51}V NMR spectra and that the main resonance is reproducibly at −510 ppm $\Delta\nu_{1/2}$=28±7 Hz.

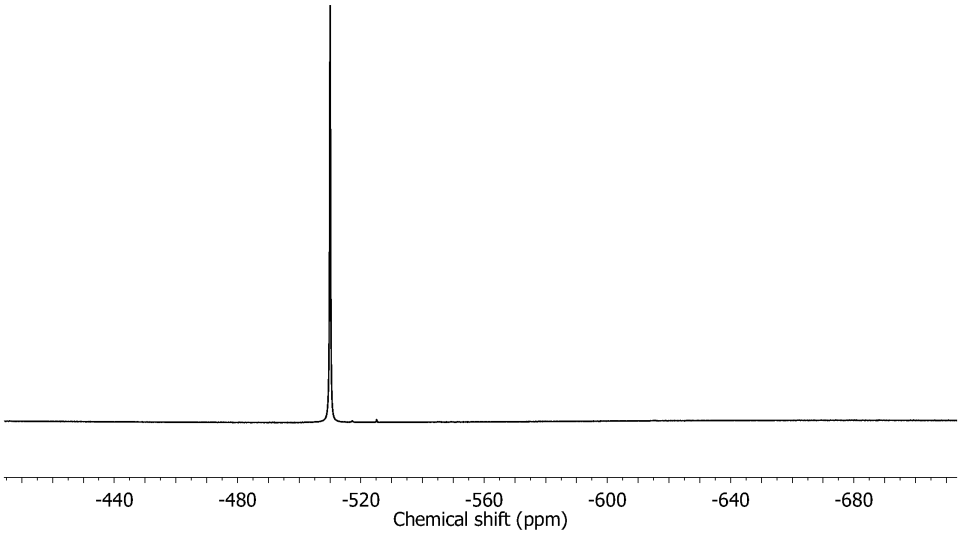

Figure S2.6. ^{51}V NMR of the "purified" green product. The main chemical resonance at −510 ppm ($\Delta\nu_{1/2}$ = 28±7 Hz) composes ca. 99% of the integration.

Additional evidence that the ^{51}V NMR chemical shift reported (−507 ppm) for "$Co_4V_2W_{18}$" and that obtained in this work (−510 ppm) are the same chemical species

A question that came up early in this work is if the 2014 literature[2] ^{51}V NMR report of a −506.8 (error bars unstated) ppm resonance with a peak width of $\Delta\nu_{1/2}$=30.5 Hz (error bars unstated) (in unbuffered D_2O or borate buffer pH 9.0 at room temperature) the same as the main resonance at −510±0.5 ppm ($\Delta\nu_{1/2}$ = 28±7 Hz) that we observe for "**$Co_4V_2W_{18}$**" dissolved in unbuffered H_2O/D_2O at room temperature. In some sense this is just the questions of: (i) what were the precise conditions of the two measurements; are they the same or different? (ii) What then, are the error bars of the two measurements being compared? And (iii) how does the referencing employed in the two studies affect the observed chemical shifts?

To address the first question, one would like to examine a sample of "**$Co_4V_2W_{18}$**" prepared by the 2014,[2] Synthesis #2, by ^{51}V NMR under the precise conditions used in the 2014 study. However, insufficient detail was given in those studies to be able to reproduce exactly the NMR figures of interest, namely Figures S6 and S7 of that paper.[2] Indeed, Figure S8 of those studies[2] claims to display the ^{51}V NMR spectra of "**$Co_4V_2W_{18}$**" in D_2O and 40 mM sodium borate buffer, but does not explicitly state which set of conditions is for which of the spectra given. Furthermore, the concentration of "**$Co_4V_2W_{18}$**" used in the ^{51}V NMR aging and heating experiments is not reported (Figures S6 and S7 of that study, respectively), making it impossible to know, and then use, "identical" conditions to those particular experiments.[2]

Hence, we conducted ^{51}V NMR as follows: using 2 μM "**$Co_4V_2W_{18}$**" from synthesis 2A, first in pure, unbuffered D_2O and, separately, in 0.1 M sodium borate buffer at pH 9.0, both at room temperature. In comparison to the 2014 paper's ^{51}V NMR peak at −507 ppm (and $\Delta\nu_{1/2}$=30.5 Hz) we observe a resonance at −510 ppm ($\Delta\nu_{1/2}$=28±7 Hz) observed in unbuffered pure D_2O.

However, when we conducted the same control in pH 9.0 borate buffer with 20% D_2O we did not observe the −510 peak; instead, we observed a moderately broad peak at −543 ppm ($\Delta\nu_{1/2}$= ca. 170 Hz), Figure S7. The absence of the −510 peak can be explained by the decomposition of *cis*-$V_2W_4O_{19}^{4-}$ (which we have assigned to this resonance; see the main text), because *cis*-$V_2W_4O_{19}^{4-}$ is known to be unstable above pH 8.[9] Hence, precisely how the authors were able to observe the −507 species in borate buffer is not 100% clear, and is likely related to the precise conditions under which the spectra were collected, including aging time.

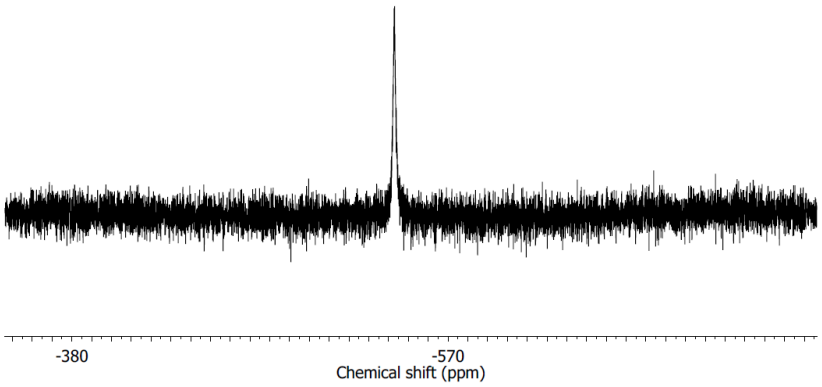

Figure S2.7. ^{51}V NMR spectrum of "**$Co_4V_2W_{18}$**" after one hour in 0.1 M NaB buffer, pH=9.0.

To address the second and third questions of the estimated error bars on the ^{51}V NMR chemical shifts, we performed the following experiment to give an *estimate* of the variance in our chemical shift values vs what others might obtain, especially with respect to the referencing method employed. Specifically, we obtained the ^{51}V NMR of neat $VOCl_3$ (the standard ^{51}V NMR 0.0 ppm reference) at 25 °C by tuning, locking, and shimming on authentic *cis*-$V_2W_4O_{19}^{4-}$ in 50% D_2O (all of our NMR chemical shifts were determined using D_2O as an internal lock—no significant changes were observed in controls using 10, 50, or 99.9% D_2O), then replacing that

sample with the neat $VOCl_3$ sample and then collecting the ^{51}V NMR spectrum of $VOCl_3$ unlocked and without additional shimming, Figure S8. (Further details are provided in the Experimental section of the main text.) The observed ^{51}V NMR chemical shift for $VOCl_3$ obtained in this manner was +1.4 ppm, that is, positive of the nominally expected 0.0 ppm value for this standard ^{51}V NMR reference compound. This result suggests that, again as one estimate, errors on the order of *ca.* ±1.4 ppm in ^{51}V NMR chemical shifts can probably easily be present, depending on the exact method of referencing (i.e. external via substitution, in a sealed capillary, or deuterium locked). Hence, the −510 ± 0.5 ppm resonance reproducibly observed herein has a chemical shift closer to −510 −1.4 = −511.4 ppm vs $VOCl_3$, by the external substitution method. However, to avoid confusion and maintain internal consistency, we will continue to denote the observed resonance as at −510±0.5 ppm, because in our work this is the *observed resonance* for any given sample, locked on and hence referenced to D_2O, to a 2-sigma, ±0.5 ppm precision.

Unfortunately, the exact method of ^{51}V NMR referencing in the original report was not given,[2] although a similar error of ±1–2 ppm is not unreasonable. Additionally, we observe a ~23 ppm shift for ^{31}P NMR for **$Co_4P_2W_{18}$** compared to the literature value (*vide infra*).

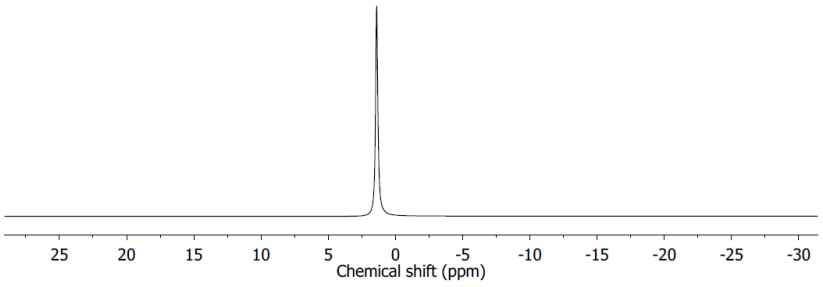

Figure S2.8. ^{51}V NMR of neat $VOCl_3$ at 25 °C demonstrating that the NMR reference is not 0.0 ppm but rather +1.4 ppm—suggesting that the error due to referencing, especially when comparing ^{51}V NMR between different labs, is likely on the order of ≥1–2 ppm.

For the sake of completeness, we also searched the literature for more evidence on the factors that are known to influence the precise chemical shift and line width of *cis*-$V_2W_4O_{19}^{4-}$: they include solvent, pH, counter ions, and temperature.[9,10] As a demonstration of this, the observed resonance for the TBA salt of both "**$Co_4V_2W_{18}$**" and *cis*-$V_2W_4O_{19}^{4-}$ in d^3-acetonitrile was obtained and found, interestingly, to shift to the −507 ppm value provided in the 2014 paper, although the line width is now *ca.* 2-fold narrower, $\Delta\nu_{1/2}$= 12 ±1 Hz, Figure S2.9.

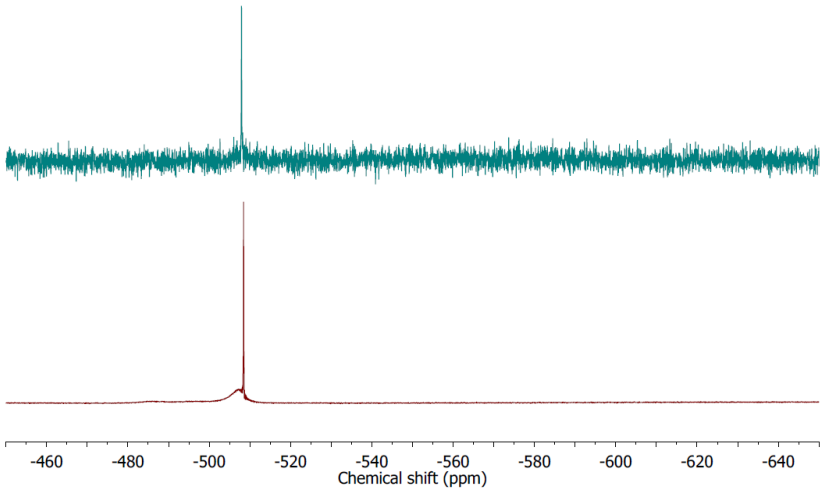

Figure S2.9. ^{51}V NMR of the "**$Co_4V_2W_{18}$**" from 2A (top) as well as *cis*-$V_2W_4O_{19}^{4-}$ (bottom) TBA^+ salts in d_3-acetonitrile. These spectra demonstrate that the predominant resonance for authentic *cis*-$V_2W_4O_{19}^{4-}$, as well as for a sample of "**$Co_4V_2W_{18}$**" prepared by Synthesis #2, is at −507 ppm ($\Delta\nu_{1/2}$ = 12 ±1 Hz). Both samples were conducted at the same mass loading (ca. 5 mg in 1 mL) since the precise composition of the TBA^+ metathesis product is not known.

Overall, then, the available evidence argues that the reported[2] −507(1) and herein observed −510(1.4) ppm resonances *are almost surely one and the same within experimental error*, especially in light of the evidence in the main text that authentic *cis*-$V_2W_4O_{19}^{4-}$ and "**$Co_4V_2W_{18}$**" show this identical, superimposable resonance when examined under identical NMR conditions. Their identical line widths within experimental error ($\Delta\nu_{1/2}$=30.5 in the 2014 report[2] compared to $\Delta\nu_{1/2}$=28±7 herein) provide additional, compelling evidence that the two resonances are one and

the same, especially when considering that if any Co(II) was present in the compound giving rise to the −510 ppm resonance, that signal would have been much more broadened. We conclude, therefore, that the observed main ^{51}V NMR resonance observed in the 2014[2] and the present studies correspond to the same chemical species.

Linewidth discussion for $Zn_4P_2W_{18}O_{68}^{10-}$ and $Co_4P_2W_{18}O_{68}^{10-}$

The polyoxometalates $Zn_4P_2W_{18}O_{68}^{10-}$ and $Co_4P_2W_{18}O_{68}^{10-}$ were synthesized according to literature procedures.[11,12] The more soluble Li^+ salt of $Zn_4P_2W_{18}O_{68}^{10-}$ was obtained by boiling the K^+ salt with $LiClO_4$ and gravity filtering the solution with a Whatman #5 paper to remove the $KClO_4$. ^{31}P NMR was then collected on the *ca.* 5 mM solution of the Li^+ salt of $Zn_4P_2W_{18}O_{68}^{10-}$ in 10% D_2O on a 500 MHz Varian NMR with a sweep width from −49.6 to 199.6 ppm (40322.6 Hz), 256 scans, 1 s relaxation delay, 45° pulse angle, and 0.813 s acquisition time. The ^{31}P NMR resonance of $Zn_4P_2W_{18}O_{68}^{10-}$ is observed at −4.8 ppm (referenced to H_3PO_4 using D_2O as an internal lock) with a narrow peak width of $\Delta\nu_{1/2} = 2.6$ Hz. The chemical shift is within 0.5 ppm of the literature value, though we could not find any literature information as to the peak width.[11] The ^{31}P NMR spectrum of $Co_4P_2W_{18}O_{68}^{10-}$ was collected on a 5 mM solution of the Na^+ salt in 10% D_2O at room temperature on a 500 MHz Varian NMR with a sweep width from 1767.7 ppm to 1900.2 ppm (27000 Hz), 256 scans, 1 s relaxation delay, 45° pulse angle, and 0.813 s acquisition time. The observed resonance is greatly shifted to 1832 ppm (referenced to H_3PO_4 using D_2O as an internal lock), with the expected much greater peak width of $\Delta\nu_{1/2} = 337$ Hz. The chemical shift observed is reasonably close to the reported literature value of 1855 ppm and the $\Delta\nu_{1/2} = 400$ Hz and since were are measuring the NMR of paramagnetic species. The line widths were determined as discussed in the Experimental section of the main text.

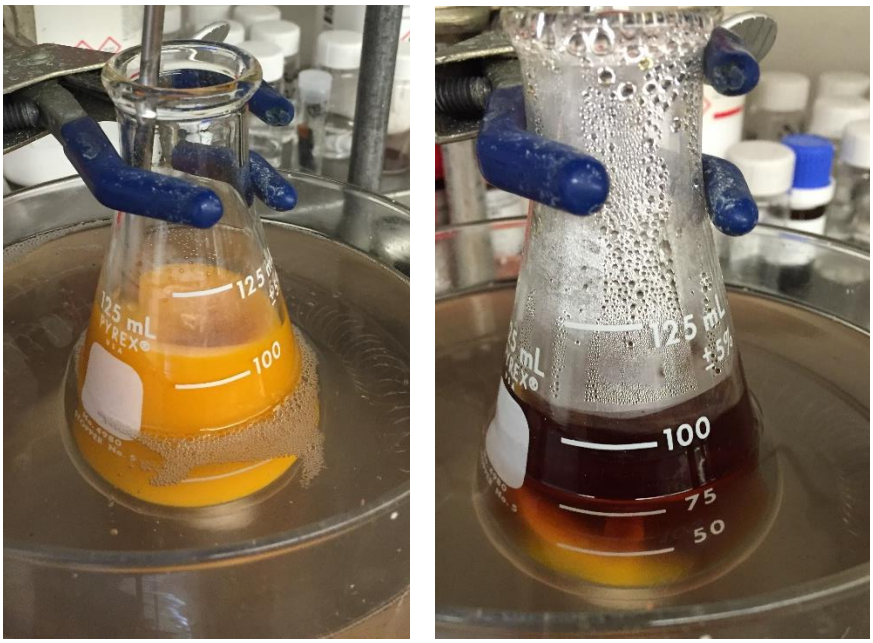

Figure S2.10. Photographs of reaction solution following the Original[1] synthesis procedure: V_2O_5 solution prior to addition of cobalt or tungstate (left) and after heating for 40 minutes at 70˚C for 40 minutes in the presence of cobalt and tungsten (right).

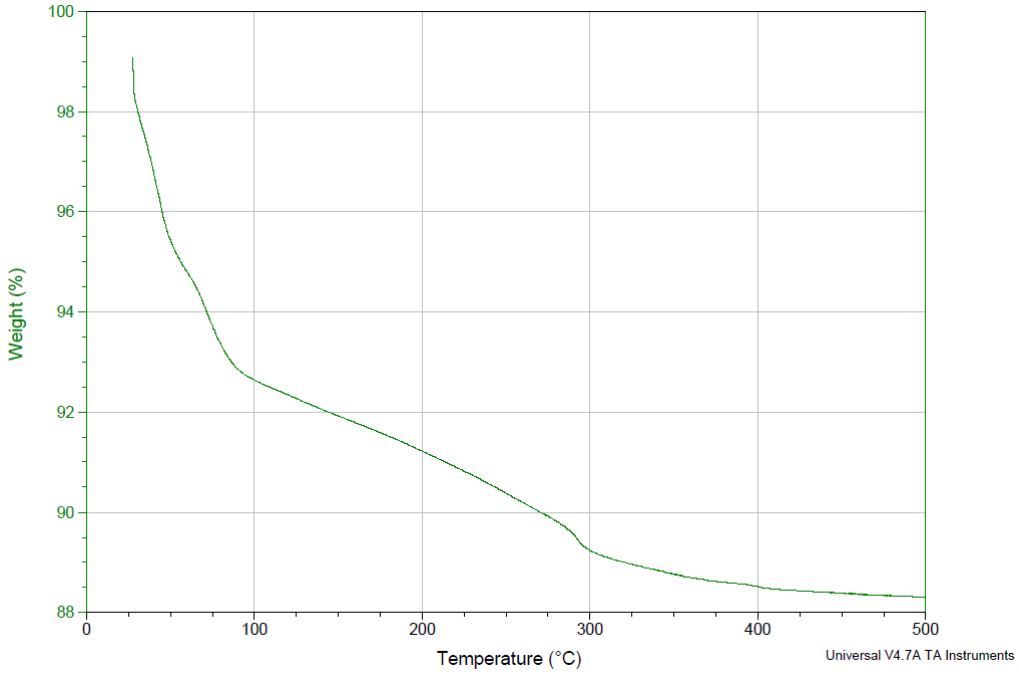

Figure S2.11. TGA of "**$Co_4V_2W_{18}$**" obtained following the original[1] synthesis procedure. The TGA demonstrates a 11.69% weight loss at 500 ˚C corresponding to the loss of ~37 H_2O if one assumes the "**$Co_4V_2W_{18}$**" is pure and has an empirical formula of "$Na_{10}[Co_4(H_2O)_2(VW_9O_{34})_2]\bullet 37H_2O$".

Figure S2.12. Photographs of reaction solution following the procedure used in the 2014 synthesis[2] prior to heating (left) and after heating at 80 °C for two hours (right).

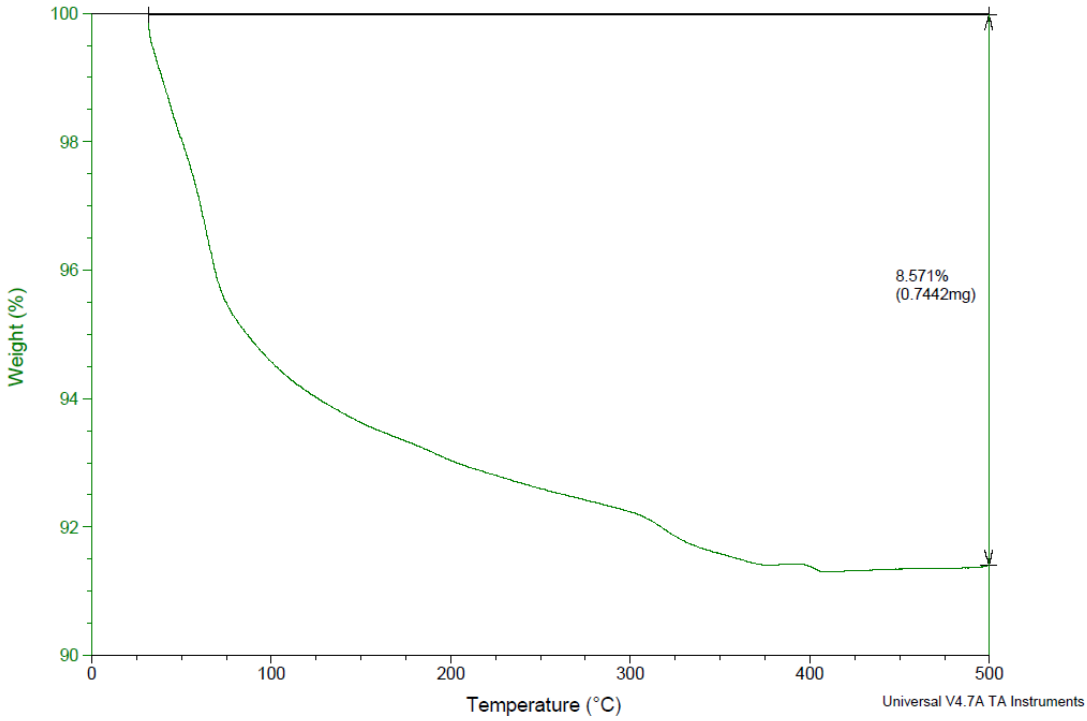

Figure S2.13. TGA of "**$Co_4V_2W_{18}$**" collected following the procedure used in the 2014 synthesis.[2] The TGA demonstrates a 8.571% weight loss corresponding to 26 equivalents of water assuming a pure compound of empirical formula "$Na_{10}[Co_4(H_2O)_2(VW_9O_{34})_2]\bullet 26H_2O$".

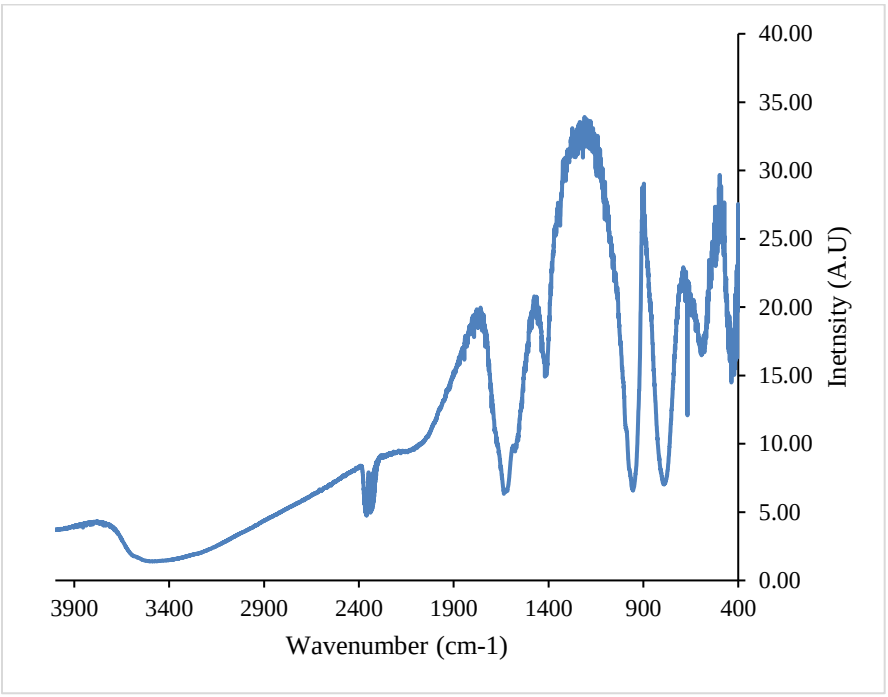

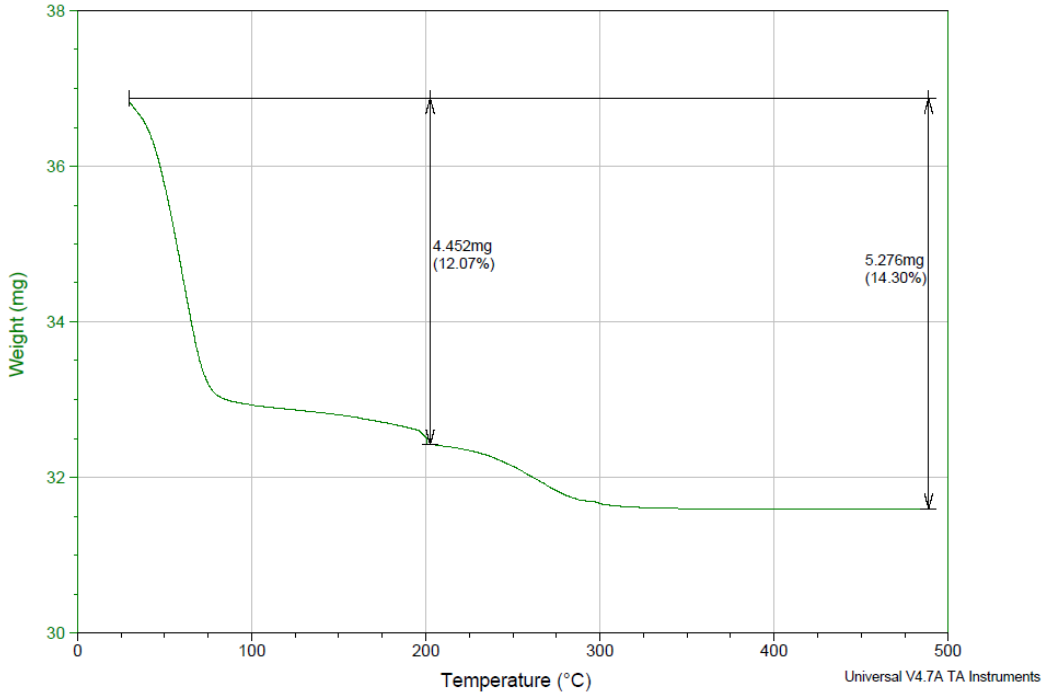

Figure S2.14. FT-IR and TGA of authentic *cis*-$V_2W_4O_{19}^{4-}$ synthesized according to Pope and Flynn.[13] The 12.07 and 14.30% weight change correspond respectively to 9.4 and 11.4 equivalents of water calculated for $Na_4[V_2W_4O_{19}]\cdot XH_2O$.

REFERENCES

1 Li, B.; Yan, Y.; Li, F.; Xu, L.; Bi, L.; Wu, L. *Inorg. Chim. Acta,* **2009**, 362, 2796.

2 Lv, H.; Song, J.; Geletii, Y. V.; Vickers, J. W.; Sumliner, J. M.; Musaev, D. G.; Kögerler, P.; Zhuk, P. F.; Bacsa, J.; Zhu, G.; Hill, C. L. *J. Am. Chem. Soc.* **2014**, *136* (26), 9268.

3 Yergey, J.; Heller, D.; Hansen, G.; Cotter, R. J.; Fenselau, C. *Anal. Chem.* **1983**, *55* (2), 353.

4 Holclajtner-Antunović, I.; Bajuk-Bogdanović, D.; Popa, A.; Uskoković-Marković, S. *Inorg. Chim. Acta* **2012**, *383*, 26.

5 Uehara, K.; Kasai, K.; Mizuno, N. *Inorg. Chem.* **2007**, *46* (7), 2563.

6 Darensbourg, M. *Inorganic Syntheses*; John Wiley & Sons, **1998**; Vol. 32, 247.

7 Finke, R. G.; Droege, M. W.; Cook, J. C.; Suslick, K. S. *J. Am. Chem. Soc.* **1984**, *106* (19), 5750.

8 Suslick, K. S.; Cook, J. C.; Rapko, B.; Droege, M. W.; Finke, R. G. *Inorg. Chem.* **1986**, *25* (2), 241.

9 Andersson, I.; Hastings, J. J.; Howarth, O. W.; Pettersson, L. *J. Chem. Soc., Dalton Trans*. **1996**, No. 13, 2705.

10 Leparulo-Loftus, M. A.; Pope, M. T. *Inorg. Chem.* **1987**, *26* (13), 2112.

11 Finke, R. G.; Droege, M. W.; Domaille, P. J. *Inorganic Chemistry* **1987**, *26* (23), 3886.

12 Yin, Q.; Tan, J. M.; Besson, C.; Geletii, Y. V.; Musaev, D. G.; Kuznetsov, A. E.; Luo, Z.; Hardcastle, K. I.; Hill, C. L. *Science* **2010**, *328* (5976), 342.

13 Flynn, C. M.; Pope, M. T. *Inorg. Chem.* **1971**, *10* (11), 2524.

Table S3.1. Comparison of characterization data for the **$Co_4V_2W_{18}$** used herein, following the original[1] and 2014[2] syntheses for **$Co_4V_2W_{18}$**. Reproduced from reference 3 with permission. Hence, the citations below to the "main text" or the "Experimental section" *refer to reference 3*.

sample number	evaporation time[a]	yield[b] (g)	yield[c] (%)	^{51}V NMR[d] δ (ppm), $\Delta\nu_{1/2}$ (Hz), (%)	FT-IR[e] (cm^{-1})	elemental[f] (%)
1A	12 days	0.476	8.3	−510, 41 (97) −525, N.O. (3)	3400(br), 1620(d), 1405(s), 955, 881, 818, 761, 695, 511, 484	**Co: 3.51** **W: 61.6** V: 1.62 Na: 4.88
2A	31 days	0.55	9.9	−510, 23 (88) −559, 69 (12)	3400(br), 1620(d), 1400(d), 951, 879, 810, 752, 694, N.O., 469	**Co: 5.05** **W: 54.0** V: 1.88 Na: 4.89 **C: 0.55**
2B	13 days	2.55	45.9	−510, 19 (90) −559, N.O. (10)	3400(br), 1620(s), 1411(w), 959, 885, 820, 749, 688, N.O., 485	not conducted
2C	11 days	1.04	18.7	−510, 22 (95) −559, 86 (5)	3400(br), 1620(d), 1405(s), 954, 882, 812, 761, 693, 512, 491	Co: 4.95 W: 55.8 V: 1.83 Na: 5.83
"purified"	N/A	1.39	–	−510, 28 (99) −517, N.O. (0.4) −525, 35 (0.6)	3400(br), 1620(d), 1400(d), 932, 880, 833, N.O., 693, N.O., 485	**Co: 1.00** **W: 52.9** V: 1.80 **Na: 9.56**

[a] Product was collected after a significant amount of brown crystals had visibly accumulated in the beaker used for the slow evaporation.

[b] The yield is the mass of the material obtained after drying as described in the Experimental section of the main text.

[c] The percent yield is calculated based on tungsten. Although the number of hydrates is likely variable, the change in percent weight for each elemental component is relatively small for the different hydrates. Hence, the percent yield was determined assuming the empirical formula $Na_{10}[Co_4V_2W_{18}O_{68}]\cdot 26H_2O$.

[d] The ^{51}V NMR resonances observed for the freshly synthesized and then freshly dissolved material (5 mg in 1 mL of unbuffered 10% D_2O at room temperature). The peaks are the instrument readings relative to $VOCl_3$ (calculated from the D_2O lock) in ppm; the peak widths are reported in *italics* in Hz (see the Experimental section for more details); *N.O.* (not observed) is used where the signal-to-noise was too low for accurate determination. The integration is shown in parentheses (the total integration was set to 100).

[e] FT-IR peaks of the material obtained, 2 wt % in KBr. Peak descriptors are provided where appropriate, and are not given when the peaks are not well resolved. N/A is used for peaks that were observed in the 2014 or original syntheses, but not observed herein. vb = very broad, d = doublet, w= weak, and s = strong.

[f] Elemental analysis obtained from Galbraith Laboratories. Differences of greater than 0.4 wt % error are reported in **bold** and the cobalt wt % in the "Purified" sample is in red to highlight the importance of this low cobalt result.

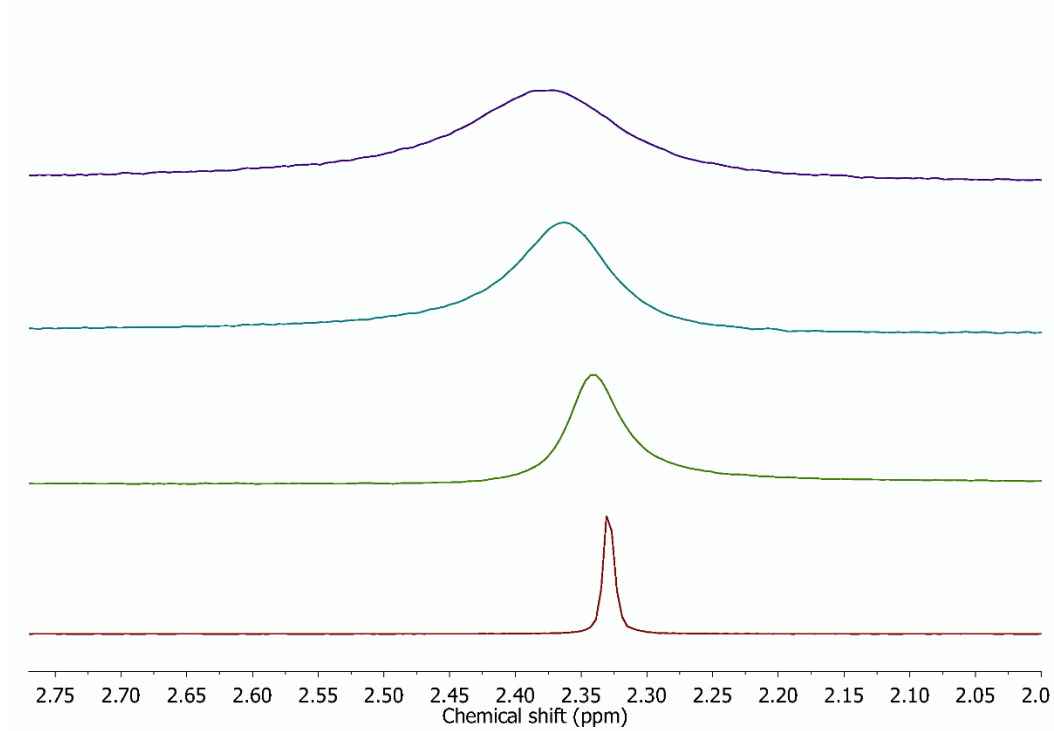

Figure S3.1. Example ^{31}P NMR spectra of pH 8.0 NaPi (0.1 M) buffer with [$Co(NO_3)_2$] ranging from 0, 10, 20 and 30 μM from bottom to top. The ^{31}P NMR resonance broadens linearly with the [Co(II)] and also shifts downfield at higher [Co(II)]. The FWHM of each peak was fit using VnmrJ software and is plotted in Figure S2.

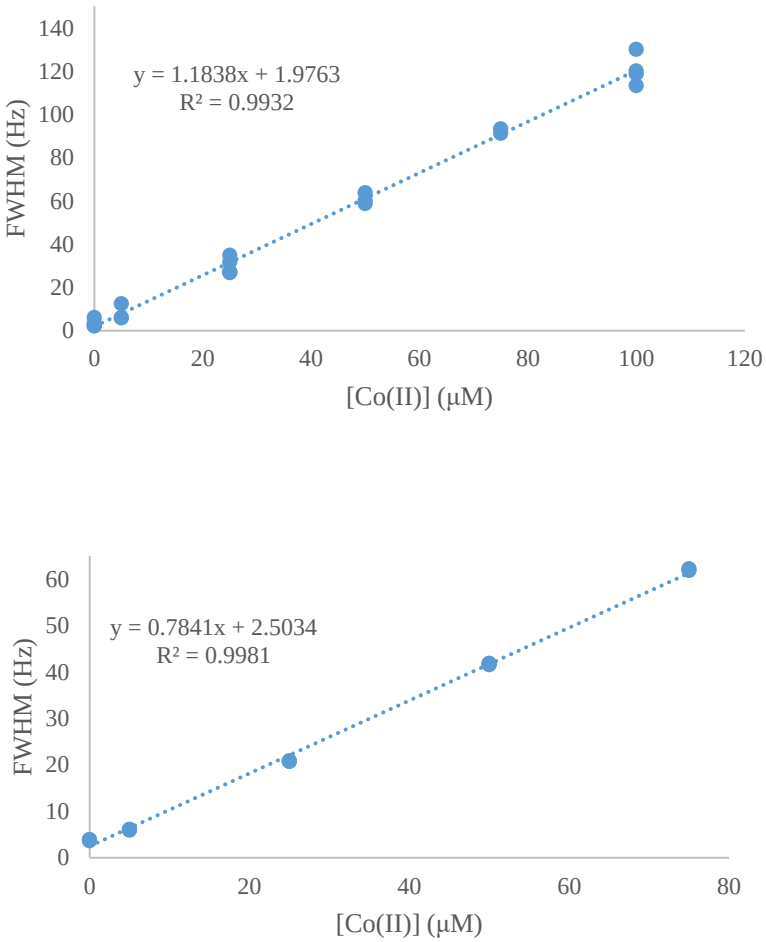

Figure S3.2. ^{31}P NMR line broadening calibration curves for pH 8.0 (top) and 5.8 (bottom). Every point consists of at least 3 data points acquired over twelve hours. The R^2 values for both linear regressions are good, R^2 = 0.993 and 0.998, respectively.

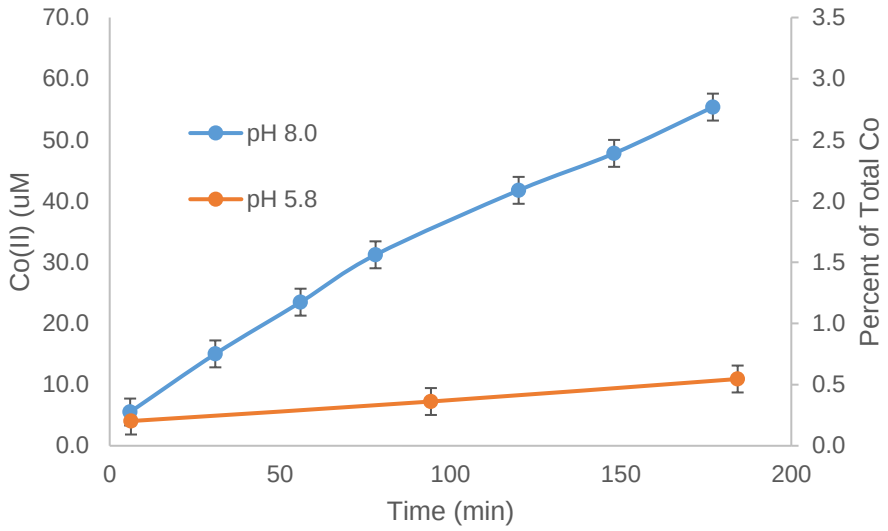

Figure S3.3. [$Co(II)_{aq}$] (left y-axis) and the percent of total $Co(II)_{dissociated}$ (right y-axis) vs. time for $\mathbf{Co_4P_2W_{18}}$ determined using ^{31}P NMR line broadening analysis.

Phenomenological Discussion of $Co(II)_{aq}$ Induced Line Broadening and Implications for Ion Pairing, Exchange Rates of Co(II)/HPO_4^{2-} or PO_4^{3-}, and Rationalization of Why the Intact POMs Do Not Contribute to the Observed Line Broadening.

Notable for the Co(II)-induced line broadening of the ^{31}P NMR resonance of NaPi is the drastic five orders of magnitude difference in concentrations of these species, 5-100 μM and 100 mM for $Co(NO_3)_2$ and NaPi, respectively. Even in the smallest concentration for Co(II), 5 μM, quantitative line broadening of a single ^{31}P NMR resonance is observed. Furthermore, the working Co(II) concentration range of this ^{31}P NMR line-broadening technique is 2-4 orders of magnitude higher concentrations of Co(II) than is soluble thermodynamically at equilibrium. (At pH 8.0 in 0.1 M NaPi, the maximum equilibrium solubility of Co(II) is ~15 nM (calculated using the solubility constant for $Co_3(PO_4)_2$ of 2.05 x 10^{-35} M^5 and the Henderson-Hasselbach equation for the pKa of HPO_4^{2-}/PO_4^{3-} of 12.6.) The precipitation of $Co_3(PO_4)_2$ is obviously kinetically slow, while the chemical exchange of HPO_4^{2-}, and $H_2PO_4^{1-}$ as ligands for Co(II) is faster than the NMR timescale (the ligand exchange rates of Co(II) are on the order of 200-1000 picoseconds,[4] and the ^{31}P NMR relaxation time of PO_4^{3-} ranges from 5-1000 ms).[5] A 500 ms ^{31}P NMR relaxation time ($t_{1/2}$ estimated from the FID) is observed herein for 0.1 M NaPi pH 8.0 in the absence of Co(II). Hence, Co(II) plus HPO_4^{2-} or PO_4^{3-} must exchange at $\geq 10^5$ s^{-1}. This chemical exchange contributes to the observed line width, making the observed ^{31}P NMR line width a convolution of both the Co(II) induced paramagnetic relaxation, and the chemical exchange of Co(II) with HPO_4^{2-} or PO_4^{3-}.

The mechanism of broadening caused by Co(II) helps explain why the intact Co-POM does not contribute to the observed line broadening: it is a large *polyanion* and will not readily interact

(e.g., ion pair) with the phosphate *anion*. Its slower diffusion through solution will also hinder the fast exchange required to broaden the bulk buffer's ^{31}P NMR line.

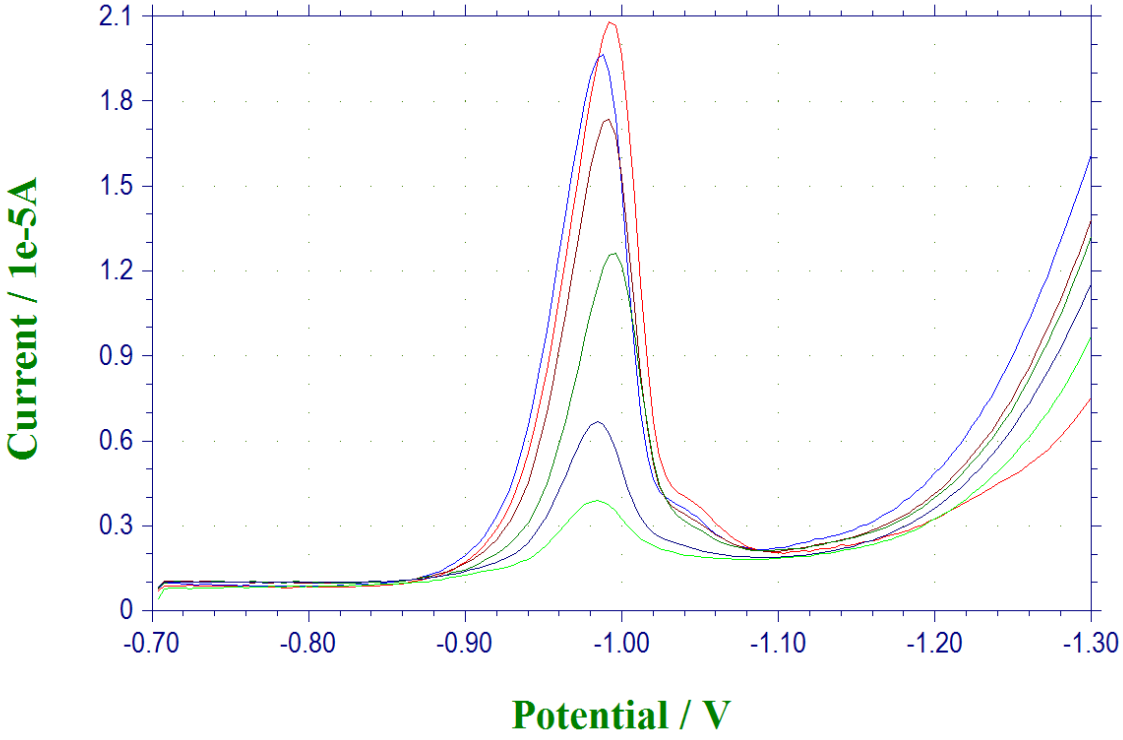

Figure S3.4. Sample differential pulse voltammograms of $Co(II)_{aq}$ showing voltammograms for 2, 5, 10, 15, 20, and 25 μM Co(II) from bottom to top in 0.1 M NaPi pH 8.0.

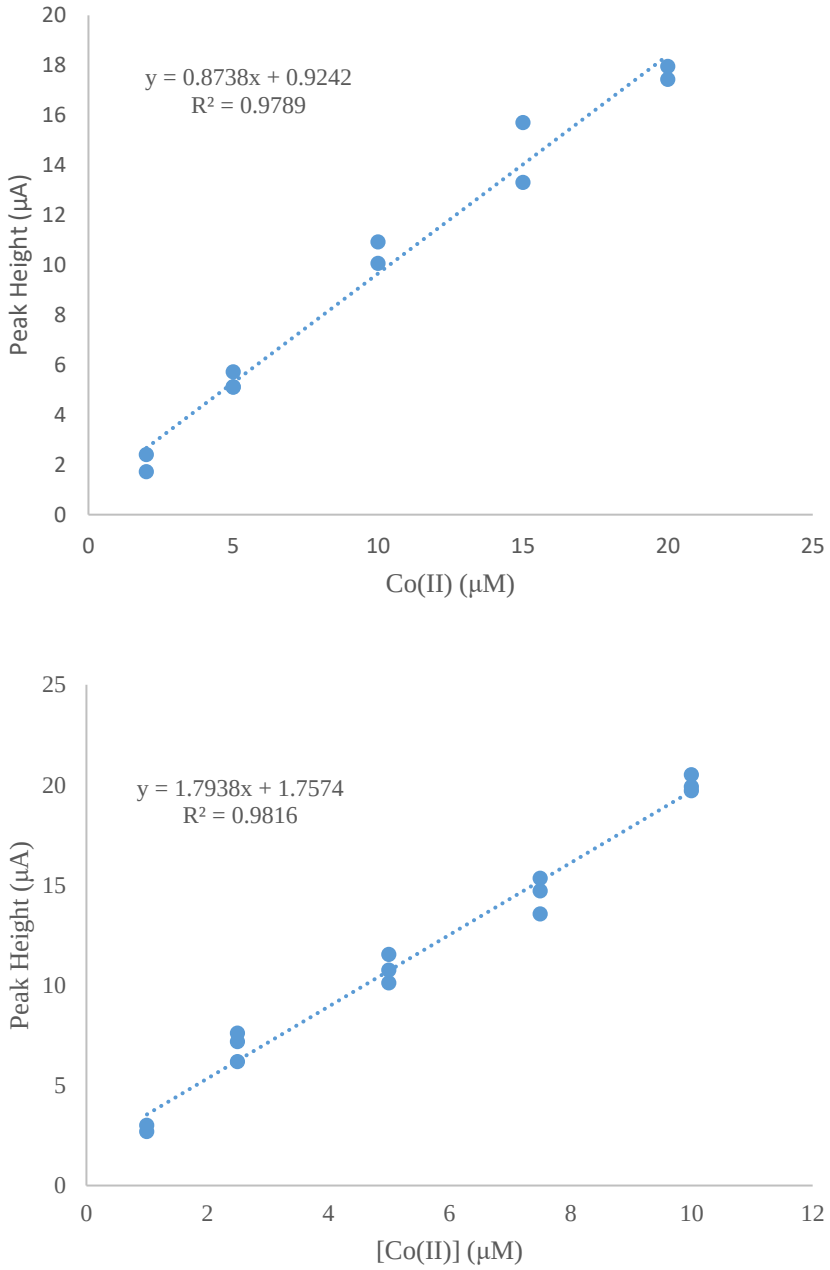

Figure S3.5. Calibration curves for cathodic stripping of $CoDMG_2$ complex 0.1 M NaPi pH 8.0 (Top) and 0.1 M NaB pH 9.0 (bottom).

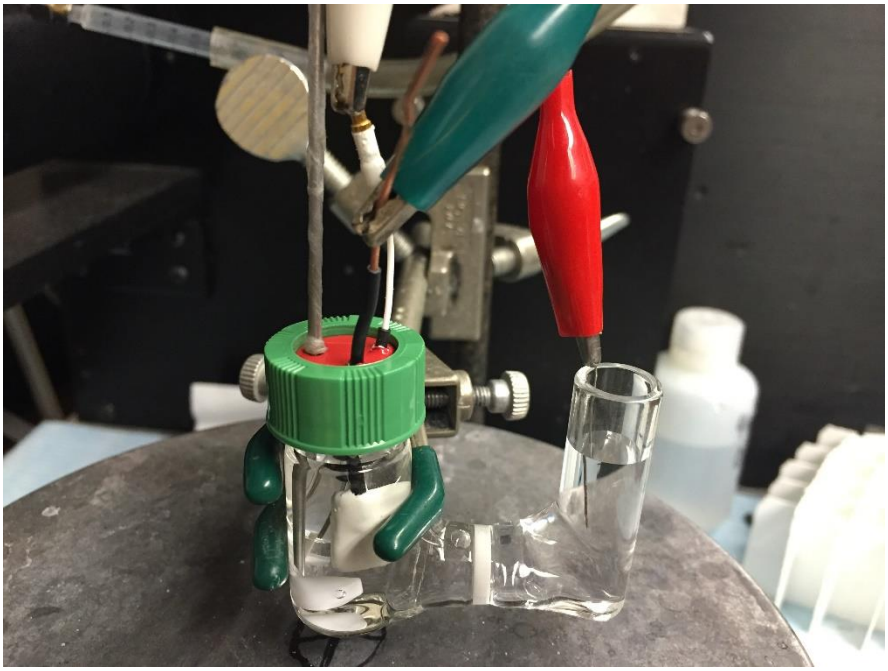

Figure S3.6. Photograph of the custom built U-cell employed for O_2 quantification experiments.

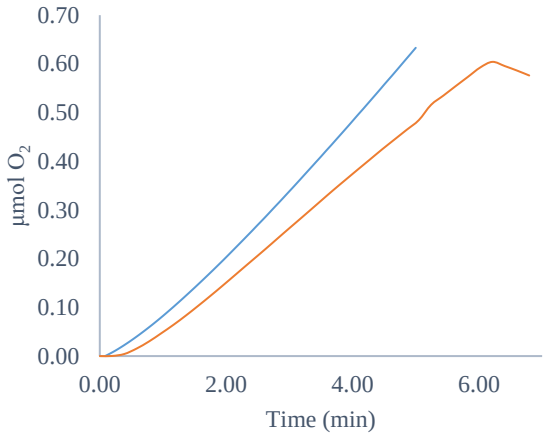

Figure S3.7. Representative O_2 evolution profile beginning with 5 µM **$Co_4V_2W_{18}$** precatalyst in 0.1 M NaPi pH 8. The blue trace represents the expected O_2 production calculated by integrating the current and converting the charge to equivalents of O_2. The orange line represents the O_2 measured by the Ocean Optics FOXY-R O_2 detection probe. The slight induction period in the measured O_2, could be due to film accumulation, bubble formation, or lag time of the O_2 sensor, but has no significant influence on the interpretation of the results. The measured [O_2] also begins to decline after 6 min due to O_2 equilibration with the headspace or O_2 loss from the cell. The Faradaic efficiency is, however, still 100 ± 5 %.

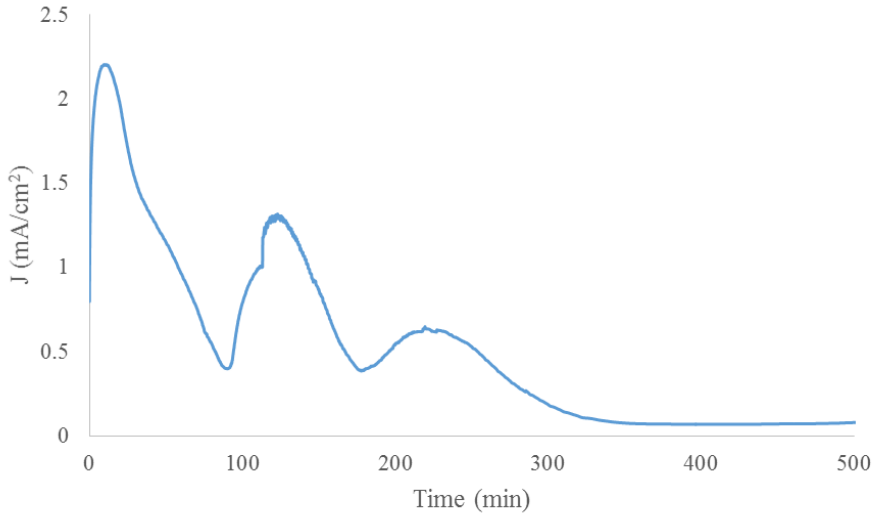

Figure S3.8. Prolonged WOC beginning with 5 μM $\mathbf{Co_4V_2W_{18}}$ in pH 8.0 0.1 M NaPi on the 0.071 cm^2 glassy carbon electrode. A similar J vs t trace is reproducibly observed in controls using a different glassy carbon electrode and also when using $Co(NO_3)_2$ in place of $\mathbf{Co_4V_2W_{18}}$. Hence, the above trace is apparently either not an artifact, or a reproducible one. The above phenomenon of spikes and valleys is *not* observed in a control using a gold electrode and, hence, the above pattern appears to be specific to glassy carbon electrodes with CoO_x. The detailed shape of the above J vs t trace—which would seem to suggest catalyst deactivation followed by formation of new catalyst, then its deactivation, apparently at "new" sites within the glassy carbon—has not been investigated and, hence, remains ill-understood. The decreasing J parts of the above J vs t trace may involve poor CoO_x film adhesion to the glassy carbon as just one possible deactivation mechanism.

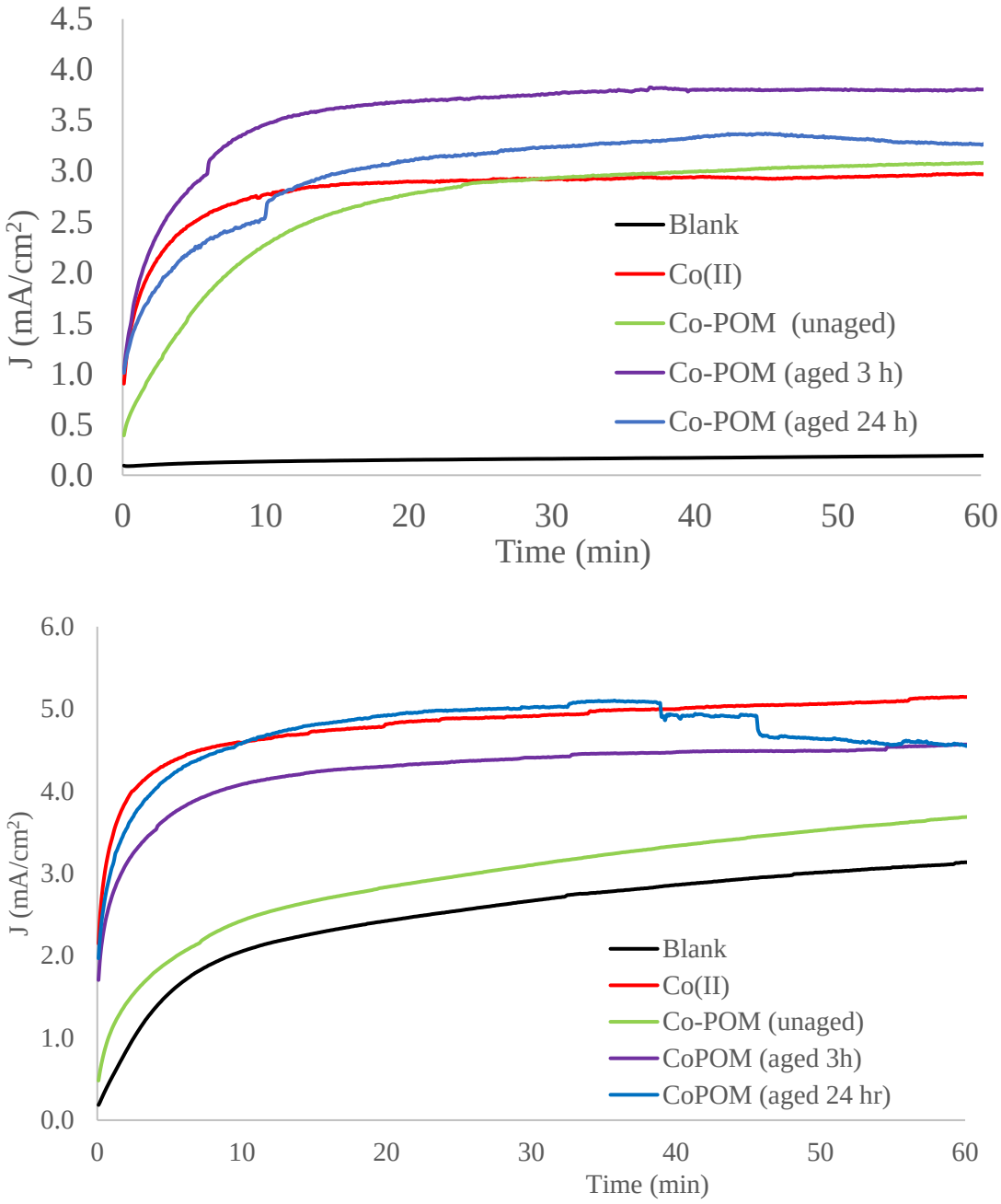

Figure S3.9. Prolonged electrolysis of 23 μM $Co(NO_3)_2$ and 5 μM **$Co_4V_2W_{18}$** both unaged (less than 5 min) and aged in 0.1 M NaPi pH =8.0 (top) and NaB pH 9.0 (bottom). The large background current for pH 9.0 0.1 M NaB has been observed previously[6] and is likely due to impurities in the borate electrolyte.

Discussion of the Prolonged Electrolysis Experiments.

As noted in the main text, when beginning with **$Co_4V_2W_{18}$** there are small (≤30%) differences in the activity of the films, as well as discernable differences in the J vs t profiles, vs those seen for just $Co(II)_{aq}$ and NaPi—although the effects are small and arguably approaching negligible within experimental error. For example, when beginning with **$Co_4V_2W_{18}$** the WOC activity is either somewhat lower, as is the case in pH 5.8 NaPi shown in Figure 4 of the main text, or somewhat (ca. ~30%) higher activity, as is the case in pH 8.0 NaPi, Figure S3.8—although, again, the effect is relatively small, and may not be beyond experimental error. However, *if* real, then this small effect may be due to other species being present (such as *cis*- $V_2W_4O_{19}^{4-}$, or other POM fragments derived from **$Co_4V_2W_{18}$** hydrolysis) in comparison to films formed from just Co(II) and NaPi. In addition, Table 2 of the main text documents a ca. 37% higher activity for $Co(NO_3)_2$ when *cis*-$V_2W_4O_{19}^{4-}$ is deliberately added to a WOC experiment at pH 5.8, although the activity for this mixture is the same within experimental error of the otherwise same experiment performed without *cis*-$V_2W_4O_{19}^{4-}$ at pH 8.0. The precise reason(s) for the relatively small difference in activity is not 100% clear, again assuming the effect is real / beyond experimental error. *If* real, then possible explanations include: the speciation of the cations present; the precise composition and properties of the films deposited when starting with **$Co_4V_2W_{18}$** as opposed to just Co(II); or other, presently unknown causes. Worth noting here are the results in the main text demonstrating that the films deposited from solutions of **$Co_4V_2W_{18}$** do *not* show discernable different compositional or morphological properties from the films derived from just $Co(NO_3)_2$.

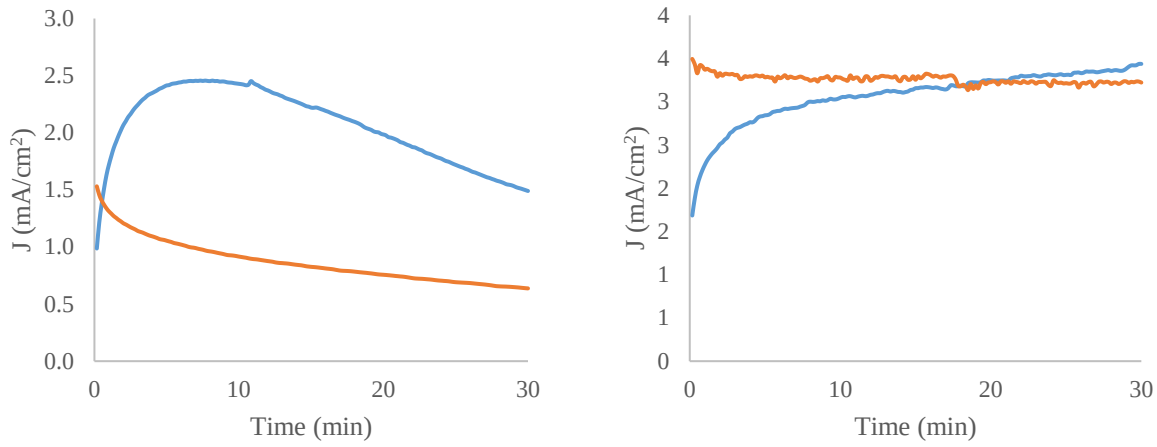

Figure S3.10. Electrolysis of a 5 μM solution of $\mathbf{Co_4V_2W_{18}}$ (blue curve) in 0.1 M, pH 8.0 NaPi (left), and 0.1 M, pH 9.0 NaB (right) at 1.1 V for 30 minutes. The electrodes were then rinsed, placed into a buffer-only solution, and electrolysis was restarted (orange curve).

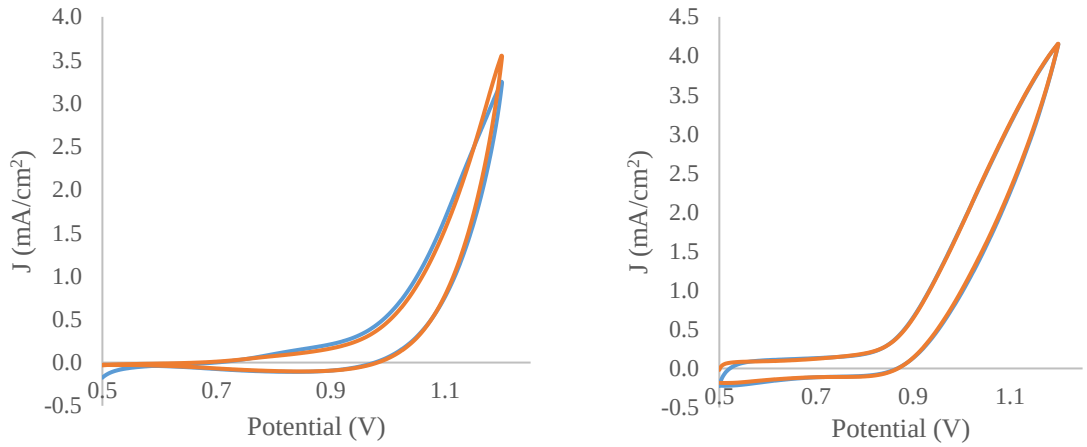

Figure S3.11. CVs of the films after the 30 min bulk electrolysis in Figure S10 in 5 μM solutions of $\mathbf{Co_4V_2W_{18}}$ (blue curves) in 0.1 M, pH 8.0 NaPi (left), and 0.1 M, pH 9.0 NaB (right) and in the buffer-only solutions (orange curves). The resultant CVs are nearly indistinguishable, indicating that the electrode-bound film carries all of the observed electrocatalytic current.

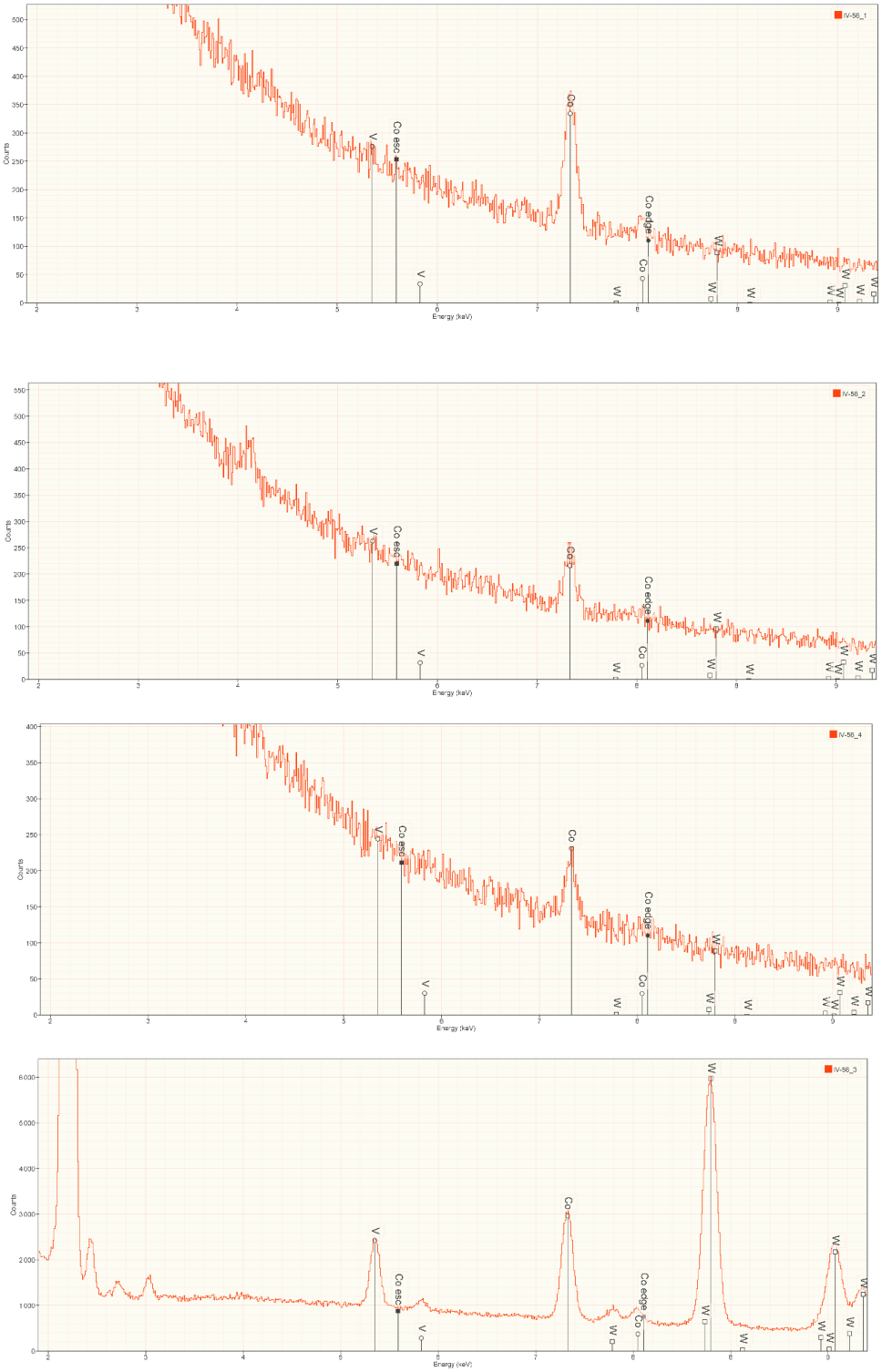

Figure S3.12. EDX spectra collected on the SEM samples in Figure 7 of the main text at 15.0 keV NaPi pH 8.0, 5.8, NaB pH 9 and drop cast solution bottom (top to bottom respectively). The EDX spectra demonstrate that the electrodeposited film *does not contain any detectable vanadium or tungsten,* thereby ruling out Co-POM or any other POM fragment as part of the heterogeneous (CoO_x) WOCatalyst film deposited on the electrode.

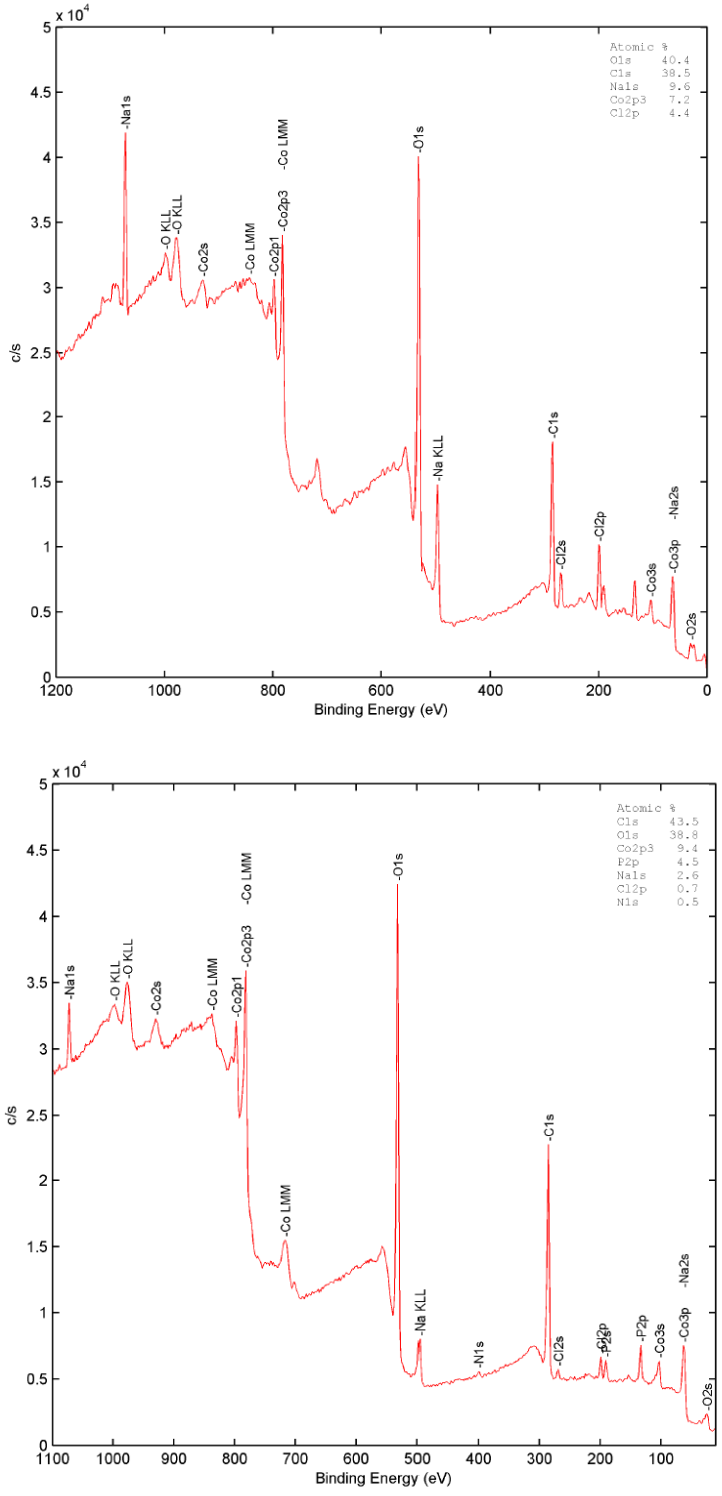

Figure S3.13. XPS spectra of CoO_x film formed from the electrolysis of 5 μM **$Co_4V_2W_{18}$** in 0.1 M NaPi pH 8 (top) and pH 5.8 (bottom) demonstrating the presence of Co, P, and Na with a slight contamination with Cl. Notably, the surface of the film *does not contain any detectable vanadium or tungsten,* demonstrating once again that the film does not contain **$Co_4V_2W_{18}$** or any other POM fragment.

Discussion of the similarities and differences of the present vs the 2014 study.[1]

Although the conditions for this and the previous study[1] are not exactly the same, and although the chemical vs electrochemical oxidants are a major difference known to influence the nature of the true catalyst,[7] the [**$Co_4V_2W_{18}$**], [buffer], buffer identity and pH are all within a small range or the same, Table S3.2. This in turn implies that the (in)stability of **$Co_4V_2W_{18}$** should be quite similar in both studies (Table S3.2).[2] It is inescapable that the prior study's claim that **$Co_4V_2W_{18}$** is hydrolytically stable is questionable because the present study shows that it decomposes between 87(±18) to 102(±12)%, that is, 100% within experimental error, after 3 h of aging in 0.1M NaPi (pH 5.8 or 8.0) or NaB (pH 9.0).

The reason for the drastic difference in conclusions about the stability of **$Co_4V_2W_{18}$** can be understood if one examines the methodology used previously. The previous studies probed the stability of **$Co_4V_2W_{18}$** using ^{51}V NMR, UV-Vis, FT-IR and mass spectrometry.[2] We have recently published a paper detailing the pitfalls of those studies,**Error! Bookmark not defined.** with the most important points being (i) the observed ^{51}V NMR resonance of −506.8 was incorrectly assigned to **$Co_4V_2W_{18}$** and should actually be assigned to a *cis*-$V_2W_4O_{19}^{4-}$ impurity; (ii) the observed UV-Vis spectrum is a convolution of several species; (iii) the prior FT-IR is also convolution of several species (and is relatively insensitive to the precise POM structure because of this); and (iv) the prior mass spectrometry studies are non-definitive and furthermore were conducted on the TBA^+ salt in acetonitrile—conditions that have little to no bearing on *the aqueous chemistry speciation* of **$Co_4V_2W_{18}$**.

In summary the techniques employed in the 2014 study[2] are not direct, compelling, or quantitative evidence of the stability of **$Co_4V_2W_{18}$** under the prior study's conditions.

Table S3.2. Comparison of the conditions under which **$Co_4V_2W_{18}$** stability has been determined. The previous work[2] employed multiple conditions, so the range of those values is reported in the table. Note that the conditions of the prior[1] and the present studies are closely similar, albeit not exactly identical, in most respects. That said, the difference in the chemical oxidant used in the prior study[1], vs the electrochemical oxidation used in the current study, is a major difference known to influence the identity of the true catalyst,[7] and hence is shown in bold below to highlight that difference.

	This Work	***Previous Work***
Buffer	NaPi, NaB	NaPi, NaB
[Buffer] (mM)	100	80-120
pH	5.8-9.0	6.2-9.0
[$Co_4V_2W_{18}$] (μM)	5.0	2.0
Co(II) leached(%)	87-100 (within 3 hours)	None "…high hydrolytic stability."
Oxidant	**Electrochemical: 1.1 V vs. Ag/AgCl using glassy carbon**	**Photochemical: 1.0 mM $[Ru(bpy)_3]Cl_2$ and 5.0 mM $Na_2S_2O_8$ 455 nm irradiation**

Discussion of previous literature[2] attempts to disprove CoO_x when studying $Co_4V_2W_{18}$ for WOC.

Attempts to disprove the presence of CoO_x in previous studies utilized dynamic light scattering (DLS) and *tetra-n*-heptylammonium nitrate-toluene extraction, which extracts anionic species into toluene via ion paring with the alkyl ammonium.[2] However, definitive claims of a single homogeneous catalyst cannot be made because of several issues associated with both of these CoO_x control experiments: (i) DLS detection limits for size or concentration of the detected species were not determined, an important issue since smaller particles are known to be more active WOCatalysts.[8] (ii) The acquired DLS spectrum reports that the count rate is too low for accurate measurement, which is not compelling disproof of nanoparticles.[2] Furthermore, (iii) the precipitation of $Ru(bpy)_3^{3+}$ with anionic POM WOCatalysts is known (such as **$Co_4P_2W_{18}$**, with a

K_{sp} of *ca.* 8 x 10^{-25} M^5)[7] and a $\{\mathbf{Co_4V_2W_{18}}\}_x\{Ru(bpy)_3^{2+}\}_y$ precipitate from both the pre and post reaction solution is reported and characterized in the Supporting Information of the 2014 study.[2] The presence of this precipitate greatly complicates any straight-forward analysis of discussion of the true WOCatalyst, as discussed elsewhere in greater detail.[7] Additionally, (iv) the *tetra-n*-heptylammonium nitrate-toluene extraction technique should not be selective towards only the intact $\mathbf{Co_4V_2W_{18}}$, but theoretically to any anion. It is conceivable that CoO_x nanoparticles formed in solution from $Co(II)_{aq}$ could be stabilized[9] by the anionic decomposition side products (i.e., POMs or anionic fragments), so that those *anionic colloids* would, therefore and for example, also be extracted into the toluene.

For the kinetic studies in the 2014 paper,[2] controls with 8 μM $Co(II)_{aq}$ and authentic CoO_x were performed and do appear to have lower O_2 production activity than solutions with 2 μM $\mathbf{Co_4V_2W_{18}}$ (Figure S19, Table S4 of that study).[2] However, no error bars are reported and one might guess that once error bars are added, the kinetic traces and O_2 yields *might well be the same within experimental error*, a possibility that is also not ruled out by the prior study (nor assessed in the current study).

In short, we have demonstrated that $\mathbf{Co_4V_2W_{18}}$ is both impure as synthesized[3] and highly unstable in 0.1 M NaPi (pH 5.8 or 8.0) or NaB (pH 9.0). Therefore, even though the previous studies used $Ru(bpy)_3^{3+}$ as a chemical oxidant vs the electrochemical oxidation employed herein, and even though such precise conditions are known to sometimes matter greatly in determining the true POM-derived WOCatalyst,[7] one must conclude that the identity of the true WOCatalyst when beginning with $\mathbf{Co_4V_2W_{18}}$ under both chemical and photochemical oxidation[2] is unclear at present and merits careful, further detailed re-examination.

REFERENCES

1 Li, B.; Yan, Y.; Li, F.; Xu, L.; Bi, L.; Wu, L. *Inorg. Chim. Acta* **2009**, *362*, 2796-2801.

2 Lv, H.; Song, J.; Geletii, Y. V.; Vickers, J. W.; Sumliner, J. M.; Musaev, D. G.; Kögerler, P.; Zhuk, P. F.; Bacsa, J.; Zhu, G.; Hill, C. L. *J. Am. Chem. Soc.* **2014**, *136*, 9268-9271.

3 Folkman, S. J.; Kirner, J. T.; Finke, R. G. *Inorg. Chem.* **2016**, *55*, 5343-5355.

4 Ma, H.; Wan, C.; Zewail, A. H. *PNAS* **2008**, *105* (35), 12754.

5 S. Dufour, E. Thiaudière, G. Vidal, J. L. Gallis, N. Rousse and P. Canioni, *J Magn Reson B*, 1996, **113**, 125–135.

6 Smith, A. M.; Trotochaud, L.; Burke, M. S.; Boettcher, S. W. *Chem. Commun.* **2015**, *51*, 5261-5263.

7 (a) Stracke, J. J.; Finke, R. G. *ACS Catal.* **2013**, *3*, 1209-1219. (b) Stracke, J. J.; Finke, R. G. *ACS Catal.* **2014**, *4*, 79-89. (c) Stracke, J. J.; Finke, R. G. *ACS Catal.* **2014**, *4*, 909-933.

8 Blakemore, J. D.; Gray, H. B.; Winkler, J. R.; Müller, A. M. *ACS Catal.* **2013**, *3*, 2497-2500.

9 Wang, Y.; Weinstock, I. A. *Chem. Soc. Rev.* **2012**, *41*, 7479-7496.

APPENDIX III. SUPPORTING INFORMATION FOR CHAPTER IV.

Table S4.1. Compilation of other POMs used in WOCatalysis that are not discussed in the main text.

Polyoxometalate	system	notes	Ref.
$[Mn_4(H_2O)_2(PW_9O_{34})_2]^{10-}$	Mn analog of **$Co_4P_2W_{18}$**. Electrocatalytic oxidation, pH 7 NaPi (50 mM), amorphous carbon disc. WOCatalysis current at potentials >1.0 V vs. Ag/AgCl	Very unstable, decomposes within 30 min. Formation of MnO_x is claimed to not be important because MnO_x is not an effective WOCatalyst.	1
$[Co^{II}(bpy)_3]_6(H_2bpy)$ $[(Co^{II}bpy)_2P$ $Mo_8{}^{VI}Mo_4VO_{40})]_3$ $[(Co^{II}bpy)(PMo_8{}^{VI}$ $Mo_4VO_{40})]\cdot 16H_2O$	Co/Mn-POM-bpy hybrid. $Co(bpy)_3^{2+}$ countercation. Uses photochemical $Ru(bpy)_3^{2+}$ persulfate system. Claim of homogeneous WOC.	Stability not quantified. Very complex speciation and stability issues. WOCatalyst not known.	2
$Na_{12}[\{Co^{II}{}_7As^{III}{}_6O_9(OH)_6\}$ $(A\text{-}\alpha\text{-}SiW_9O_{34})_2]\cdot 8H2O$	Well characterized in solid state. Uses photochemical $Ru(bpy)_3^{2+}$ persulfate system. Claim of homogeneous WOC.	Not well characterized in solution. Co_7 core likely dissociates due to labile Co(II). Stability not known. WOCatalyst not known	3
$[(A\text{-}\alpha\text{-}SiW_9O_{34})_2Co_8$ $(OH)_6(H_2O)_2(CO_3)_3)]^{16-}$	Single xtal gives evidence for solid state structure. Use photochemical $Ru(bpy)_3^{2+}$ persulfate system. Claim of homogenous WOC with 1436 TTOs and 10 s^{-1} TOF.	Carbonate and labile Co(II) hold core together; likely dissociation of $Co(II)_{aq}$ in aqueous solutions. Stability and WOCatalyst not known	4
$K_{10}H_2[Ni_5(OH)_6(OH_2)_3$ $(Si_2W_{18}O_{66})]\bullet 34H_2O$	Single crystal, Ft-IR, TGA of solid. UV-Vis, DLS of soln. Uses photochemical $Ru(bpy)_3^{2+}$ persulfate system. Claim of homogeneous WOC.	Leaching of Ni^{2+} not conducted. Stability not unequivocally known.	5
$K_3[H_3Ag^{I}PW_{11}O_{39}]\bullet 12H_2O$	1D chain as solid. ^{31}P NMR, ESR, UV-Vis, Raman in solution. Oxidized by $S_2O_8^{2-}$, forms Ag(II) and Ag(III). Compares with Ag salts. 1st order wrt Ag-POM.	Strong evidence for molecular catalysis. Leached Ag quantitation needed.	6
$Cs_9[(\gamma\text{-}PW_{10}O_{36})_2$ $Ru_4O_5(OH)(H_2O)_4]$	Single crystal. Acid-base titration, CV in solution. Use photochemical $Ru(bpy)_3^{2+}$ persulfate system.	Leached Ru not detected. Evidence is consistent with homogeneous WOCatalysis, but not definitive.	7
$[Fe_{11}(H_2O)_{14}(OH)_2(W_3O_{10})_2$ $(\alpha\text{-}SbW_9O_{33})_6]^{27-}$	Single crystal, XPS of solid. Uses photochemical $Ru(bpy)_3^{2+}$ persulfate system. Compare with other Fe systems, including Fe_2O_3, and $\alpha\text{-}Fe_2O_3$ nanoparticles.	Good controls, consistent with homogeneous WOCatalysis. Leached Fe should be quantified.	8
$[Cu_5(OH)_4(H_2O)_2(A\text{-}\alpha\text{-}$ $SiW_9O_{33})_2]^{10-}$	Single crystal. Little solution characterization. Use photochemical	Stability of Cu-POM not known. True catalyst not identified.	9

	$Ru(bpy)_3^{2+}$ persulfate system. No comparison to CuO_x.		
$K_7[Co^{III}Co^{II}(H_2O)W_{11}O_{39}]$	DLS, CV, Ft-IR, EDX, and catalyst recycling. Uses photochemical $Ru(bpy)_3^{2+}$ persulfate system. Compares to Co^{2+} and claims to rule out CoO_x.	Amount of leached Co(II) not determined. Data consistent with homogeneous WOCatalysis, but not definitive.	10
$[\{Co(H_2O)_3\}_2\{CoBi_2W_{19}O_{66}(OH)_4\}]^{10-}$ and $([Co_{2.5}(H_2O)_6\{Bi_2W_{19.5}O_{66}(OH)_4\}]^{8-}$	Substitutional disorder of metals in crystal structure. CV, UV-Vis, FT-IR of recovered material. Photochemical $Ru(bpy)_3^{2+}$ persulfate system.	Stability not definitively determined. Substitutional disorder at redox metal site complicates analysis of WOCatalysis results.	11
$[\{Co_4(\mu\text{-}OH)(H_2O)_3\}(Si_2W_{19}O_{70})]^{11-}$	Single crystal. UV-Vis, magnetic susceptibility. Photochemical $Ru(bpy)_3^{2+}$ persulfate system.	Thermally unstable, yields decomposition products capable of WOCatalysis.	12
$[\alpha_1$- and α_2-$P_2W_{17}O_{61}Ru^{III}(H_2O)]^{7-}$	Ru analogs of **α_1- and α_2-CoP_2W_{17}** employed. Ft-IR, CV, UV-Vis, ^{31}P NMR. Cerium(IV) ammonium nitrate as oxidant.	Insufficient evidence for stability of Ru-POM. Dominant catalyst not known.	13
Three different Ni-POMs synthesized.	Single crystal structure. Photochemical $Ru(bpy)_3^{2+}$ persulfate system. UV-Vis, DLS, $THpANO_3$ extraction. <4.7% decomposition. Controls with $Ni(II)_{aq}$ did not produce as much O_2.	Evidence is consistent with homogeneous WOCatalysis.	14
Four Co-POMs synthesized.	Single Crystal. DLS, ^{31}P NMR, UV-Vis, $THpANO_3$ extraction	Leached $Co(II)_{aq}$ not effectively measured. Evidence consistent with homogeneous WOCatalysis, albeit not definitive.	15
Cs salt of $Co_4P_2Mo_xW_y$ analog of $Co_4P_2W_{18}$	Insoluble POM salt in nafion/carbon black. Linear sweep voltammetry, chronoamperometry, O_2 yield.	POM structure and true catalyst not known.	16
$Co_4P_2W_{18}$ embedded in Zr(IV) MOF-545	Elemental analysis, UV-Vis, SEM-EDS used to characterize composite. DFT used to determine POM placement in MOF. Photoexitation of TCPP-MOF and reduction of $S_2O_8^{2-}$.	Insufficient evidence for stoichiometry and/or structure of catalyst. Co(II) leaching not quantified. Products not quantified. The true catalyst is not known—and is quite possibly not "Co-POM@MOF" as claimed, but instead "CoO_x@MOF".	17

Synthesis of $Na_{10}[Co_4(H_2O)_2(PW_9O_{34})_2]\cdot 27H_2O$. The **$Co_4P_2W_{18}$** used herein is the same sample used in our 2011 paper,[18] which was synthesized according to Yin et al. and was

recrystallized twice from water.[18,19] The purity of **$Co_4P_2W_{18}$** was confirmed using FT-IR which matched previous literature, plus elemental analysis for cobalt.[18] The interested reader is directed to earlier publications for more characterization data and details regarding the synthesis.[18,19]

Synthesis of $Na_{16}[Co_9(H_2O)_6(OH)_3(HPO_4)_2(PW_9O_{34})_3]\bullet 43H_2O$. The **$Co_9P_5W_{27}$** material was provided by Professor J.R. Galán-Mascarós, and was synthesized and characterized according to literature.[20,21,22] The purity of **$Co_9P_5W_{27}$** was confirmed using Ft-IR and UV-Vis. For synthesis and characterization details, the reader is directed to earlier publications.[21]

Synthesis of $Na_{16}[\beta,\beta\text{-}[Co_4(H_2O)_2(P_2W_{15}O_{56})_2]\bullet 39H_2O$. **$Co_4P_4W_{30}$** was synthesized according to the literature,[23,24,25,26] adapted to obtain the isomerically pure, symmetric *ββ* complex. In that synthesis the pH is lowered to pH ~3 because it has been demonstrated that a mixture of isomers will convert to the symmetric *ββ* complex at a pH of ca. 3.[24,25] First, the precursors $K_6\alpha$-$[P_2W_{18}O_{62}]$ and $Na_{12}[\alpha\text{-}P_2W_{15}O_{56}]\bullet 18H_2O$ were synthesized according to the literature and their identities were confirmed by FT-IR in comparison to the IR spectra in *Inorganic Syntheses*[23] and elsewhere.[26] The obtained $Na_{12}[\alpha\text{-}P_2W_{15}O_{56}]\bullet 18H_2O$ was then used for the synthesis of $Na_{16}[\beta,\beta\text{-}Co_4(H_2O)_2(P_2W_{15}O_{56})_2]\bullet 39H_2O$. First, $Co(NO_3)_2\bullet 6H_2O$ (1.84 g, 2.5 mmol) and NaCl (2.93 g, 50 mmol) were dissolved in 50 mL of water in a 100 mL beaker with stirring until the solids had fully dissolved. Then $Na_{12}\alpha\text{-}[P_2W_{15}O_{56}]\bullet 18$ (5.00 g, 1.25 mmol) was added all at once with stirring, and the solution was heated to 50 °C during which the solution became brown/green. Concentrated HCl was then added until the solution had a pH of 3 (measured by pH paper). The solution was stirred at 50 °C for an additional 1.5 h before being placed into a refrigerator at 5 °C for 2 days. The green/brown product was collected via suction through a medium glass-fritted filter, rinsed with 10 mL absolute ethanol three times, then with 10 mL diethyl ether 3 times, and then air dried for 4 days. After drying the product was collected in a pre-weighed vial (2.912 g, 57 % yield). The

identity of the product was confirmed using Ft-IR, ^{31}P NMR and compared to the FT-IR and ^{31}P NMR data previously collected for isometrically pure [*β,β*-$Co_4(H_2O)_2(P_2W_{15}O_{56})_2]^{16-}$ (Figures S4.1 and S4.2).[23,24] The number of waters of hydration was determined using TGA. The observed vs the expected (in parentheses) percent by mass of each element for Na_{16}[*ββ*-$Co_4(H_2O)_2(P_2W_{15}O_{56})_2$]•$39H_2O$ (8,772 AMU) are: Co 2.62 (2.69), P 1.33 (1.41), W 59.6 (62.9), and Na 3.63 (4.19) wt. %. The observed values arrange from 0.07 to 3.3 wt. % low. However, the observed empirical formula is $Na_{14.2}Co_{4.0}P_{3.9}W_{29.2}$ in comparison to the expected $Na_{16}Co_{4.0}P_{4.0}W_{30}$, consistent with the "**$Co_4P_4W_{30}$**" structure also confirmed by IR and ^{31}P NMR (*vide supra*). The systematic low elemental analysis could be explained if one considers the possibility that Na_{16}[*ββ*-$Co_4(H_2O)_2(P_2W_{15}O_{56})_2$]•$39H_2O$ may have absorbed water at the Galbraith facility, because of the much higher relative humidity in Knoxville, TN (the location of Galbraith) than Fort Collins, CO (the location of Colorado State University). The expected elemental analysis for the hypothetical higher hydrate Na_{16}[*ββ*-$Co_4(H_2O)_2(P_2W_{15}O_{56})_2$]•**60**$H_2O$ (9,151 AMU) (i.e., absorption of 20 equiv. of water) is: Co 2.58, P 1.35, W 60.3, and Na 4.27 wt. %, which is much closer to the values obtained from Galbraith. In short, because the FT-IR and ^{31}P NMR characterization of Na_{16}[*ββ*-$Co_4(H_2O)_2(P_2W_{15}O_{56})_2$]•$39H_2O$ are consistent with prior literature,[23,24,26] and because the analysis confirms the basic structure of the **$Co_4P_4W_{30}$** core of this Co-POM, the material was used without further purification.

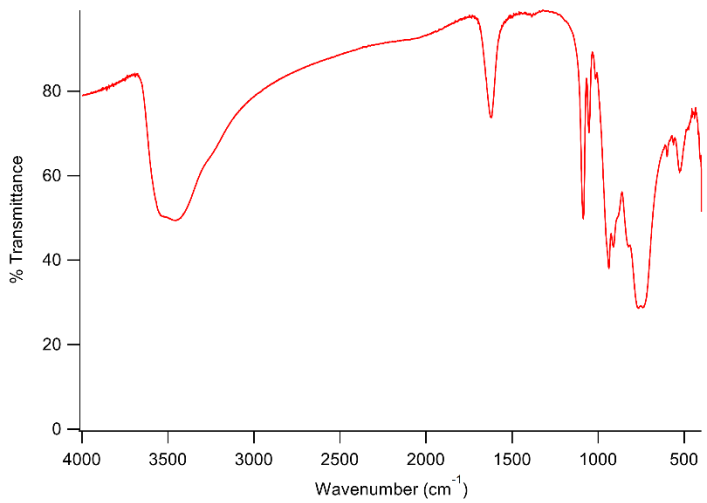

Figure S4.1. FT-IR of $Na_{16}[\beta,\beta\text{-}Co_4(H_2O)_2(P_2W_{15}O_{56})_2]\bullet 39H_2O$ in a KBr pellet. The peaks observed in the fingerprint region from 600-1300 cm^{-1} are consistent with prior literature.[23,26]

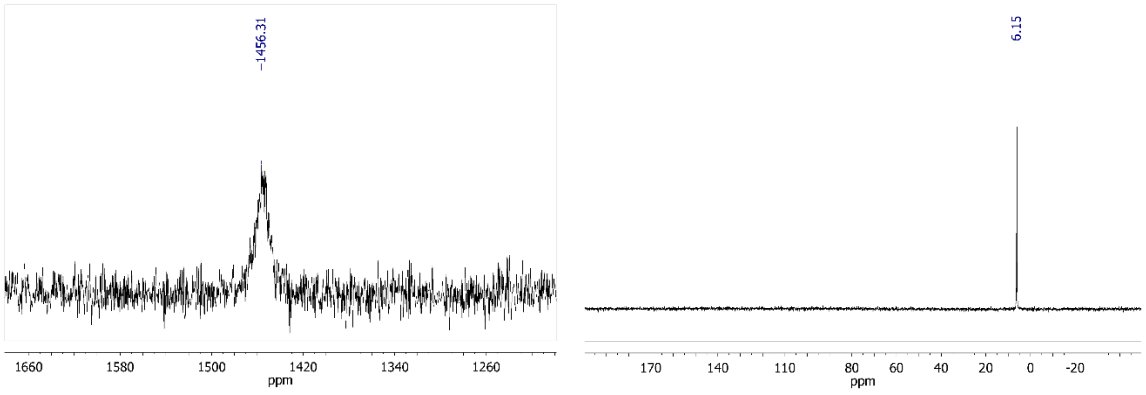

Figure S4.2. ^{31}P NMR peaks of $Na_{16}[\beta,\beta\text{-}Co_4(H_2O)_2(P_2W_{15}O_{56})_2]\bullet 39H_2O$ in 25% D_2O. The ^{31}P resonance for the P atoms nearest the paramagnetic cobalt centers is shown on the left and has an appreciable downfield shift and peak broadening. The ^{31}P NMR peak for the P atoms further from the four Co(II) atoms is shown on the right. Both of these ^{31}P NMR peaks are consistent with prior literature for $Na_{16}[\beta,\beta\text{-}Co_4(H_2O)_2(P_2W_{15}O_{56})_2]$.[23,24,25] The lack of other detectable peaks is consistent with the isometrically pure nature of the sample.

Synthesis of $K_5[Co(H_2O)PW_{11}O_{39}]\bullet 14H_2O$. **$CoPW_{11}$** was synthesized using a procedure adapted from literature methods.[27,28,29] First, $[Na_3PW_{12}O_{34}]\bullet 12H_2O$ was synthesized according to literature.[30] Then $[Na_3PW_{12}O_{34}]\bullet 12H_2O$ (10.2 g, 3.2 mmol) was dissolved in 20 mL of water, $Co(NO_3)_2\bullet 6H_2O$ (0.95 g, 3.2 mmol) was dissolved into 5 mL of water, and the two solutions were mixed and stirred at 90° C for ~30 min. Next, potassium acetate (8 mL, 10 M, pH 7.0) was added

dropwise over 1 minute. The solution was stirred an additional 2 min then filtered through a medium frit glass filter via suction. The solution was cooled to 60° C and 35 mL of methanol was added and the solution was stored at 5° C overnight. The solid, purple product was then collected on a medium a fritted filter via suction with aspiration until dry. The product was then redissolved in a minimum amount of water at 60° C, cooled to room temperature, and then placed stored at 5° C overnight. The purple crystalline product was then collected with a medium fritted filter via suction until the product was dry, and was then collected in a pre-weighed scintillation vial (9.39 g, 92% yield). The waters of hydration were determined by TGA to be 8% by mass corresponding to 14 equivalents of water/Co-POM. The product was characterized via FT-IR, ^{31}P NMR, and elemental analysis to confirm the product identity and purity, consistent with prior literature (Figures S4.3 and S4.4).[27,28,29,31] The observed vs the expected (in parentheses) elemental analysis for $K_5[Co(H_2O)PW_{11}O_{39}]\bullet 14H_2O$ (3,201 AMU) was: Co 1.61 (1.84), P 0.83 (0.97), W 62.0 (63.2), and K 5.70 (6.11) wt. %, which are once again systematically low by 0.14 to 1.16 wt. %. The observed empirical formula is $K_{5.3}Co_1P_{1.0}W_{12.3}$ vs. the expected $K_5Co_1P_1W_{11}$, meaning that the elemental ratios are correct within 12% error. However note that, absorption of just 3 equiv. of water yields the empirical formula $K_5[Co(H_2O)PW_{11}O_{39}]\bullet 17H_2O$ (3,255 AMU) and the calculated elemental analysis becomes: Co 1.81, P 0.95, W 62.1, K 6.0 %, which gives <0.3 absolute error in any wt. %. Thus because the FT-IR and ^{31}P NMR are consistent with prior literature,[29,31] and because the elemental analysis ratios are the same within 12% error, the material was used without further purification.

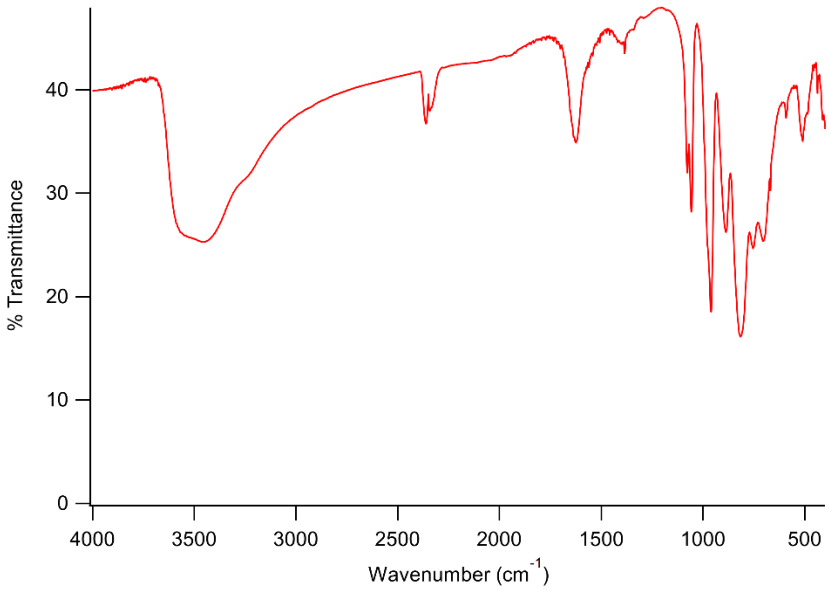

Figure S4.3. FT-IR of $K_5[Co(H_2O)PW_{11}O_{39}]\bullet 14H_2O$ in a KBr pellet. The peaks present in the fingerprint region are consistent with prior FT-IR literature.[31]

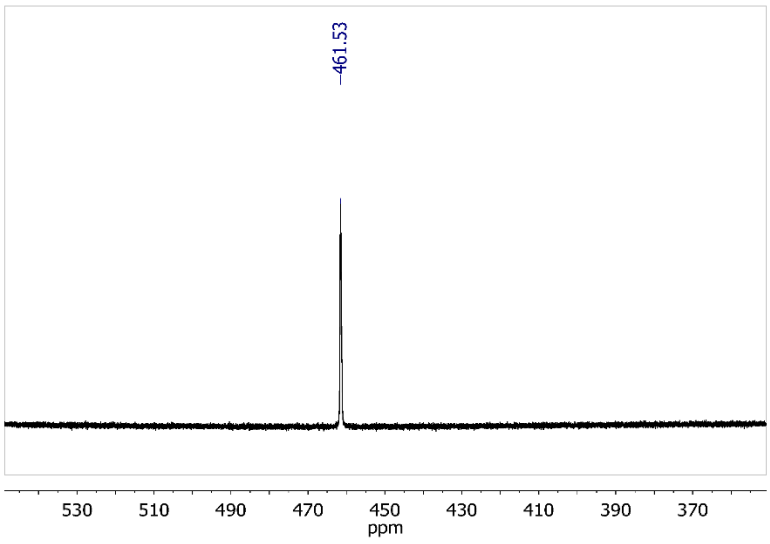

Figure S4.4. ^{31}P NMR of $K_5[Co(H_2O)PW_{11}O_{39}]\bullet 14H_2O$ in 25% D_2O. The presence of a single resonance at *ca.* −460 ppm is consistent with prior ^{31}P NMR literature for $[Co(H_2O)PW_{11}O_{39}]^{11-}$.[29]

Synthesis of $K_8[\alpha_1\text{-}Co(H_2O)P_2W_{17}O_{61}]\bullet 17H_2O$. The synthesis of **$\alpha_1$-$CoP_2W_{17}$** was conducted using the isolated lacunary $K_9[\alpha_1\text{-}LiP_2W_{17}O_{61}]$ isomer from $K_{12}\alpha\text{-}[H_2P_2W_{12}O_{48}]$.[32,33] First, $K_6\alpha\text{-}[P_2W_{18}O_{62}]$ was converted to $K_{12}[\alpha\text{-}H_2P_2W_{12}O_{48}]$ by dissolving $K_6\alpha\text{-}[P_2W_{18}O_{62}]$ (92 g, hydrates unknown; ~17 mmol) into 300 mL of water, mixed with an aqueous tris(hydroxymethyl)aminomethane (200 mL, 2 M) and stirred for 30 min. Next KCl (80 g, 1 mol) was added with stirring. After the KCl had dissolved, aqueous K_2CO_3 (200 mL, 2 M) was added with stirring causing a white ppt to form. The white $K_{12}[\alpha\text{-}H_2P_2W_{12}O_{48}]$ product was collected via a coarse fritted filter and dried overnight via suction from aspiration, then washed two times with 50 mL ethanol and filtered to dryness, 66.93 g collected.

Next, $K_9[\alpha_1\text{-}LiP_2W_{17}O_{61}]$ was prepared from the collected $K_{12}[\alpha\text{-}H_2P_2W_{12}O_{48}]$ (hydrates unknown). First, a 500 mL aqueous solution of LiCl (1 M) and HCl (20 mM) was prepared and $K_{12}[\alpha\text{-}H_2P_2W_{12}O_{48}]$ (40 g, hydrates unknown; ~10 mmol) was added all at once and stirred until clear (~2 min). Next, aqueous Li_2WO_4 (50 mL, 1M) was added with stirring over ~20 s. Immediately after the Li_2WO_4 addition, HCl (110 mL, 1 M) was added dropwise over 2 min. Next KCl (200 mL, saturated solution) was added quickly with stirring and a white ppt formed instantly. The product was collected and dried via suction through a medium fritted filter. The product was then resusupended in ethanol (250 mL, reagent grade) then collected again via a medium fritted filter, and allowed to dry on the filter overnight. The product was collected (32.725 g) and its purity was examined using ^{31}P NMR with peaks found at δ= −9.0 and −13.1 ppm. Peaks at δ= +0.1 and −13.3 ppm consistent with the α_2 isomer was observed (5 % integration).[32] Three repeated syntheses did not give purer material by ^{31}P NMR. This is not unexpected because $[\underline{\alpha_1}\text{-}LiP_2W_{17}O_{61}]^{9-}$ is known to convert to $[\underline{\alpha_2}\text{-}LiP_2W_{17}O_{61}]^{9-}$ in solution.[32,34] As such, the synthesis

was continued because we also made the **α_2-CoP_2W_{17}** isomer and have it available for comparison and WOCatalysis experiments (*vide infra*).

The last step of the synthesis places a Co(II) atom into the lacuna of the $[\alpha_1\text{-}LiP_2W_{17}O_{61}]^{9-}$. $Co(NO_3)_2 \bullet 6H_2O$ (0.68 g, 2.3 mmol) was dissolved in lithium acetate buffer (40 mL, pH 4.7, 1 M) and was heated to 50° C. Next, $K_9[\alpha_1\text{-}LiP_2W_{17}O_{61}]$ (9.97 g, ~2 mmol) was added all at once and was stirred for 15 min. Finally, KCl (5.9 g, 80 mmol) was added and stirred for 15 min. The solution was then cooled to room temperature and the red precipitate was collected and dried via a medium fritted filter. The product was redissolved into a minimum amount of boiling water and allowed to recrystallize at room temperature twice before finally collecting and drying on a medium fritted filter; 7.542 g collected, 75% yield based upon $K_8[\alpha_1\text{-}Co(H_2O)P_2W_{17}O_{61}] \bullet 17H_2O$ (4,859 AMU); the hydrates were determined by TGA. Only the Co elemental analysis was obtained to ensure that excess Co(II) was not present as a counter cation, calculated 1.24%, (1.12% found). The final product was characterized by FT-IR and ^{31}P which were consistent with literature (Figures S4.5 and S4.6).[29,32,33,34]

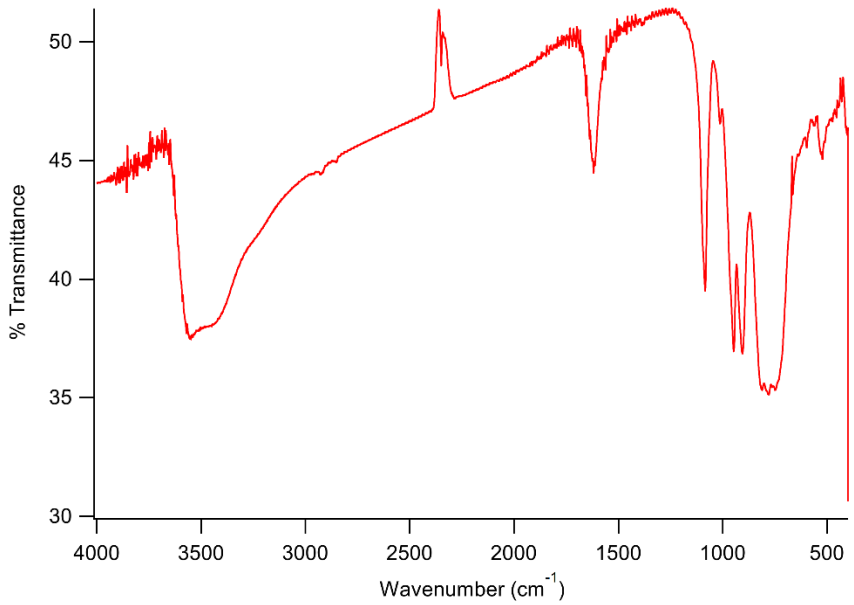

Figure S4.5. FT-IR of $K_8[\alpha_1\text{-}Co(H_2O)P_2W_{17}O_{61}]\bullet 17H_2O$ in a KBr pellet, which is consistent with the FT-IR values in the literature.[32]

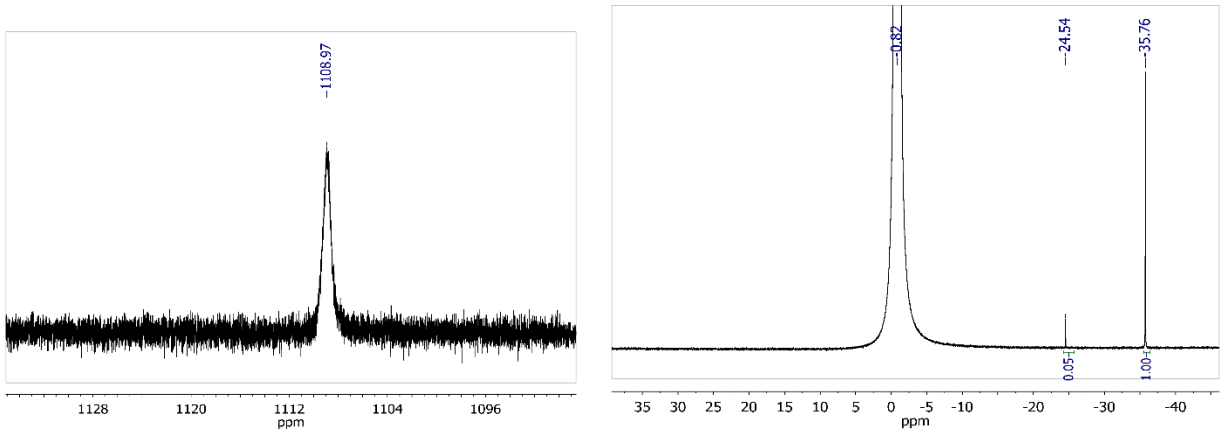

Figure S4.6. ^{31}P NMR of $K_8[\alpha_1\text{-}Co(H_2O)P_2W_{17}O_{61}]\bullet 17H_2O$ in unbuffered 25% D_2O. The P atom closer to the cobalt atom is shown on the left with a ^{31}P NMR resonance at ~1108 ppm.[29] The P atom further from the cobalt atom is shown on the right and contains a concentric H_3PO_4 insert as reference. The peak at −36 ppm is the desired $[\alpha_1\text{-}Co(H_2O)P_2W_{17}O_{61}]^{8-}$, and the peak at −25 ppm is $[\underline{\alpha_2}\text{-}Co(H_2O)P_2W_{17}O_{61}]$ which is present at ~5% based on integration.[29]

Synthesis of $K_8[\alpha_2\text{-}Co(H_2O)P_2W_{17}O_{61}]\bullet 15H_2O$. **$\alpha_2$-$CoP_2W_{17}$** was synthesized from the lacunary $K_{10}[\alpha_2\text{-}P_2W_{17}O_{61}]$ according to the literature from the $K_6\alpha\text{-}[P_2W_{18}O_{62}]$ precursor.[29,32,35]

First, $K_6\alpha\text{-}[P_2W_{18}O_{62}]$ (62.22 g, hydrates unknown) was dissolved into 150 mL of water at 40° C

with stirring, then aqueous $KHCO_3$ (250 mL,1 M) was added to the $K_6\alpha$-$[P_2W_{18}O_{62}]$ solution with stirring and the temperature was maintained at 40° C for 1 h. Next, the reaction flask was placed into an ice bath for 30 min. The white $K_{10}[\alpha_2$-$P_2W_{17}O_{61}]$ product was collected with a medium fritted filter with suction via aspiration for 1 h. The product was then redissolved in 100 mL of boiling water then filtered through celite and left at 5° C overnight. The product was then collected with a medium fritted filter and washed three times with 50 mL water, then three times with 50 mL anhydrous EtOH, and then three times with 50 mL anhydrous diethyl ether, followed by drying under aspiration overnight. The yield of the lacunary $K_{10}[\alpha_2$-$P_2W_{17}O_{61}]$ was 49.8 g. Next, $K_{10}[\alpha_2$-$P_2W_{17}O_{61}]$ (25 g, 5.3 mmol) was dissolved into 100 mL of water at 90° C and $Co(NO_3)_2$•$6H_2O$ (1.686 g, 5.8 mmol) was added with stirring. After 15 min of stirring KCl (15 g, 200 mmol) was added with stirring and the solution was cooled to room temperature then cooled to 5° C overnight. The red $K_8[\alpha_2$-$Co(H_2O)P_2W_{17}O_{61}]$ product was collected with a medium fritted filter to dryness via aspiration. The product was then ground in a mortar and pestle, then redissolved into a minimum amount of boiling water and allowed to cool to room temperature. The red product was then again collected via filtration through a medium fritted filter and dried overnight via aspiration. The red product was ground in a mortar and pestle and then collected and weighed in a scintillation vial. The yield was 19.32 g, 74% yield based on $K_8[\alpha_2$-$Co(H_2O)P_2W_{17}O_{61}]$•$15H_2O$ (4,823 AMU); the equivalents of water was determined using TGA. The identity was confirmed using FT-IR ^{31}P NMR and elemental analysis and were found to be consistent with literature spectra (Figures S4.7 and S4.8).[27,29,32,35] Only the Co elemental analysis was obtained to ensure that excess Co(II) was not present as a counter cation, calculated 1.21%, and 1.11% found.

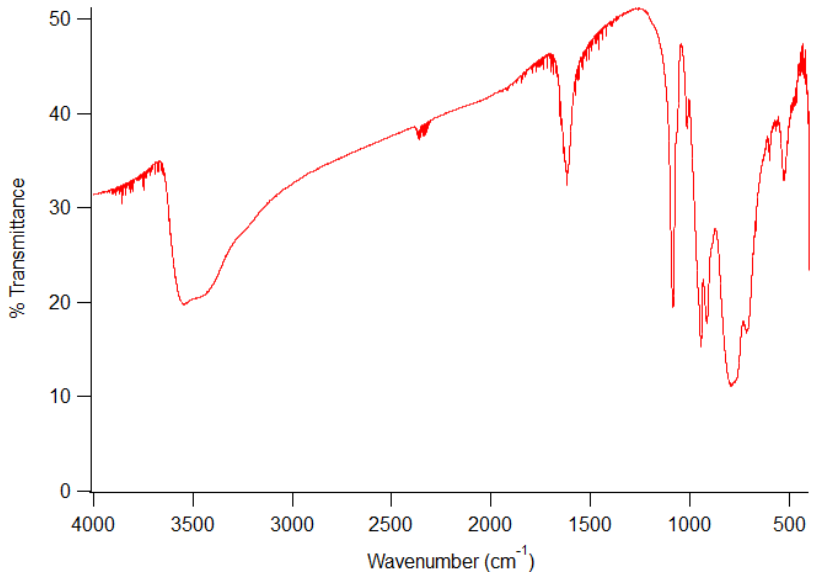

Figure S4.7. FT-IR of $K_8[\alpha_2\text{-}Co(H_2O)P_2W_{17}O_{61}]\bullet 15H_2O$ in KBr.[32]

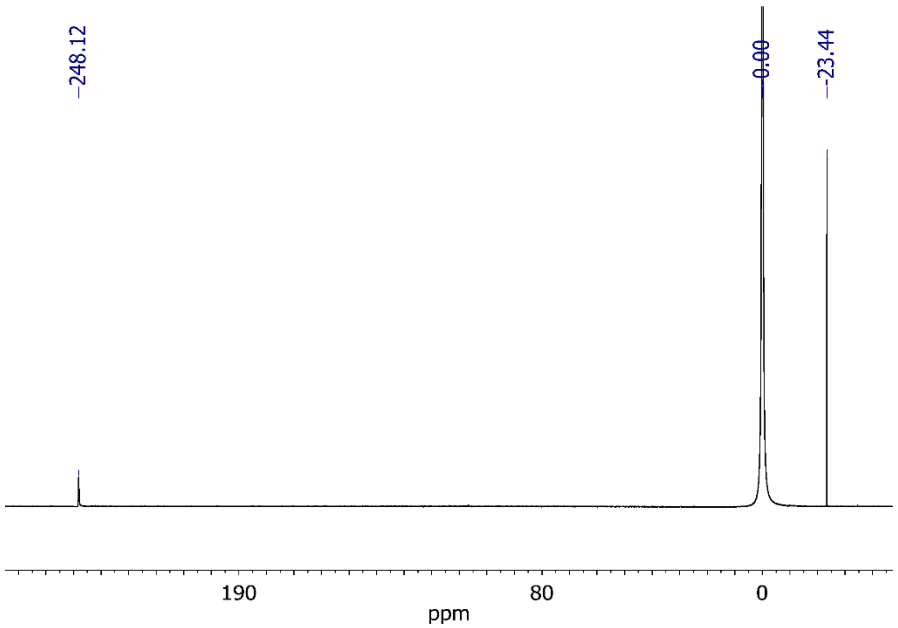

Figure S4.8. ^{31}P NMR of $K_8[\alpha_2\text{-}Co(H_2O)P_2W_{17}O_{61}]\bullet 15H_2O$ in unbuffered 25% D_2O with a concentric H_3PO_4 insert as reference (0.00 ppm). The peak at +248 ppm (FWHM=33 Hz) belongs to the P atom closer to the Co (literature values are +250 ppm, FWHM=25 Hz) , and the peak at −23 ppm (FWHM=3 Hz) belongs to the P atom that is further from the Co (literature values are −23.7, FWHM=5 Hz).[29]

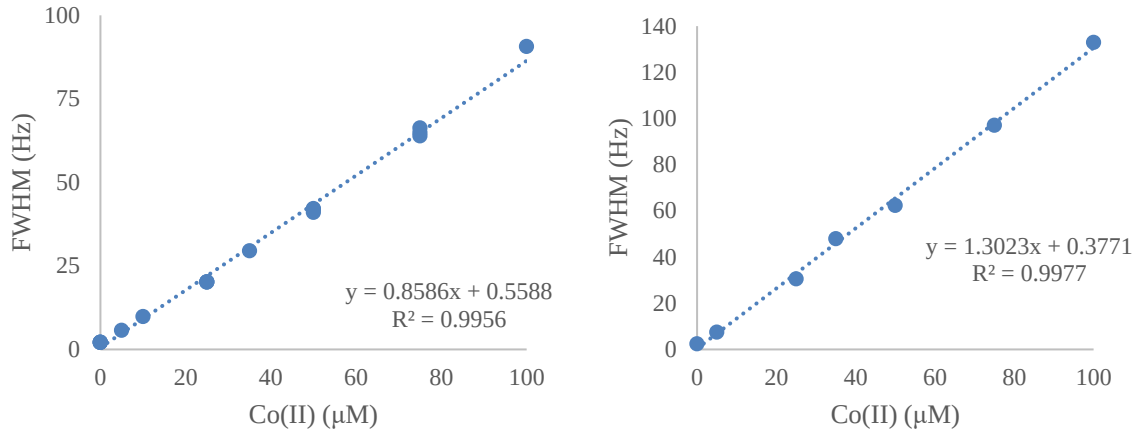

Figure S4.9. Calibration curves for the $Co(II)_{aq}$-induced line broadening of the NaPi ^{31}P NMR peak. The $Co(NO_3)_2$ concentration is plotted against the full-width at half-maximum (FWHM) for 0.1 M NaPi pH = 5.8 (left) and 0.1 M NaPi pH = 8.0 (right).

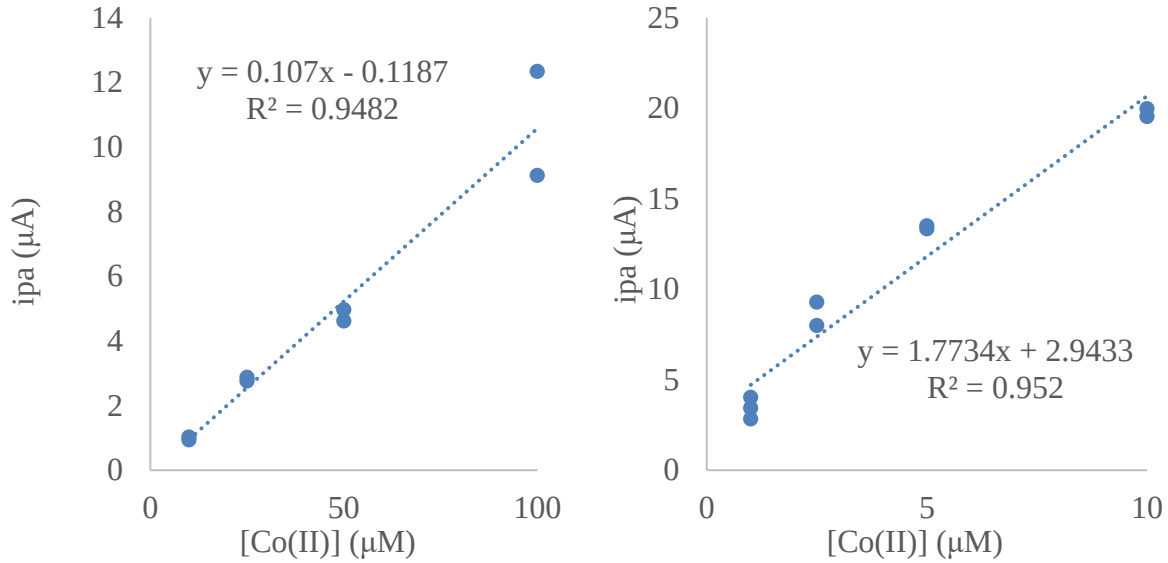

Figure S4.10. Calibration curve for the adsorptive cathodic stripping experiments in 0.1 M NaPi pH=8.0 (left) and 0.1 M NaB pH=9.0 (right). The $Co(NO_3)_2$ concentration (µM) in shown on the x-axis and the peak anodic current (µA) is shown on the y-axis.

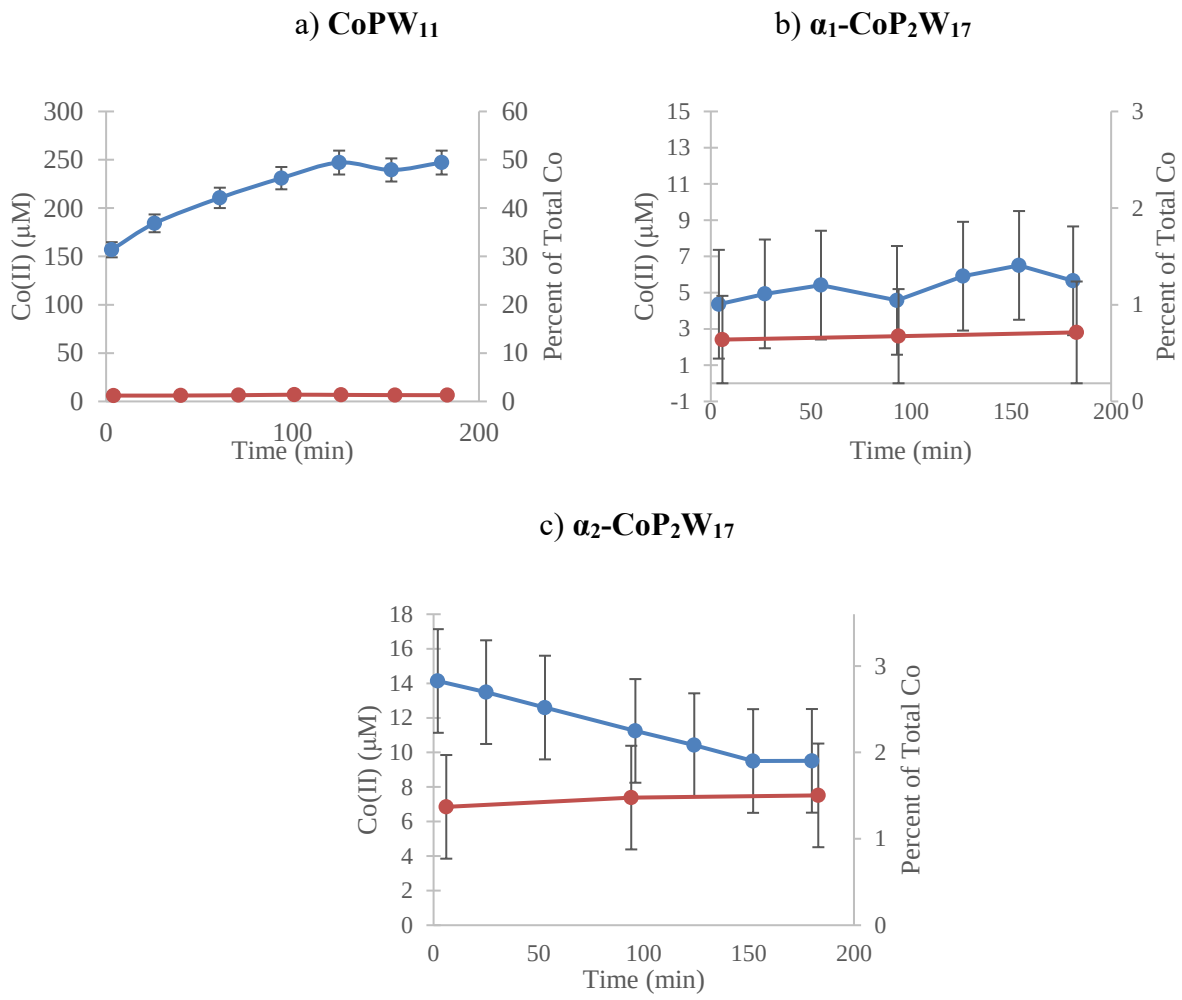

Figure S4.11. The $Co(II)_{aq}$ concentration vs time determined by $Co(II)_{aq}$ induced line broadening in 0.1 M NaPi (pH 5.8, red and pH 8.0, blue) for 500 μM solutions of a) **$CoPW_{11}$**; b) **α_1-CoP_2W_{17}**; and c) **α_2-CoP_2W_{17}**. The value for the $Co(II)_{aq}$ concentration was determined by fitting the observed ^{31}P NMR linewidths of the NaPi to the calibration curve generated with authentic $Co(NO_3)_2$. The percent of total cobalt refers to the percent of cobalt that is detected in solution compared to the total Co(II) bound in the individual Co-POM. Error bars are the standard deviation from three repeat experiments. The lines between points have been added to guide the eye and, hence, are not fit to any specific equation.

The pH 5.8 vs 8.0 ^{31}P Line-Broadening Data for $Co_4P_4W_{30}$: A Discussion of An Apparent Systematic Difference of ~20%, ~16(±~3) μM Apparent $Co(II)_{aq}$

The ~20% lower $Co(II)_{aq}$ measured in pH=5.8 in the absence of EDTA of 62(±1) (vs 78(±2) in pH 8.0), a difference of ~16(±~3) μM, is of interest as it bears on the accuracy and any systematic errors in the ^{31}P phosphate NMR line-broadening method. This ~20% difference has at least three possible explanations. The possibility of *stronger* ion pairing between $Co(II)_{aq}^{2+}$ [*ββ*-$Co_4(H_2O)_2(P_2W_{15}O_{56})_2]^{16-}$ at *lower* pH 5.8 does not make much sense, at least at first glance. Given that the speciation of $Co(II)_{aq}$ does not change significantly in the pH 5.8-8.0 range (existing as $Co(H_2O)_6^{2+}$ and not for example the lesser charged "$Co(H_2O)_5(OH)^{+}$"),[36] argues against a change in speciation of at least $Co(II)_{aq}$ as the reason for the apparently lower $Co(II)_{aq}$ measured in pH=5.8. However, the known coordinated water pK_a values for $[Co_4(H_2O)_2(P_2W_{15}O_{56})_2]^{16-}$ are 3.5(±0.1) and 5.3(±0.1),[37] so that at pH 8.0 it is implied that at least the di-deprotonated, now overall 18 minus $[Co_4(OH)_2(P_2W_{15}O_{56})_2]^{18-}$ is present, and that *should* have stronger ion-pairing to $Co(H_2O)_6^{2+}$, which could explain the systematic ~16(±~3) μM difference between the pH 5.8 and 8.0 $Co(II)_{aq}$ measurements.

A third, possible explanation for the pH-dependent apparent $Co(II)_{aq}$ derives from the pK_a of 7.2 for $H_2PO_4^{1-}$. This second pKa of phosphoric acid means that $H_2PO_4^{1-}$ will be the dominant species at pH 5.8, but that the dianion, HPO_4^{2-}, will dominate at pH 8.0 (the pK_a of HPO_4^{2-} is 12.4). The resultant, expected increased affinity for $Co(II)_{aq}$ by dianionic HPO_4^{2-} (i.e., and at the higher pH 8.0) is therefore also a plausible explanation for why the ^{31}P line broadening method detects ~20%, ~16(±3) μM, more $Co(II)_{aq}$ at the higher pH.

Overall, the conclusion from the pH dependent, apparent $Co(II)_{aq}$ detection results is that the ^{31}P NMR phosphate line-broadening method comparisons are best done at the same pH, or

with controls such as using EDTA as done herein in Figure 4.4 in the main text, to get an idea of the inter-pH systematic error. The bottom line for the work herein is that the pH 5.8 vs pH 8.0 ^{31}P line broadening looks to contain a at most ~20%, ~16(±~3) μM difference in the pH 5.8 vs pH 8.0 data and in the absence of EDTA that that needs to be considered when interpreting any inter-pH, ^{31}P phosphate line-broadening data. That said, the ready work-around is simply to do the added EDTA experiments as done in Figure 4.4 in the main text, experiments that detect a total Co(II) present that is consistent to within a small error, 85(±4) μM.

a) **α_1-CoP_2W_{17}** pH=5.8 NaPi

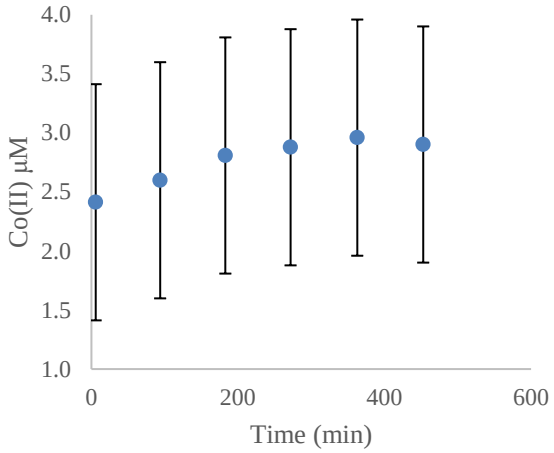

b) **α_2-CoP_2W_{17}** pH=5.8 NaPi

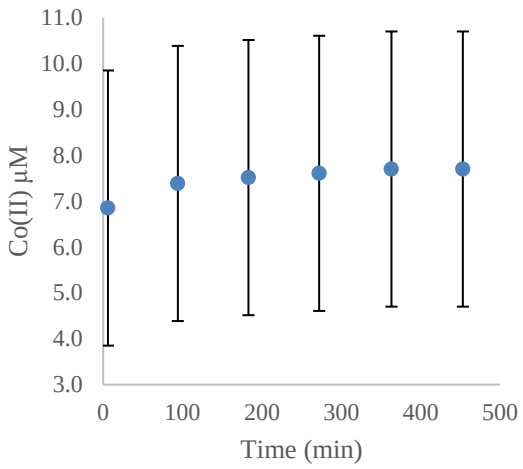

c) **α_1-CoP_2W_{17}** pH=8.0 NaPi

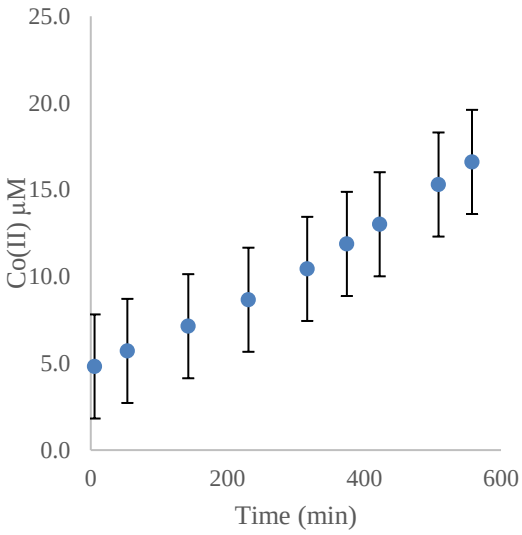

d) **α_2-CoP_2W_{17}** NaPi pH= 8.0 NaPi

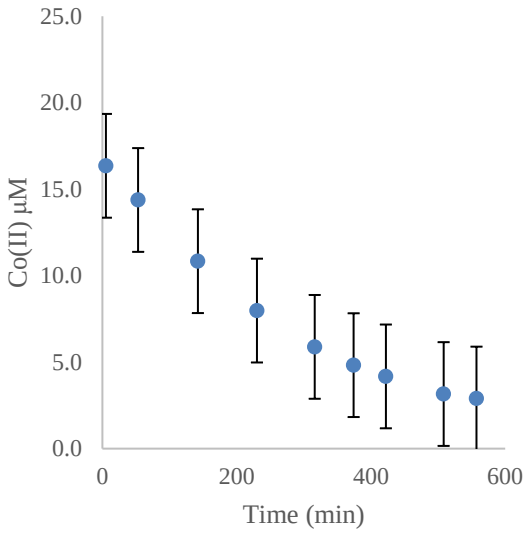

Figure S4.12. ^{31}P NMR line broadening over the longer period of 7-10 hrs of: a) **α_1-CoP_2W_{17}** pH=5.8 NaPi; b) **α_2-CoP_2W_{17}** pH=5.8; c) **α_1-CoP_2W_{17}** pH=8.0; and d) **α_2-CoP_2W_{17}** NaPi pH= 8.0. Note the expanded scale in Figures S4.12a and S4.12b relative to the error bars of repeat measurement.

Discussion of the Decrease in $Co(II)_{aq}$ concentration from α_2-CoP_2W_{17} in 0.1 M NaPi pH= 8.0.

One possible explanation for the decrease in observed $Co(II)_{aq}$ from **α_2-CoP_2W_{17}** in 0.1 M NaPi pH=8.0 (Figures S4.11 and S4.12) is that α_2-$Co(H_2O)P_2W_{17}O_{61}^{8-}$ initially (and quickly) leaches Co(II) and becomes the lacunary α_2-$P_2W_{17}O_{61}^{10-}$ POM which then yields trivacant $P_2W_{15}O_{56}^{12-}$ as is known to form from $[P_2W_{18}O_{62}]^{6-}$ at pH ≥8.[37,38] The $P_2W_{15}O_{56}^{12-}$ could then react with Co(II) to form $Co_4(H_2O)_2(P_2W_{15}O_{56})_2^{16-}$ which would remove 2 equivalents of Co(II) per $P_2W_{15}O_{56}^{12-}$ unit from solution—an overall decrease in the $Co(II)_{aq}$ concentration. The experiments needed to confirm this hypothesis are beyond the scope of this paper, but would likely include ^{31}P NMR on the Co-POMs at a much higher concentration, (i.e., and because the concentration of the $[Co_4(H_2O)_2(P_2W_{15}O_{56})_2]^{16-}$ in these experiments would only be in the 1-4 μM range, approximately 1000 times lower than the concentration needed for ^{31}P NMR for detection of $[Co_4(H_2O)_2(P_2W_{15}O_{56})_2]^{16-}$ and other Co-POMs).

Table S4.2. O_2 yield (μmol) from 5 min electrolysis using a 1 cm^2 glassy carbon electrode in 3 h aged 500 μM Co-POMs in each respective buffer solution. These values were determined by converting the total charge passed in coulombs to μmol of O_2 (i.e., using the conversion of $1O_2/4e^-$).

	Buffer System		
Polyoxometalate	**0.1 M NaPi pH 5.8**	**0.1 M NaPi pH 8.0**	**0.1 M NaB pH 9.0**
$Co_4P_2W_{18}$	0.12 ± 0.11	0.65± 0.17	0.8 ± 0.3
$Co_9P_5W_{27}$	0.4 ± 0.2	0.8 ± 0.1	0.8 ± 0.3
$Co_4P_4W_{30}$	0.3 ± 0.2	0.8 ± 0.4	1.8 ± 0.9
$CoPW_{11}$	0.13 ± 0.11	1.1 ± 0.2	2.3 ± 0.5
α_1-CoP_2W_{17}	0.05 ± 0.03	0.3 ± 0.06	0.9 ± 0.1
α_2-CoP_2W_{17}	0.07 ± 0.06	0.3 ± 0.1	0.4 ± 0.1

Discussion of the WOCatalysis activity of CoO_x derived from $Co(II)_{aq}$ compared with the WOCatalysis activity from the Co-POMs.

It is of considerable interest to compare the relative rates of WOCatalysis derived from CoO_x formed from $Co(II)_{aq}$ to those for the intact Co-POM. While some assumptions and approximations are needed to do so, *initial estimates* can be obtained as follows: the total WOCatalysis activity can be expressed as the i_{total} and since the Faradiac efficiency is ~100%. The i_{total} can, in turn, be written as the sum of the activity from the Co-POM ($i_{Co\text{-}POM}$) and the activity derived from $Co(II)_{aq}$ ($i_{Co(II)}$) in the form of CoO_x:

$$i_{total} = i_{Co(II)} + i_{Co-POM} \quad (1)$$

The initial Co-POM concentration ($[Co\text{-}POM]_i$) can be written in its simplest form as equal to the concentration of intact Co-POM after aging ($[Co\text{-}POM]_t$) plus the concentration of $Co(II)_{aq}$ detected ($[Co(II)]_{aq,t}$) according to equation 2.

$$[Co - POM]_i = [Co - POM]_t + [Co(II)]_{aq,t} \quad (2)$$

The assumptions behind eqs (1) and (2) include that: (i) there are only Co-POM and CoO_x WOCatalysts present; (ii) that each $Co(II)_{aq}$ becomes an active site in CoO_x; and (iii) that Co-POM decomposition yields only $Co(II)_{aq}$ and no other, active, lacunary or other Co-POM.

The normalized WOCatalysis activity of the intact Co-POM ($I_{Co\text{-}POM}$) or $Co(II)_{aq}$ ($I_{Co(II)}$) can then be determined under the above assumptions /approximations using equations 3 and 4:

$$i_{Co-POM} = [Co - POM]_t \, x \, I_{Co-POM} \quad (3)$$

$$i_{Co(II)} = [Co(II)]_{aq,t} \, x \, I_{Co(II)} \quad (4)$$

The relative rate of $Co(II)_{aq}$ when compared with the intact Co-POM then becomes equation 5:

$$\frac{I_{Co(II)}}{I_{Co-POM}} = \frac{i_{Co(II)}\ x\ [Co-POM]_t}{i_{Co-POM}\ x\ [Co(II)]_{aq,t}} \quad (5)$$

An example calculation is the case for Co-POM WOCatalysis seen in Tables 4.1 and 4.2 of the main text of **α_1-CoP_2W_{17}** in 0.1 M NaPi pH=5.8, where the percent decomposition is ~0.6% and the percent WOCatalysis that can be accounted for by the $Co(II)_{aq}$ is ~30%. If one then makes the further assumption / approximation that the ~0.6% and ~30% values are precise (i.e., are exactly 0.6% and 30%, respectively, so that in turn the $[Co(II)]_{aq,t}$= 0.6 %, the $[Co\text{-}POM]_t$=99.4% and that $i_{Co(II)}$=30% and $i_{Co\text{-}POM}$=70%), then the relative WOCatalysis activity of $Co(II)_{aq}$ according to eq. 6, becomes 70 times that of the intact Co-POM—a previously unavailable *estimate* of the relative WOCatalysis activity of the Co-POM vs that of the $Co(II)_{aq}$ released and in the form of CoO_x:

$$\frac{I_{Co(II)}}{I_{Co-POM}} = \frac{i_{Co(II)}\ x\ [Co-POM]_t}{i_{Co-POM}\ x\ [Co(II)]_{aq,t}} = \frac{30\ x\ 99.4}{70\ x\ 0.6} = 70 \quad (6)$$

One can of course use the data ranges and error bars in Tables 4.1 and 4.2 of the main text to repeat the calculations above to get the range of the relative WOCatalysis activities of the Co-POM vs that of the $Co(II)_{aq}$ released, again under the assumptions stated above that lead to eq 6. Deliberately biasing the estimate as much as possible in favor of the Co-POM (i.e., assuming maximum decomposition and minimum contribution from CoO_x to the current) and for this case of the most stable Co-POM examined (**α_1-CoP_2W_{17}**) yields the following ratio (see Tables 4.1 and 4.2 for the error bars that lead to the following input values for eq. 6): (10 x 98.8) / (90 x 1.2) ≈ 10. Biasing the calculation the other way, towards the CoO_x (while using the lower limit of 0.2

μM $Co(II)_{aq}$ (which equals 99.96%) seen for **α_1-CoP_2W_{17}** as given in Table 4.1) yields: (50 x 99.96) / (50 x 0.04) ≈ 2500. Hence, the *estimate* as to the relative WOC activity for the most stable Co-POM WOCatalysis seen (given the data in Tables 4.1 and 4.2) of **α_1-CoP_2W_{17}**, compared to that for the leached $Co(II)_{aq}$, is ~70, with a range to the estimate of 10-2500.

Repeating these calculations at pH=8, again for the most stable **α_1-CoP_2W_{17}** and using the data in Table 4.1 and 4.2 of the main text, yields (90 x 98.8) / (10 x 1.2) ≈ 740 for the relative activity of the Co(II)aq derived CoO_x compared to **α_1-CoP_2W_{17}**. If one biases the calculation as much as possible towards Co-POM-based catalysis, then the activity ratio is ≥(60 x 98.2) / (40 x 1.8) ≈ ≥80. That is, at pH=8 CoO_x is an even more kinetically dominant catalyst than is the most stable Co-POM examined, **α_1-CoP_2W_{17}**.

Cyclic voltammograms of 3 h aged Co-POMs after 5 min electrolysis in the original Co-POM solution (red) and the same electrode in a buffer-only solution (blue).

This section presents the CVs that were not presented in Figure 4.5 of the main text. Each pH (5.8, 8.0 and 9.0) are presented on separate pages. The red traces are the CVs of the electrode in the original electrolyzed Co-POM solution, and the blue traces are the CVs of the electrodes after they have been removed from the Co-POM solution, rinsed and placed into a buffer-only solution. Most of the CVs with and without the Co-POM are superimposable, suggesting that CoO_x is the dominant catalyst. In the cases where the electrolyzed Co-POM solution (red trace) has higher current than the buffer-only solution (blue trace), the interpretation is that a solution-based species is responsible for the observed catalysis.

Cyclic Voltammograms of Aged POMs NaPi **pH 5.8**

$Co_4P_2W_{18}$ in 0.1 M NaPi pH 5.8

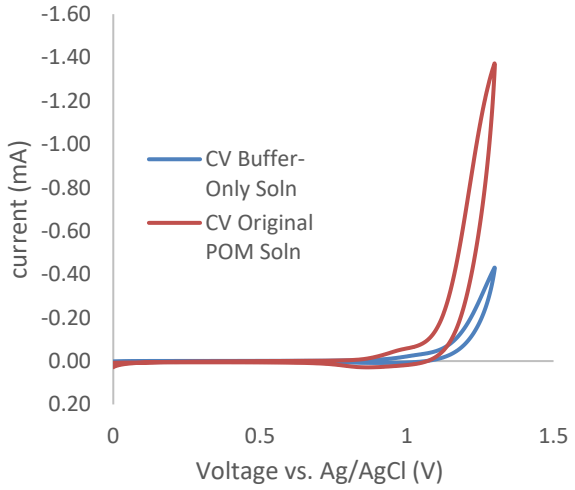

$Co_9P_5W_{27}$ in 0.1 M NaPi pH 5.8

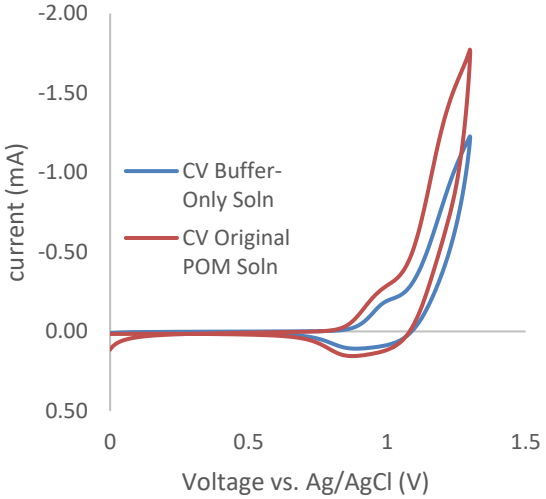

$Co_4P_4W_{30}$ in 0.1 M NaPi pH 5.8

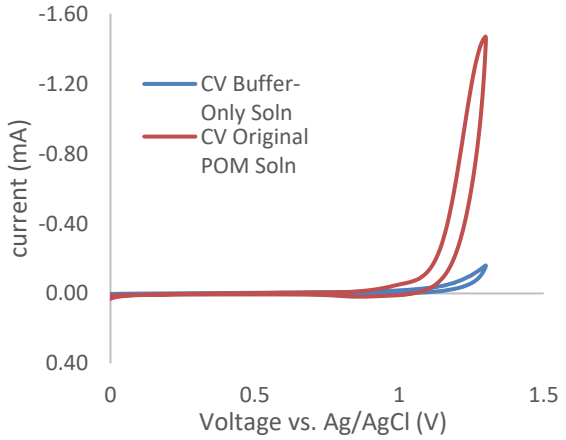

$CoPW_{11}$ in 0.1 M NaPi pH 5.8

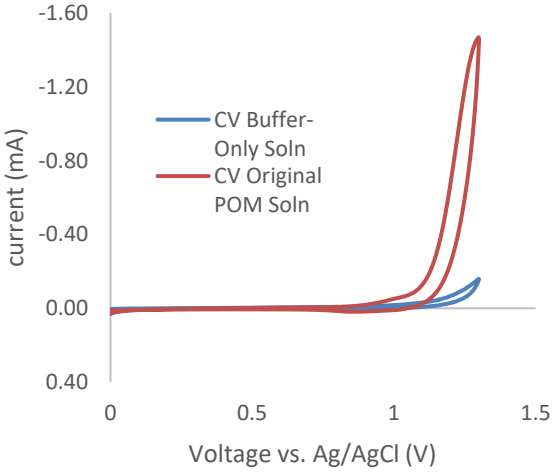

α_2-CoP_2W_{17} in 0.1 M NaPi pH 5.8

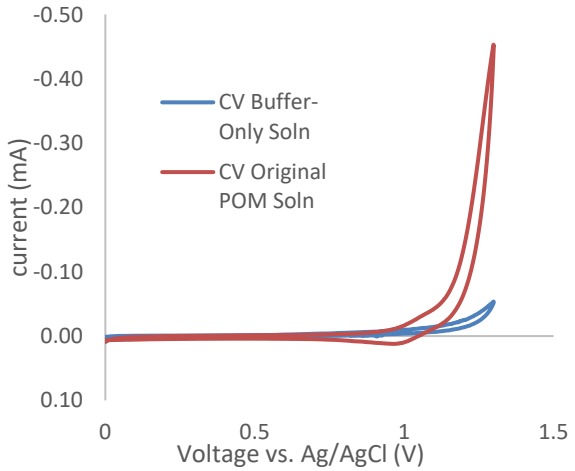

Cyclic Voltammograms of Aged POMs NaPi **pH 8.0**

$Co_9P_5W_{27}$ in 0.1 M NaPi pH 8.0

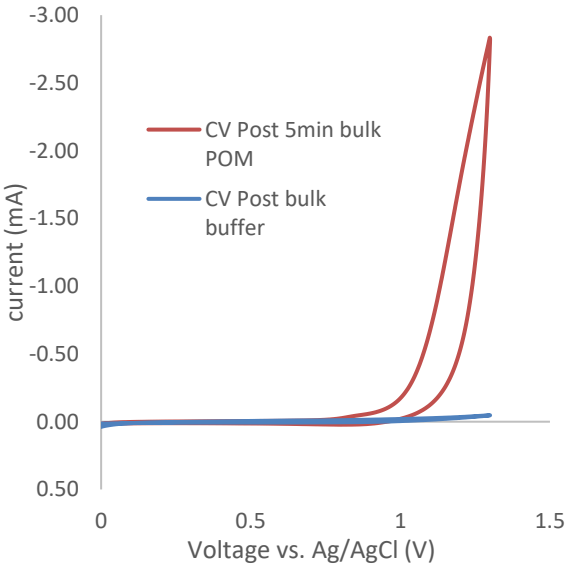

$Co_4P_4W_{30}$ in 0.1 M NaPi pH 8.0

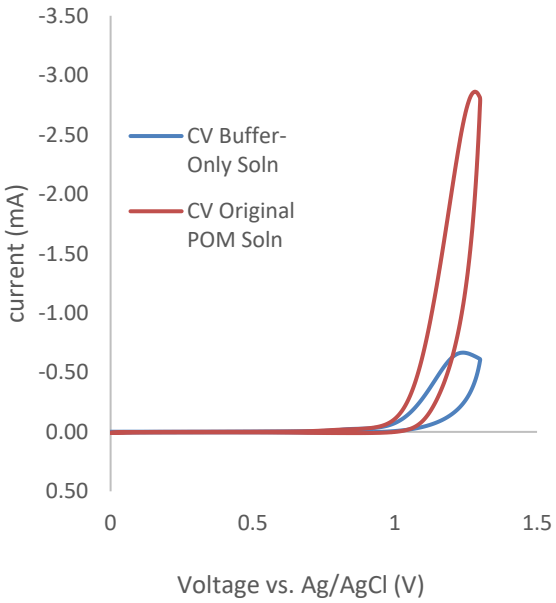

$CoPW_{11}$ in 0.1 M NaPi pH 8.0

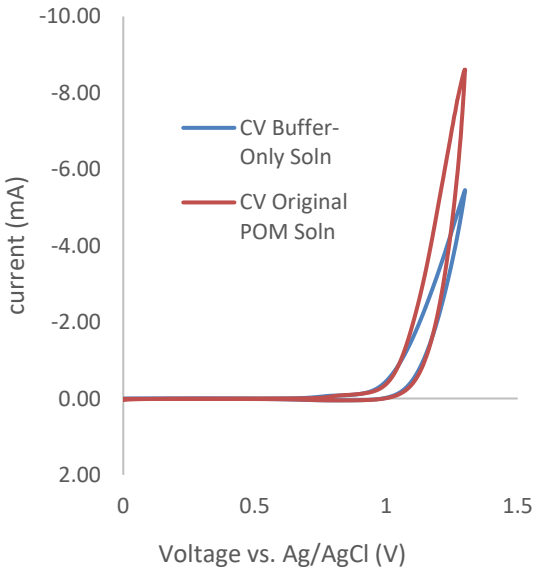

α_1-CoP_2W_{17} in 0.1 M NaPi pH 8.0

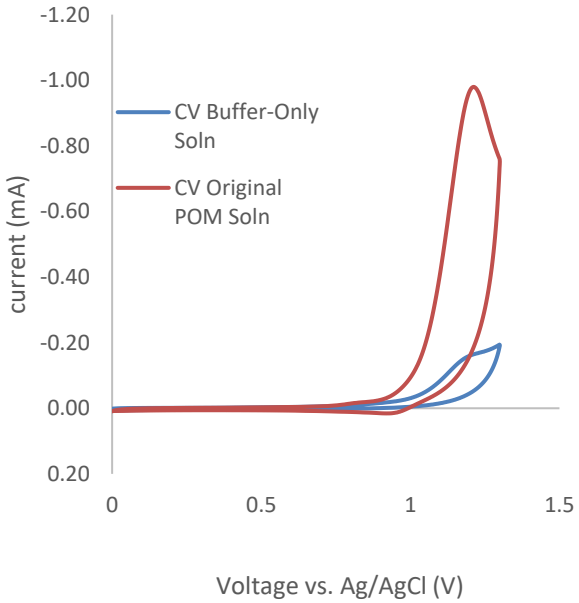

Cyclic Voltammograms of Aged POMs NaB **pH 9.0**

$Co_4P_2W_{18}$ in 0.1 M NaB pH 9.0

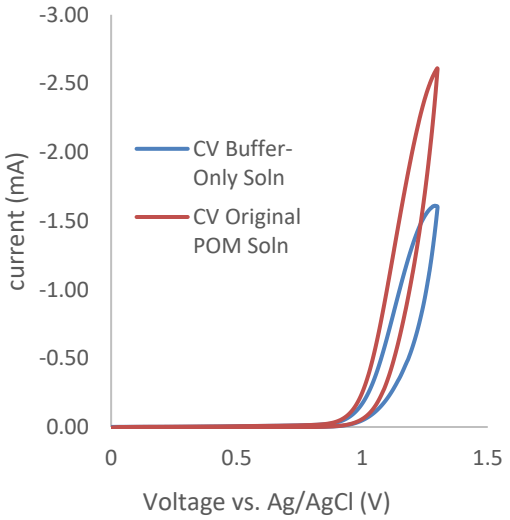

$Co_9P_5W_{27}$ in 0.1 M NaB pH 9.0

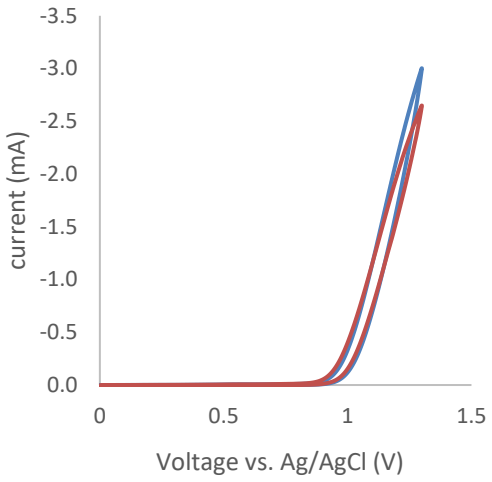

$Co_4P_4W_{30}$ in 0.1 M NaB pH 9.0

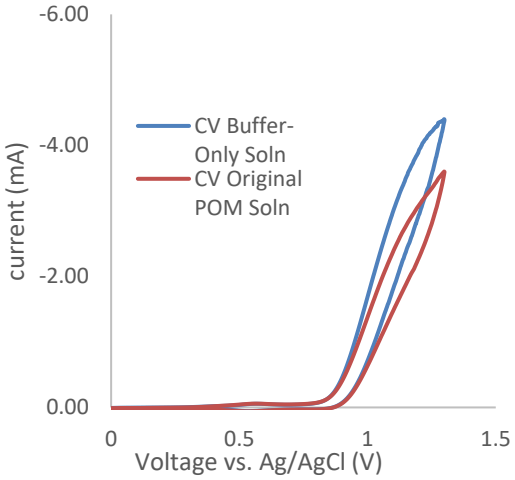

$CoPW_{11}$ in 0.1 M NaB pH 9.0

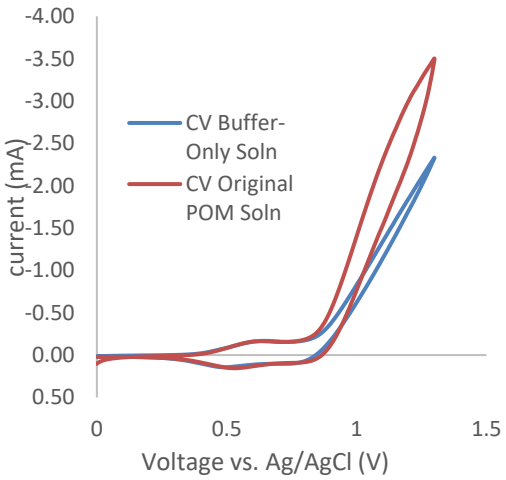

α_1-CoP_2W_{17} in 0.1 M NaB pH 9.0

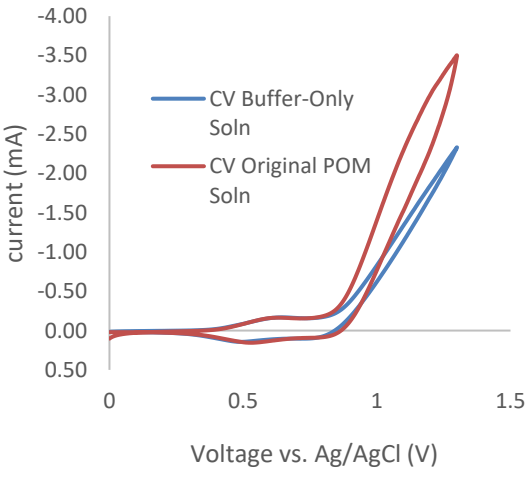

α_2-CoP_2W_{17} in 0.1 M NaB pH 9.0

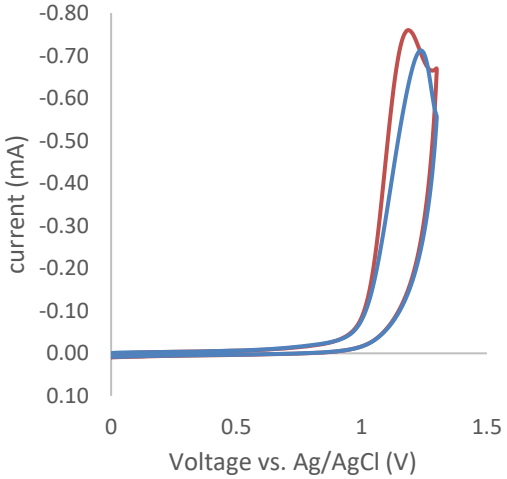

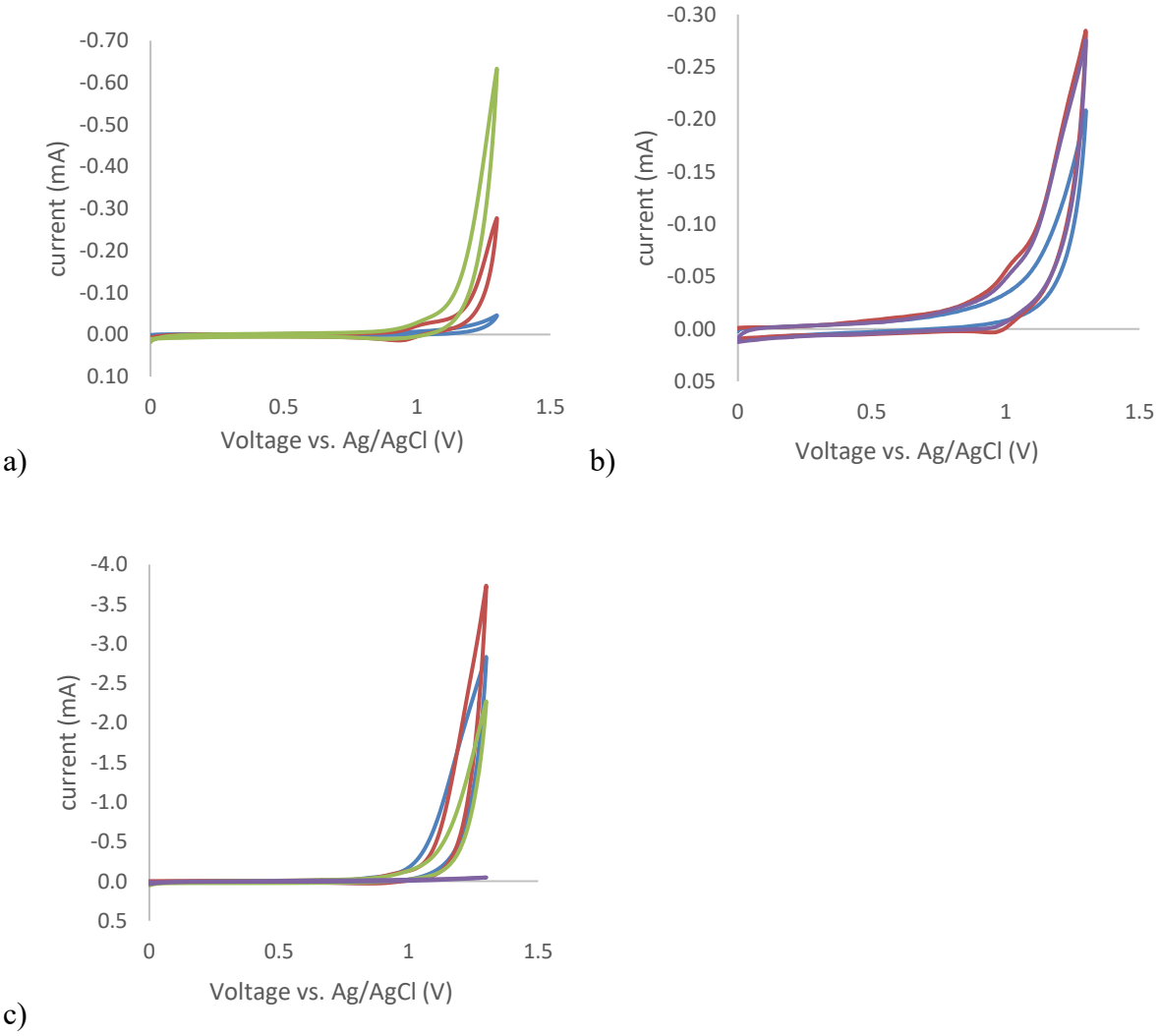

Figure S4.13. Cyclic voltammograms: a) **α_1-CoP_2W_{17}** aged 3 h in 0.1 M NaPi pH 5.8 electrodes post 5 min controlled potential electrolysis in the original Co-POM solution (red), in a buffer-only solution (blue) (the same as Figure 4.3c of the main text), and then additionally the CV of the electrode-bound film after 30 min electrolysis (green) showing that the catalytic current increases with prolonged electrolysis. b) **α_2-CoP_2W_{17}** aged 3 h in 0.1 M NaPi pH 8.0 with 100μM EDTA added just before the following experiments: prior to electrolysis (red), after 5 min controlled potential electrolysis in the original Co-POM solution (blue), and after 5 min electrolysis in a buffer-only solution (purple). These results reveal that the WOCatalysis activity from **α_2-CoP_2W_{17}** is not significantly affected by the presence of EDTA. c) **$Co_9P_5W_{27}$** in 0.1 M NaPi pH=8.0 after 3 hours of aging in the original Co-POM solution: prior to electrolysis (red), after 5 min electrolysis (blue), after 30 min electrolysis (green), and in a buffer-only solution after 30 min electrolysis (purple). These experiments demonstrate that the WOCatalysis current diminishes over time from **$Co_9P_5W_{27}$** and that no significant deposition of film occurs.

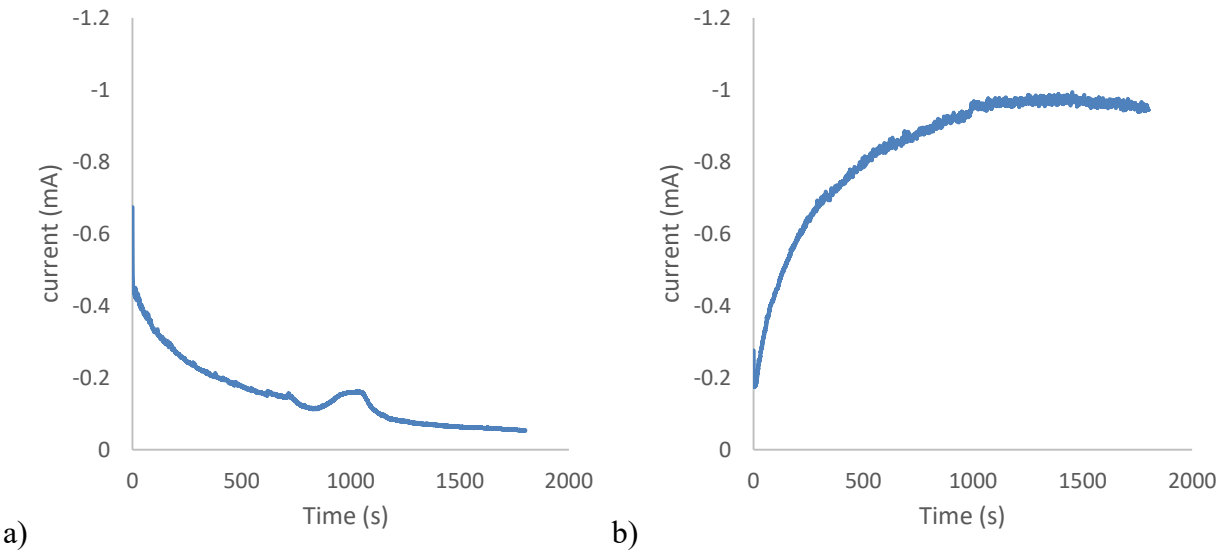

Figure S4.14. Current vs. time for the electrodes used for SEM and XPS in the main text a) 500 µM **$Co_4P_2W_{18}$** in 0.1 M NaPi pH 8.0 with 600 µM EDTA (10 equiv./ $Co(II)_{aq}$), the low and diminishing WOCatalysis current is evidence against film deposition. b) 500 µM **α_2-CoP_2W_{17}** in 0.1 M NaPi pH 8.0. The growth of WOCatalysis is consistent with the deposition of catalytically active CoO_x.

Discussion of the Prolonged Electrolysis of 3 h Aged 500 µM α_1-CoP_2W_{17} in 0.1 M NaPi pH 5.8.

We examined a 3 h aged solution of 500 µM **α_1-CoP_2W_{17}** in 0.1 M NaPi pH 5.8—conditions where **α_1-CoP_2W_{17}** decomposes by only 0.6(±0.6)%, the lowest decomposition observed herein, Table 4.1 of the main text, conditions where the intact **α_1-CoP_2W_{17}** accounts for 70(±20)% of the observed WOCatalysis activity when compared with $Co(II)_{aq}$, Table 4.2 of the main text. In this experiment CV was conducted *after 3h aging but prior to electrolysis* (Figure S4.15, red). Next, constant potential electrolysis was conducted for 30 min, followed by CV in the post-electrolysis Co-POM solution (Figure S4.15, blue). The electrodes were then removed and rinsed then placed into a buffer-only solution and CV was conducted again (Figure S4.15, green). The constant potential i vs t curve shown in Figure S4.15 exhibits an increase in WOCatalysis current throughout the experiment, consistent with the formation of a more catalytically active

species.[18,39,40] Furthermore, the WOCatalysis current increases for the CV after electrolysis (Figure S4.15, blue), which is also consistent with the formation of a more catalytically active species.[18,39,40] However, unlike the other cases examined,[18,39,40] CV in the buffer-only solution shows a significantly diminished current, meaning that the active WOCatalyst is not an electrode-bound species. Furthermore, no film is observable to the naked eye, and XPS of the electrode (Figure S4.16) shows only C and O, meaning that heterogeneous CoO_x is not formed from 500 μM **α_1-CoP_2W_{17}** in 0.1 M NaPi pH=5.8.

The reason for the increase in the WOCatalysis current in Figure S4.15 is not currently known, but demonstrates the formation of a solution-based species that is the dominant WOCatalyst. One possibility is that dimerization of **α_1-CoP_2W_{17}** occurs in a similar manner to the formation[41] of $[(\alpha_2\text{-}P_2W_{17}O_{61}Co^{IV})_2O]^{14-}$ from $[\alpha_2\text{-}Co^{II}(H_2O)P_2W_{17}O_{61}]^{8-}$ and the (**α_1-CoP_2W_{17}**)$_2$ dimer is the active WOCatalysis species.[41] Determining the precise nature of the solution based active species from 500 μM **α_1-CoP_2W_{17}** in 0.1 M NaPi pH=5.8 is beyond the scope of this paper, but is of interest and merits further investigation.

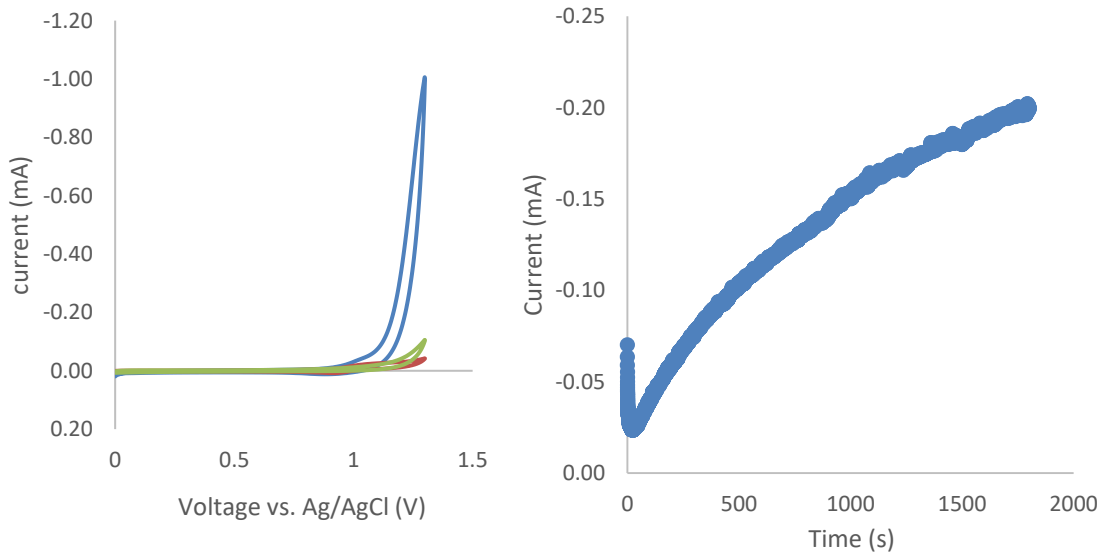

Figure S4.15. CVs (left) and constant potential electrolysis (right) curves of 3 h aged 500 μM **α_1-CoP_2W_{17}** in 0.1 M NaPi pH 5.8.The red CV corresponds to the aged **α_1-CoP_2W_{17}** solution prior to electrolysis, the blue CV corresponds to the **α_1-CoP_2W_{17}** solution after the electrolysis at 1.1 V, and the green CV corresponds to the CV in the buffer-only solution of the electrodes that have been rinsed. The increase in anodic current for over time is evidence for the formation of a more catalytically active species, with the increase in current in the CV after electrolysis being consistent with the formation of a more catalytically active species. Interestingly, and unlike the other cases examined, CV in the buffer-only solution shows a significantly diminished current (left, green)—meaning that the active WOCatalyst is not electrode bound CoO_x.

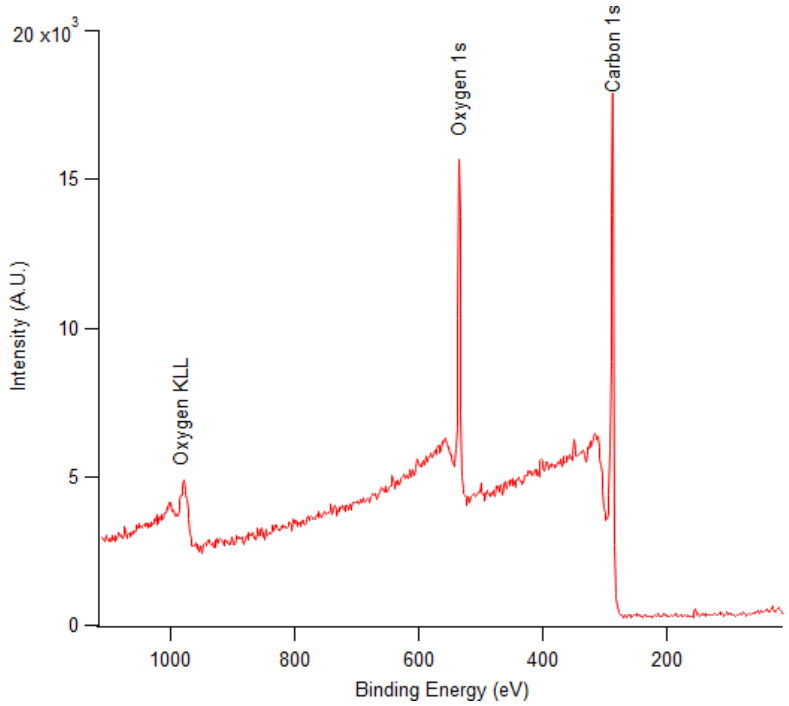

Figure S4.16. XPS of the glassy carbon electrode from the constant potential electrolysis of 3 h aged 500 μM **α_1-CoP_2W_{17}** in 0.1 M NaPi pH 5.8. Noteworthy here is that only C and O are detected, meaning that detectable electrode-bound CoO_x is not formed.

A Brief Discussion of the Error Bars in Table 4.2.

The large error bars inherent in the low, μM detection of $Co(II)_{aq}$ and, hence, some of the values in Table 4.2 in the main text could, in principle be lowered ~2-fold by performing 4 times more (so 3 x 4 = 12 total, requiring 8 more) repetitions at each pH value (i.e., that would be expected, then, in turn to reduced the error bars down by ~$(4)^{1/2}$ or ~2-fold, assuming a normal distribution of data that is affected by random error only[42]). That said, reducing the error by ~2-fold for all the 12 entries in Table 4.2 would require 12 repetitions for each of our 18 conditions (i.e, 216 WOCatalysis experiments given the 3 hrs of aging in each experiment), hence ~650 hrs to reduce the error bars by only half for all the measurements in Table 4.2. That large number of experiments would require a good reason to justify the required, considerable effort. However, a high interest in a specific Co-POM could result in ~2-fold lower error bars with ~8 more experiments.

REFERENCES

1 Goberna-Ferrón, S.; Soriano-López, J.; Galán-Mascarós, J. R. *Inorganics* **2015**, *3* (3), 332–340.

2 Zhang, C.; Lin, X.; Zhang, Z.; Long, L.-S.; Wang, C.; Lin, W. *Chem. Commun.* **2014**, *50* (78), 11591–11594.

3 Chen, W.-C.; Wang, X.; Qin, C.; Shao, K.-Z.; Su, Z.-M.; Wang, E. *Chem. Commun.* **2016**.

4 Wei, J.; Feng, Y.; Zhou, P.; Liu, Y.; Xu, J.; Xiang, R.; Ding, Y.; Zhao, C.; Fan, L.; Hu, C. *Chem. Sus. Chem* **2015**, 8, 2630.

5 Zhu, G.; Glass, E. N.; Zhao, C.; Lv, H.; Vickers, J. W.; Geletii, Y. V.; Musaev, D. G.; Song, J.; Hill, C. L. *Dalton Trans.* **2012**, *41* (42), 13043–13049.

6 Cui, Y.; Shi, L.; Yang, Y.; You, W.; Zhang, L.; Zhu, Z.; Liu, M.; Sun, L. *Dalton Trans.* **2014**, *43*, 17406–17415.

7 Besson, C.; Huang, Z.; Geletii, Y. V.; Lense, S.; Hardcastle, K. I.; Musaev, D. G.; Lian, T.; Proust, A.; Hill, C. L. *Chem. Commun.* **2010**, *46* (16), 2784–2786.

8 Du, X.; Ding, Y.; Song, F.; Ma, B.; Zhao, J.; Song, J. *Chem. Commun.* **2015**.

9 Yu, L.; Du, X.; Ding, Y.; Chen, H.; Zhou, P. *Chem. Commun.* **2015**.

10 Song, F.; Ding, Y.; Ma, B.; Wang, C.; Wang, Q.; Du, X.; Fu, S.; Song, J. *Energy Environ. Sci.* **2013**, *6* (4), 1170.

11 Evangelisti, F.; Car, P.-E.; Blacque, O.; Patzke, G. R. *Catalysis Science & Technology* **2013**, *3* (12), 3117.

12 Zhu, G.; Geletii, Y. V.; Kögerler, P.; Schilder, H.; Song, J.; Lense, S.; Zhao, C.; Hardcastle, K. I.; Musaev, D. G.; Hill, C. L. *Dalton Trans.* **2012**, *41* (7), 2084.

13 Nishiki, K.; Umehara, N.; Kadota, Y.; Lopez, X.; Poblet, J. M.; Mezui, C. A.; Teillout, A.-L.; Mbomekalle, I. M.; Oliveira, P. D.; Miyamoto, M. *Dalton Trans.* **2015**.

14 Han, X.-B.; Li, Y.-G.; Zhang, Z.-M.; Tan, H.-Q.; Lu, Y.; Wang, E.-B. *J. Am. Chem. Soc.* **2015**, *137* (16), 5486–5493.

15 Han, X.-B.; Zhang, Z.-M.; Zhang, T.; Li, Y.-G.; Lin, W.; You, W.; Su, Z.-M.; Wang, E.-B. *J. Am. Chem. Soc.* **2014**, *136* (14), 5359–5366.

16 Martin-Sabi, M.; Soriano-López, J.; Winter, R. S.; Chen, J.-J.; Vilà-Nadal, L.; Long, D.-L.; Galán-Mascarós, J. R.; Cronin, L. *Nature Catalysis* **2018**, *1* (3), 208–213.

17 Paille, G.; Gomez-Mingot, M.; Roch-Marchal, C.; Lassalle-Kaiser, B.; Mialane, P.; Fontecave, M.; Mellot-Draznieks, C.; Dolbecq, A. *J. Am. Chem. Soc.* **2018**, *140* (10), 3613–3618.

18 Stracke, J. J.; Finke, R. G *J. Am. Chem. Soc.* **2011**, *133*, 14872–14875.

19 Yin, Q.; Tan, J. M.; Besson, C.; Geletii, Y. V.; Musaev, D. G.; Kuznetsov, A. E.; Luo, Z.; Hardcastle, K. I.; Hill, C. L. *Science* **2010**, *328*, 342–345.

20 Goberna-Ferrón, S.; Vigara, L.; Soriano-López, J.; Galán-Mascarós, J. R. *Inorg. Chem.* **2012**, *51*, 11707–11715.

21 Galán-Mascarós, J. R.; Gómez-Garcia, C. J.; Borrás-Almenar, J. J.; Coronado, E. *Adv. Mater.* **1994**, *6* (3), 221–223.

22 Weakley, T. J. R. *J. Chem. Soc., Chem. Commun.* **1984**, No. 21, 1406–1407.

23 Darensbourg, M. *Inorg. Synth.*; John Wiley & Sons, 1998; Vol. 32, pages 175-182.

24 Ruhlmann, L.; Costa-Coquelard, C.; Canny, J.; Thouvenot, R. *Inorg. Chem.* **2007**, *2007*, 1493–1500.

25 Ruhlmann, L.; Schaming, D.; Ahmed, I.; Courville, A.; Canny, J.; Thouvenot, R. *Inorg. Chem.* **2012**, *51* (15), 8202–8211.

26 Finke, R. G.; Droege, M. W.; Domaille, P. J. *Inorg. Chem.* **1987**, *26* (23), 3886–3896.

27 Weakley, T. J. R.; Malik, S. A. *J. Inorg. Nucl. Chem.* **1967**, *29*, 2935–2944.

28 Tourné, C. M.; Tourné, G. F.; Malik, S. A.; Weakley, T. J. R. *J. Inorg. Nucl. Chem.* **1970**, *32*, 3875–3890.

29 Jorris, T. L.; Kozik, M.; Casan-Pastor, N.; Domaille, P. J.; Finke, R. G.; Miller, W. K.; Baker, L. C. W. *J. Am. Chem. Soc.* **1987**, *109*, 7402–7408.

30 Bailar, J. C.; Booth, H. S.; Grennert, M. *Synth.*; Booth, H. S., Ed.; John Wiley & Sons, Inc., **1939**; pp. 132–133.

31 Li, J.; Wang, J.; Zhang, L.; Sang, X.; You, W. *J. Coord. Chem.* **2017**, *70*, 2950–2957.

32 Contant, R.; Klemperer, W. G.; Yaghi, O. *Inorg. Synth.*; Ginsberg, A. P., Ed.; John Wiley & Sons, Inc., **1990**; pp. 104–111.

33 Samonte, J. L.; Pope, M. T. *Can. J. Chem.* **2001**, *79*, 802–808.

34 Contant, R.; Ciabrini, J.-P. *J. Chem. Res.* **1982**, 50–51.

35 Lyon, D. K.; Miller, W. K.; Novet, T.; Domaille, P. J.; Evitt, E.; Johnson, D. C.; Finke, R. G. *J. Am. Chem. Soc.* **1991**, *113*, 7209–7221.

36 Baes, C.; Mesmer, R. *The Hydrolysis of Cations*; John Wiley & Sons, 1976.

37 Ruhlmann, L.; Nadjo, L.; Canny, J.; Contant, R.; Thouvenot, R. *Eur. J. Inorg. Chem.* **2002**, *2002*, 975–986.

38 Finke, R. G.; Droege, M. W.; Domaille, P. J. *Inorg. Chem.* **1987**, *26* (23), 3886–3896.

39 Stracke, J. J.; Finke, R. G. *ACS Catal.* **2014**, *4*, 909–933.

40 Folkman, S. J.; Finke, R. G. *ACS Catal.* **2017**, *7*, 7–16.

41 Barats-Damatov, D.; Shimon, L. J. W.; Weiner, L.; Schreiber, R. E.; Jiménez-Lozano, P.; Poblet, J. M.; de Graaf, C.; Neumann, R. *Inorg. Chem.* **2014**, *53* (3), 1779–1787.

42 Taylor, J. *An Introduction to Error Analysis the Study of Uncertainties in Physical Measurements*, 2nd ed.; University Science Books, 1982.

APPENDIX IV. SUPPORTING INFORMATION FOR CHAPTER V.

Discussion of the elemental analysis, the approximate average molecular formula of the Co_3O_4 nanoparticles, OAc^- surface coverage of Co_3O_4 nanoparticles, and the binding mode of the OAc^- surface ligand.

The elemental analysis of the cobalt-oxide particles synthesized from EtOH/water is 56.0 % Co, 34.4 % O, 7.5 % C, 2.0 % H, and 1.2 % N. Assuming that all of the carbon originates from OAc^-, one would expect 4.7 mM OAc^- in a 1.5 mg/mL solution of the digested particles, and we observe 4.3 ± 0.6 mM OAc^- from the quantitative NMR experiments, values in good agreement. This quantitative agreement between the elemental analysis and quantitative NMR in turns supports the conclusion *that OAc^- quantitatively accounts for all of the carbon in the sample*.

Given that the only source of deliberately introduced N in the synthesis is as NH_4OH, the presence of nitrogen in the elemental analysis suggests that NH_4^+ is present in the product (and even though NH_3 will be present at the pH = 9.8 of our synthesis given the approximate pKa of NH_4^+ of ca. 9.2 that should be higher in EtOH / water). We attempted several methods to detect and quantify NH_4^+, including the Berthelot test,[1] but were unsuccessful in identifying and quantifying NH_4^+ due to incompatibilities between the the test and the cobalt-oxide nanoparticles and other conditions as elaborated on in a footnote.[2] However, because NH_4^+ is the only source of nitrogen added to the reaction, Ockham's razor suggests that NH_4^+, along with H^+, are the counterions present for the OAc^- observed in the cobalt oxide nanoparticle product.

Proposing an Approximate Molecular Formula for Cobalt-Oxide Nanoparticles Synthesized in EtOH/water. As noted in the Introduction of the main text, even just an approximate "average molecular formula" has been unavailable previously for what are otherwise referred to in the literature generally as "cobalt-oxide nanoparticles" or "Co_3O_4 nanoparticles"—a hypothetical material that, in reality, is probably almost never actually present since the true product is closer to "Co_3O_4•ligands•countercations". Hence, we decided to see how far we could proceed in formulating an approximate, average molecular formula that more precisely describes the average composition of the Co_3O_4 nanoparticle product prepared in EtOH/water. As noted in the main text, the *empirical formula* is $Co_{3.00\pm0.01}O_{6.80\pm0.01}C_{1.97\pm0.05}H_{6.3\pm0.2}N_{0.3\pm0.3}$. We also know that acetate quantitatively accounts for all of the observed carbon in the sample. Therefore, one formulation is $Co_3O_4(O_2C_2H_3)(NH_4)_{0.3}(H_xO)$, where X is ≈ 2.7. This approximate, average

molecular formula can be rewritten as of $\{[Co_3O_4(O_2C_2H_3)]^-[(NH_4^+)_{0.3}(H^+_{0.7})]^+\bullet(H_2O)\}_{\sim 216}$. The slightly idealized net reaction stoichiometry is given in eq. 1 from the main text, reproduced below and (as noted in the main text) in which the only counter cation shown is NH_4^+, thereby simplifying the observed mixed $[(NH_4^+)_{0.3}(H^+_{0.7})]$ (which, if that had been written instead, would then just require 0.7 equiv of NH_3 to also be among the products):

$$\begin{array}{l} 3Co(OAc)_2\cdot 4H_2O \\ +\ 6NH_4OH \\ +\ 1/2O_2 \end{array} \xrightarrow[\begin{array}{c}75\ ^\circ C \\ 3\ h\end{array}]{EtOH/water} \begin{array}{l} 1/\sim 216[Co_3O_4(OAc^-)(NH_4^+)\cdot(H_2O)]_{\sim 216} \\ +\ 5(NH_4)(OAc) \\ +\ 14H_2O \end{array} \qquad (1)$$

Surface Coverage and Binding Mode of the OAc^- Surface Ligands on the Cobalt-Oxide Nanoparticles. If one assumes the density of the Co_3O_4 particle is similar to that of the bulk ($6.11 g/cm^3$), and if one uses the average particle diameter of 3 nm to determine the surface area and number of Co_3O_4 equivalents in each particle, then one calculates ~2,827 $Å^2$ and ~216 units per particle, respectively, as rough estimates of these values. The surface area and number of Co_3O_4 units implies that each acetate anion (also 216/particle) would have ~13 $Å^2$ on the surface, which is plenty of room for an acetate molecule and a counter-cation equivalent of xH_3O^+ plus $(1-x)NH_4^+$ ($x \approx 0.7$). Furthermore, the FT-IR spectrum of the nanoparticles has peaks corresponding to OAc^- at 1552 and 1409 cm^{-1} corresponding to the asymmetric C−O and symmetric C−O stretching modes. The energy splitting of these peaks, $\Delta\nu_{as\text{-}s}$=143 cm^{-1}, is consistent with the acetate undergoing a bridging or bidentate (and therefore covalent) surface binding.[3,4,5] In short, the size and surface-coverage data as well as the IR data are consistent with the average formulation of $\{[Co_3O_4(O_2C_2H_3)]^-[(NH_4^+)_{0.3}(H^+_{0.7})]^+\bullet(H_2O)\}_{\sim 216}$.

Discussion of why the methyl protons of OAc^- bound to Co_3O_4 nanoparticles are not detectable by ^{1}H NMR. ^{1}H NMR line broadening in the present system could be caused by either a long correlation time from relatively slow rotation of the particles (thereby shortening T_2) or by enhanced relaxation caused by the paramagnetic particles (thereby shortening T_1). Given[6] that paramagnetic induced line broadening for $Co(II)_{aq}$ is expected to be via an inner-sphere mechanism, in order for the methyl protons on acetate to be broadened, the implication is that acetate is bonded directly to the Co(II). However, at the low pH of H_2SO_4 used in the digested solutions, $Co(H_2O)_6^{2+}$ is formed and OAc^- present is fully protonated to HOAc (pK_a=4.8), meaning

that no paramagnetic line broadening is expected for uncoordinated, freely diffusing HOAc in the digested solutions, in turn permitting HOAc to be quantified.

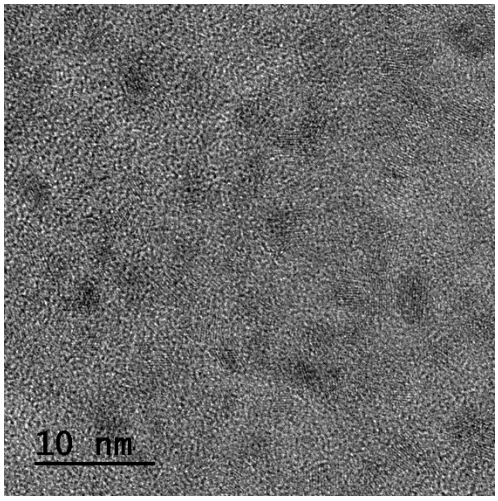

Figure S5.1. High magnification TEM of the Co_3O_4 nanoparticles synthesized in EtOH. HRTEM for this same sample is presented in Figure 1b of the main text. This image shows greater particle detail due to the higher magnification.

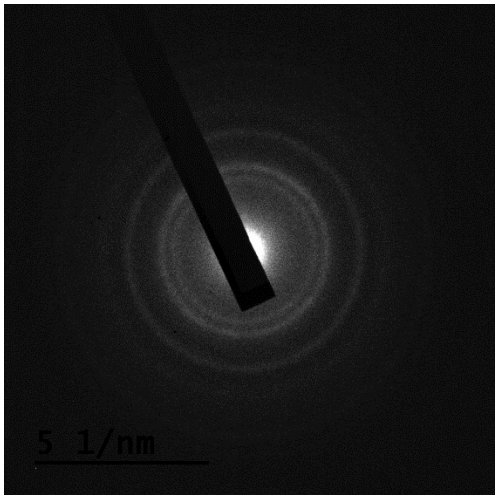

Figure S5.2. SAED of the Co_3O_4 nanoparticles synthesized in EtOH/water, showing the crystallinity of the particles.

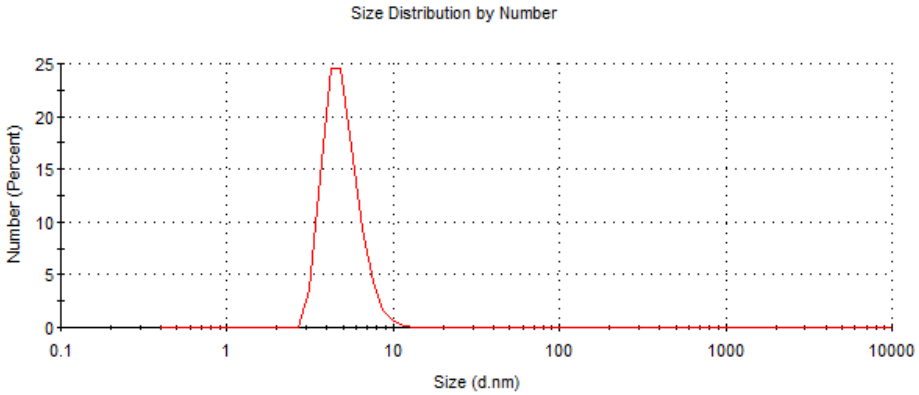

Figure S5.3. DLS size distribution by number of Co_3O_4 nanoparticles synthesized in EtOH/water, re-dissolved in neutral water (0.4 mg/mL) ~5 nm hydrodynamic radius (2-10 nm range).

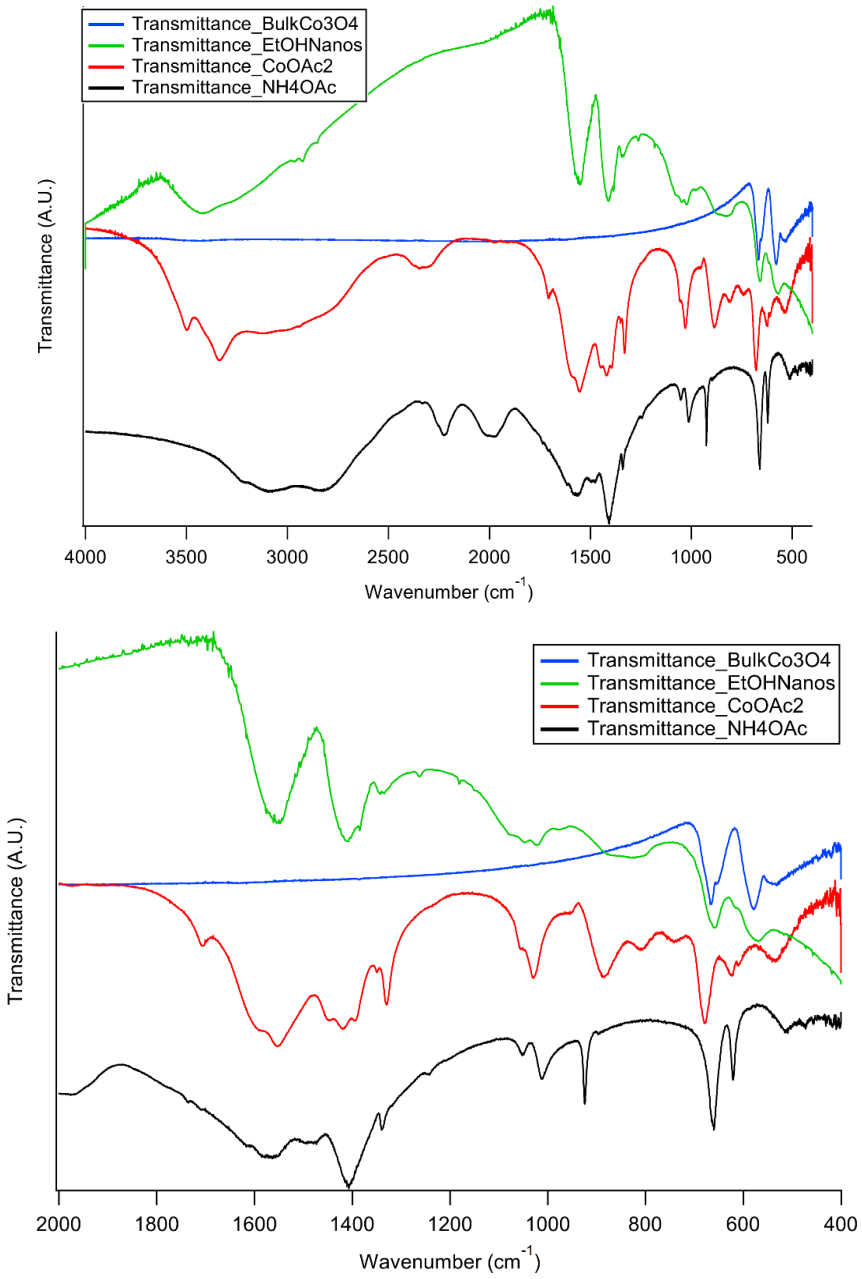

Figure S5.4. FT-IR spectrum of: the Co_3O_4 nanoparticles synthesized in EtOH/water, bulk (commercial) Co_3O_4 powder, $Co(OAc)_2•4H_2O$, and NH_4OAc at 2 wt %in KBr pellets. The full spectrum is on top and the fingerprint region from 2000 cm^{-1} on is expanded on the bottom. The bulk Co_3O_4 powder does not contain a peak at ca. 1550 and 1410 cm^{-1}, yet the nanoparticles, $Co(OAc)_2•4H_2O$, and NH_4OAc do contain those peaks. This indicates the 1550 and 1410 cm^{-1} bands most likely originate from OAc^- and not surface hydroxyl groups as previously assigned.[7]

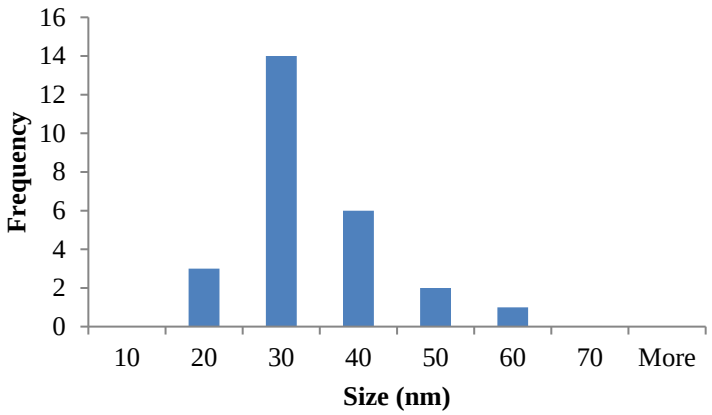

Figure S5.5. TEM size histogram (frequency vs diameter) for only the Co_3O_4 nanoparticles formed in water (size range: 20-60 nm). Larger, ~400 nm particles of β-$Co(OH)_2$ are also observed.

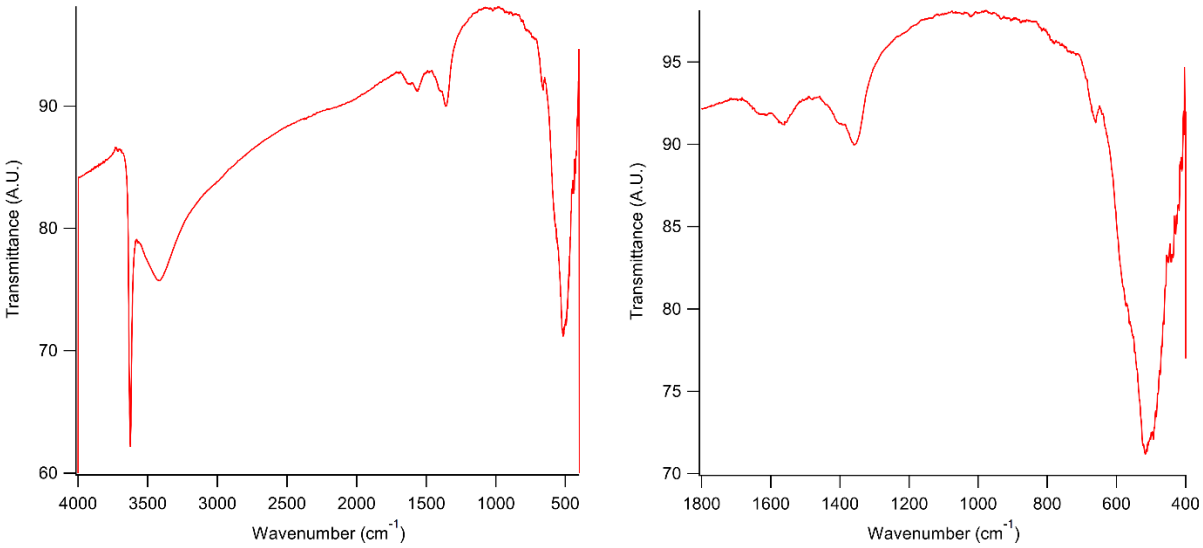

Figure S5.6. FT-IR of the CoO_x nanoparticles synthesized in water. The left image shows the full 400–4000 cm^{-1} range, and the right image shows the fingerprint 400–1800 cm^{-1} range.

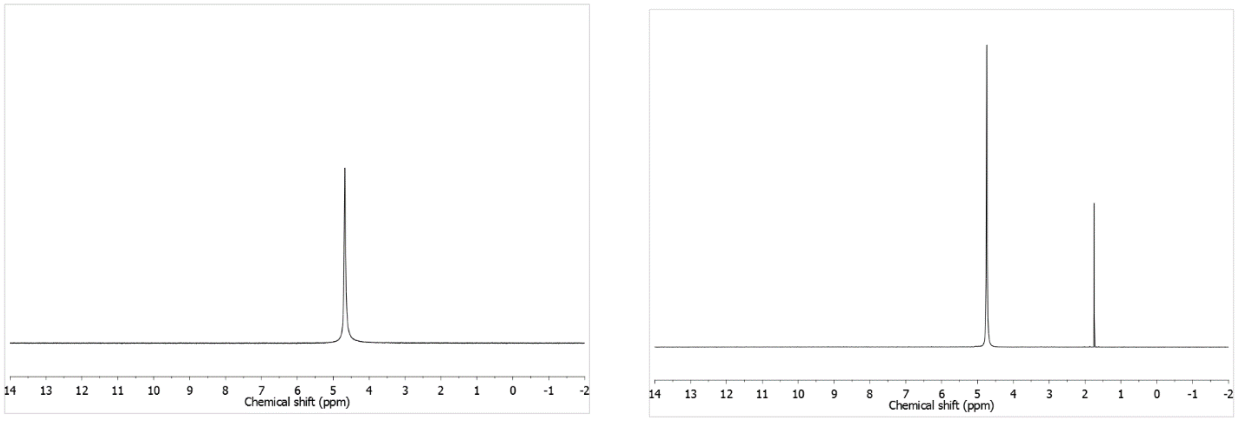

Figure S5.7. ^{1}H NMR of the freshly dissolved (left) and digested (right) Co_3O_4 nanoparticles synthesized from EtOH/water. The signal at ca. 4.8 ppm is the residual H_2O signal, while the signal at 1.7 ppm is assigned to HOAc based on spiking experiments with authentic acetic acid. Both solutions contain 1.5 mg/mL of the particles (collected under identical NMR conditions). This control demonstrates that acetate is not detectable by ^{1}H-NMR in solutions of intact nanoparticles (left-most spectrum). This implies that the ^{1}H-NMR signal for the acetate on the surface is broadened beyond detection (or possibly shifted outside the spectral window examined).

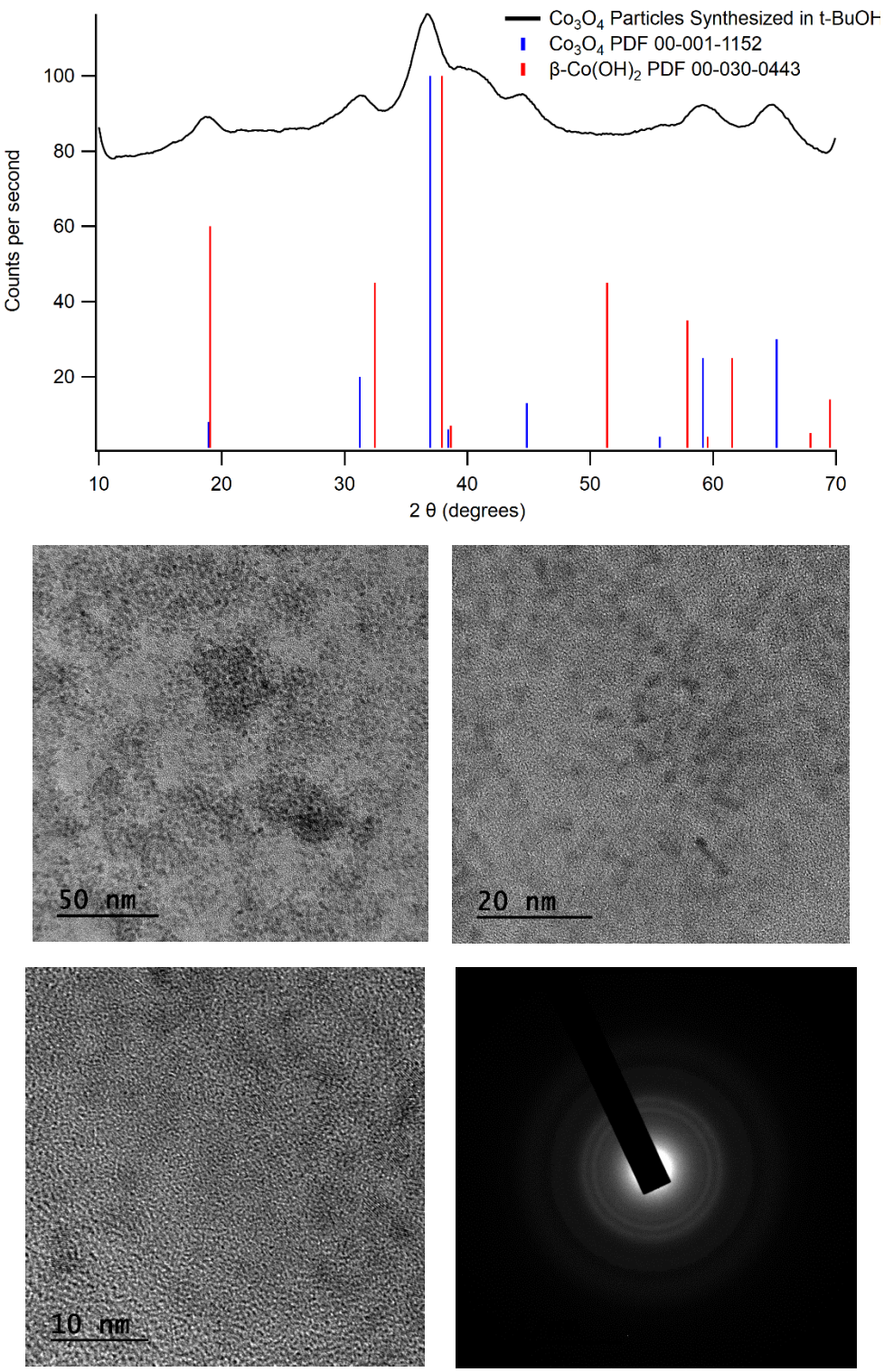

Figure S5.8. PXRD (top), 50, 20 and 10 nm scale HRTEM images (middle left, right, and bottom left), and SAED (bottom right) of Co_3O_4 particles synthesized in *t*-BuOH.

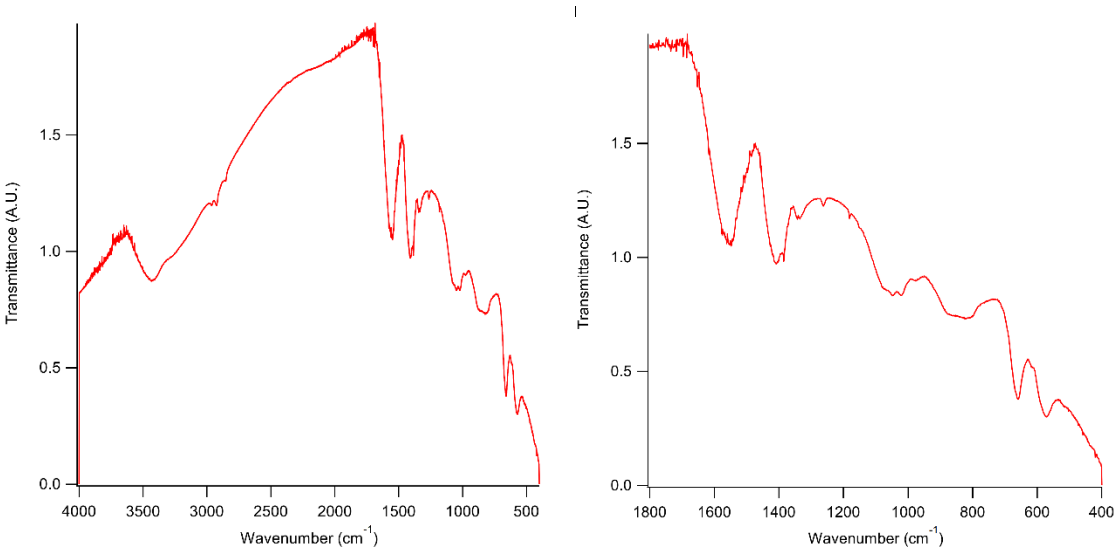

Figure S5.9. FT-IR of the Co_3O_4 particles synthesized in *t*-BuOH/water. The full 400–4000 cm^{-1} is shown on the left and a zoom of the fingerprint region from 1800 cm^{-1} on is shown on the right.

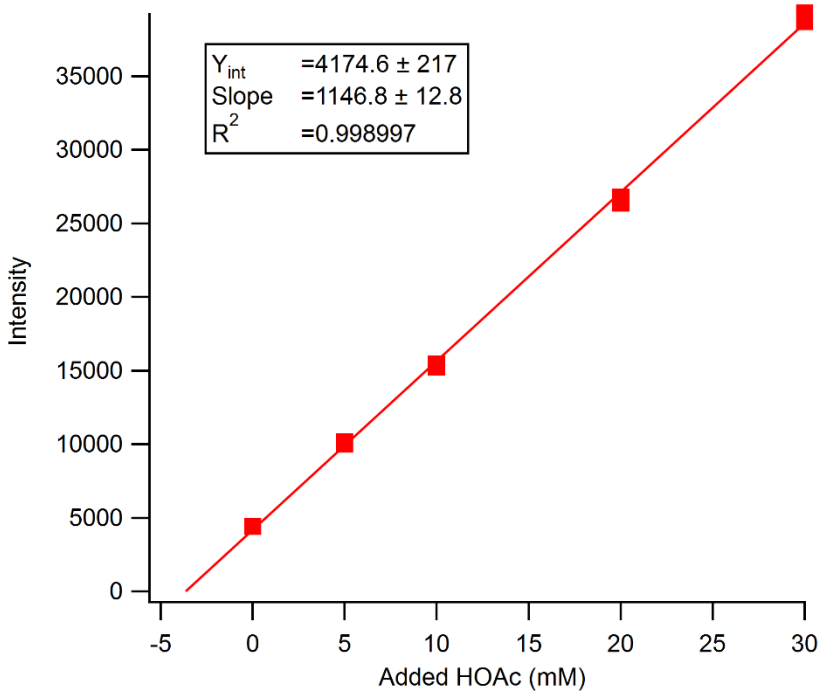

Figure S5.10. Integration of the 1.7 ppm peak vs [HOAc] for the digestion of the Co_3O_4 nanoparticles synthesized in *t*-BuOH. The [HOAc], determined as described in the main text, is 3.6 ± 0.2 mM in the 1.5 mg/mL digested solution.

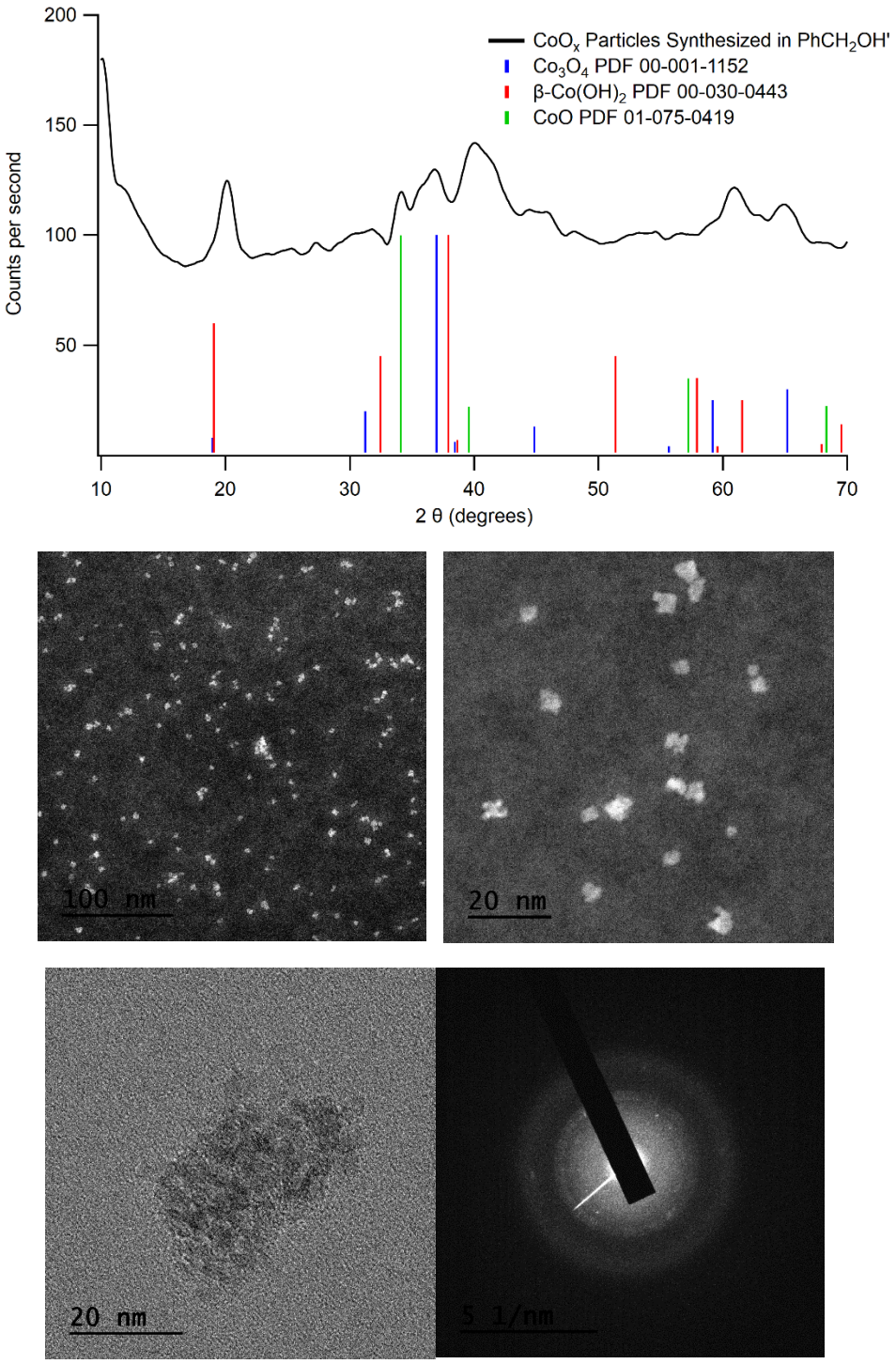

Figure S5.11. PXRD (top), HAADF-STEM (middle left and right), HRTEM (bottom left), and SAED (bottom right) of CoO_x nanoparticles synthesized in $PhCH_2OH$/water.

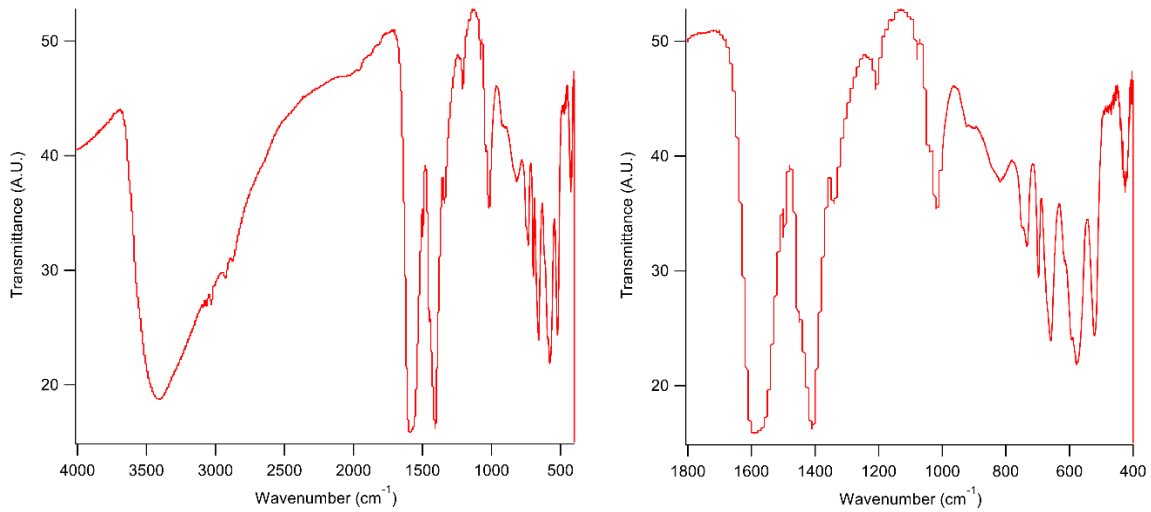

Figure S5.12. FT-IR of CoO_x nanoparticles synthesized in $PhCH_2OH$/water. The full 400–4000 cm^{-1} is shown on the left and a zoom of the fingerprint region from 1800 cm^{-1} on is shown on the right.

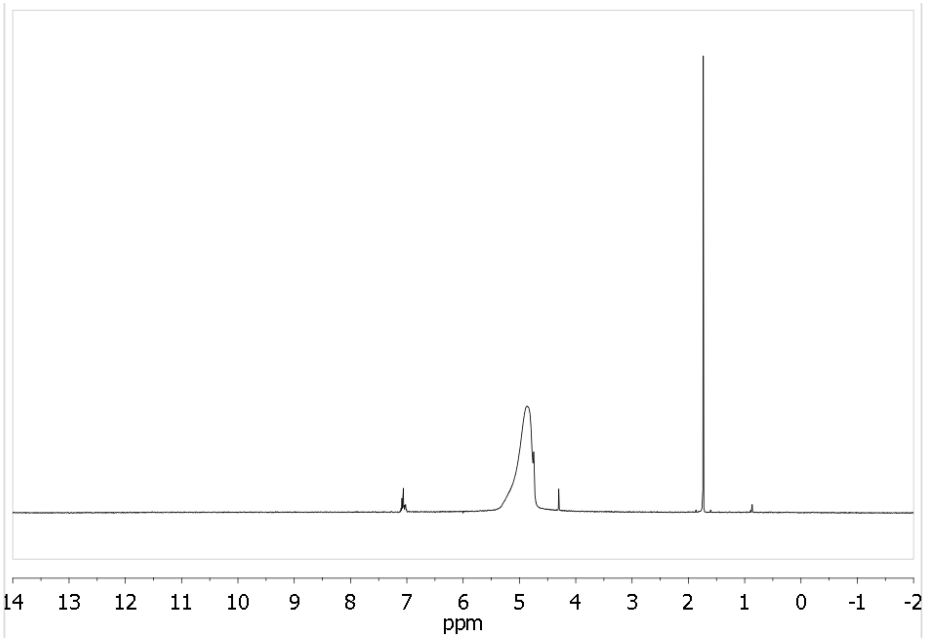

Figure S5.13. ^{1}H-NMR spectrum of CoO_x nanoparticles synthesized in $PhCH_2OH$/water. The peaks at 4.3 and 7 ppm are the methylene protons and the ring protons of $PhCH_2OH$, respectively. The peak at 1.7 ppm is the methyl group of OAc^-. Quantitative NMR and standard additions was used to determine $[PhCH_2OH] = 0.78 \pm 0.02$ mM and $[OAc^-] = 4.1 \pm 0.3$ mM in a 1.5 mg/mL solution.

Control Synthesis Employing an Eight-Fold Longer Reaction Time of 24 hrs in Search of a Higher Yield of the Co_3O_4 Product

A synthesis was conducted exactly the same as in the main text, but with the exception that instead of refluxing for 3 hours, the reaction was refluxed for 24 hours to test the hypothesis that we simply had not let the reaction go long enough to obtain the highest yield of crystalline Co_3O_4. However, after 24 hours of reflux approximately half of the solution had evaporated by escaping out of the top of the reflux column. A turbid light brown solution remained in the round bottomed flask that was still refluxing at 75 °C after 24h. Collection of the material was followed in the same manner as described in the main text via washing with acetone and centrifugation. After drying, 176 mg of material was collected in a scintillation vial, indicating no increase in the desired Co_3O_4 product yield in comparison to the yields reported in the main text (i.e., of 115 and 200 mg corresponding to a 12 to 22% yield based on $Co(OAc)_2•4H_2O$ for the 3 hr reflux). However, the product composition did change some as seen in Figure S14, with the appearance of some β-CoOOH phase (perhaps related somehow due to the solvent or other reactant evaporation, or just a slower formation of the β-CoOOH phase made possible over the eight-fold longer, 24 hr reaction time, or some other at present unknown reason).

However, the main finding from this control synthesis is clear: longer reaction times past 3 hrs, and at least without additional precautions to retard solvent evaporation, do not provide higher yields of the desired Co_3O_4. Hence, we recommend a 3 hour reaction time at least presently because it leads to phase-pure particles and gives 115 and 200 mg yields that are as good or better than the 120 mg obtained under autoclave conditions.[8]

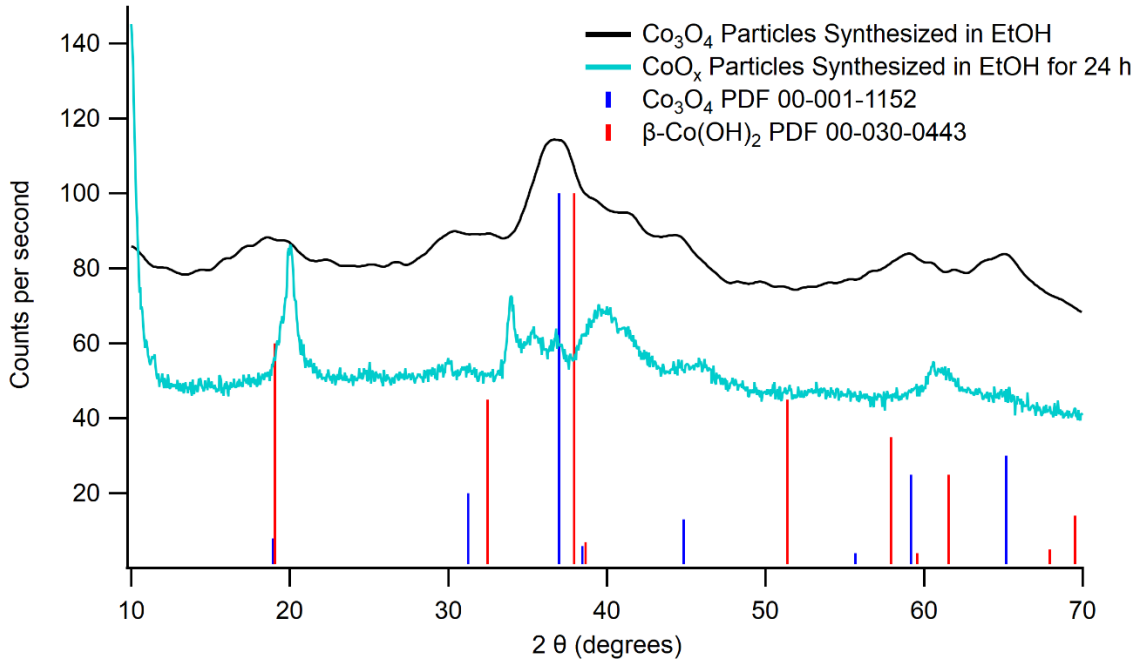

Figure 5.14. PXRD pattern of Co_3O_4 nanoparticles synthesized in ethanol for three hours (black, top) and, separately, for 24 hours (light blue, bottom). The blue and red lines are for the Co_3O_4 and β-CoOOH phases, respectively. This demonstrates that heating for 24 hrs in search of a higher yield of Co_3O_4 leads, instead, to an impure product containing a β-CoOOH phase.

REFERENCES

1 Grasshoff, K.; Kremling, K.; Ehrardt, M. *Methods of Seawater Analysis*; Third; Wiley-VCH, 1999.

2 The digestion of the Co_3O_4 nanoparticles relies upon a strong acid, reductive procedure to reduce substitutionally inert Co^{3+} to substitutionally labile Co^{2+}. On the other hand, the Berthelot test for NH_4^+ uses alkaline and oxidizing conditions to form *indophenol* in the presence of phenol, hypochlorite, and NH_4^+.[1] Under the conditions for the Berthelot test, the solution becomes dark and cloudy, suggesting that cobalt-oxide nanoparticles have reformed. Centrifuging the solution does remove the insoluble particles, but a strongly absorbing species is still present that overlaps with the indophenol absorption. We attempted using EDTA as a control to prevent reformation of the particles, but the strongly absorbing species was again formed, preventing the quantification of the desired indophenol product of the Berthelot test for the presence of NH_4^+. In short, the Berthelot test for NH_4^+ looks to be incompatible with the cobalt oxide nanoparticles and other conditions of their formation.

3 Deacon, G. B.; Phillips, R. J. *Coord. Chem. Rev.* **1980**, *33*, 227–250.

4 Deacon, G. B.; Huber, F.; Phillips, R. J. *Inorg. Chim. Acta* **1985**, *104*, 41–45.

5 Rotzinger, F. P.; Kesselman-Truttmann, J. M.; Hug, S. J.; Shklover, V.; Grätzel, M. *J. Phys. Chem. B* **2004**, *108*, 5004–5017.

6 Folkman, S. J.; Finke, R. G. *ACS Catal.* **2017**, *7*, 7–16.

7 Wei, P.; Hu, B.; Zhou, L.; Su, T.; Na, Y. *Journal of Energy Chemistry* **2016**, *25*, 345–348.

8 Grzelczak, M.; Zhang, J.; Pfrommer, J.; Hartmann, J.; Driess, M.; Antonietti, M.; Wang, X. *ACS Catal.* **2013**, *3*, 383–388.

LIST OF ABBREVIATIONS

General Abbreviations

Co-POM, cobalt-based polyoxometalate;

WOCatalysis, water-oxidation catalysis;

WOCatalyst, water-oxidation catalyst;

WOPrecatalyst, water oxidation precatalyst;

NaOAc, sodium acetate;

NaPi, sodium phosphate buffer;

NaB, sodium borate buffer;

LMCT, ligand-to-metal charge transfer;

TOF, turnover frequency;

EtOH, ethanol;

t-BuOH, *tert*-butyl alcohol;

$PhCH_2OH$, benzyl alcohol;

OAc^-, acetate.

TBA^+, tetra-*n*-butylammonium$^+$;

DMG, dimethylgloxime;

EDTA, ethylenediaminetetraacetic acid;

CoO_x, heterogeneous cobalt oxide;

Abbreviation of Co-POMs

$Co_4V_2W_{18}$, $Co_4V_2W_{18}O_{68}^{10-}$;

$Co_4P_2W_{18}$, $Co_4P_2W_{18}O_{68}^{10-}$;

$Co_4P_4W_{30}$, $[Co_4(H_2O)_2(P_2W_{15}O_{56})_2]^{16-}$;

$Mn_4V_2W_{18}$, $Na_{10}[Mn_4(H_2O)_2(VW_9O_{34})_2]$;

$Co_6V_3W_{24}$, $Na_{17}[(Co(OH_2)Co_2VW_9O_{34})_2(VW_6O_{26})]$;

$Co_9P_5W_{27}$, $[Co_9(H_2O)_6(OH)_3(HPO_4)_2(PW_9O_{34})_3]^{16-}$;

$Co_4P_4W_{30}$, $[Co_4(H_2O)_2(P_2W_{15}O_{56})_2]^{16-}$;

$CoPW_{11}$, $[Co(H_2O)PW_{11}O_{39}]^{5-}$;

α_1-CoP_2W_{17}, $[\alpha_1\text{-}CoP_2W_{17}O_{61}]^{8-}$;

α_2- CoP_2W_{17}, $[\alpha_2\text{-}CoP_2W_{17}O_{61}]^{8-}$;

Instrumentation and Techniques

CV, cyclic voltammetry

TGA, thermogravimetric analysis;

PXRD, powder X-Ray diffraction;

HRTEM, high-resolution transmission electron microscopy;

SEM, scanning electron microscopy;

XPS, x-ray photoemission spectroscopy.

SAED, selected area electron diffraction;

DLS, dynamic light scattering;

DPV, differential pulse voltammetry;